# FINAL TECHNICAL REPORT

| | |
|---|---|
| Federal Agency and Organization Element to Which Report is Submitted | Office of Fossil Energy<br>U.S. Department of Energy<br>National Energy Technology Laboratory |
| Federal Grant or Other Identifying Number Assigned by Agency | DE-FE0032119 |
| Project Title | Multi-Sourced Collaboration for the Production and Refining of Rare Elements and Critical Metals |
| PD/PI Name, Title and Contact Information (e-mail address and phone number) | Rick Q. Honaker, Ph.D., Professor<br>University of Kentucky<br>230 MMRB, 504 Rose Street<br>Lexington, Kentucky, 40506-0107<br>Phone: (859) 257-1108 (Work)<br>Phone: (859) 333-0189 (Mobile)<br>Email: rick.honaker@uky.edu |
| Name of Submitting Official, Title, and Contact Information (e-mail address and phone number), if other than PD/PI | Rick Q. Honaker, Ph.D., Professor<br>University of Kentucky<br>230 MMRB, 504 Rose Street<br>Lexington, Kentucky, 40506-0107<br>Phone: (859) 257-1108 (Work)<br>Phone: (859) 333-0189 (Mobile)<br>Email: rick.honaker@uky.edu |
| Submission Date | June 3, 2023 |
| Unique Entity Identifier (UEI) | H1HYA8Z1NTM5 |
| Recipient Organization (Name and Address) | University of Kentucky Research Foundation<br>109 Kinkead Hall<br>500 South Limestone Street<br>Lexington, Kentucky, 40526-0001 |
| Project/Grant Period (Start Date, End Date) | 12/1/2021 – 2/28/2023 |
| Reporting Period End Date | 2/28/2023 |
| Report Term or Frequency (annual, semi-annual, quarterly, other) | Final |
| Signature of Submitting Official (electronic signatures are acceptable) | 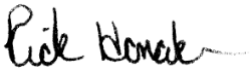 |

# EXECUTIVE SUMMARY

The project objective was to develop a feasible and cost-effective method for recovering rare earth elements (REEs) and critical materials (CMs) from coal and coal byproducts, resulting in high-purity individually separated REEs and CMs. The targeted REEs included Y, Pr, Nd, Gd, Dy, and Sm, with a purity of over 99.5%, while the CMs included Co, Mn, Ga, Sr, Li, Ni, Zn, and Ge, with a purity of over 90%. The project aimed to design a prototype facility capable of producing 1-3 tonnes/day of high-purity REO mixes. The work was divided into four designated circuits: 1) REE extraction and concentration, 2) REE separation and purification, 3) RE metal production, and 4) CM production. To achieve these goals, the project involved 11 tasks, including technology reviews, research, process flow diagram development, mass balance estimation, and preliminary technical-economic analysis. The project team included researchers from the University of Kentucky, University of Alabama and Virginia Tech as well as process specialists from Argonne National Laboratory. MP Materials provided technical support regarding rare earth markets and processing while Alliance Coal performed resource assessment.

The project included a market analysis for Nd/Pr, Tb, Dy, Gd, Y, Co, Mn, Li, Sr, Ga, Ni, Zn, and Ge. These analyses provided insights into the supply and demand trends as well as historic and future projections of market price relative to purity requirements for these elements. Two coal resources were selected for the project: the West Kentucky No. 13 (Baker) Seam and an undisclosed lignite resource in the Illinois coal basin. The estimated quantities of REEs in these resources were calculated based on production samples and drilling data. It was estimated that there is adequate supply for an operation producing one metric ton daily of higher purity mixed rare earth oxides (MREO) for approximately 20 years at a site located in western Kentucky.

In Circuit 1, project data was obtained from a pilot heap leach and REE concentration facility. It was concluded that the existing circuit, which generated a MREO concentrate, two types of CM mixed products, and Li- and Sr-containing waters, would be suitable feed for circuits 2-4. Data from the first-of-its-kind coal coarse refuse heap leach pilot pad played a crucial role in estimating reliable elemental concentrations of the pregnant leaching solution (PLS). The average total REE concentration in the PLS was found to be 28.6 ppm.

In Circuit 2, several concepts were explored including a novel process referred to as solvent-assisted chromatography (SAC). This concept involved a novel columnar reactor that incorporated multiple mixer/settlers, thereby enabling the operation of counter-flowing aqueous and organic phases. A static steady-state model (with no inflow or outflow) was developed in Matlab to evaluate the concept and the simulation results showed significant promise. The next stage involved modeling simultaneous inflows and outflows to assess the recirculating load of the aqueous and organic phases. Unfortunately, due to project time constraints, the necessary debugging and development could not be completed to fully evaluate the technology. As a result, a combined plasma distillation process, along with ionic liquid electrowinning, was selected as the technology-of-choice that can combine the performance objectives of both circuits 2 and 3. This approach allows integration of refining and REE metal production into an efficient unit.

Molten salt electrowinning was considered as an alternative for circuit 3 following circuit 2 purification circuit utilizing the novel SAC process. A mass and energy balance of Nd reduction to metal in a fluoride containing molten salt electrolyte was conducted. Comparisons were made

with the current state of Asian molten salt electrorefining, and potential improvements in siphoning rare earth metals (REM) from the reactor were presented. Geometric and control system enhancements were implemented to improve efficiency. It was determined that the minimum anode-to-cathode spacing was a limiting factor. Utilizing a spacing below the minimum would lead to contamination of the reduced metal with carbon. A cost estimate was performed for the production of 1 tonne per day, which yielded a total of $2.29 million for the nine electrowinning (EW) cells required.

As previously stated, the selected option for circuits 2 and 3 was a plasma distillation process, which initially separates rare earth elements (REEs) from other elements. This is followed by selective electrowinning in various ionic liquids. The selection was made on the basis of thermodynamic modeling and experimental data previously published by a project partner. The combination offers an innovative approach to integrated refining and RE metal production.

For Circuit 4, an extensive literature review was conducted for the processing of the CMs. Of particular interest was the Ge aqueous process, as Ge is not soluble in aqueous mineral acids. Several flowsheets were recommended that involved mineral processing and hydrometallurgy processes. However, the ultimate decision was to utilize a combined plasma and ionic liquid process as well to produce individual high-purity concentrates of Zn, Ni, Co, Mn, and Mg. A separate flowsheet for Li and Sr was recommended, which would yield carbonates of these elements. Due to the lack of suitable experimental data at this time, a process recommendation could not be provided but several methods have been proposed for consideration.

Lastly, a techno-economic analysis (TEA) was conducted to assess the effectiveness of the proposed process for further investigation. The TEA results revealed a capital expense (CapEx) of $737 million and an annual operational expense (OpEx) of $220 million. Due to the selected elements, the hypothetical heap leach pad can produce 1 metric tonne per day of REO equivalent, but a conscious decision was made to only treat targeted REEs, resulting in the production of 0.4 metric tonne of REM. An estimated annual revenue of $90.87 million was projected based on standard market pricing information provided by the funding agency. During the TEA, ten different modules were evaluated for costing purposes. The precipitation circuit was identified as the largest single operational expense, followed by the Mg/Mn process due to the amount of treated metal. In terms of capital expenditures, the heap leach process incurred the highest cost, followed by the Mg/Mn process. The scalability of the plasma process is a crucial consideration since the reactors cannot be scaled beyond the largest demonstrated size due to their reliance on surface area of the slag and vapor phase.

Additionally, a supplemental cost analysis was conducted for Li and Sr, which was not included in the TEA due to existing uncertainties. This preliminary analysis provided a break-even price for lithium carbonate based on solution concentration.

The purity estimate for the REEs are generally 98%±2% to produce a metal. The purity level being lower than the project objective was due to the lack of specific experimental data needed to tighten the tolerance of the estimates. Based on literature and previous experience, the CMs are estimated as follows; Ga (95%+, metal), Sr (95%+, carbonate), Li (95%+, carbonate), Ni (98%±2%, metal), Zn (95%+, metal sponge), Ge (95%+, metal), Co (98%±2%, metal), and Mn (98%±2%, metal).

# TABLE OF CONTENTS

# LIST OF FIGURES

# LIST OF TABLES

# 1.0 INTRODUCTION

## 1.1 OBJECTIVES

The primary objective of this project is to identify, evaluate, test and ultimately scale and commercialize advanced refining and metal production technologies capable of extracting high purity rare earth (RE) and critical metals from coal-based sources economically and in an environmentally friendly manner. Previously, the Recipient successfully designed, constructed, and operated a pilot scale rare earth processing facility that uses conventional approaches to extract and recover rare earth elements (REEs). Operational data from this facility has demonstrated the ability to successfully produce rare earth oxide (REO) concentrates at grades exceeding 90% and at production rates of 10 to 100 g/day. It is currently being expanded to 110 kg/year. However, this facility does not have the capability to produce individually separated high purity (ISHP) REEs. Through this nine-month effort, the project team will deliver a pathway and research plan to apply advanced technologies for ISHP production from coal-based sources and reduction to metal that will minimize environmental impact and reduce capital and operating expenses by more than 20% over conventional processes while delivering, at a minimum, the following rare and critical metals: (REEs) Y, Pr, Nd, Gd, Dy and Sm of greater than 99.5% purity, and (Critical Minerals [CM]) Co, Mn, Ga, Sr, Li, Ni., Zn and Ge of greater than 90% purity.

## 1.2 APPROACH

The proposed scope of work will identify and evaluate advanced refining and metal production technologies for individually separated high purity REEs as well as CMs. The effort has been divided into 11 different tasks to provide the project deliverables within a nine month project duration. These tasks will be undertaken to: 1) complete a thorough literature review of currently available refining and metal reduction technologies; 2) complete a resource and market analyses; 3) technically and economically evaluate and assess advanced processes proposed by the team for separation and purification of rare earth and critical elements as well as metal reduction processes proposed needed to produce high-purity metals; 4) develop novel process flow diagrams capable of producing high purity rare and critical metals; 5) complete a preliminary techno-economic analysis of the process options; and 6) develop a Technical Research Plan that will focus on the development of innovative separation and purification technologies and metal reduction processes for the production of rare and critical metals.

## 1.3 SCHEDULE AND MILESTONE STATUS

### 1.3.1 Project Schedule

The project had a formal start date of December 1, 2021 and was originally scheduled to end on August 31, 2022. The project involved eleven work tasks focused on the production of five individual rare earth metals (i.e., Y, Pr, Nd, Gd, and Dy) of greater than 99.5% purity, and five individual critical minerals [CM]) (i.e., Co, Mn, Ga, Sr, and Li) of greater than 90% purity. An opportunity was presented to increase the work scope to include Sm as well as Ni, Zn and Ge. Due

to the expanded work scope, the end date was extended to February 28, 2023. The schedule by task and subtask is provided in Figure 1, which also indicates the completion date of major project milestones.

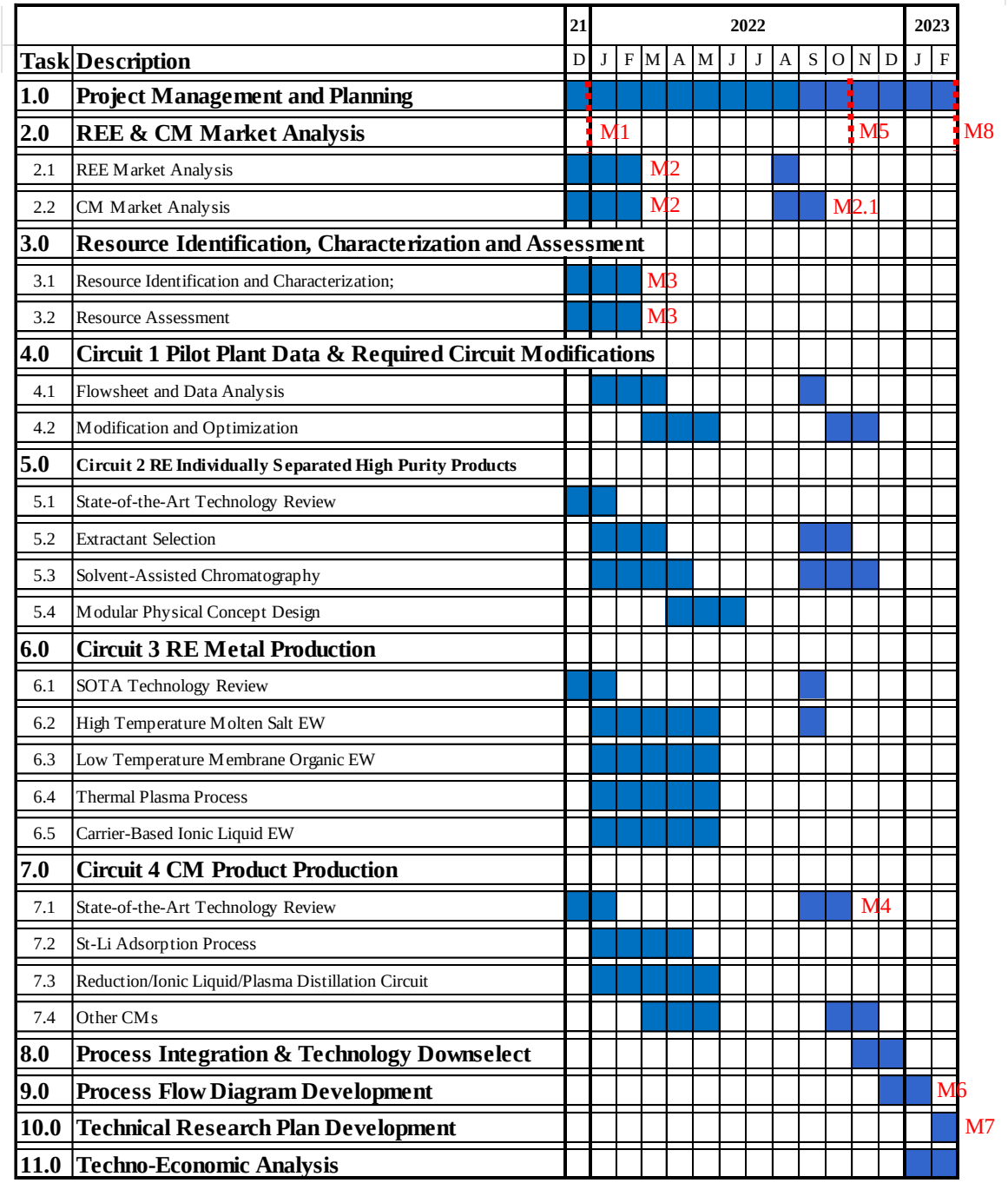

Figure 1. Project schedule for the 15-month project; start date = December 1, 2021, end date = February 28, 2023.

*1.3.2 Project Milestones*

Table 1 provides a list of project milestones, planned completion and actual completion dates, completion verification method and comments regarding status.

Table 1. Project milestone status.

| No. | Milestone Title & Description | Completion Date | | Verification Method | Comments on Status |
|---|---|---|---|---|---|
| | | Plan | Actual | | |
| 1 | Modified Project Management Plan | 12/31/21 | 1/14/22 | PMP approved by the NETL program manager | Modified plan was submitted on 1/5/22, edited by NETL, corrected and final version submitted on 1/14/2022. |
| 2 | Market Analysis Complete | 2/28/22 | 3/31/22 | Submission of Research Progress Performance Report | Completed; subsequently revised based on review by Program Manager; re-submitted 6/1/2023 |
| 2.1 | Market Analysis (Sm, Ni, Zn, Ge) Complete | 9/30/22 | 10/17/22 | Submission of Research Progress Performance Report | Completed; subsequently revised based on review by Program Manager; re-submitted 6/1/2023 |
| 3 | Resource Assessment Complete | 2/28/22 | 3/31/22 | Submission of Research Progress Performance Report | Completed |
| 4 | Purity Product Estimates Complete | 5/31/22 | 11/30/22 | Submission of Research Progress Performance Report | Completed |
| 5 | Teaming Plan Complete | 6/30/22 | 1/15/23 | Submission of Research Progress Performance Report | Completed |
| 6 | Flow Diagram Complete | 7/31/22 | 1/31/23 | Submission of Research Progress Performance Report | Completed |
| 7 | Technical Research Plan Completed | 8/31/22 | 4/17/23 | Submission of Final Report | Completed; subsequently revised ba on review by Program Manager; re-submitted 6/1/2023 |
| 8 | Final Technical Report Completed | 8/31/22 | 6/1/23 | Submission of Final Report | Completed |

# 2.0 PRODUCTS RESULTS AND DISCUSSION

## 2.1 Task 1.0 – Project Management & Planning

## 2.2 Task 2.0 – REE & CM Market Analysis

### *2.2.1 Subtask 2.1 – REE Market Analysis*

Introduction

While there are some functional similarities across the lanthanide series, the markets for certain groups, pairs, and individual rare earth elements (REEs), each carry their own unique characteristics. Historically, there has been a degree of reflexivity among the REEs, as the idiosyncratic price environments for each element have prompted new product introductions when certain prices were low, and substitutions when prices were high. Furthermore, there are only a few specific minerals proven to support commercial extraction of REEs, meaning that the relative abundance of each element in the market largely mirrors the distribution of what is found in these commercial minerals. As a result of this complex balance of factors, when describing the market for each REE, it is necessary to make contextual reference to lanthanides more broadly to fully illustrate market dynamics.

Rare earth metal (REM) pricing correlates closely with the related rare earth oxide (REO) pricing, and across the REEs there is generally negligible margin for metal reduction based on spot prices for the metal and oxide respectively. VAT policies in China deterring export of intermediate materials have historically drawn criticism from the World Trade Organization, and industry participants have pointed towards these policies as a hurdle for private sector investment in rare earth metal production. This context (combined with material handling considerations) helps explain why industry participants tend to talk in terms of REOs rather than REMs, with the pricing of the latter implicitly tied to the former. Given the focus area of this project, special attention will be paid to describing post-oxide processing, but market sizing will be provided on an oxide basis. By the same token, the purity provided for each REO specification represents what is believed to be the highest volume specification of that material in the market. Table 2 below summarizes pricing, production, and market sizes for the elements of interest.

Table 3. summarizes the specifications associated with the pricing and market sizing provided.

Table 2. Pricing, Production, and Market Size per REE of Interest

| Material | Price ($/kg) | Global Production* | Estimated Market Size ($M) |
|---|---|---|---|
| NdPr | 133 | 46,000 | 6,118 |
| Tb | 1,775 | 440 | 781 |
| Dy | 460 | 1,780 | 819 |
| Gd | 68 | 2,500 | 170 |
| Y | 11 | 10,000 | 110 |

*(MTPA)

Table 3. Material Specifications for REEs of Interest

| REEs | Purity | Incoterms | Requirements* |
|---|---|---|---|
| NdPr | 99% | EXW China | 25% $Pr_6O_{11}$ (+/- 2%), 75% $Nd_2O_3$ (+/- 2%), < 0.05% Ce, < 0.03% Sm |
| Tb | 99.99% | FOB China | < 20ppm Dy, < 10ppm Gd |
| Dy | 99.5% | FOB China | < 0.1% Ho, < 0.1% Tb |
| Gd | 99.5% | EXW China | < 0.1% Sm + Eu, < 30ppm Fe |
| Y | 99.999% | FOB China | < 1ppm Ho, < 1ppm Er |

*All percentages are wt %

*Neodymium & Praseodymium* - Neodymium and praseodymium are very similar – so much so, in fact, that historically they were thought to consist of a single element ("didymium") up until the late 19th century. Neodymium and praseodymium tend to be found in a ratio of approximately 3:1 in commercial minerals. The applications and markets for neodymium and praseodymium overlap considerably. Today, neodymium and praseodymium, which are collectively called "NdPr" in commercial settings, together represent a strong majority of overall rare earth elements (REEs) used in permanent magnets. Broadly, magnetic applications represent the largest market for all REEs in dollar terms, and this share is forecasted to grow as higher performance systems of electrified motion take over in many industries.

For general purpose magnetic applications, the neodymium and praseodymium are effectively interchangeable, a fact that has led some upstream processors to forgo separating them in bulk volumes. There are specialized applications for which one of the two elements is required (or preferred), but the volumes needed for these applications are considerably smaller than those for NdPr-containing magnets; thus, neodymium and praseodymium prices tend to be highly correlated. Those applications specifically requiring neodymium or praseodymium tend to rely on them for their photonic properties rather than magnetic properties, an example being neodymium-doped yttrium-aluminum-garnet (YAG) for solid-state laser gain media. Praseodymium specifically also finds use as pigment for specialized ceramic materials.

While NdPr-containing permanent magnets serve as crucial components indirectly enabling trillions of dollars of end-use markets, when directly defining the rare earth market as terminating at the oxide, global production of NdPr is roughly 46,000 metric tons per annum by recent estimates. As of February 1, 2022 (the reference date for all spot prices included herein), the spot price for NdPr oxide was $133/kg for 2N purity (99%). Together, these values equate to a market size of over $6 billion. Industry analysts generally forecast faster demand growth for magnetics-related REEs, reflected as a compound annual growth rate (CAGR) of over 5% for the decade ahead. This near-term growth is expected to primarily tighten supply for NdPr oxide globally but will also likely have impacts on dysprosium and terbium, as will be described subsequently.

The largest producer of NdPr oxide is the Northern Rare Earth group operating in Baotou, Inner Mongolia, China. Mountain Pass in California, USA; Jiangxi Copper in Mianning, Sichuan Province, China; and Mount Weld in Australia are the next three largest actively mined resources for NdPr production. An overwhelming majority of NdPr oxides are reduced to metal in China by operations residing within the state-directed smelting quota system. This metal is then generally

made into NdFeB alloy in China as well before being used by magnet-makers in China or being exported to those few rare earth magnet-makers with operations outside of China.

*Dysprosium* - Like NdPr, the dysprosium market is primarily driven by magnetic applications. Also, like neodymium, dysprosium shares a functionally similar elemental pair in terbium, and the two tend to be found in a ratio of roughly 4:1 (respectively) in commercial minerals. This relative abundance contributes to terbium carrying a higher price than dysprosium. The reference spot price for terbium oxide at 4N purity (99.99%) is $1775/kg, while for dysprosium oxide it is $460/kg at 2N purity (99%). Recent estimates of global terbium oxide production was 440 metric tons per annum (MTPA), with dysprosium oxide at 1,780 MTPA. Using reference oxide prices, this equates to a combined terbium and dysprosium oxide market size of over $1.5 billion. Like with NdPr, dramatic demand growth for high performance magnets is expected to drive unit pricing and the market size higher in the decade ahead.

In magnets, dysprosium (and terbium) serves to increase coercivity by stabilizing the boundaries between grains, which is especially crucial for magnets in operating conditions with elevated temperatures. To fulfill this function, only a small amount of dysprosium is needed relative to NdPr, though the exact proportions are closely guarded by magnetic alloy and magnet makers. Given the higher price and greater scarcity of dysprosium compared to NdPr, metallurgists over time have tried to reduce the amount of dysprosium needed for magnets at performance parity; these efforts have succeeded to a certain extent, but generally dysprosium remains a requirement for higher coercivity magnets. This requirement is particularly troublesome from a supply chain resiliency perspective, as a significant portion of global dysprosium supply is questionably traceable and thought to originate from artisanal mining operations in South China and Myanmar utilizing in-situ, unlined acid leaching methods that fall far short of American safety standards.

There are relatively few uses for dysprosium outside of permanent magnets. While terbium has found some use in photonic applications, the same has generally not held true for dysprosium, and over time, these uses have seemingly waned as escalated pricing has pushed designers towards substitute materials and technologies. That said, both elements are the key ingredients of Terfenol-D, a leading magneto-restrictive material. This market is somewhat opaque as it is controlled by a small number of firms, and primary historical use was in underwater acoustics systems tied to defense applications. This material has more recently been used in fuel injection systems, various sensors, actuators, and transducers. This market is assumed to be considerably smaller than the market for permanent magnets.

*Gadolinium* - While gadolinium does figure into magnetic applications as well, its market consists of considerably more diverse end-use applications than those of NdPr and dysprosium. Historically, some magnet alloys featured gadolinium prominently, but today it is generally found in small amounts as a dopant (or impurity) at levels closer to that of dysprosium than NdPr.

Gadolinium is unique in its usage as a contrast agent for magnetic resonance (MR) based medical imaging. This application could be considered "magnetic," as the mechanism by which gadolinium works is magnetically interacting with water molecules in the body to create "T1 contrast" (light spots) on MR images. Despite some development efforts to move towards iron and manganese-based substitutes, all FDA-approved MR contrast agents in commercial use today rely on

gadolinium. The purity for pharmaceutical grade gadolinium is expected to be considerably higher than what is needed elsewhere, making it a specialty chemical likely requiring further refining than compositionally comparable material for alternative applications.

Gadolinium finds other medical imaging-related usage in gadolinium oxysulfide ("GOS") based scintillators for x-ray intensification (both newer digital systems and older film cassettes). It is also used in specialty glass material that shields radiation. Another gadolinium application is its emergent use as laser gain media; potassium-gadolinium-tungstate (KGW) based materials with other lanthanide dopants have grown in popularity as a substitute to rare earth doped yttrium-based materials for certain photonic use cases. The final gadolinium application of note is found in nuclear control rods.

The reference spot price for gadolinium oxide is $68/kg at 3N purity (99.9%). Recent estimated of global gadolinium production are 2,500 MTPA. These values equate to a gadolinium oxide market size of slightly under $200 million.

*Yttrium* - Similar to gadolinium, yttrium also finds its main uses outside of magnetics. Yttrium is part of a common host material for photonics applications, yttrium-aluminum-garnet (YAG), and is also a component of certain ceramic mixtures and alloys, primarily alongside zirconia in yttria-stabilized zirconia (YSZ), but also found with aluminum and magnesium. The reference spot price for yttrium oxide is $11/kg at 99.999% (5N) purity. Recent estimates put global yttrium production at 10,000 metric tons per annum. These values together equate to a market size of slightly over $100 million.

Yttrium's similar atomic structure to the lanthanides makes it an especially effective host material for laser gain media, as both YAG and yttrium oxide can effectively host a variety of dopants depending on the absorptive and emissive qualities desired. There are varied types of laser gain media, and monocrystal YAG requires production via long duration, high heat processing known as the Czochralski method. YAG is by far the most dominant solid state laser gain media (excluding simple LEDs and fiber-based systems) by market share across all end-uses. For similar functional reasons, yttrium is also an increasingly important component of scintillators for positron emission tomography (PET) in the form of lutetium-yttrium-orthosilicate (LYSO).

Yttrium once again plays a similar functional role in ceramics as a molecule with a structure that compliments the inherent strengths of a more "active" counterpart, in this case zirconia. YSZ has a wide variety of applications ranging from dentistry (non-metallic crowns) to refractory coatings in jet engines and gas turbines. The material's hardness, durability, thermal properties, and relatively established supply chains for those applications mentioned make it an appealing choice for emergent ceramic materials related to electrification as well. These qualities, together with particularly high plasma resistance, have also made yttrium a growing constituent of anti-plasma material required of semiconductor manufacturing.

Yttrium has also found some use in phosphors, particularly those used to coat certain LEDs, but this application is challenging to analyze as over time it has attracted a wide variety of substitute materials and technologies with limited transparency across largely Asia-based OEMs. Similarly, yttrium compounds are used catalytically to support ethylene polymerization, but broad variation

among substitutes and limited transparency makes generalized, commercial analysis of this application challenging.

While any materials used in quantum computing are necessarily early in their development and commercialization lifecycles, there are several materials with early promise that feature yttrium alongside other lanthanide dopants. Yttrium has also historically been a component of certain superconducting materials, but it remains to be seen if and how this application may achieve commercial significance.

*Samarium* - Like NdPr, the samarium market is primarily driven by magnetic applications. Samarium is alloyed with cobalt in magnets that are particularly well-suited to applications in which the operating environment has a high temperature. The reference spot price for samarium oxide at 99.9% (3N) purity is $40/kg. Recent estimates of global samarium production were 3,880 metric tons per annum. Using the reference oxide price, this equates to a samarium oxide market size of $155 million. For a time, SmCo magnets were the strongest formulation available, but in the past decades they have been surpassed by sintered NdFeB magnets across many sets of operating conditions for end-use applications. Consequently, demand growth is expected for SmCo magnets in the decade ahead as more electrified motion use cases gain market share, but this growth is generally expected to be more modest than that of sintered NdFeB magnets.

There are relatively few uses for samarium outside of permanent magnets. Like the other lanthanides, samarium is both used in specialty alloys and in photonic applications as well. However, publicly available information about samarium's specific uses and benefits in these applications is sparse. Samarium's magnetic and non-magnetic applications alike are generally associated with the military industrial base, so the market is opaque. In September 2022 samarium came up in the news as the Pentagon halted orders for F-35's based on the turbomachine's magnets containing samarium from China. This development highlighted the urgency to decouple supply chains for rare earth elements with sensitive end-use applications.

### *2.2.2 Subtask 2.2 – CM Market Analysis*

*Cobalt* - The commercial uses of cobalt include around 42% as super alloys in aircraft engines and gas turbines, primarily due to its temperature stability, 9% in cemented carbides for cutting and wear-resistant applications, 16% in various other metallic applications, and 33% in a variety of chemical applications as an oxidation catalyst. Cobalt-alloys are typically corrosion-resistant and wear-resistant and thus used in orthopedic implants. Alloys containing cobalt are also used to produce permanent magnets [1].

The major growth area for cobalt use involves the production of lithium-ion battery cathodes primarily for electric vehicles (EV). Cobalt has excellent thermal stability and high energy density, which are important properties for extending battery life and the number of miles between charge events. The amount of cobalt used in a typical EV battery is 13.3 kg [2, 3]. In 2021, Tesla announced that work performed in collaboration with Japanese scientists reduced the amount of cobalt per EV to 14 kg. Based on this achievement, the amount of Co that was needed to produce Tesla's 1 million EVs in 2021 was around 14,000 metric tons. By 2040, it is estimated that 45 million EVs will be produced annually [4]. At the reduced Co content, the amount of Co needed

to meet demand from EV production is estimated to be 630,000 metric tons. The total amount of cobalt produced in 2021 was only 170,000 metric tons worldwide. For this reason, cobalt supply is considered to be one of the biggest threats to the EV supply chain, which explains the significant effort to reduce the amount needed per EV or identify a substitute.

The sources and amount of known cobalt reserves present additional concerns. In 2021, the Democratic Republic of the Congo (DRC) supplied 70.6% of the total worldwide production as shown in Table 4 [1]. According to Figure 2, the pressure on cobalt supply has resulted in a 300% increase in market value over the past two years [5]. Cobalt prices rapidly increased and reached a peak in 2018 with a maximum value of $95,000 per metric ton. Reasons for the 2018 peak included anticipation of a rapid increase in EV production. However, a significant rise in EV production failed to occur which eventually resulted in a sharp drop in Co value in 2019. However, the start of significant EV production and announcements of several EV battery manufacturing facilities resulted in a sharp rise in market values in 2021. It is estimated that the value of cobalt will be around $86,994 per metric ton in 2023 [5]. Illegal labor practices and environmental issues are commonly associated with the mining environment in the DRC. In addition, nearly 100% of the production is shipped to China for purification, metal production and manufacturing. Furthermore, Congo possesses 46% of the total worldwide reserves of cobalt, a total of 7.6 million tons. Note that the known reserve base would only support 12 years of EV production at the 45 million per annum level, which does not consider the other Co applications.

Table 4. Worldwide cobalt production and reserves in 2021*

| **Country** | **2021 Production (metric tons)** | **Reserves (metric tons)** |
|---|---|---|
| United States | 700 | 69,000 |
| Australia | 5,600 | 1,400,000 |
| Canada | 4,300 | 220,000 |
| China | 2,200 | 80,000 |
| Congo | 120,000 | 3,500,000 |
| Cuba | 3,900 | 500,000 |
| Indonesia | 2,100 | 600,000 |
| Madagascar | 2,500 | 100,000 |
| Morocco | 2,300 | 13,000 |
| New Guinea | 3,000 | 47,000 |
| Philippines | 4,500 | 260,000 |
| Russia | 7,600 | 250,000 |
| **Total** | **170,000** | **7,600,000** |

*Source: [1] USGS, 2022.


Figure 2. Market price variations of cobalt in recent years [5].

*Manganese* - Manganese (Mn) is the fourth most common metal by tonnage after iron, aluminum, and copper. It is a transitional metal that is used in a number of alloys including stainless steel and provides strength, workability, and resistance to wear [6]. Manganese's use in iron and steel production represents 85% to 90% of its total demand, whereas it's second largest application is in aluminum alloys, which typically contain 1.5% manganese [7]. For example, nearly 37,800 tons of manganese metal were used in 2020 for aluminum beverage cans [8,9] as an example.

A growing application involves the use of Mn as a stabilizer in lithium-ion batteries (LIBs), which represents less than 1% of global demand [10]. Specifically, manganese in a lithium battery used for electric vehicles provides a cathode structure that is less resistant to electron flow. Due to the cost of nickel, recent developments are focused on substituting a portion of the nickel in LIBs with manganese, as described by for Volkswagen [11]. Although increasing nickel content maximizes energy density as shown in Figure 3, manganese provides an opportunity to reduce cost. According to the International Energy Agency (IEA), currently, the amount of manganese used in an electric vehicle (EV) is 24.5 kg, while the amount used to manufacture a single conventional car is 11.2 kg, which is primarily in the steel and aluminum alloys [3]. Based on a targeted EV production of 45 million worldwide annually by 2040, the corresponding Mn demand increase would be by 0.6 million tons annually, which would only require a 3% increase in the current supply. The battery application requires high purity electrolytic manganese metal (HPEMM) which is 4N (99.99%) purity, or high purity manganese sulfate monohydrate ($MnSO_4 \cdot H_2O$), which is projected to be in short supply due to the growth in battery manufacturing. It is noted that China has the majority of the refining capacity and, thus, is the supplier of 90% of the world's high purity manganese [12].

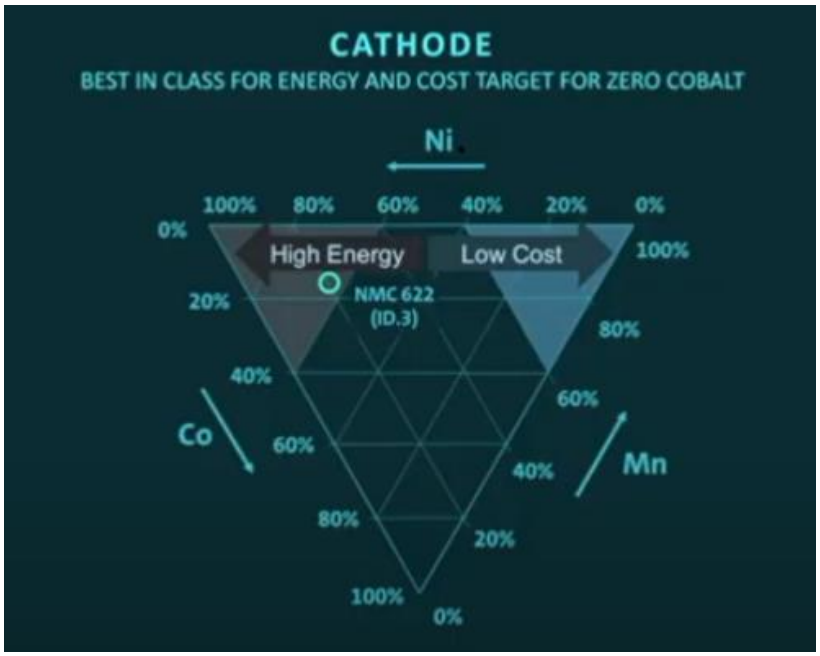


Figure 3. Substitution of Ni and Co with Mn in EV battery cathodes [11]

The market value for manganese ore peaked at $7.2/metric ton in 2016, decreased to $4.2/metric ton in 2019, and has since steadily increased to a present value of $4.5/metric ton in 2022 as shown in Figure 4. The current trading value of manganese ore is $4.5/metric ton [13].


Figure 4. Market price variations of manganese in recent years in yuan per metric ton.

The global manganese alloy market size was USD 25,615.7 million in 2019 and is projected to reach USD 42,004.4 million by 2027, exhibiting a compound annual growth rate (CAGR) of 7.4% during the forecast period [14].

According to Mordor Research, the global manganese market is projected to grow at a CAGR of over 4.0% between 2021 and 2026. Much of this anticipated growth was attributed to an increase in EV demand. The disposable and rechargeable battery space is the second largest consumer of manganese today [15].

The primary worldwide suppliers of manganese are (in order of production): South Africa, Gabon, and Australia, as shown in Table 5 [1]. Total worldwide supply of manganese has held fairly steady at around 20 million tons annually. The U.S. reliance on other countries for Mn ore is close to

Table 5. Worldwide manganese production and reserves in 2021*

| **Country** | **2020 Production (mt * $10^3$)** | **2021 Production (mt * $10^3$)** | **Reserves (mt * $10^3$)** |
|---|---|---|---|
| United States | - | - | - |
| Australia | 3,330 | 3,300 | 270,000 |
| Brazil | 494 | 400 | 270,000 |
| Burma | 254 | 250 | N/A |
| China | 1,340 | 1,300 | 54,000 |
| Cote d'Ivoire | 525 | 500 | N/A |
| Gabon | 3,310 | 3,600 | 61,000 |
| Georgia | 186 | 190 | N/A |
| Ghana | 637 | 640 | 13,000 |
| India | 632 | 600 | 34,000 |
| Kazakhstan | 158 | 160 | 5,000 |
| Malaysia | 347 | 360 | N/A |
| Mexico | 198 | 200 | 5,000 |
| South Africa | 6,500 | 7,400 | 640,000 |
| Ukraine | 578 | 670 | 140,000 |
| Vietnam | 121 | 120 | N/A |
| Other Countries | 260 | 260 | Small |
| **Total** | **18,900** | **20,000** | **1,500,000** |

*Source: [1]

100% with the major sources being Gabon (67%), South Africa (18%), and Mexico (11%) (USGS Annual Commodities Report, 2022). The U.S. imports of Mn increased by 20% in 2021 relative to 2020. It is noted that South Africa has 30% of the world's manganese reserves.

Manganese demand is primarily driven by increased steel production to support infrastructure development in countries such as China, India, Brazil, and South Africa. SiMn alloy production primarily occurs in China (70%) and India (12%) [1]. These same two countries also produce 50% of the FeMn. Recently, production levels of steel in China were impacted by their energy crisis and coordinated maintenance outages, which drove the price of steel upward. Moreover, the COVID pandemic greatly impacted manganese demand through reduced steel demand for construction and infrastructure projects as well as a decrease in automotive manufacturing due to constrained chip production [16].

*Lithium* - The most common use of lithium is in the manufacturing of lithium-ion batteries. The primary reason for lithium's use in this application is due to the fact that lithium has the highest potential to lose electrons among all elements [17]. In 2020, the total worldwide production of lithium was 82,500 metric tons and increased to around 100,000 tons in 2021. Of the total lithium produced in 2021, nearly 74% was utilized for batteries. Other applications of lithium include ceramics and glass (14%), lubricating greases (3%), continuous casting molding flux (2%), polymer production (2%), and air treatment (1%) [1]. Another unique property of lithium is that it is the lightest of all metals with a specific gravity of 0.45. This makes it ideal as an additive with aluminum to form a low weight, high strength alloy.

Lithium-ion batteries are the anticipated energy source for electric vehicles (EVs). There is approximately 8.9 kg of lithium in each EV which means that 8,900 tons of lithium is needed to build the batteries for 1 million EVs. Due to the anticipated near exponential growth in EV production, a supply-demand deficit of 5,000 metric tons is expected in 2022 with battery manufacturers accelerated capacity expansion [18]. A 30% growth is expected through 2025. From another estimate, the lithium market will nearly double in seven years growing from $3.83 billion in 2021 to $6.62 billion in 2028 [19]. A negative side effect of this application is that lithium metal is very reactive to air and water. As a result, fires developed from Li ion batteries during an accident involving an EV, for example, are difficult to extinguish and, thus, a known safety concern.

The market value for lithium carbonate was relatively flat for several years prior to 2021 as shown in Figure 4 [20]. However, prices escalated exponentially and reached a maximum value in November 2022 that was 14 times the pre-2021 value. The rise in market value reflected the anticipated production increase in lithium-ion batteries, especially those associated with EVs. However, EV production is currently lower than anticipated which has caused lithium carbonate prices to drop to $41,650/t (or 297,500 CYN/t). It is noted that remarkable value increases of lithium products occurred within 11 months in 2021. For example, from January 2021 to November 2021 lithium carbonate ($Li_2CO_3$) prices rose from $7,000/metric ton to $26,200/metric ton; lithium hydroxide (LiOH) prices increased from $9,000/metric ton to $27,400/metric ton; spodumene (lithium containing mineral) market prices increased from $450/metric ton to $2,300/metric ton; and lithium metal prices increased from $77,000/metric ton to $97,000/metric ton.[20]

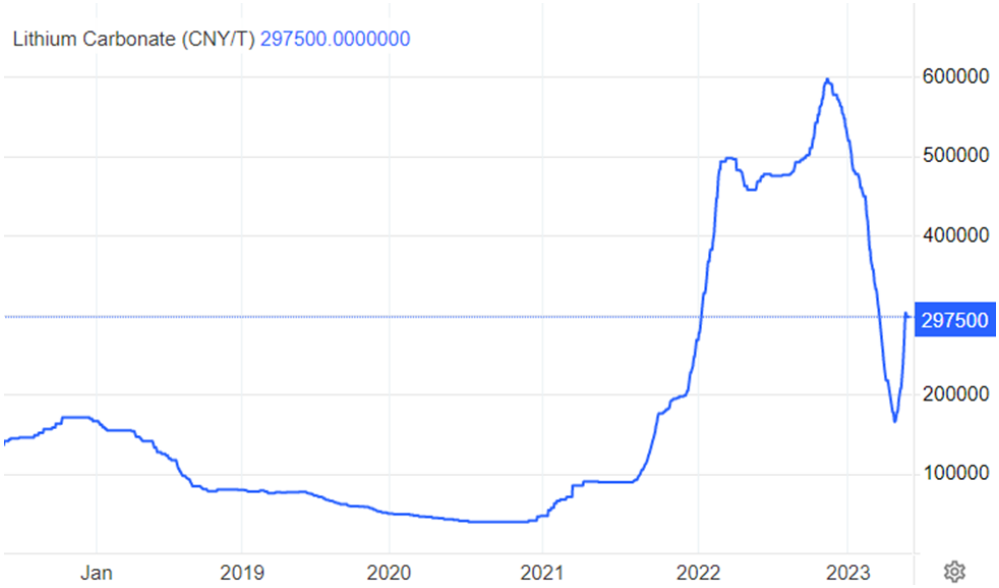


Figure 5. Market value variability of lithium carbonate in recent years [20].

Table 6 shows the total lithium reserves and 2021 production estimates by country [1]. The world's largest lithium producer is Australia (55%) followed by Chile (26%). The worldwide lithium production total in 2021 was around 100,000 metric tons. However, many producers have announced expanded production for 2022 and 2023 including operations in Australia (+250,000

Table 6. Worldwide lithium production from mining and remaining reserves in 2021*

| Country | 2021 Production (metric tons) | Reserves (metric tons) |
|---|---|---|
| United States | Unknown | 750,000 |
| Argentina | 6,200 | 2,200,000 |
| Australia | 55,000 | 5,700,000 |
| Brazil | 1,500 | 95,000 |
| Chile | 26,000 | 9,200,000 |
| China | 14,000 | 1,500,000 |
| Portugal | 900 | 60,000 |
| Zimbabwe | 1,200 | 220,000 |
| Other Countries | - | 2,700,000 |
| **Total** | **100,000** | **22,000,000** |

*Source: [1] USGS, 2022.

metric tons), U.S. (+5,000 metric tons), Argentina (+25,000 metric tons), and Chile (+100,000 metric tons) (Source: S&P Global, Commodities 2022). In the U.S., it was reported that Tesla signed a 10-year lithium supply agreement with Piedmont Lithium, Inc., who owns a lithium property in North Carolina [21]. Currently, the Albemarle's Silver Peak in Nevada is the only lithium mine operating in the U.S.

*Strontium* - Strontium is an element that has similar physical and chemical properties to calcium and barium. Strontium metal is extremely reactive to air and water and ignites spontaneously. common applications of strontium nitrate include pyrotechnics and the production of signals, such as flares, as ignition of strontium provides the bright red color in flares and fireworks. Nearly 75% of strontium is used in glass of cathode ray tubes (CRT) for color televisions to prevent x-ray emission, however, use in this application is on the decline due to the use of field emission displays (FED) and liquid crystal displays (LCD). There are three common commercial forms of strontium:

- Strontium aluminate used in glow in the dark toys;
- Strontium nitrate and carbonate for the manufacturing of fireworks providing a deep red color; and
- Strontium chloride in toothpaste for sensitive teeth.

In 2021, 40% of the strontium was used in ceramic ferrite magnets, 40% in pyrotechnics/signals, and 20% in other applications including drilling fluids/electrolytic production of zinc/master alloys/pigments and fillers [1]. Substitution in these applications is possible but typically has a negative impact on performance/desired effect. For example, replacement with barium in ceramic ferrite magnets reduces the maximum operating temperature [22].

As indicated in Table 7, the total world mine production of strontium in 2021 was 360,000 tons [1]. The U.S. does not produce strontium and has not done so since 1959 [1]. The primary source of strontium for the U.S. is Mexico (80%) in addition to relatively smaller amounts sourced from Germany and China.

Table 7. Worldwide strontium mineral (celestite) mine production in 2020 and 2021*

| **Country** | **2020 Production (metric tons)** | **2021 Production (metric tons)** |
|---|---|---|
| United States | - | - |
| Argentina | 700 | 700 |
| China | 80,000 | 80,000 |
| Iran | 90,000 | 90,000 |
| Mexico | 33,500 | 35,000 |
| Spain | 150,000 | 150,000 |
| **Total** | **350,000** | **360,000** |

*Source: [1] USGS, 2022

The worldwide strontium market was valued at $449.9 million in 2020 and is projected to reach $711.5 million by 2028, growing at a compound annual growth rate (CAGR) of 5.9% from 2021 to 2028. Growth is attributed to the use in the dental industry for tooth-sensitive paste [23]. Strontium was removed from the 2022 Final List of Critical Minerals as published in the Federal Register (87 FR 10381)[24].

*Gallium* - Gallium is a soft, silver solid metal at room temperature and under standard pressure. However, the melting point of gallium is just slightly higher than room temperature (29.76°C) [25]. This property, along with the ability to efficiently diffuse into a metal lattice, is valuable in Ga's use to lower the melting points of alloys. Notably, gallium has the largest liquid range among metals with a boiling point of 2,400°C.

Gallium at a purity level of 99.9999% (6N) is commonly used as a dopant in semiconductor substrates. Gallium arsenide (GaAs) and gallium nitride (GaN) represent 98% of gallium use, while GaAs makes up 95% of the total [26].

GaAs is a type III/V semiconductor with high electron mobility and a high saturated electron velocity relative to silicon, enabling it to function at frequencies over 250 Hz. The semiconductors produced using GaAs are not sensitive to heat because of their wide bandgap. The market value of GaAs was $7.5 billion in 2016, of which 53% was in cell phones and 27% in other wireless communications. Increased use in future years is primarily associated with smartphone advancements [27].

The electrons in gallium nitride crystals move 30% faster than silicon electrons [28]. The use of gallium nitride (GaN) in wide bandgap semiconductors provides high-efficiency power transistors and integrated circuits. Favorable characteristics include higher breakdown strength, faster switching speed, higher thermal conductivity and lower on-resistance, power devices relative to silicon-based devices. As a result of its high electron mobility, GaN has distinct advantage for use in radio frequency components over silicon. Gallium nitride is used in cable television transmission, commercial wireless infrastructure, and power electronics [29].

Furthermore, GaAs and GaN have the ability to convert electricity into light. Based on this property, their use in optoelectronic devices (laser diodes, superluminescent diodes, and light-emitting diodes (LEDs)) had an overall market value of $18.5 billion in 2016 [1, 30]. Aluminum gallium arsenide (AlGaAs) is used in high-powered infrared laser diodes.

The supply of gallium is primarily obtained as a byproduct from bauxite mining and processing. However, a significant amount is reportedly associated with zinc sulfide ores, e.g., sphalerite mineralization. The average Ga feed grade in a bauxite ore that is considered a good Ga source is 50 ppm. During the processing of bauxite, gallium is recovered from the sodium hydroxide solution generated from the Bayer process and subsequently extracted using an ion-exchange resin. Approximately 15% of the Ga is recovered during the processes used for extraction with the remaining reporting to various waste streams, including the red mud [31, 32].

Total production of gallium has varied significantly over the past decade due to oversupply and COVID issues but is recently on an upward trend, primarily due to the demand associated with

smart phone technologies. Total worldwide production in 2021 was 430,000 kilograms as shown in Table **8**. High-purity gallium production was 225,000 kg in 2021 which represented a 5% increase from 2020. China accounts for 84% of the worldwide low-purity gallium capacity [1]. All other suppliers have relatively small production capabilities. High purity gallium metal is 99.9999% Ga and low-purity gallium 99.99% pure (4N) Ga. Worldwide primary low-purity gallium production capacity in 2021 was 774,000 kg/yr; high-purity production capacity 325,000 kg/yr; and secondary high-purity production capacity 273,000 kg/yr [1].

Table 8. Worldwide gallium production in 2020 and 2021*

| **Country** | **2020 Production (kg)** | **2021 Production (kg)** |
|---|---|---|
| United States | - | - |
| China | 317,000 | 420,000 |
| Japan | 3,000 | 3,000 |
| Republic of Korea | 2,000 | 2,000 |
| Russia | 5,000 | 5,000 |
| **Total** | **327,000** | **430,000** |

*Source: [1] USGS, 2022.

The U.S. is 100% reliant on imports for gallium, and the primary source is China (53%), with 11% from the United Kingdom; 9% from Germany, 7% from Ukraine, and 20% from others. The value of gallium imports in 2017-2020 was $3 million for metal and $200 million for gallium arsenide wafers. The supply of gallium was identified as being critical by the U.S. federal government in the Federal Register (86 FR 621199). In addition, gallium is recognized as a technology critical-circuit element by the U.S. National Library of Medicine and Frontiers Media [1].

Primary low-purity (99.99%) gallium prices in China increased from $275/kg in December 2020 to $345/kg in October 2021. As of 2022, the market price had increased to around $400/kg as shown in Figure 7 [33]. The recent price increase is a result of significant environmental restrictions placed on China's bauxite producers which required importing bauxite containing lower amounts of gallium. This action significantly reduced gallium supply and COVID issues reduced demand, which led to the closures of many producers. When demand started increasing after the recovery from COVID, there was insufficient supply which elevated market prices [1]. Gallium is expected to trade at 2089.54 CNY/kg ($292.54/kg) by the end of this quarter, according to Trading Economics global macro models and analysts' expectations. Looking forward, it is estimated to trade at 2273.90 CNY/kg ($318.35/kg) within 12 months [34].

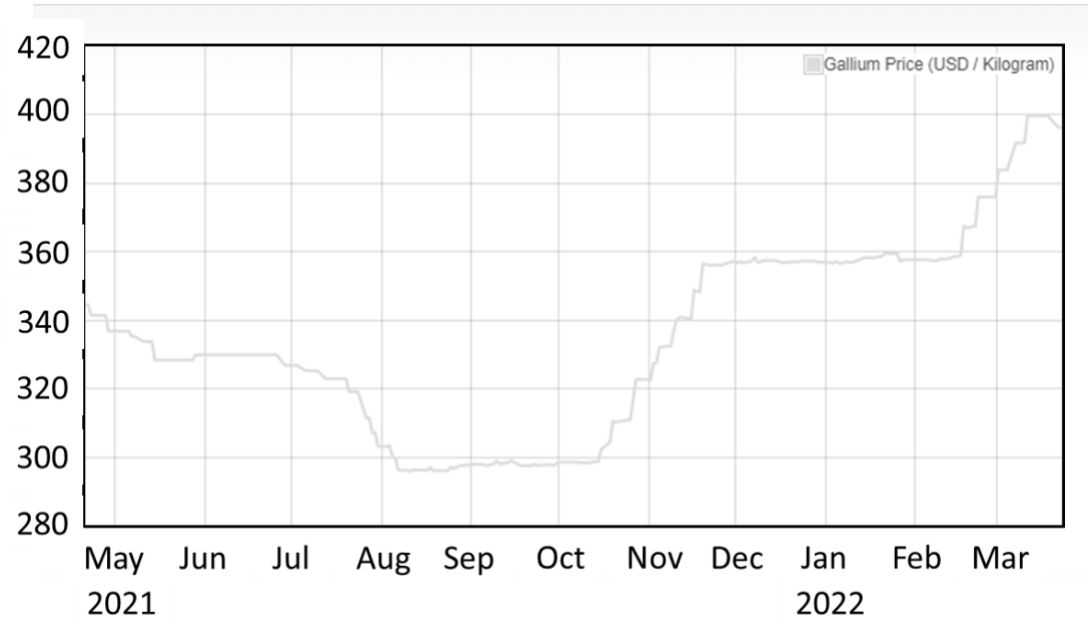


Figure 6. Gallium metal market price variability ($USD) in 2021 and 2022 [33].

The global gallium nitride materials market was valued at $90.0 million in 2019 and is projected to reach a market value of $1,294.5 million by 2031. Development of faster processors and high-frequency radio-frequency devices resulted in a demand increase in wide-bandgap semiconductor material within the electronics industry worldwide [35]. With respect to gallium arsenide (GaAs), a market growth of $2.65 billion occurred during the period 2020 to 2023 due to the rising adoption of smartphones and tablets [36] The GaAs market growth is anticipated to reach a compound annual growth (CAGR) of 6.19% from 2022 – 2027 with Asia-Pacific anticipated to contribute 78% of the growth. Similar to GaN, the primary technologies driving the growth of the GaAs market are noted to electronics related, including mobile devices and wireless communications.

*Nickel* - Nickel is a hard and ductile transition metal. These characteristics are beneficial for its primary use in stainless steel. Nickel is malleable and, for a transition metal, has relatively high electrical and thermal conductivity. Moreover, nickel is slowly oxidized by air at room temperature and is considered corrosion-resistant [37]. Regarding mineralogy, nickel is known to occur naturally in a few mineral types and geologic formations. Lateritic nickel deposits are developed from the weathering of ultramafic rock and the deposits are known for being high grade. Magmatic nickel sulfide deposits are formed from the solidification and crystallization of nickel-rich magma. Nickel sulfide minerals such as pentlandite and pyrrhotite are formed in this process to produce an ore. For nickel deposits exceeding 0.5% in grade, the resource base totals 300 million tons, of which 60% is in laterites and 40% in sulfide deposits [38, 39].

Stainless and alloy steel and nickel-containing alloys typically account for more than 85% of domestic consumption of nickel [40]. As shown in Figure 8, the main application of nickel is alloying with chromium and other metals to form stainless steel and other heat resistant steels. About 9% of world nickel production is still used for corrosion-resistant nickel plating. Other uses include alnico magnets, coinage, rechargeable batteries (e.g., nickel-iron), electric guitar strings,

microphone capsules, plating on plumbing fixtures, and special alloys such as permalloy, elinvar, and invar. Nickel is also used as a green tint in glass.

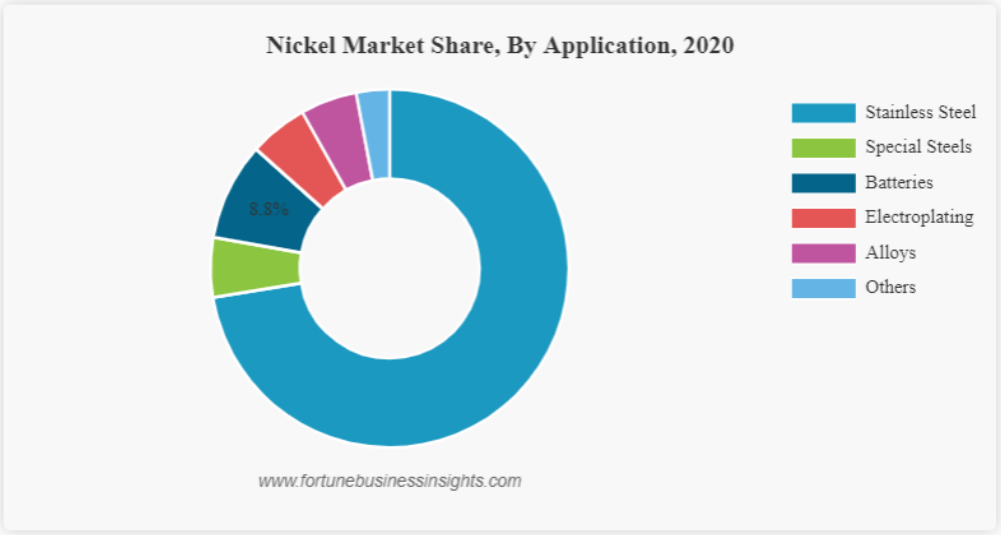


Figure 7. Distribution of nickel market utilization [40].

Increased demand for lithium-ion batteries is expected due to a projected exponential increase in electric vehicle (EV) production [4]. Utilization of nickel in EV batteries cathodes reduces the amount of cobalt needed, which alleviates supply chain concerns associated with the use of cobalt. As an added benefit, Ni also provides higher energy density and, thus, new formulations use a nickel content as high as 80%. For example, nickel cobalt aluminum (NCA) ($LiNi_xCo_yAl_zO_2$) batteries have typically contained 80% Ni and recent efforts have increased the Ni content to the same level in nickel manganese cobalt (NMC) ($LiNi_xMn_yCo_{1-x-y}O_2$) batteries [41]. According to the International Energy Agency (IEA), the share of nickel demand for battery production will increase from 9% in 2020 to around 32% in 2040 [42]. According to a recent Reuters report, Vale expects a 44% increase in nickel by 2030 due to energy transition [43].

In 2021, the worldwide mine production of nickel was 2.7 million tons, of which, approximately one-third was sourced from Indonesia due to the opening of a major production facility (Table 8) [1]. Several other countries are significant producers of Ni, including the Philippines and Russia. The U.S. accounts for a relatively minor level of production and possesses a small amount of Ni reserves. As such, the current level of domestic supply of Ni and the anticipated opening of many battery manufacturing facilities has led the U.S. to include nickel among the list of 50 individual mineral commodities in critical supply as defined in the Federal Register (87 FR 10381). It is noted that Australia, Brazil and Indonesia control the vast majority of nickel reserved worldwide. In 2021, recycled nickel in all forms accounted for approximately 52% of apparent consumption.

Table 9. Worldwide nickel production and reserves in 2021*

| Country | 2021 Production (metric tons) | Reserves (metric tons) |
|---|---|---|
| United States | 18,000 | 340,000 |
| Australia | 160,000 | 21,000,000 |
| Brazil | 100,000 | 16,000,000 |
| Canada | 130,000 | 2,000,000 |
| China | 120,000 | 2,800,000 |
| Indonesia | 1,000,000 | 21,000,000 |
| New Caledonia | 190,000 | N/A |
| Philippines | 370,000 | 4,800,000 |
| Russia | 250,000 | 7,500,000 |
| Other countries | 410,000 | 20,000,000 |
| **Total** | **2,700,000** | **>95,000,000** |

*Source: [1] USGS, 2022.

Market price for nickel was on a gradual rise increasing by 30% in 2021 prior to a spike in market value in February 2022 caused by uncertainties related to the Russian war with Ukraine. As shown in Figure 8, market prices have settled back to around $22,400 per ton. Recently, nickel prices have dropped due to the slowdown in manufacturing worldwide, in particular China and Europe [45]. On 3 May 2023, algorithm-based forecasting service WalletInvestor forecasted a long term increase in nickel price to reach $43,999 per metric tonne by May 2028 [46]. Fitch Solutions reported that the recent decline in market price was a result of oversupply caused by new production coming online. However, demand is expected to increase due to an elevation in stainless production and EV manufacturing. Fitch Solutions anticipates that the market price for nickel will rise to $29,000/metric tonne in 2028 [47]. According to Fortune Business Insights (April 2022), the global nickel market is projected to grow from $36.27 billion in 2021 to $59.14 billion in 2028 at a CAGR of 7.3% in forecast period, 2021-2028 [48].


Figure 8. Recent market price volatility for nickel [44].

*Zinc* - Zinc is the 24th most abundant element, and as a metal, is slightly brittle and shiny-gray in appearance. Zn is chemically similar to magnesium, as it has a similar atomic radius and its chemistry is dominated by the $2^+$ oxidation state. Zn has relatively low melting and boiling points and is used to form many alloys [49,50]. For example, a familiar application of Zn is in brass, which is an alloy with Cu containing 3% to 45% Zn [51]. Moreover, Zn is the fourth most widely consumed base metal and is most used as an anti-corrosive agent and a galvanization coating for iron and steel primarily [52]. Therefore, it finds widespread application in construction, automobiles, and emerging markets, such as clean energy. Moreover, the reactivity of zinc and its ability to oxidize makes it an excellent selection as a sacrificial anode for cathodic protection. Specifically, galvanizing (55%), brass and bronze (16%), and other alloys (21%) make up the major applications of Zn by percentage, while miscellaneous uses account for an additional 8% of Zn use [1]. Other applications of Zn compounds include the use of zinc oxide (ZnO) in paints and as a catalyst for the production of rubber, the use of zinc chloride ($ZnCl_2$) as an addition to lumber as a fire retardant and a wood preservative, and the use of zinc sulfide (ZnS) in luminescent pigments, x-ray and television screens, and in lasers. A niche use of zinc powder is as propellant for model rockets [53].

Regarding energy applications, Zn is also used as an anode material for alkaline batteries. Zn-based batteries are being considered as an alternative to lithium-ion batteries due to their intrinsic safety, comparable energy density, long service life, and competitive cost. Zn-based batteries would be advantageous considering the current concerns over lithium supply and general safety

concerns. Zinc's expanded use in batteries may explain the elements addition to the 2022 Final List of Critical Minerals, as per Federal Register (87 FR 10381).

The worldwide production of zinc mined in 2021 was valued at $2.4 billion with a total production level of 13 million tons [1]. As shown in Table 10, the major producers were China, Peru and Australia, followed by the U.S. and Mexico. Australia and China possess about 45% of the world's total known Zn reserves. Within the U.S., zinc is mined in five U.S. states and processed in one smelter, which is located in Clarksville, Tennessee. A secondary smelter recovering zinc from recycled materials is operating in North Carolina. Additional small-scale non-smelter operations exist which recover a small amount of zinc from recycled materials. Recycled products account for about 25% of the refined zinc produced in the U.S. in 2019 [54]. Around 740,000 tons were produced in the U.S. and 580,000 tons exported in 2021 [1]. Around 700,000 tons of refined Zn was imported in 2021, of which, 64% was from Canada. Nearly 60% of the refined zinc produced in the U.S. in 2021 (220 million tons) was from secondary materials treated in primary and secondary smelters. The secondary materials included galvanizing residues (galvanizing ashes, top-dross and bottom-dross {hard zinc}) as well as other zinc-containing materials and crude zinc oxide recovered from electric arc dust [1].

Table 10. 2021 Worldwide zinc production and reserves*

| **Country** | **2021 Production (metric tons)** | **Reserves (metric tons)** |
|---|---|---|
| United States | 740,000 | 9,000,000 |
| Australia | 1,300,000 | 69,000,000 |
| Bolivia | 490,000 | 4,800,000 |
| Canada | 260,000 | 5,400,000 |
| China | 4,200,000 | 44,000,000 |
| India | 810,000 | 9,100,000 |
| Kazakhstan | 220,000 | 12,000,000 |
| Mexico | 720,000 | 19,000,000 |
| Peru | 1,600,000 | 19,000,000 |
| Russia | 280,000 | 22,000,000 |
| Sweden | 230,000 | 3,700,000 |
| Other countries | 2,000,000 | 34,000,000 |
| **Total** | **13,000,000** | **250,000,000** |

*Source: [1] USGS, 2022.

According to Home [55], both supply and demand of zinc were down in 2022. Specifically, a 3% drop in global Zn use and a 2.6% decrease in global production of Zn were noted. The market price of Zn in September 2022 was $3,080 per tonne, which was down from a record high of $4,896 per

metric tonne in March 2022. The downward turn is largely due to a construction decline in China resulting in a drop in the demand for galvanized steel. Sharp electricity price increases in Europe have resulted in the closure of zinc smelters, which accounts for the drop in zinc production [56]. Recession fears in Europe and the U.S. is expected to cause an additional decline in demand. Notably, a Zn metal supply surplus of 27,000 tonnes occurred during the first six months of 2022 which was contrary to expectations for a supply deficit of 290,000 tonnes. This outcome resulted in a sharp drop in Zn market value in April 2022, as shown in Figure 9. Recent market *value* variations in zinc market value [57].Additional threats to the Zn market value are potential substitutes which include: Aluminum and plastics for galvanized steel in automobiles; cadmium paint and plastic coatings to replace zinc coatings; aluminum and magnesium-based alloys are replacements for zinc-based diecasting alloys [1].

With regard to battery use, it has been estimated that the market share of zinc-ion batteries will climb from 1% in 2021 to 5% in 2025, and 20% in 2030 [58]. Statista projects an increase in global zinc demand from 16,053,000 metric tonnes in 2021 to 19,662,000 metric tonnes in 2028, which is a 22% expansion in demand [59]. The increase is attributed to an elevated amount used in the manufacturing of renewable energy technologies and conventional uses. Based on a report by Wood Mackenzie, large-scale solar power plants require zinc coatings to provide low cost protection that will extend the useful life to a total of 30 years [60]. Using projections for the required increased in solar energy needed to meet climate change goals, it was estimated that zinc demand would increase by 0.8 million tonnes annually in 2040 under a based case and may be elevated by as much as 2.1 million tonnes under scenarios involving expanded solar use. This represents in an increase in zinc metal demand ranging from 5% to 13% over 2021 production levels based on solar energy expansion alone.


Figure 9. Recent market value variations in zinc market value [57].

*Germanium* - Germanium (Ge) is an elemental semiconductor that is used in transistors and other various electronic devices. In consideration of these factors, Ge is considered a technology-critical

element that is expected to experience increased future demand. Properties of the element that contributes to its valued uses are a high refraction index and low optical dispersion [61]. Germanium has properties between a metal and non-metal and, as such, is referred to as a metalloid [62] and has a crystal structure similar to diamond (carbon) [63]. Germanium also has chemical and physical properties like its lighter congener, silicon, which can be a less-expensive substitute in certain electronic applications. An alloy of germanium and silicon has become important to produce semiconductor material in high-speed integrated circuits. The addition of germanium provides significantly faster computer processing speeds than silicon metal only [64].

Germanium finds use in many high-tech applications such as electronics and solar, fiber-optic systems, night vision technologies, infrared (IR) optics, polymerization catalysts, and chemotherapy, metallurgy, and phosphors, amongst others [61]. The manufacturing of material for fiber optic communication networks, infrared night vision systems, and polymerization catalysts represent 85% of the current germanium demand [65]. Germanium tetrachloride ($GeCl_4$) is a colorless liquid that is used in the production of fiber-optic cable. Germanium dioxide ($GeO_2$) is a white powder used in the manufacturing of optical lenses and as a catalyst for plastic polyethylene terephthalate (PET) resin [61].

The available resources of germanium worldwide are relatively small. Worldwide Ge production in 2021 was around 140,000 kilograms or 140 metric tons, of which most was supplied by China [1] (Table 11). It is noted that Ge is typically associated with certain zinc and lead-zinc-copper sulfide ores. The USGS also estimated that the U.S. reserves of Ge are approximately 2500 tons at a grade as high as 0.3% and are contained within zinc ores.

Table 11. Worldwide germanium production in 2021*

| **Country** | **2021 Production (kg)** |
|---|---|
| China | 95,000 |
| Russia | 5,000 |
| Other countries | 40,000 |
| **Total** | **140,000** |

*Source: [1] USGS, 2022.

Prices for germanium dioxide ($GeO_2$) and germanium metal trended upward through 2021 and 2022 after a significant price decline since 2014, as shown in Figure 10 [66]. The price for germanium metal (minimum 99.999% purity – 5N) increased by 21% to $1,315 per kg from $1,090 per kg, and the price for germanium dioxide (minimum 99.999% purity) increased by 15% to $825 per kg from $720 per kg. The overall value is more than silver due to the expense of producing 5N purity material.

Proficient Market Insights reported that the current global market value for germanium is $274.5 million and the value will move downward by 2028 to $263.7 million by 2028, which yields a CAGR of -0.6% [67]. Market Watch, who is a market investment support company, compiles data

from multiple sources. Based on the data compilation and analysis, the global germanium market size was $248.5 million in 2022 and expected to expand to $272.4 million by 2028 with a CAGR of 1.54% [68]. The discrepancy between the two reports may be due to the uncertainty surrounding the germanium demand increase resulting from solar panel production. Gallium arsenide germanium solar cells (Gaas) are preferred over other solar cell types due to a number of factors including enhanced compatibility, scalability and functionality with the the internet of things (IoT) [69]. The global market for Gaas is projected to reach $27.7 billion by 2030 from a value of $14.5 billion in 2022, which equates to a CAGR of 8.40% [69]. Market Watch recently estimated that the germanium substrate market for solar cells will realize an annual growth rate of 13.3% [70].

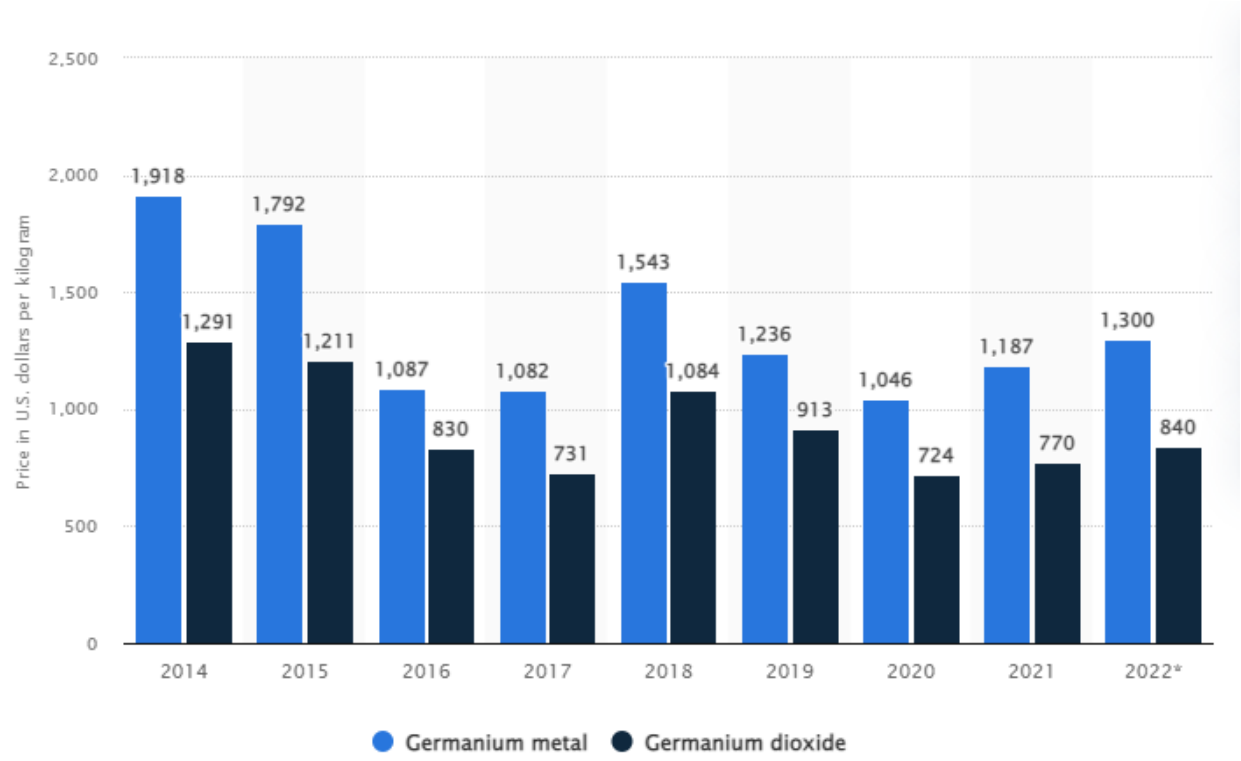


Figure 10. Market value trend for germanium from 2014 through 2022 [66].

### *2.2.3 Section References:*


[1] Mineral Commodity Report, U.S. Geological Survey.

[2] Enghag, Per (2004). "Cobalt". Encyclopedia of the elements: technical data, history, processing, applications. p. 667. ISBN 978-3-527-30666-4.

[3] The Role of Critical Minerals in Clean Energy Transition, International Energy Agency, page 6.

[4] Electric Car Forecast to 2040, Wood Mackenzie, https://www.woodmac.com/our-expertise1/capabilities/electric-vehicles/2040-forecast/.

[5] Trade Economics, 2023; https://tradingeconomics.com/commodity/cobalt.

[6] Corathers, L. A.; Machamer, J. F. (2006). "Manganese". *Industrial Minerals & Rocks: Commodities, Markets, and Uses* (7th ed.). SME. pp. 631–636. ISBN 978-0-87335-233-8.

[7] Zhang, Wensheng; Cheng, Chu Yong (2007). "Manganese metallurgy review. Part I: Leaching of ores/secondary materials and recovery of electrolytic/chemical manganese dioxide". *Hydrometallurgy*. **89** (3–4): 137–159. doi:10.1016/j.hydromet.2007.08.010

[8] The World Counts, 2023. https://www.theworldcounts.com/challenges/consumption/foods-and-beverages/aluminium-cans-facts.

[9] Manganese—It Turns Iron Into Steel (and Does So Much More), 2014. U.S. Geological Survey, Fact Sheet 2014–3087.

[10] Manganese – the third electric vehicle metal no one is talking about, 2017. Mining.com, https://www.mining.com/web/manganese-the-third-electric-vehicle-metal-no-one-is-talking-about-it-heres-how-to-take-advantage/#:~:text=A%20typical%20LMD%20battery%20uses,mix%20and%20only%204%25%20lithium.

[11] Blome, F., 2021. "EV Batteries: Challenges for the Mass Market," StorageX International Symposium, Stanford University, June 4, 2021. https://www.youtube.com/watch?v=dQZJzwUKGq0

[12] Creamer, M., 2022. "High-purity manganese facing phenomenal demand growth, PDAC hears," Mining Weekly. https://m.miningweekly.com/article/high-purity-manganese-facing-phenomenal-growth-pdac-hears-2022-06-24.

[13] Trade Economics, 2023. https://tradingeconomics.com/commodity/manganese

[14] Manganese Alloy Market Size, Share & Industry Analysis, 2020. Fortune Business Insights. https://www.fortunebusinessinsights.com/industry-reports/manganese-alloy-market-101569

[15] Manganese Market Size & Share Analysis - Growth Trends & Forecasts (2023 - 2028), 2021. Mordor Intelligence, https://www.mordorintelligence.com/industry-reports/manganese-market

[16] Manganese flake declines on steel cuts, ore prices, 2019. Argus, https://www.argusmedia.com/en/news/2034202-manganese-flake-declines-on-steel-cuts-ore-prices

[17] Evarts, E.C., 2015. "Lithium Batteries: to the limits of lithium," Nature, 526, pp. S93-S95.

[18] Lithium costs up in 2021, continuing to surge in 2022, 2022. S&P Global, https://www.spglobal.com/marketintelligence/en/news-insights/research/lithium-costs-up-in-2021-continuing-to-surge-in-2022.

[19] The global lithium market is projected to grow from USD 3.83 billion in 2021 to USD 6.62 billion in 2028 at a CAGR of 8.1% during 2021-2028, Fortune Business Insights, Report Number FBI104052. https://www.fortunebusinessinsights.com/lithium-market-104052

[20] Trade Economics, 2023. https://tradingeconomics.com/commodity/lithium

[21] Piedmont Lithium Signs Sales Agreement with Tesla, 2020. https://www.sec.gov/Archives/edgar/data/1728205/000172820520000031/ex99_1.htm

[22] Li, Z., Yi, Y., Wang, H., Yu, Z., Wu, C., Dou, H., Li, O., Sun, K., Jiang, X., and Lan, Z., 2023. "The effects of Barium Strontium Titanate (BST) on the soft magnetic properties and loss performance of MnZn ferrites," Ceramics International, Volume 49, Issue 12, pp. 19631-1964

[23] Global Strontium Market Size By Product (Strontium Carbonate, Strontium Sulfate, Strontium Nitrate), By Application (Electrical And Electronics, Pyrotechnic, Medical And Dental, Personal Care), By Geographic Scope And Forecast, 2020. Verified Market Research. https://www.verifiedmarketresearch.com/product/strontium-market/

[24] 2022 Final List of Critical Minerals, 2022. U.S. Geological Survey. https://www.federalregister.gov/d/2022-04027

[25] Zhang, Y., Evans, J.R.G., and Zhang, S., 2011. "Corrected Values for Boiling Points and Enthalpies of Vaporization of Elements in Handbooks". J. Chem. Eng. Data. 56 (2): 328–337. doi:10.1021/je1011086

[26] Greber, J. F., 2012. "Gallium and Gallium Compounds" in Ullmann's Encyclopedia of Industrial Chemistry, Wiley-VCH, Weinheim, doi:10.1002/14356007.a12_16

[27] Moskalyk, R. R., 2003. "Gallium: the backbone of the electronics industry". Minerals Engineering. 16 (10): 921–929. Bibcode:2003MiEng..16..921M. doi:10.1016/j.mineng.2003.08.003

[28] Lovati, S., 2021. "10 Things to know about GaN," Power Electronics News, https://www.powerelectronicsnews.com/10-things-to-know-about-gan/#:~:text=Gallium%20nitride%20has%20an%20electron,30%25%20faster%20than%20in%20Silicon

[29] Gallium Nitride: The Fundamental Building Block for Power Electronics, GaN Systems, https://gansystems.com/gallium-nitride-semiconductor/#:~:text=Since%20the%201990s%2C%20it%20has,see%20GaN%20in%20sensor%20technology

[30] Coleman, J.J., Jagadish, C., and Catrina, B.A., 2012. Advances in Semiconductor Lasers. pp. 150–151. ISBN 978-0-12-391066-0

[31] Frenzel, M., Ketris, M.P., Seifert, T., and Gutzmer, J., 2016. “On the current and future availability of gallium,” Resources Policy. 47, pp. 38–50

[32] Frenzel, M., Hirsch, T,, and Gutzmer, J., 2016. "Gallium, germanium, indium, and other trace and minor elements in sphalerite as a function of deposit type — A meta-analysis". Ore Geology Reviews. 76, pp. 52–78

[33] Metal Spot Price Charts, 2022. Daily Metal Prices, https://www.dailymetalprice.com/metalpricecharts.php?c=ga&u=kg&d=240

[34] Trading Economics, 2022. https://tradingeconomics.com/commodity/gallium

[35] Global Gallium Nitride Materials market is projected to reach a market value of US$ 1,294.5 Million by 2031: Visiongain Research Inc, 2022. GlobeNewswire, https://www.globenewswire.com/en/news-release/2022/02/09/2382088/0/en/Global-Gallium-Nitride-Materials-market-is-projected-to-reach-a-market-value-of-US-1-294-5-Million-by-2031-Visiongain-Research-Inc.html

[36] Gallium Arsenide Components Market by Type, Application and Geography - Forecast and Analysis 2023-2027, 2022. Technavio, pages 162. https://www.technavio.com/report/gallium-arsenide-components-market-size-industry-analysis

[37] Hammond, C.R.,.and Lide, C. R., 2018. "The elements". In Rumble, John R. (ed.). CRC Handbook of Chemistry and Physics (99th ed.). Boca Raton, FL: CRC Press. p. 4.22. ISBN 9781138561632

[38] Nickel (Ni) Ore, 2018. Geology Science. https://geologyscience.com/ore-minerals/nickel-ore

[39] Nickel reserves worldwide by country, 2020. Statista, https://www.statista.com/statistics/273634/nickel-reserves-worldwide-by-country/

[40] Nickel Market Size, Share & COVID Impact Analysis, 2022. Fortune Business Insights, Report ID: FBI106576. https://www.fortunebusinessinsights.com/nickel-market-106576

[41] Nickel in batteries, Nickel Institute. https://nickelinstitute.org/en/about-nickel-and-its-applications/nickel-in-batteries/ [42] The Role of Critical Minerals in Clean Energy Transition, International Energy Agency, page 7.

[42] The Role of Critical Minerals in Clean Energy Transition, International Energy Agency, page 7.

[43] Vale sees 44% increase in global nickel demand by 2030, 2022. Reuters, September 7. https://www.reuters.com/markets/commodities/vale-sees-44-increase-global-nickel-demand-by-2030-2022-09-07/

[44] Nickel, 2023. Trade Economics. https://tradingeconomics.com/commodity/nickel

[45] Wulandari, F., 2022. “Nickel price forecast: Will the metal continue to rise after 2022?,” Capitol.com. https://capital.com/nickel-price-forecast

[46] Nickel Forecast, Nickel Price Prediction, 2023. Wallet Investor. https://walletinvestor.com/commodity-forecast/nickel-prediction#:~:text=Nickel%20price%20(per%20metric%20ton,to%20be%20around%20%2B109.08%25.

[47] Parker, T. 2023. “Nickel could average $US32,000/t in years to come,” Australian Resources & Investment, April 6. https://www.australianresourcesandinvestment.com.au/2023/04/06/nickel-could-average-us32000-in-years-to-come/#:~:text=The%20EV%20industry%20will%20be,%2C000%2Ft%20by%202024.

[48] “With 7.3% CAGR, Nickel Market to Reach USD 59.14 Billion by 2028,” 2023. Fortune Business Insights, April 17. https://www.globenewswire.com/news-release/2023/04/17/2647795/0/en/With-7-3-CAGR-Nickel-Market-to-Reach-USD-59-14-Billion-by-2028-Fortune-Business-Insights.html#:~:text=filingsmedia%20partners-,With%207.3%25%20CAGR%2C%20Nickel%20Market%20to%20Reach%20USD%2059.14%20Billion,2028%20%7C%20Fortune%20Business%20Insights%E2%84%A2

[49] Heiserman, David L., 1992. "Element 30: Zinc". Exploring Chemical Elements and their Compounds. New York: TAB Books. ISBN 978-0-8306-3018-9.

[50] Lide, D.R., 2006. Handbook of Chemistry and Physics (87th ed.). Boca Raton, Florida: CRC Press, Taylor & Francis Group. ISBN 978-0-8493-0487-3.

[51] Ingalls, Walter Renton (1902). "Production and Properties of Zinc: A Treatise on the Occurrence and Distribution of Zinc Ore, the Commercial and Technical Conditions Affecting the Production of the Spelter, Its Chemical and Physical Properties and Uses in the Arts, Together with a Historical and Statistical Review of the Industry". The Engineering and Mining Journal: 142–6.

[52] Kropschot, S.J. and Doebrich, J.L., 2011. “Zinc—The Key to Preventing Corrosion,” U.S. Geological Survey, Fact Sheet 2011-3016.

[53] ‘Zinc’, 2023. Encyclopedia Britannica. https://www.britannica.com/science/zinc

[54] Tolcin, A. C., 2020. "Zinc". Mineral commodity summaries 2020. Reston, Virginia: U.S. Geological Survey. pp. 190–191. ISBN 978-1-4113-4362-7

[55] Home, A., 2022. “Column: Zinc caught between weakening demand and sliding supply,” Reuters, September 2022. https://www.reuters.com/markets/commodities/zinc-caught-between-weakening-demand-sliding-supply-2022-09-16/

[56] "METALS-Zinc hits 14-year high as Nyrstar cuts output due to power prices," 2021. Reuters, Staff article, October 14. https://www.reuters.com/article/global-metals/metals-zinc-hits-14-year-high-as-nyrstar-cuts-output-due-to-power-prices-idUSL4N2RA11E

[57] "Zinc", 2023. Trading Economics. https://tradingeconomics.com/commodity/zinc

[58] Li, J., 2022. "Zinc Mining & Market Outlook 2022-2025," The Assay. https://www.theassay.com/articles/the-assay-insights/zinc-market-analysis/

[59] "Zinc consumption forecast worldwide from 2021 to 2028," 2023. Statista. https://www.statista.com/statistics/1093625/global-zinc-consumption/

[60] "Solar energy to boost demand for base metals," 2021. Wood Mackenzie, August 9. https://www.woodmac.com/press-releases/solar-energy-to-boost-demand-for-base-metals/

[61] Shanks, W.C.P., Kimball, B.E., Tolcin, A.C., and Guberman, D.E., 2017. "Germanium and Indium," in Critical Mineral Resources of the United States—Economic and Environmental Geology and Prospects for Future Supply (eds.: K.J. Schulz, J.H. DeYoung, R.R. Seal, and D. C. Bradley), U.S. Geological Survey, Professional Paper 1802. https://doi.org/10.3133/pp1802

[62] Nelson. D. 2020. "4 Properties of Metalloids," Science Trends, March 3. https://sciencetrends.com/4-properties-of-metalloids/

[63] "Silicon & Germanium Crystal Structure," 2018. PhysicsOpenLab, January 28. https://physicsopenlab.org/2018/01/28/silicon-germanium-crystal-structure/

[64] Washio, K., 2003. "SiGe HBT and BiCMOS technologies for optical transmission and wireless communication systems". IEEE Transactions on Electron Devices. 50 (3), pp. 656–668.

[65] "Germanium Statistics and Information," 2023. U.S. Geological Survey, National Minerals Information Center. https://www.usgs.gov/centers/national-minerals-information-center/germanium-statistics-and-information

[66] "Price of germanium in the United States from 2014 to 2022, by type," 2023. Statista. https://www.statista.com/statistics/1061511/us-germanium-price/

[67] "Germanium Market 2023 readjusted size of USD 263.7 million by 2028 with CAGR of -0.6%: Industry Trends and Investigation Growth Rate, consumption by Regional data, Key Companies a Showing Impressive Growth," 2023. Proficient Market Insights, January 10. https://www.globenewswire.com/en/news-release/2023/01/10/2585892/0/en/Germanium-Market-2023-readjusted-size-of-USD-263-7-million-by-2028-with-CAGR-of-0-6-Industry-Trends-and-Investigation-Growth-Rate-consumption-by-Regional-data-Key-Companies-a-Showi.html

[68] "Global Germanium Market from 2023-2030 | Research Report," 2023. MarketWatch, April 20. https://www.marketwatch.com/press-release/global-germanium-market-from-2023-2030-research-report-2023-04-20

[69] "Global Gallium Arsenide Germanium Solar Cell (Gaas) Market – Industry Trends and Forecast to 2030," 2023. Data Bridge Market Research, January 2023. https://www.databridgemarketresearch.com/reports/global-gallium-arsenide-germanium-solar-cell-gaas-market

[70] "This report presents a detailed analysis of the global Germanium Substrate for Solar Cells market including market size of 13.3% CAGR valuation and growth throughout 2023 to 2030," 2013. MarketWatch, May 27, 2023. https://www.marketwatch.com/press-release/this-report-presents-a-detailed-analysis-of-the-global-germanium-substrate-for-solar-cells-market-including-market-size-of-133-cagr-valuation-and-growth-throughout-2023-to-2030-2023-05-27

## 2.3 Task 3.0 – Resource Identification, Characterization and Assessment

### *2.3.1 Subtask 3.1 – Resource Identification and Characterization*

Two sites are proposed for official consideration with regard to project deliverables, being Site 1 comprising materials from West Kentucky No. 13 (Baker) Seam, and Site 2 comprised of materials from a lignite source.

*Site 1* - Preliminary investigations identified multiple potential sources of rare earth elements (REEs) in Webster County and Hopkins County, Kentucky. The potential sources of REEs are coarse coal refuse disposal facilities owned and/or operated by Alliance Coal, LLC or a subsidiary mining company. Please see section 2.1 for further details and information.

*Site 2* - This lignite resource is located at an undisclosed sand production site in the continental USA. The resource is a rare earth and critical minerals source as evidenced by the Highly Probable Mineral Resource Estimate ("MRE") for the site. The resource is currently a byproduct of sand production for the construction industry.

The MRE for the site comprises a total mineral resource of 94.2 Mt containing a probable ore content of 1.0% - 5.3% with REEs and critical minerals (CM) containing up to 37.7 Kt CM. A high value CM assemblage exists consisting of 62.4% manganese, 14.5% REEs, 9.5% nickel, 3.7% cobalt, 3.5% zinc, 3.3% strontium, 1.9% vanadium, 0.6% lithium, 0.5% germanium 0.2% gallium and 0.04% silver. The REE mineralization has an excellent ratio of heavy and light rare earths. Mineralization occurs in a single, large, surface down, shallow, coherent at-surface mineral deposit.

The combination of grade, high value CM assemblage, low-cost jurisdiction, and existing infrastructure supports the potential to expand a world class CM business in the USA. The resource is amenable to low-cost and low impact unconsolidated material extraction techniques (e.g., open pit or long reach excavator mining), which actively mine the land as the operation progresses. It is strategically located with low-cost road, rail, and water logistics connecting it to world class manufacturing industries and customers.

*2.3.1.1 Site 1 West Kentucky No. 13 seam*

*Estimation Summary* - A preliminary estimation has been conducted for rare earth elements (REEs) in the West Kentucky No. 13 seam (WKY13) as shown in

Table 12. The estimates are not intended to meet assessment requirements as defined by the Securities and Exchange Commission's S-K 1300 rule. This estimation includes the existing refuse disposal facilities and unmined coal and parting. The refuse facilities are located on areas permitted by Alliance Coal's subsidiary companies.

Table 12. REE Summary of West Kentucky No. 13 sources.

| | In-Place Tons | In-Place Metric Tons | Total REE (ppm) | In Place Total REE Metric Tons |
|---|---|---|---|---|
| Wky No. 13-Coal | 302,251,341 | 274,197,792 | 58.84 | 15,553 |
| Wky No. 13-Parting | 80,795,385 | 73,296,337 | 333.95 | 23,800 |
| Coarse Refuse | 18,798,535 | 17,053,744 | 290.15 | 4,948 |
| Fine Refuse | 3,565,000 | 3,234,113 | 219.54 | 710 |
| **TOTAL REE** | **405,410,262** | **367,781,986** | | **45,011** |

*Estimation of Unmined Areas* - The area was modeled using Carlson Software's SurvCADD program. Output from the model includes coal and parting tons separated into controlled and uncontrolled categories. Controlled tonnages are located on properties for which Alliance Coal either owns or has existing mining rights to the property. Uncontrolled tonnages are located on properties where mining rights have not yet been obtained.

The in-place density used in the model is then converted to a dry density utilizing moisture data taken from limited corehole samples in the area. These same corehole averages are the basis from which the REE concentrations are calculated and applied to the in-place coal seam. These calculations are shown in Refuse Storage Estimation – Along with the unmined WKY13, REEs have been identified within refuse disposal sites where waste from processing of the WKY13 is stored. These waste disposal sites are in the form of either an above ground coarse only pile or an in-ground pit containing fine refuse. Location of the refuse disposal sites are shown in Figure 11.

The two above ground storage piles are identified as the Tucker Pile and the Smith Pile. Both piles are on areas currently permitted and controlled by Alliance Coal.

The presence of REEs in the coarse refuse material was determined by conducting a drilling program at each site. Boreholes were advanced through each pile and samples were collected every five (5) feet. These samples were analyzed, and the resulting assay data was used to complete geologic models for each site.

While the Tucker Pile is comprised of only WKY13 refuse, the Smith Pile was originally constructed with West Kentucky No. 9 seam refuse, then completed with WKY13 refuse. The estimate considers only the WKY13 refuse (See Table 14).

*Refuse Storage Estimation* – Along with the unmined WKY13, REEs have been identified within refuse disposal sites where waste from processing of the WKY13 is stored. These waste disposal

sites are in the form of either an above ground coarse only pile or an in-ground pit containing fine refuse. Location of the refuse disposal sites are shown in Figure 11.

The two above ground storage piles are identified as the Tucker Pile and the Smith Pile. Both piles are on areas currently permitted and controlled by Alliance Coal.

The presence of REEs in the coarse refuse material was determined by conducting a drilling program at each site. Boreholes were advanced through each pile and samples were collected every five (5) feet. These samples were analyzed, and the resulting assay data was used to complete geologic models for each site.

While the Tucker Pile is comprised of only WKY13 refuse, the Smith Pile was originally constructed with West Kentucky No. 9 seam refuse, then completed with WKY13 refuse. The estimate considers only the WKY13 refuse (See Table 14).

Table 13. In-Place Coal & Parting Summary (REE Concentration).

| | REE Concentration (ppm) | | Parting (kg) | | Coal (kg) | |
|---|---|---|---|---|---|---|
| | Parting | Coal | Controlled | Uncontrolled | Controlled | Uncontrolled |
| CERIUM (Ce) | 123.46 | 14.43 | 6,448,502 | 2,350,444 | 2,914,354 | 898,562 |
| DYSPROSIUM (Dy) | 6.01 | 1.14 | 313,968 | 114,440 | 230,015 | 70,919 |
| ERBIUM (Er) | 4.21 | 0.81 | 219,824 | 80,125 | 163,314 | 50,353 |
| EUROPIUM (Eu) | 1.82 | 0.42 | 95,309 | 34,740 | 85,784 | 26,449 |
| GADOLINIUM (Gd) | 10.34 | 2.50 | 539,810 | 196,758 | 504,955 | 155,689 |
| HOLMIUM (Ho) | 1.60 | 0.22 | 83,586 | 30,467 | 44,751 | 13,798 |
| LANTHANUM (La) | 53.08 | 6.50 | 2,772,436 | 1,010,538 | 1,312,959 | 404,815 |
| LUTETIUM (Lu) | 0.87 | 0.59 | 45,630 | 16,632 | 120,066 | 37,019 |
| NEODYMIUM (Nd) | 50.62 | 7.10 | 2,643,675 | 963,605 | 1,434,612 | 442,324 |
| PRASEODYMIUM (Pr) | 17.47 | 5.70 | 912,533 | 332,613 | 1,151,560 | 355,052 |
| SAMARIUM (Sm) | 13.81 | 3.62 | 721,483 | 262,976 | 731,900 | 225,662 |
| SCANDIUM (Sc) | 16.11 | 5.28 | 841,430 | 306,696 | 1,067,028 | 328,989 |
| TERBIUM (Tb) | 0.76 | 0.49 | 39,808 | 14,510 | 99,298 | 30,616 |
| THULIUM (Tm) | 0.95 | 0.17 | 49,648 | 18,096 | 33,441 | 10,311 |
| YTTERBIUM (Yb) | 3.16 | 1.17 | 165,223 | 60,223 | 235,863 | 72,722 |
| YTTRIUM (Y) | 29.66 | 8.70 | 1,549,385 | 564,742 | 1,757,936 | 542,012 |
| **TOTAL REE** | **333.95** | **58.84** | **17,442,249** | **6,357,604** | **11,887,840** | **3,665,292** |

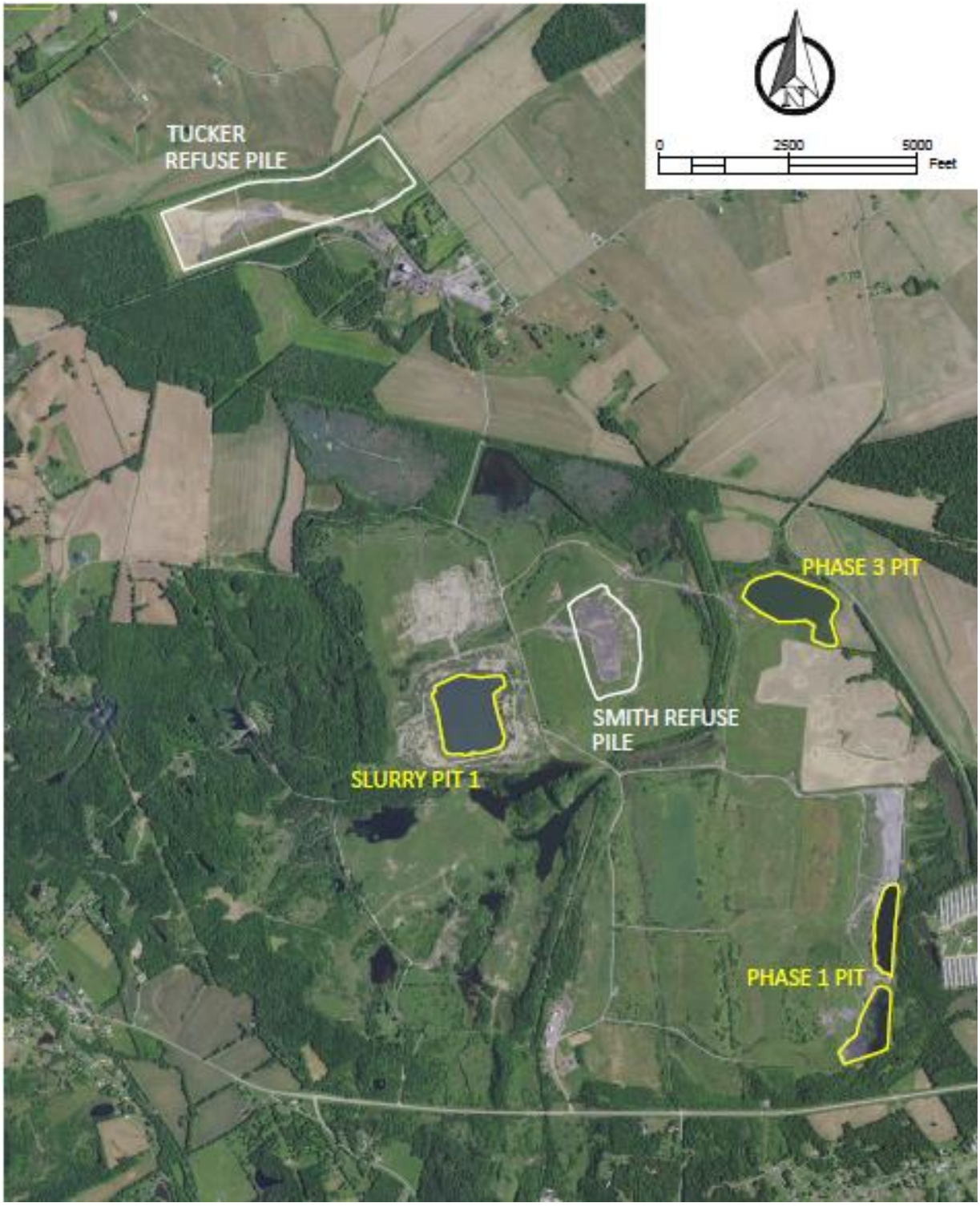


Figure 11. Map showing the location of the coarse and fine WKY13 sources.

Table 14. Coarse Refuse Summary (REE Concentration).

| | Smith (ppm) | Smith (kg) | Tucker (ppm) | Tucker (kg) | TOTAL (kg) |
|---|---|---|---|---|---|
| CERIUM (Ce) | 101.02 | 56,757 | 104.22 | 1,718,844 | 1,775,601 |
| DYSPROSIUM (Dy) | 2.80 | 1,573 | 4.42 | 72,957 | 74,530 |
| ERBIUM (Er) | 3.03 | 1,702 | 1.96 | 32,396 | 34,098 |
| EUROPIUM (Eu) | 1.93 | 1,084 | 1.95 | 32,093 | 33,177 |
| GADOLINIUM (Gd) | 10.21 | 5,736 | 9.30 | 153,334 | 159,071 |
| HOLMIUM (Ho) | 0.60 | 336 | 0.80 | 13,250 | 13,585 |
| LANTHANUM (La) | 46.21 | 25,960 | 48.42 | 798,595 | 824,555 |
| LUTETIUM (Lu) | 1.30 | 732 | 1.22 | 20,191 | 20,923 |
| NEODYMIUM (Nd) | 43.11 | 24,220 | 46.17 | 761,466 | 785,686 |
| PRASEODYMIUM (Pr) | 13.04 | 7,325 | 12.60 | 207,799 | 215,124 |
| SAMARIUM (Sm) | 10.66 | 5,989 | 11.33 | 186,854 | 192,843 |
| SCANDIUM (Sc) | 19.91 | 11,188 | 17.99 | 296,622 | 307,810 |
| TERBIUM (Tb) | 1.24 | 695 | 0.73 | 11,964 | 12,659 |
| THULIUM (Tm) | 0.63 | 353 | 0.58 | 9,530 | 9,883 |
| YTTERBIUM (Yb) | 3.99 | 2,241 | 3.88 | 63,987 | 66,229 |
| YTTRIUM (Y) | 26.05 | 14,635 | 24.72 | 407,666 | 422,301 |
| **TOTAL REE** | **285.73** | **160,526** | **290.30** | **4,787,549** | **4,948,075** |

In addition to the coarse refuse facilities, there are three (3) fine refuse disposal sites located on the Smith property and the resource is quantified in

Table 15. These sites consist of two (2) incised pits and one (1) combination pit (embankment and incised). Refuse was disposed of within these sites by pumping the fine refuse material from the static thickener at the Dotiki preparation plant to the pits.

The quantity of fine refuse material in each pit is calculated by using the preparation plant throughput. Generally, 20% of the plant reject is considered fine refuse and would be pumped from the static thickener. A review of disposal records identified the timeframe for which material was pumped into each fine refuse site. Applying the fine refuse reject factor of 20% to the total waste stream, the tons of fine refuse placed into each site can be calculated for the given timeframe. The REE concentration within the fine refuse was calculated using laboratory data supplied by the University of Kentucky.

Table 15. Fine Refuse Summary (REE Concentration).

| | Fines (ppm) | [1]P1 (kg) | [2]P3 (kg) | [3]SP1 (kg) | TOTAL (kg) |
|---|---|---|---|---|---|
| CERIUM (Ce) | 74.93 | 80,215 | 26,172 | 135,958 | 242,346 |
| DYSPROSIUM (Dy) | 4.68 | 5,005 | 1,633 | 8,482 | 15,120 |
| ERBIUM (Er) | 2.70 | 2,892 | 944 | 4,902 | 8,738 |
| EUROPIUM (Eu) | 1.34 | 1,438 | 469 | 2,437 | 4,344 |
| GADOLINIUM (Gd) | 5.50 | 5,889 | 1,921 | 9,981 | 17,791 |
| HOLMIUM (Ho) | 0.92 | 990 | 323 | 1,678 | 2,991 |
| LANTHANUM (La) | 37.24 | 39,865 | 13,007 | 67,567 | 120,438 |
| LUTETIUM (Lu) | 0.39 | 415 | 135 | 704 | 1,254 |
| NEODYMIUM (Nd) | 33.67 | 36,042 | 11,760 | 61,089 | 108,890 |
| PRASEODYMIUM (Pr) | 8.99 | 9,625 | 3,140 | 16,314 | 29,079 |
| SAMARIUM (Sm) | 6.46 | 6,917 | 2,257 | 11,723 | 20,897 |
| SCANDIUM (Sc) | 15.80 | 16,917 | 5,520 | 28,673 | 51,110 |
| TERBIUM (Tb) | 0.82 | 881 | 287 | 1,492 | 2,660 |
| THULIUM (Tm) | 0.40 | 424 | 138 | 719 | 1,281 |
| YTTERBIUM (Yb) | 2.57 | 2,749 | 897 | 4,659 | 8,306 |
| YTTRIUM (Y) | 23.12 | 24,749 | 8,075 | 41,948 | 74,772 |
| **TOTAL REE** | **219.54** | **235,013** | **76,678** | **398,327** | **710,018** |

*[1] Phase 1 Pit*
*[2] Phase 3 Pit*
*[3] Slurry Pit 1*

### *2.3.1.2 Site 2 Lignite Source*

The MRE represents the first probable mineral resource reported within the site and confirms the region as an untapped critical mineral (CM) area. See Table 16 for the resource summary. The MRE is based on 12 drill holes totaling 830 feet. The MRE is supported by 50 real time production samples. The MRE is planning more drill holes to prove both the local and regional resource (see Figure 12 for drill hole information). The MRE is expected to sustain growth due to accelerated land consolidation. The site's CM business builds a platform to become the leader in the U.S. CM supply chains.

Table 16. Lignite total critical mineral resource.

| | | | | | THM assemblage | | | | |
|---|---|---|---|---|---|---|---|---|---|
| **Site Project** | **Cut off** | **Tons** | **Ore %** | **TCM** | **Mn** | **REE** | **Ni/Co** | **Zn** | **Other** |
| | *(CM %)* | *(Mt)* | *(%)* | *(Kt)* | *(%)* | *(%)* | *(%)* | *(%)* | *(%)* |
| **Total Mineral Resource** | **N/A** | **94.2** | **0.63-5.3** | **~37.7** | **62.4** | **14.5** | **13.2** | **3.5** | **6.4** |

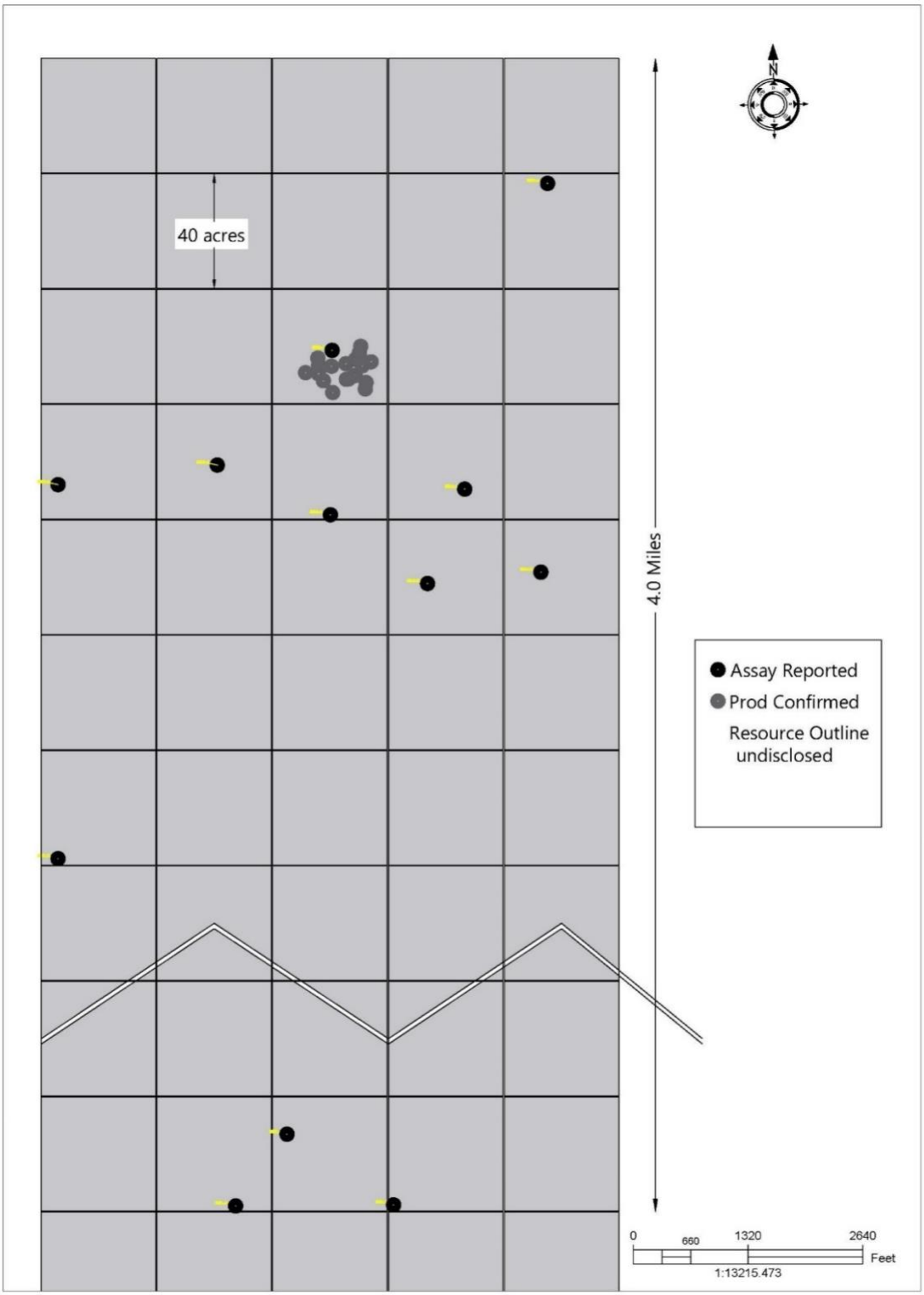


Figure 12. Project MRE drill holes and production sampling

The site covers over 600 acres of rare earth elements (REEs), cobalt, nickel, manganese, and other minerals. The project is strategically located near low-cost road, rail, and water logistics connecting it to world class manufacturing industries and customers. The site is in a region of more than 100 square miles that could reach to 10,000 square miles.

The MRE intends to confirm that the deposit is one of the largest CM deposits in the U.S., with a high in-situ value underpinned by a product assemblage of high value CM and heavy and light rare earth elements. The shallow unconsolidated nature of the mineralization enables the potential for simple mining operations such as open pit or dredge.

*Mineral Resource Estimate* - The MRE for the project comprises 94 Mt at 0.63 - 5.3% probable CM ore, containing up to 37.7 Kt. Mineralization occurs as a single, large, and coherent near-surface deposit. The MRE incorporates results from 12 sonic drill core holes for a total of 830 feet drilled in 2014, 2018, and 2021. Fifty production samples were sampled in 2021 and sampling continued in 2022. The deposit has a high proportion of critical minerals (CM), including the subset of rare earth elements (REEs).

Table 17. In-situ grades of rare earth elements and other critical minerals.

| **Mn** | | **REEs** | | **Ni/Co** | | **Zn** | | **Other** | |
|---|---|---|---|---|---|---|---|---|---|
| **%** | **(t)** | **%** | **(t)** | **%** | **(t)** | **%** | **(t)** | **%** | **(t)** |
| 62.4 | ~22,500 | 14.5 | ~6,858 | 13.2 | 4,777 | 3.5 | 1,253 | 6.4 | 3,555 |

*Rare Earth Elements* - Test work to date has highlighted that the rare earth minerals at the site contain a high percentage of rare earth oxides (REOs), with heavy to light rare earths ratio showing 32% heavy and 68% light.

*Drill Hole Exploration Program* - All drilling for the project has been roto sonic. This method alternates advancement of a core barrel and a removeable casing (casing is used when needed to maintain sample integrity). The core barrel utilized for this project is 4” in diameter with a 6” diameter outer casing. The core barrel is retrieved from the ground and the samples are recovered directly from the barrel into a plastic sleeve. All holes are drilled vertically. The sonic drilling method has been shown to provide representative unconsolidated samples across a variety of deposits as it is a direct sampling method of the formation(s). At times water is used to create head on the formation to help prevent run-up.

A roto-sonic drill rig with a 10-foot core barrel is used to obtain direct 10-foot samples of the unconsolidated geological formations hosting the mineralization in the project area. All holes are drilled vertically, which is essentially perpendicular to the mineralization. The sonic cores are used to produce approximately 4 kg samples for heavy liquid separation as well as further mineralogical analysis. Each core is measured, and the recovery is calculated as length of recovered core divided by length drilled (typically 10’).

Some interpretation is involved, as the material can expand or compact as it is recovered from the core barrel into the plastic sleeve. Samples are logged for lithological, geological, and mineralogical parameters in the field to help aid in determining depositional environment, major geologic units, and mineralized zones.

All samples are sieved, and estimates made for the CM %. Logging is both qualitative (sorting, color, lithology) and quantitative (estimation of CM %) to help support the integrity of the Exploration Results and MRE. Photographs are taken of the sonic cores.

The unconsolidated sonic cores are sampled by splitting the core using a 58" sample knife then recovering an even fillet with a trowel along the entire length of the sample interval. Samples are collected directly to the pre-labelled/pre-tagged sample bags; the remaining sample is further split into a replicate/archival sample.

*Sample Analysis Methodology* - Roto-sonic drill core samples, typically 10 ft, as well as real-time production samples are sent to SGS North America facility in Denver, Colorado. Samples are subjected to size fraction analysis, heavy-liquid separation, and chemical analysis. Samples are density separated then the fractions are analyzed by inductively coupled plasma – mass spectrometry (ICP-MS).

*Mining and Metallurgical Methods and Parameters* - The MRE assumes that the deposit will be mined by standard mineral open pit methods that may include a combination of hydraulic excavator/shovel or dredge. Metallurgical testing has been conducted, with bulk samples collected from the upper mineralized horizons only. Products were analyzed by ICP-MS. Product information has not been included in the block model at this stage of the project.

*Estimation of Distribution* – To provide an estimation of distribution Table 18 is provided which show in the first Prod % the mass distribution component of the assayed elements from samples derived from production sources. For the Core % column, this distribution is derived from the % mass of REEs only. The last Prod % column is to provide a mass % distribution on REEs only for direct comparison to Core %.

Table 18. Resource assessment of rare earth elements and other critical minerals for Site 2.

| Element | Mass Range (kg) | Elemental Distribution in Product (%) | Elemental Distribution in Core (%) | REE Distribution in Product (%) |
|---|---|---|---|---|
| Scandium | 9,666 – 81,317 | 0.19 | 2.8 | 1.6 |
| Lanthanum | 132,950 – 1,118,467 | 2.60 | 16.5 | 17.3 |
| Cerium | 193,994 – 1,632,012 | 3.80 | 26.5 | 27.0 |
| Praseodymium | 27,521 – 231,529 | 0.54 | 4.1 | 3.6 |
| Neodymium | 114,340 – 961,908 | 2.24 | 14.8 | 15.2 |
| Samarium | 22,202 – 186,778 | 0.43 | 2.9 | 3.0 |
| Europium | 4,812 – 40,478 | 0.09 | 0.8 | 0.7 |
| Gadolinium | 24,701 – 207,801 | 0.48 | 3.2 | 3.3 |
| Terbium | 3,416 – 28,741 | 0.07 | 0.6 | 0.5 |
| Dysprosium | 20,873 – 175,599 | 0.41 | 2.8 | 2.8 |
| Holmium | 4,501 – 37,864 | 0.09 | 0.7 | 0.6 |
| Erbium | 12,662 – 106,524 | 0.25 | 1.7 | 1.8 |
| Thulium | 1,755 – 14,676 | 0.03 | 0.5 | 0.2 |
| Ytterbium | 10,528 – 86,294 | 0.20 | 1.5 | 1.4 |
| Lutetium | 1,672 – 14,064 | 0.03 | 0.5 | 0.2 |
| Yttrium | 154,234 – 1,297,528 | 3.02 | 20.1 | 20.8 |
| Gallium | 5,925 – 49,846 | 0.15 | - | - |
| Cobalt | 144,895 – 1,218,958 | 3.73 | - | - |
| Manganese | 2,427,127 – 20,418,685 | 62.41 | - | - |
| Nickel | 370,048 – 3,113,102 | 9.51 | - | - |
| Silver | 1,616 – 13,594 | 0.04 | - | - |

| | | | | |
|---|---|---|---|---|
| Vanadium | 72,717 – 611,745 | 1.87 | - | - |
| Zinc | 135,199 – 1,137,392 | 3.47 | - | - |
| Germanium | 17,775 – 149,538 | 0.46 | - | - |
| Strontium | 124,427 – 1,046,763 | 3.31 | - | - |
| Lithium | 7,272 – 61,174 | 0.55 | - | - |
| Total | | 100.00 | 100.00 | 100.00 |

### *2.3.2 Subtask 3.2 – Resource Assessment*

#### *2.3.2.1 West Kentucky No. 13 Coarse Refuse Source*

The pilot-plant tests involving the West Kentucky No. 13 coarse refuse source will involve heap leaching and production of a pregnant leach solution (PLS) at a rate of 5800 gallons/minute. The production of the individual rare earth metals from the proposed pilot plant is provided in Table 8. The recovery of each rare earth element (REE) from the PLS was assessed based on previous study for upstream concentration (A Unique Collaboration of Coal-based REEs and the U.S.'s Largest Rare Earth Producer - FE000053) and estimates for downstream purification (Demonstration of Scaled-Production of Rare Earth Oxides and Critical Materials from Coal-Based Sources using Innovative, Low Cost Process Technologies and Circuits - DE-FE0031827) and metal making processes. Likewise, the estimated production levels of the other critical metals are provided in Table 9.

Table 8. Rare earth metal production estimates from the treatment of the West Kentucky 13 coarse refuse material by the proposed pilot plant facilities.

| Rare Earth Metal | Elemental Process Feed Rate (kg/hr.) | Product Production Rate (kg/day) | Product Production Rate (mt/yr.) | Annual Revenue Value ($/yr.) |
|---|---|---|---|---|
| Yttrium | 15.8 | 195 | 71 | 564,427 |
| Praseodymium | 0.6 | 8 | 3 | 293,170 |
| Neodymium | 2.2 | 49 | 18 | 2,031,225 |
| Samarium | 2.4 | 32 | 12 | 26,655 |
| Gadolinium | 4.7 | 83 | 30 | 1,706,526 |
| Dysprosium | 2.7 | 38 | 14 | 4,632,453 |

Table 9. Critical material production estimates from the treatment of the West Kentucky 13 coarse refuse material by the proposed pilot plant facilities.

| Rare Earth Metal | Elemental Process Feed Rate (kg/hr.) | Product Production Rate (kg/day) | Product Production Rate (mt/yr.) | Annual Revenue Value ($/yr.) |
|---|---|---|---|---|
| Germanium | 0.13 | **ND | - | - |
| Gallium | 0.23 | 624 | 228 | 69,201,095 |
| Manganese | 269.56 | 33 | 12 | 59,016 |
| Cobalt | 24.01 | 300 | 110 | 3,805,848 |
| Nickel | 78.22 | 713 | 260 | 6,911,928 |
| Zinc | 80.37 | 1378 | 503 | 1,588,838 |
| Strontium | *ND | - | - | - |
| Lithium | 28.84 | 587 | 214 | 13,181,971 |

*ND = Non-detected in feed. **ND = Element not detected downstream.

It should be noted that the most significant contribution to revenue is gallium, which is an element that is critical for electronic chip manufacturing. Lithium is the next most significant in terms of revenue followed by nickel, dysprosium, cobalt, neodymium, gadolinium, and zinc.

*2.3.2.2 Subtask 3.2.2 –Lignite Sand-Production Source*

The lignite source is currently a waste product of construction sand production. The leachability of the lignite source is superior to the West Kentucky No. 13 coarse refuse source. According to laboratory leaching experiments, nearly 95% of the rare earth elements (REEs) and critical materials (CM) can be leached from the lignite source using 0.5 M sulfuric acid ($H_2SO_4$) solution with no pretreatment required other than particle size reduction to an 80% passing size of around 150 microns. As such, tank leaching at a solids concentration of 20% by weight was assumed in this case instead of heap leaching. To allow a direct comparison with the production values determined for the West Kentucky No. 13 course (Tables 8 and 9), the same PLS volume flow rate of 5,800 gpm was used for the elemental production. The solids flow rate of lignite into the leaching system was 350 tph. Using the elemental concentration of the average lignite sample, daily and annual production rates were determined along with the metal contributions to annual revenue were estimated as shown in Tables 10 and 11.

Rare earth production provides the most significant impact on annual revenue with praseodymium, neodymium, and dysprosium combining to generate an annual contribution to the total revenue of around $129 million. However, manganese is estimated to provide a significant impact of $25 million while cobalt and nickel are close behind with a combined total of nearly $30 million.

Table 10. Rare earth element production estimates from the treatment of the lignite material produced as a waste product from construction sand.

| Rare Earth Metal | Elemental Process Feed Rate (kg/hr.) | Product Production Rate (kg/day) | Product Production Rate (mt/yr.) | Annual Revenue Value ($/yr.) |
|---|---|---|---|---|
| Yttrium | 130 | 1593 | 581 | 4,623,783 |
| Praseodymium | 36 | 480 | 175 | 18,138,513 |
| Neodymium | 1062 | 1831 | 668 | 75,683,830 |
| Samarium | 25 | 341 | 125 | 280,165 |
| Gadolinium | 20 | 356 | 130 | 7,365,178 |
| Dysprosium | 21 | 289 | 105 | 34,960,998 |

Table 11. Critical mineral production estimates from the treatment of the lignite material produced as a waste product from construction sand.

| Rare Earth Metal | Elemental Process Feed Rate (kg/hr.) | Product Production Rate (kg/day) | Product Production Rate (mt/yr.) | Annual Revenue Value ($/yr.) |
|---|---|---|---|---|
| Germanium | *ND | - | - | - |
| Gallium | *ND | - | - | - |
| Manganese | 943 | 14,235 | 12 | 25,147,684 |
| Cobalt | 60 | 744 | 110 | 9,440,691 |
| Nickel | 216 | 1,968 | 260 | 19,071,663 |
| Zinc | 49 | 832 | 503 | 959,476 |
| Strontium | *ND | - | - | - |
| Lithium | 10 | 68 | 214 | 1,519,031 |

*ND = Non-detected in feed

## 2.4 Task 4.0 – Circuit 1 Pilot Plant Data & Required Circuit Modifications

### *2.4.1 Subtask 4.1 – Flowsheet and Data Analysis*

To describe the proposed flowsheet, it is necessary to provide context for the reasons in deciding upon certain configurations. For Circuit 1, staged precipitation tests conducted prior to the start of this project by VT were conducted to evaluate the precipitation characteristics of selected critical elements and contaminant elements as a function of pH. As Figure 13 shows, by raising the pH of a leachate from coal to around 4.5, nearly all Fe and most Al were precipitated, while the majority of the critical elements remained in the solution. Therefore, Fe and Al in the leachate can be largely removed by removing the precipitate formed at pH 4.5. Subsequently, critical elements begin to precipitate with an increase in the solution pH. When the pH of the solution reached around 9.0, rare earth elements (REEs), Co, Mn, Ge, and Ga were precipitated, while Li and Sr remained in solution. Although the precipitation curve of Zn and Ni is not presented in the Figure 13, a prior study performed by the project team confirmed that Zn and Ni precipitate in a similar pH range as Co and Mn. Therefore, after staged precipitation, the critical elements contained in the leachate were separated into two material streams: precipitate rich in REEs, Co, Mn, Ge, Ga, Zn, and Ni, and a solution rich in Li and Sr with some contaminate elements, such as Ca and Mg.

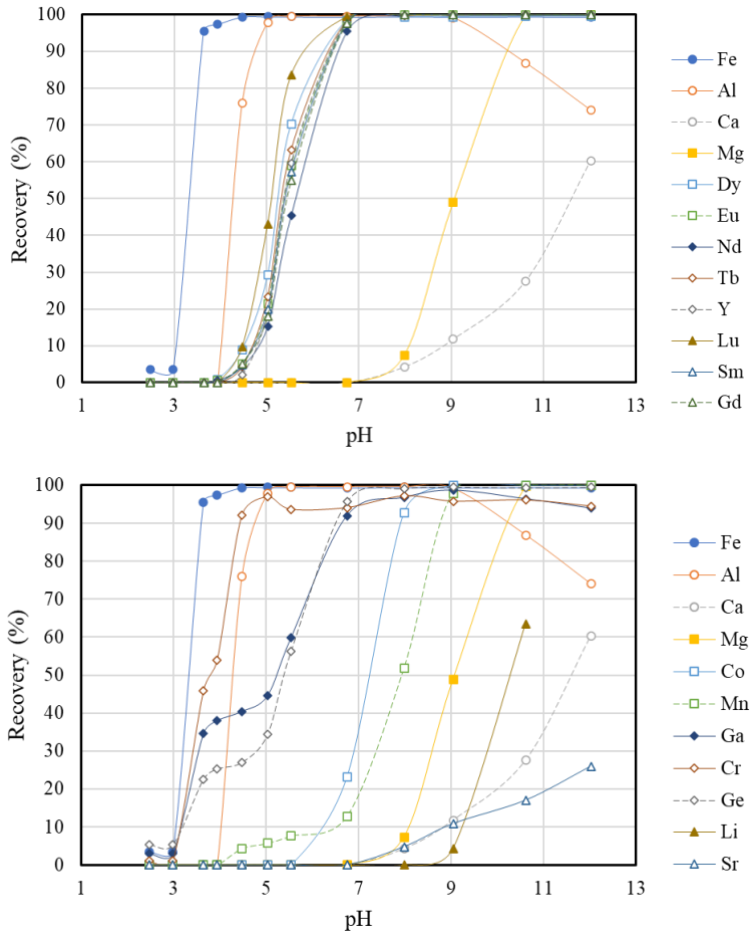


Figure 13. Precipitation recovery of selected critical elements and contaminant elements as a function of pH.

To make use of the REE and critical mineral (CM) characteristics and produce useful products, including rare earth metals (REMs), the following flow sheet is proposed to produce four (4) product streams to meet the requirements of the project referenced in [1] (see Figure 13). At this time, staged precipitation which creates several distinct products, is favored owing to the downstream selection of pyrometallurgical methods (to be discussed in later sections). The products include a REE product containing Ga and Ge, a CM product containing Co, Ni, and Zn, a Mn and Mg product, and waters containing Sr and Li. The PLS from the proposed heap leach is shown in Table 19 which shows the elemental assay. Table 20 shows the oxides generated in the test circuit shown in Figure 14. The intermediate CM products have been formed as precipitates previously in another DOE sponsored project [1] as shown in Table 21and Table 22.

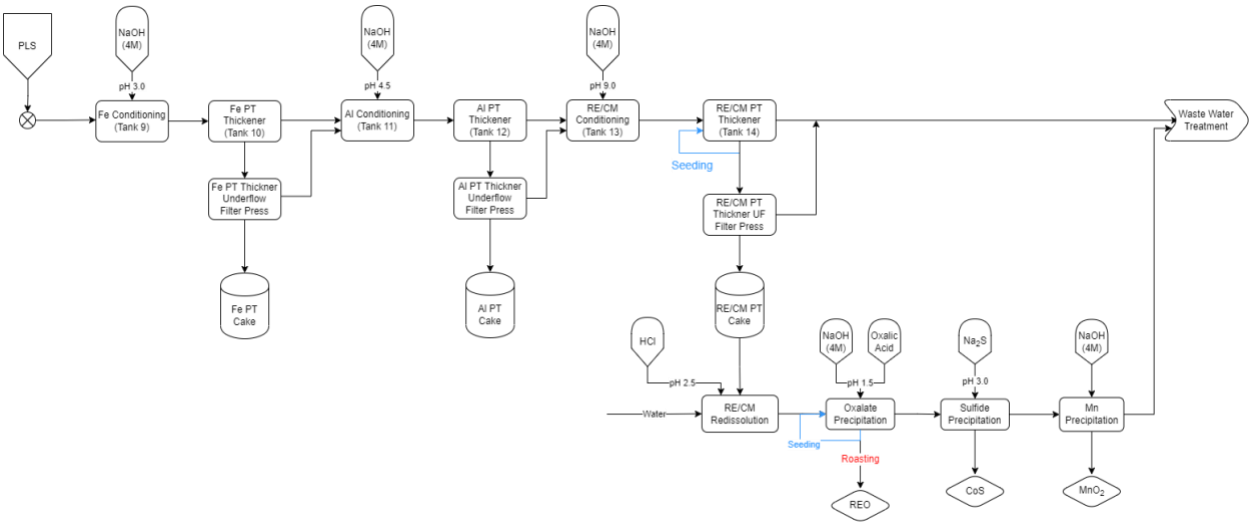


Figure 14. Pilot Plant Schematic Flowsheet of PLS4 (test) from project [1] upon which the data in this report is based upon.

Table 19. PLS 4 Data compared to the average heap leach concentration from the running of the heap leach commenced in [2].

| Element | PLS4 Data | Heap Leach Average |
|---|---|---|
| Sc | 0.35 | 0.99 |
| Y | 4.91 | 12.02 |
| La | 0.13 | 0.26 |
| Ce | 0.99 | 1.82 |
| Pr | 0.18 | 0.44 |
| Nd | 1.20 | 2.17 |
| Sm | 0.80 | 1.80 |
| Eu | 0.22 | 0.49 |
| Gd | 1.40 | 3.57 |
| Tb | 0.21 | 0.49 |
| Dy | 1.19 | 2.08 |
| Ho | 0.20 | 0.53 |
| Er | 0.49 | 1.00 |
| Tm | 0.06 | 0.15 |
| Yb | 0.31 | 0.70 |
| Lu | 0.05 | 0.16 |
| | | |
| Mg | 877.79 | 2415.55 |
| Mn | 68.85 | 204.63 |
| Co | 7.21 | 18.23 |
| Ni | 20.16 | 59.38 |
| Zn | 20.48 | 61.01 |
| Cu | 4.35 | 10.76 |
| | | |
| Se | 9.37 | 8.95 |
| Sr | NR | NR |
| Ge | NR | 0.10 |
| Ga | 0.07 | 0.18 |
| Li | 7.13 | 21.90 |
| | | |
| Al | 1038.90 | 2419.78 |
| Ca | 322.35 | 432.13 |
| Fe | 2079.23 | 4352.67 |

Table 20. Heap leach pregnant leach solution rare earth product*

| Elements | Elemental Concentration | | Elemental MW | Oxide Form | Oxides Concentration |
|---|---|---|---|---|---|
| | mg/kg | % dry weight | g/mol | | % dry weight |
| Sc | 287 | 0.0 | 45 | Sc2O3 | 0.04 |
| Y | 303804 | 30.4 | 89 | Y2O3 | 38.58 |
| La | 2889 | 0.3 | 139 | La2O3 | 0.34 |
| Ce | 28337 | 2.8 | 140 | CeO2 | 3.48 |
| Pr | 9080 | 0.9 | 141 | Pr6O11 | 1.10 |
| Nd | 69877 | 7.0 | 144 | Nd2O3 | 8.15 |
| Sm | 54613 | 5.5 | 150 | Sm2O3 | 6.33 |
| Eu | 16037 | 1.6 | 152 | Eu2O3 | 1.86 |
| Gd | 111411 | 11.1 | 157 | Gd2O3 | 12.84 |
| Tb | 16656 | 1.7 | 159 | Tb4O7 | 1.96 |
| Dy | 123926 | 12.4 | 163 | Dy2O3 | 14.22 |
| Ho | 12564 | 1.3 | 165 | Ho2O3 | 1.44 |
| Er | 27816 | 2.8 | 167 | Er2O3 | 3.18 |
| Tm | 3192 | 0.3 | 169 | Tm2O3 | 0.36 |
| Yb | 15534 | 1.6 | 173 | Yb2O3 | 1.77 |
| Lu | 2067 | 0.2 | 175 | Lu2O3 | 0.24 |
| **TREE** | 798091 | 79.8 | | **∑REO** | **95.89** |
| **Al** | 4294 | 0.4 | 13 | Al2O3 | 1.22 |
| **Ca** | 44847 | 4.5 | 40 | CaO | 6.28 |
| **Fe** | 8865 | 0.9 | 56 | Fe2O3 | 1.27 |

*Note: Oxalates converted to oxides by roasting.

Table 21. Heap leach pregnant leach solution Co, Ni, and Zn product*

| Elements | Elemental Concentration | | Elemental MW | Oxide Form | Oxides Concentration |
|---|---|---|---|---|---|
| | mg/kg | % dry weight | g/mol | | % dry weight |
| **TREE** | 2768.3 | 0.3 | | | **0.33** |
| Al | 5960.3 | 0.6 | 13 | Al2O3 | 1.70 |
| Ca | 1427.9 | 0.1 | 40 | CaO | 0.20 |
| Co | 56371.3 | 5.6 | 28 | CoO | 8.86 |
| Cu | 9724.6 | 1.0 | 64 | CuO | 1.22 |
| Fe | 10556.5 | 1.1 | 56 | Fe2O3 | 1.51 |
| Mg | 26914.2 | 2.7 | 24 | MgO | 4.49 |
| Mn | 17784.4 | 1.8 | 55 | MnO2 | 2.81 |
| Na | 33888.2 | 3.4 | 23 | Na2O | 4.57 |
| Ni | 187197.6 | 18.7 | 59 | NiO | 28.93 |
| Se | 251.1 | 0.0 | 79 | SeO2 | 0.04 |
| Sr | 78.2 | 0.0 | 88 | SrO | 0.01 |
| Zn | 136566.9 | 13.7 | 65 | ZnO | 17.02 |

*Note: Sulfides converted to oxides by roasting.

Table 22. Heap leach pregnant leach solution Mg/Mn product*

| Elements | Elemental Concentration | | Elemental MW | Oxide Form | Oxides Concentration |
|---|---|---|---|---|---|
| | mg/kg | % dry weight | g/mol | | % dry weight |
| **TREE** | 8465.0 | 0.8 | | | **1.03** |
| Al | 67481.9 | 6.7 | 13 | Al2O3 | 19.21 |
| Ca | 1046.7 | 0.1 | 40 | CaO | 0.15 |
| Co | 200.6 | 0.0 | 28 | CoO | 0.03 |
| Cu | 26.9 | 0.0 | 64 | CuO | 0.00 |
| Fe | 2530.3 | 0.3 | 56 | Fe2O3 | 0.36 |
| Mg | 217721.9 | 21.8 | 24 | MgO | 36.29 |
| Mn | 142053.3 | 14.2 | 55 | MnO2 | 22.47 |
| Na | 57405.7 | 5.7 | 23 | Na2O | 7.74 |
| Ni | 1095.8 | 0.1 | 59 | NiO | 0.17 |
| Se | 643.2 | 0.1 | 79 | SeO2 | 0.09 |
| Sr | 0.0 | 0.0 | 88 | SrO | 0.00 |
| Zn | 365.1 | 0.0 | 65 | ZnO | 0.05 |

*Note: Hydroxides converted to oxides by roasting.

The process begins with the representation of the heap leach. It is important to note that the heap leach concept depends on the West Kentucky No. 13 coarse refuse propensity to autogenerate sulfuric acid ($H_2SO_4$) from the oxidation of contained pyrite ($FeS_2$). To account for the variation of seasonal temperature and rainfall effects on the generation of the appropriate amount of acid, a controlled pyrite bio-oxidation step is added as a potential mitigation method. As conceived, the heap leach receives liquid in the form of make-up water, or water recycled back from the primary precipitation stage. Following leaching, iron precipitation is performed by raising the solution pH. An important option of this process is the use or blending of lignite sources for additional REE recovery. Iron precipitate derived from the process will be returned to coarse refuse impoundment from whence it originated or incorporated into areas of spent heap leach material for disposal. Techniques for rendering these refuses inert at closure make them ideal for containing this material. Increasing the pH further will result in an Al/Sc rich precipitate that will be settled in much the same manner via pond.

Following Al/Sc precipitation, further pH adjustment induces the precipitation of REEs. A thickener is utilized to decrease the volume reporting to the filter press for the recovery of this precipitate. The REEs are captured via an additional precipitation step and re-leached and precipitated via an oxalic acid precipitation step. The resulting precipitate is then roasted into an oxide form. For additional recovery the lixiviant is further processed by the introduction of $Na_2S$ which will selectively induce a CoS precipitate. The pH of the lixiviant is then adjusted to produce a Mn rich concentrate for recovery. The remaining liquid is then sent for additional processing to recover Li and Sr.

### *2.4.2 Subtask 4.2 – Modification and Optimization*

Please note that very little modification of the proposed flows sheet has been required. The full import of the deliverable of this task will be found in the flowsheet and TEA sections.

### *2.4.3 Section References*


[1] Honaker, R.Q., Werner, J., Nawab, A., Zhang, W., Noble, A., Yang, X. and Free, M., 2023. "Demonstration of Scaled-Production of Rare Earth Oxides and Critical Materials from Coal-Based Sources," DOE Contract No. DE-FE0031827, Final Technical Report, 1080 pages.

[2] Rosenthal, M., 2022. "A Unique Collaboration of Coal-based REEs and the U.S.'s Largest Rare Earth Producer" Final Technical Report, MP Materials/DOE, Project Number: 89243320CFE000053-0001; 221 pages.


## 2.5 Task 5.0 – Circuit 2 RE Individually Separated High Purity Products

### *2.5.1 Subtask 5.1 – State-of-the-Art Technology Review*

*Extractant Types* - When selecting a suitable extractant for solvent extraction or in this case solvent assisted chromatography, the choices fall into one of three categories: cation, anion, and solvating exchangers [1]. The three types vary by the mechanism in which the aqueous ion is loaded into the organic phase. Most importantly these reactions can be controlled by adjusting the pH of the solution. Due to the effects of Le Chatelier's principle, this allows specificity in which elements are stripped or loaded into preferred phases [2]. The relationship between the amount of a specific ion in the organic vs aqueous phase can be modeled in two ways: distribution coefficients and percent extracted. The distribution coefficient is defined in equation 1 [1].

$$D = \frac{[REE^{3+}]_{org}}{[REE^{3+}]_{aq}} \tag{1}$$

Here, $D$ represents the distribution coefficient; $[REE^{3+}]_{org}$, the concentration of the rare earth element in the organic phase; and $[REE^{3+}]_{aq}$, the concentration of the rare earth in the aqueous phase. In brief, the distribution coefficient represents the ratio of organic to aqueous concentrations of an element. The other characterization, percent extracted, is defined in equation 2 [1].

$$E = \frac{[REE^{3+}]_{org}}{[REE^{3+}]_{feed}} \tag{2}$$

In this equation, $E$ denotes the percent extracted. Using these characteristics correlations can be established between either distribution coefficient or percent extracted and pH. Often times these relationships resemble that of a titration curve due to the nature of the phase change.

*Cation Exchangers*

$$REE^{3+} + 3HA \rightleftharpoons REEA_3 + 3H^+ \tag{3}$$

Cation exchangers consist of the organic molecule, A, and an extra hydrogen ion, H. When a rare earth element, REE, is extracted by an anionic exchanger, the mechanism of the reaction is to load the REE into organic phase by replacing the hydrogen ions (cation). This reaction is modeled in equation 3 [1]. As a result, the hydrogen ions remain in the aqueous phase increasing the pH of the solution. Therefore, this reaction can be controlled by adjusting the pH of the system. Another

name for cation exchangers is acidic exchanger due to the production of the hydrogen ion. A collection of cation exchangers can be found in Table 23.

Table 23. List of cation exchangers and their extraction diagrams.

| Extractant Type | Literature References |
|---|---|
| Versatic 10 [3] | 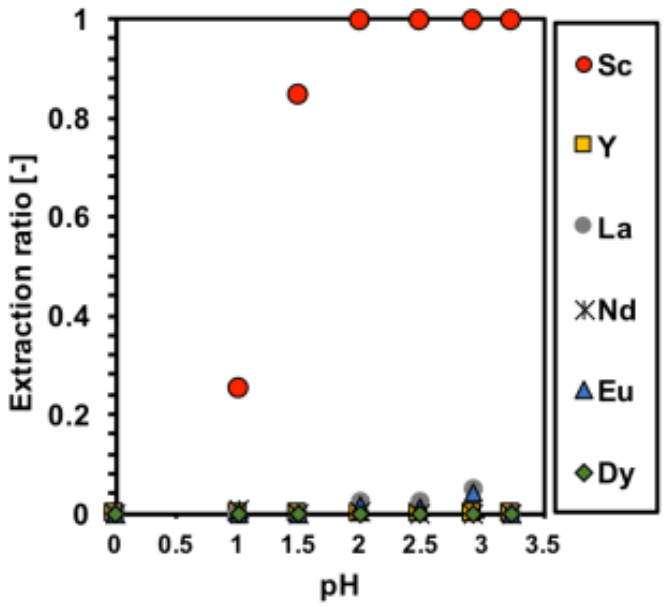 Figure 4. Extraction ratio of REE ions using 1 mM PC-88A+100 mM Versatic 10, an aqueous phase: 0.1 mM $M^{n+}$. |
| DEHPA [4,5] | 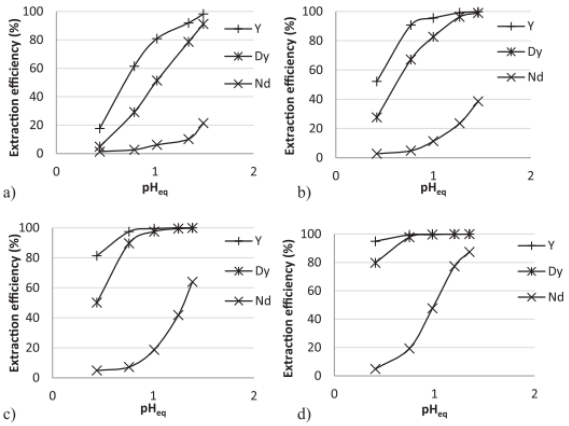 Fig. 3. Effect of equilibrium pH on the extraction efficiency of Y(III), Dy(III), and Nd(III) at different concentrations of D2EHPA and initial REE concentration of 0.005 mol/L for each element, a) 0.03 mol/L D2EHPA, b) 0.06 mol/L D2EHPA, c) 0.09 mol/L D2EHPA, d) 0.15 mol/L D2EHPA. |

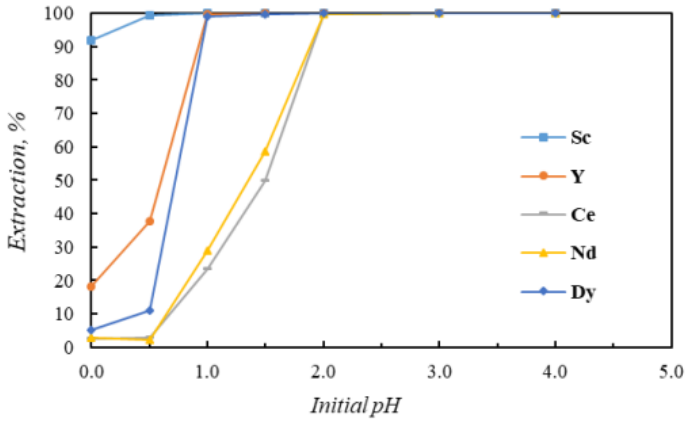


Fig 3.5 Effect of initial on the extraction efficiency of REEs.

*C(D2EHPA) = 0.2 M; $V_A/V_O$=1:1; t = 10 min.*

HEHEHP [6]

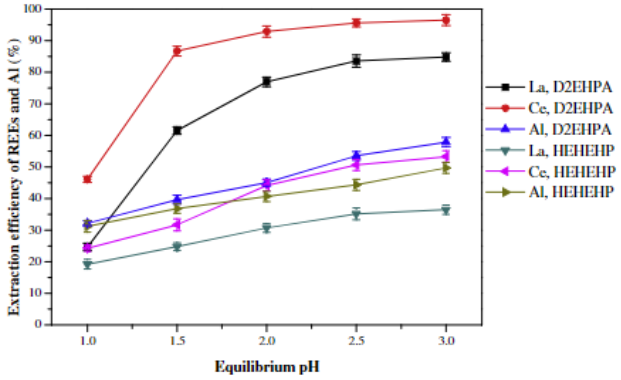


**Fig. 10.** REEs and Al extraction with 0.5 mol/L D2EHPA and HEHEHP at O/A = 1:1, ambient temperature for 10 min.

PC88A [7,8]

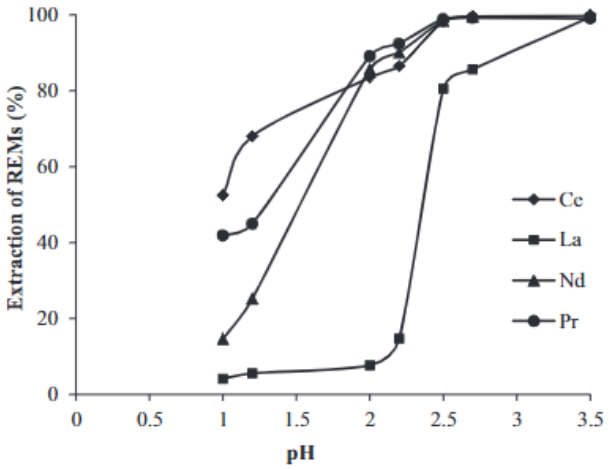


**Fig. 1.** Effect of equilibrium pH. (Aqueous: Leach liquor of REMs; Organic: 5% PC88A + 3% ID; O/A ratio: 1:1; Time: 5 min.)

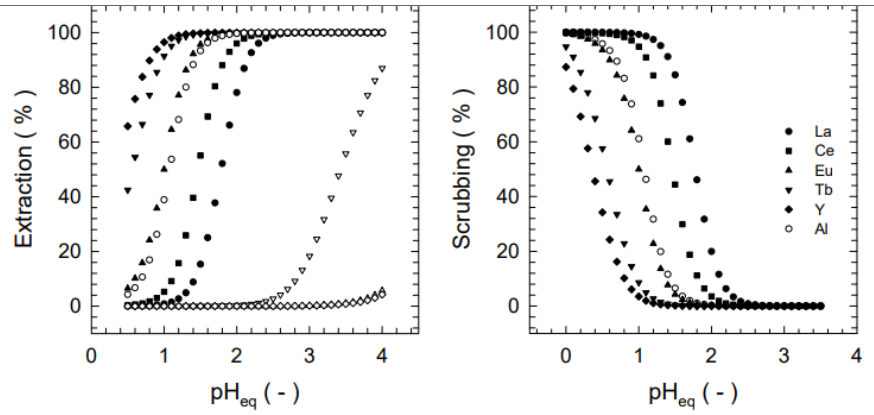


Cyanex 272 [9,10]

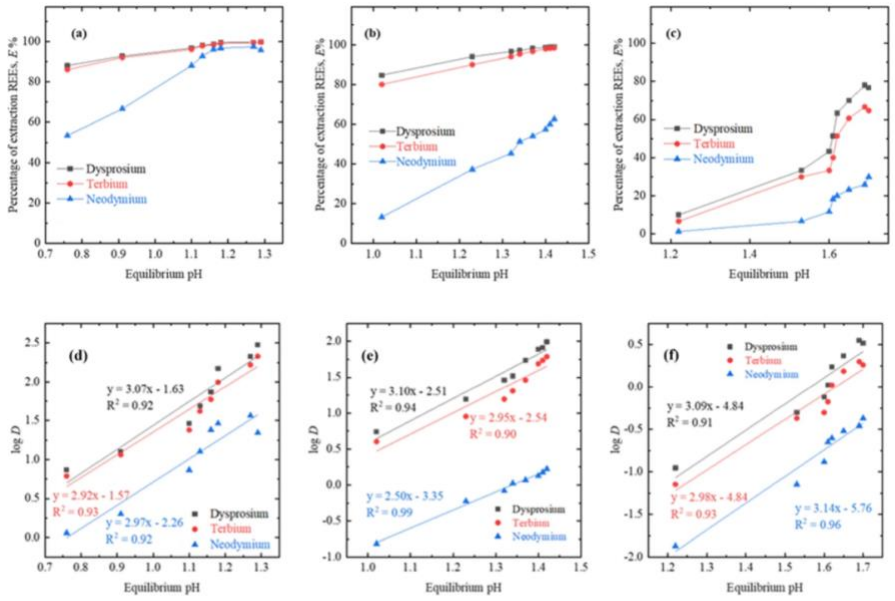


Effect of equilibrium pH using (**a**) D2EPHA, (**b**) PC 88A, and (**c**) Cyanex 272 as extractant systems for REEs extraction and Plots of log *D* as a function of equilibrium pH for (**d**) D2EPHA, (**e**) PC 88A, and (**f**) Cyanex 272. Experimental conditions: aqueous feed: 1500 mg/L $Dy^{3+}$, 1500 mg/L $Tb^{3+}$ and 1500 mg/L $Nd^{3+}$, organic feed = 0.8 mol/L phosphorous based extractants, phase ratio A/O = 1:1, temperature = 298 K, and contact time = 60 min.

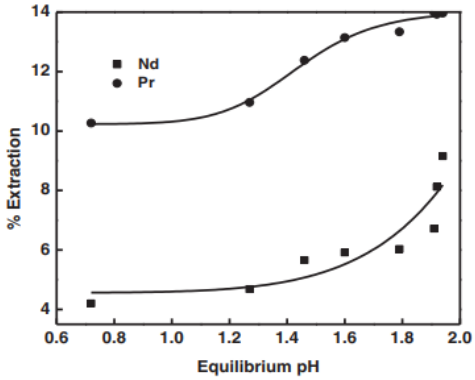


**Fig. 5.** Effect of equilibrium pH on extraction of Nd and Pr with 0.15 M Cyanex 272 at A:O = 1:1.

| | |
|---|---|
| Cyanex 301 [11] | 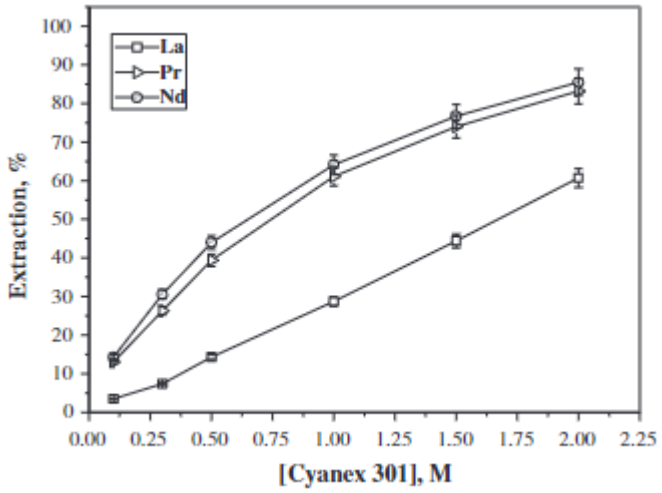 |

In addition to those listed in table 1, Versatic 11, Naphthenic acids**,** EHEHPA, HBTMPP, P507, P229, and Cyanex 302 are examples of acidic exchangers [12].

*Anion Exchangers*

$$R_4N \cdot X + REE^{3+} + 3X^- \rightleftharpoons R_4N \cdot REEX_4 \quad (4)$$

Anion exchangers are typically primary or quaternary amines. When the organic compound, $R_4N$, reacts with the REE and similar anion, the reactants are loaded into the organic phase. This reaction is depicted in equation 4 [1]. The anionic species can be added to the system via a salt or an acid. Occasionally, anion exchangers are referred to basic exchangers due to their mechanism. Select anion exchangers can be seen in

Table 24.

Table 24. List of anion exchangers and their extraction diagrams.

| **Extractant Type** | **Literature References** |
|---|---|
| Primene JM-T [13] | 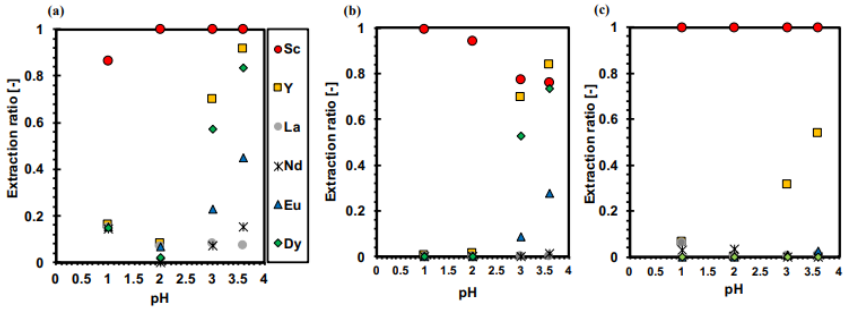 <br>Figure 3. Extraction ratio of REE ions using (a) 1 mM PC-88A and 5 mM primene JM-T, (b) 1 mM PC-88A and 5 mM Cyanex 272 and (c) 1 mM PC-88A and 5 mM TBP in *n*-dodecane. Aqueous phase: 0.1 mM $M^{n+}$. |

Aliquat 336 [14]

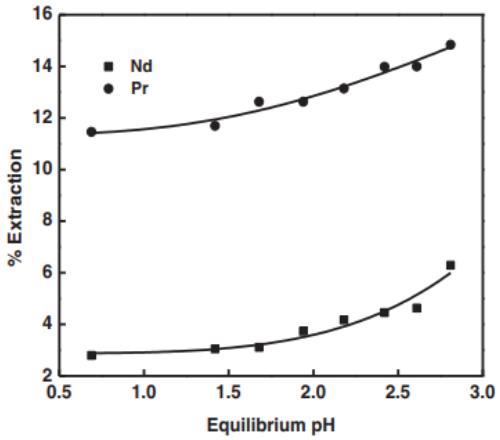


**Fig. 6.** Effect of equilibrium pH on extraction of Nd and Pr with 0.15 M Aliquat 336 at A:O = 1:1.

Furthermore, N1923 and Adogen 464 are examples of basic exchangers [12].

Solvating Exchangers

$$REEX_3 \cdot xH_2O + 3A \rightleftharpoons REEX_3A_3 + xH_2O \quad (5)$$

Solvating exchangers produce water as a product as the result of the hydrated REE being loaded into the organic phase. This reaction is represented by equation 5 [1]. "Nevertheless, a significant difference between solvating and basic extractant can be observed in the organic phase or at the interface. While the solvating extractant only reacts with the metal salt to form an adduct, the basic extractant anion reacts with the metal salt to form negatively charged metal complexes that electrostatically interact with the basic extractant cation" [15]. Additionally, these solvents are sometimes referred to as neutral exchangers. A list of these solvating exchangers can be found in Table 25.

Table 25. List of solvating exchangers and their extraction diagrams.

| Extractant Type | Literature References |
|---|---|
| TBP [16] | 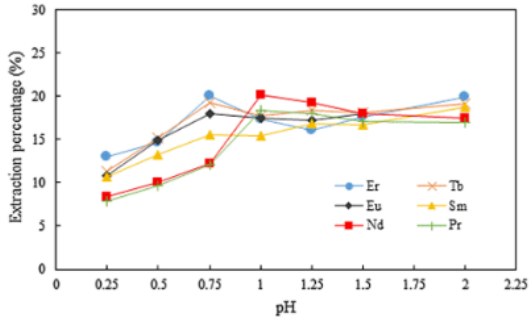 **Fig. 1.** Effect of $pH_i$ on the extraction of REEs using TBP at 20 °C and O/A ratio of 1:1 in chloride media diluted with kerosene.<br> 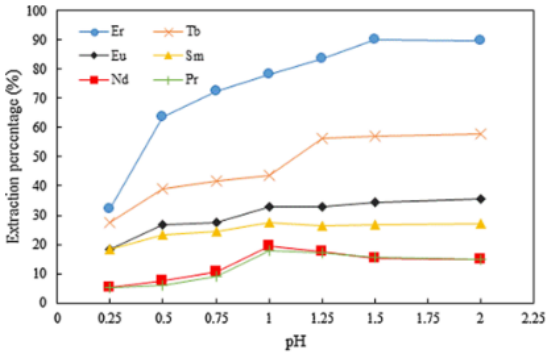 **Fig. 2.** Effect of $pH_i$ on the extraction of REEs using Cyanex 572 at 20 °C and O/A ratio of 1:1 in chloride media diluted with kerosene. |
| TOPO [17] | 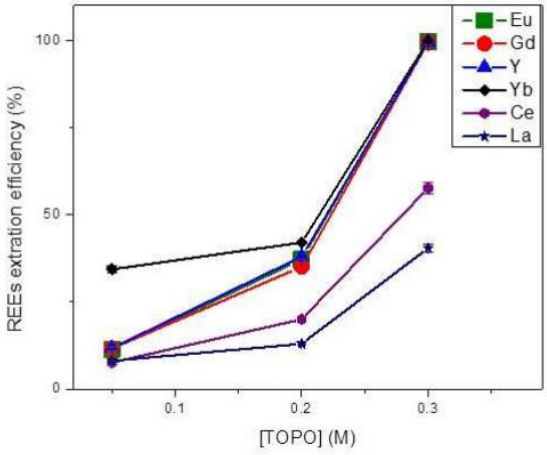 Figure 8. REEs extraction efficiency as a function of TOPO concentration. |

Also, DBBP and Cyanex 921 are examples of additional neutral exchangers [12].

*Solvent Extraction Technologies* - Solvent extraction technologies generally fit into two classifications: mixer-settlers and column extractors [18]. Both operate according to similar principles: forced mixing and a density separation via gravity. Mixer settlers are the most common technique and commonly consist of a series of agitators and decanters chained together within a counter-current methodology. On the other hand, column extractors are more analogous to distillation columns in that they contain multiples stages blended together often seamlessly. Furthermore, column extractors can be further divided into static and agitated categories. This breakdown can be seen in Figure 15.

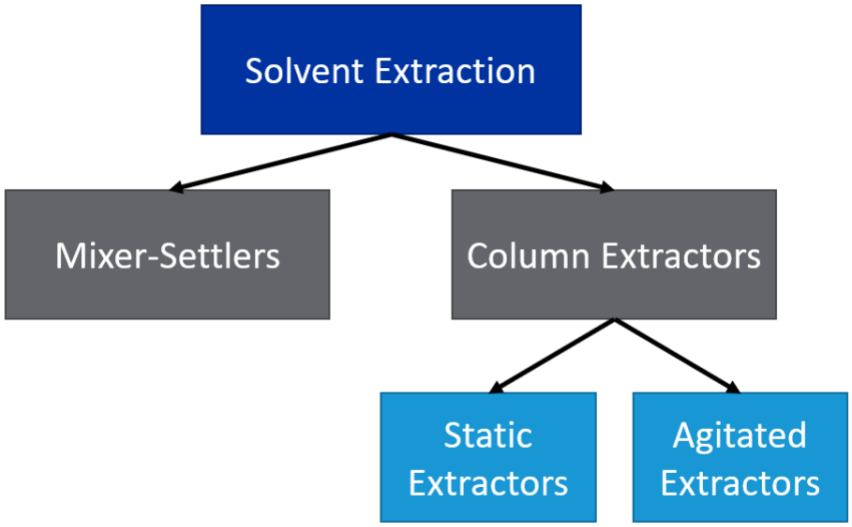


Figure 15. Diagram depicting the categorization of solvent extraction technologies.

As with most technologies, the most suitable technology is dependent upon the design parameters required by that specific system. A comparison of these design features and their fields of industrial application can be found in.

Two important factors to consider when designing a solvent extraction system are the flow rate and extractant volume of the equipment. When innovating within constraints, the amount of physical space that a system requires can be critical. For example, while mixer-settlers are the simplest solvent extraction technology, their simplicity comes at the cost of additional volume. Despite a more complex design, column extractors are in general more space efficient than mixer settlers. This is because there are rarely clearly defined boundaries for mixing and settling within an extractor column. Since this is the case, when comparing the two technologies, the space that a piece of equipment requires must be compared on a number of stages per unit length basis. In the analogy to a distillation column, this is like defining the height of a transfer unit. On the other hand, the rate at which the product is produced is also a variable of consideration. This parameter will be dependent upon the flow rate within the system. Since the diameter of the column is also a factor of design, the flow rate is defined on a volumetric flow rate per unit cross sectional area basis. A comparison of these properties of various solvent extraction techniques can be found in Figure 16

Table 26.

Two important factors to consider when designing a solvent extraction system are the flow rate and extractant volume of the equipment. When innovating within constraints, the amount of physical space that a system requires can be critical. For example, while mixer-settlers are the simplest solvent extraction technology, their simplicity comes at the cost of additional volume. Despite a more complex design, column extractors are in general more space efficient than mixer settlers. This is because there are rarely clearly defined boundaries for mixing and settling within an extractor column. Since this is the case, when comparing the two technologies, the space that a piece of equipment requires must be compared on a number of stages per unit length basis. In the analogy to a distillation column, this is like defining the height of a transfer unit. On the other hand, the rate at which the product is produced is also a variable of consideration. This parameter will be dependent upon the flow rate within the system. Since the diameter of the column is also a factor of design, the flow rate is defined on a volumetric flow rate per unit cross sectional area basis. A comparison of these properties of various solvent extraction techniques can be found in Figure 16

Table 26. Comparison of the features and uses of different solvent extraction equipment [18].

| **Type of Extractor** | **General Features** | **Fields of Industrial Application** |
|---|---|---|
| Mixer-settlers<br>• Stirred vessels with integral or external settling zones | • High stage efficiencies with long residence time<br>• Suitable with high-viscosity liquids<br>• Can be adjusted in the field (good flexibility)<br>• With proper mixer-settler design, can handle systems with low to high interfacial tension<br>• Can handle high production rates | • Petrochemical<br>• Nuclear<br>• Fertilizer<br>• Metallurgical |
| Static extraction columns<br>• Spray column<br>• Baffle column<br>• Packed column<br>• Sieve tray column | • Deliver low to medium mass-transfer efficiency<br>• Simple construction (no internal moving parts)<br>• Low capital cost<br>• Low operating and maintenance costs<br>• Best suited to systems with low to moderate interfacial tension<br>• Can handle high production rates | • Petrochemical<br>• Chemical<br>• Food |

| | | |
|---|---|---|
| Rotary-agitated columns<br>• Rotary disc contactor (RDC)<br>• Asymmetric rotating disc (ARD) contactor<br>• Oldshue-Rushton column<br>• Scheibel column<br>• Kühni column | • Can deliver moderate to high efficiency (many theoretical stages possible in a single column)<br>• Moderate capital cost<br>• Low operating cost<br>• Can be adjusted in the field (good flexibility)<br>• Suited to low to moderate viscosity (up to several hundred centipoise)<br>• Well suited to systems with moderate to high interfacial tension<br>• Can handle moderate production rates | • Petrochemical<br>• Chemical<br>• Pharmaceutical<br>• Metallurgical<br>• Fertilizer<br>• Food |

.

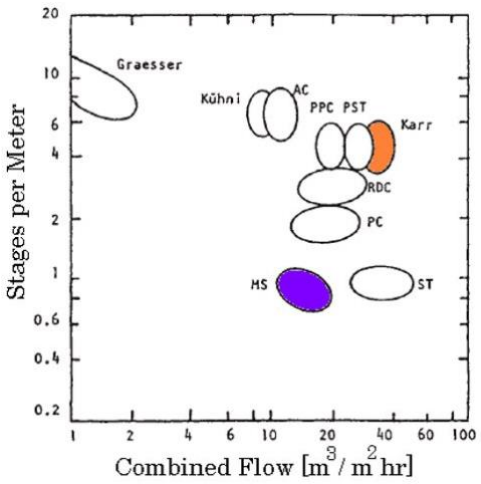


AC - Agitated Cell

PPC - Pulsed Packed Column

PST - Pulsed Sieve Tray

RDC - Rotating Disk Contactor

PC - Packed Column

MS - Mixer-Settler

ST - Sieve Tray

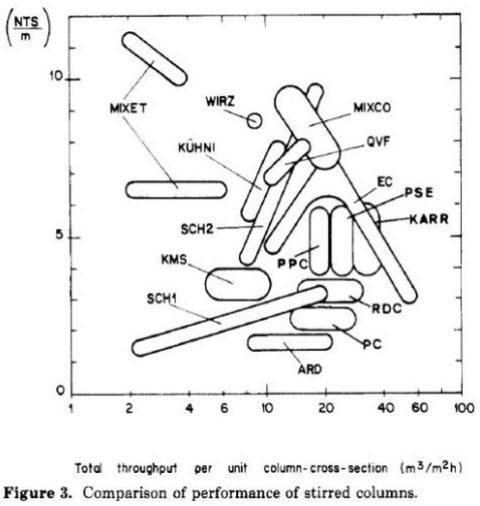


**Figure 3.** Comparison of performance of stirred columns.

ARD - axisymmetric rotating disk

SCH - Scheibel

MIXCO -mixed column

EC - enhanced coalescence

KMS - Kuhni mixer-settler

PSE - pulsed sieve plate extractor

MIXET - mixer-settler extraction column

Figure 16. Charts comparing the volumetric flowrate per unit cross sectional area versus the number of stages per unit height [19, 20].

*Mixer-Settlers* - The most common solvent extraction technology is the mixer-settler. As the name suggests, there are two stages: a mixing stage and a settling stage [21]. The mixing stage forces contact between the aqueous and organic phases through agitating the solution. This forced convection encourages the mass transfer of specific elements from one phase to the other. Next, the solution flows into a settling tank. Because the liquid and organic phases are immiscible, phase disengagement occurs due to density differences. The light phase can be extracted from the top and the heavy phase can be extracted from the bottom. Furthermore, these individual streams can be run countercurrent to additional mixer-settlers for continued separation. A depiction of one mixer settler unit is showcased in Figure 17.

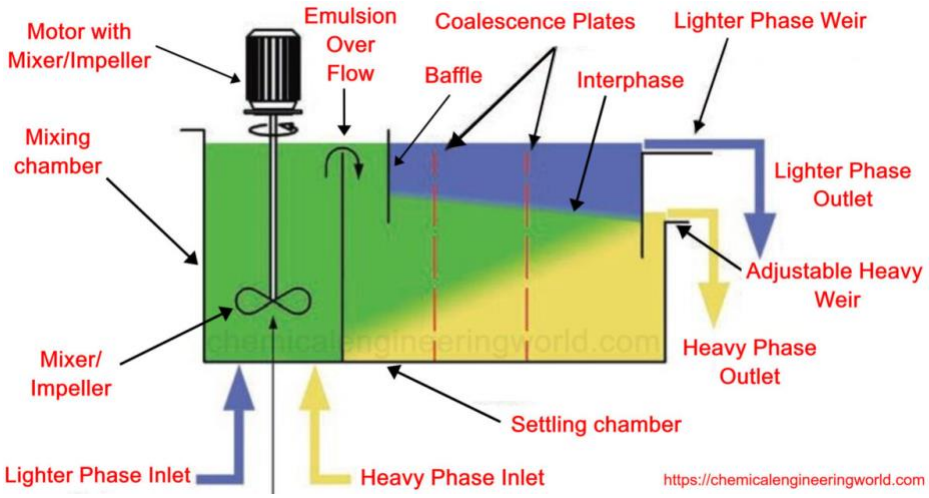


Figure 17. A mixer-settler operating unit diagram [21].

*Column Extractors* - An alternative to the conventional mixer-settlers is the column extractors. Column extractors are most analogous to a distillation column. Instead of liquid and vapor phases, column extractors have aqueous and organic phases [22]. Also, both operate on the principle of

separating the internal phases by density. At its most basic, column extractors encourage contact between the aqueous and organic phases by forcing them into intimate contact with each other as they either flow counter currently. In other words, the heavier phase enters from the top, so that as it settles to the bottom it must interact with the lighter phase that is entering the column through the bottom. This principle can be seen in Figure 18.

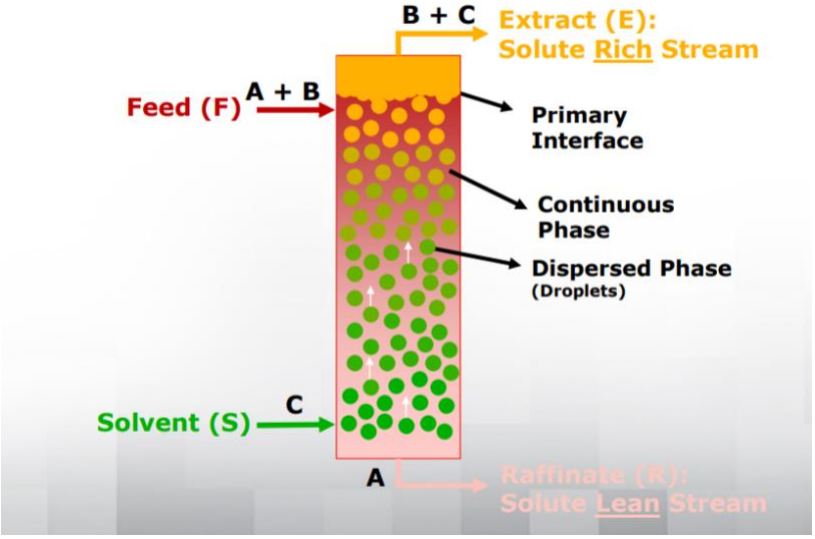


Figure 18. Diagram of a column extractor [22].

These column extractors can be further designed to enhance efficiency between the aqueous and organic interactions. In general, there are two approaches: static and agitated column extractors [18]. As the names suggests, agitated columns add a moving element to the internal structure whereas static columns do not.

*Static Column Extractors* - As aforementioned, static columns seek to enhance separations through non-moving internal designs. Overall, these columns seek to encourage these phase interactions though an increase in internal surface area. A few of the most popular designs for static columns can be found in Figure 19.

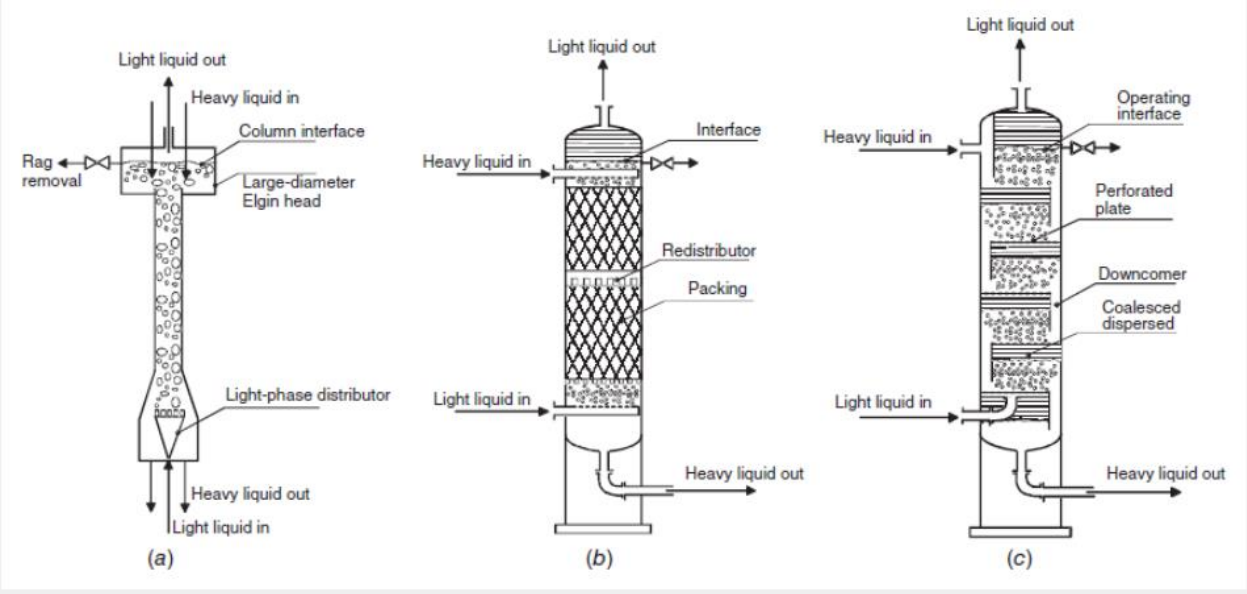


Figure 19. Diagram of a) Spray Column, b) packed column, and c) sieve tray column [18].

The three main types of static columns are spray, packed, and sieve tray columns [18]. Spray columns are the most basic of the three. This technology simply runs the streams in the countercurrent manner [18]. Therefore, this design has the least amount of surface area possible between the three designs. The other two technologies are most familiar to the distillation industry: packed and sieve tray columns. Packed columns implement various packing material into the column to force the flow of the two phases to take indirect routes [18]. As the two phases are forced closer into contact with one another, the transfer of elements from one phase to the other becomes more efficient. Finally, sieve tray columns operate by minimizing axial mixing [23]. The sieve trays provide a surface area for which the interaction between the two phases is encouraged.

*Agitated Column Extractors* - The counterpart to static columns is agitated column extractors. These technologies incorporate a moving element to encourage phase interactions through forced convection in addition to the contact that the phases are already having due to their density differences. There are many different designs for agitated columns, but the most general designs are the rotating disc contactor, Scheibel, and Karr column [18]. A diagram of the rotating disc column can be seen in Figure 20.

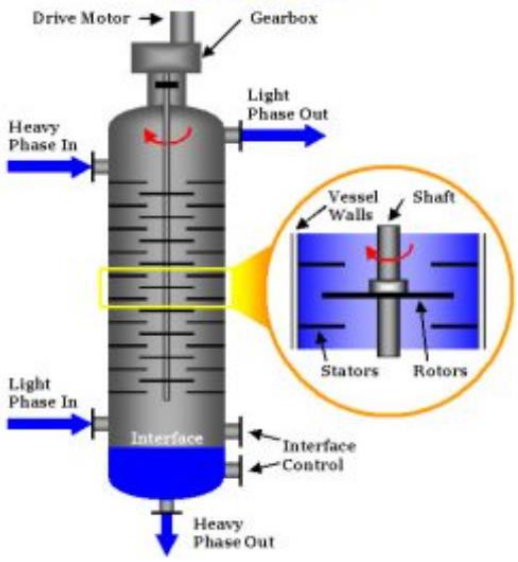


Figure 20. Diagram of a rotating disc contactor column [24].

As the name suggests, rotating disc contactor columns operate using smooth disks being turned by a central shaft [23]. Each rotating disc section is separated by baffles to encourage centripetal mixing without allowing the solution to avoid agitation by moving up the sides. Instead, for the phases to reach their respective outlets, they must move through several stages of forced convection.

A diagram of the Scheibel column, also referred to as a rotating-impeller column, can be seen in Figure 21.

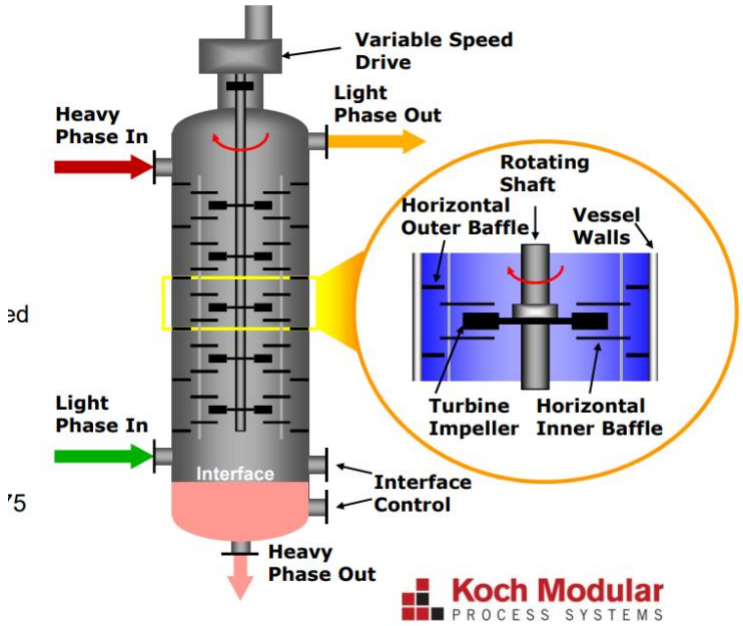


Figure 21. Diagram of a Scheibel column [24].

The Scheibel column shares a similar principle to the rotating disk contactor: mixing in the direction perpendicular to the flow of the fluids. The primary difference between the designs is that the Scheibel column incorporates turbine impellers instead of rotating disks [18]. This increases turbulence and subsequently the phase interactions. Furthermore, the baffle structure is slightly different allow the fluid to flow within a different pattern structure. This baffle design is what allows the column to have a higher efficiency [18].

Finally, the Karr column, also known as a reciprocating plate column, can be seen in Figure 22. The Karr column provides mixing in a direction opposite to that of the rotating disc contactor and Scheibel columns. The internal plates of a Karr column a designed with multiple holes through them to allow the fluid to pass through it [18]. However, these plates are also connected to an internal shaft which simultaneously moves the plates up and down in a jigging motion [24]. Here, the mixing of the two phases is parallel to the direction of flow. The force of this mixing can also push the direction of flow forwards and backwards for increased turbulence.

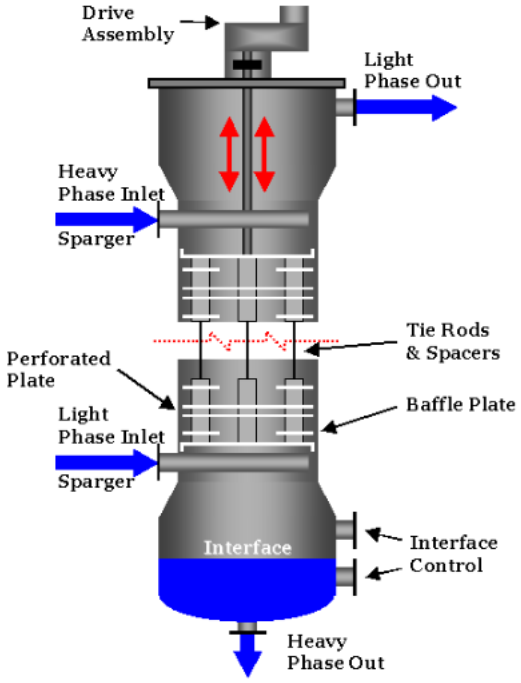


Figure 22. Diagram of a Karr column [24].

Taken as a whole, these columns may be considered a starting point for the propensity to assist solvent assisted chromatography

*Market Utilization of Separation and Purification Techniques* - As part of the project a survey was conducted of sites performing separations and purification of REEs at or near commercial in scale. The facilities located were (see Figure 23):

1. NeoMetals in Estonia;
2. Solvay in La Rocelle France;
3. Lynas in Malaysia;
4. MP Materials in USA;

5. Blue Line/Lynas in USA;
6. Ucore in Canada;
7. IBC in USA;
8. Rare Earth Salts in USA.

Neometals in Estonia was previously Silmet Rare Metals. From an investor presentation [25], Neo metals provides insights into their global supply chain which includes domestic sources such as those processed by Energy Fuels in Utah (see Figure 24). Another interesting discovery is what appears to be Energy Fuels diversification of feed stocks. Energy Fuels is a uranium and vanadium producer, which means they are permitted to process radioactive materials. This appears to allow them to process monazite type materials from sands as shown by a source in Georgia and more recently by a press release from Iperion [26]. From observed photos shown (see Figure 25), it appears that Neometals utilizes conventional SX Technologies.

From publicly available sources [27] Solvay has acquired La Rochelle facility located in France. Appearances (see Figure 26) indicate a standard solvent extraction system. Lyans also is operating and standard solvent extraction flow sheet (see Figure 27 and 22) which appears to produce La, Ce and a Nd/Pr product. Subsequently, it appears that there is a joint project in Texas with Blue Line for the processing of heavy rare earths [30][31]. Not much information is available other than DOD funding appears to have been procured for this project.

Other notable mentions for near commercial separations technologies in this space are Ucore, Rare Earth Salts, and IBC. Ucore which is a Canadian Company claiming access to what they term "Rapid SX" which appears to be a derivative of standard SX technologies [32]. Other technologies are Rare Earth Salts [34][35] utilize which appears to be an electrochemical method to produce a rare earth oxide at the cathode using a multistage electrochemical process [36]. From press releases [34] it appears that they have separated europium oxide with a purity of 99.9% and Yttrium oxide with a purity of 99.8%. They note that the first commercial deliveries of lanthanum oxide occurred in 2020. IBC out of Salt Lake City Utah is notable in the production of molecular recognition ligands for the separation of REEs. Press releases from Ucore indicate that they had option to acquire the technology but did not exercise the option.

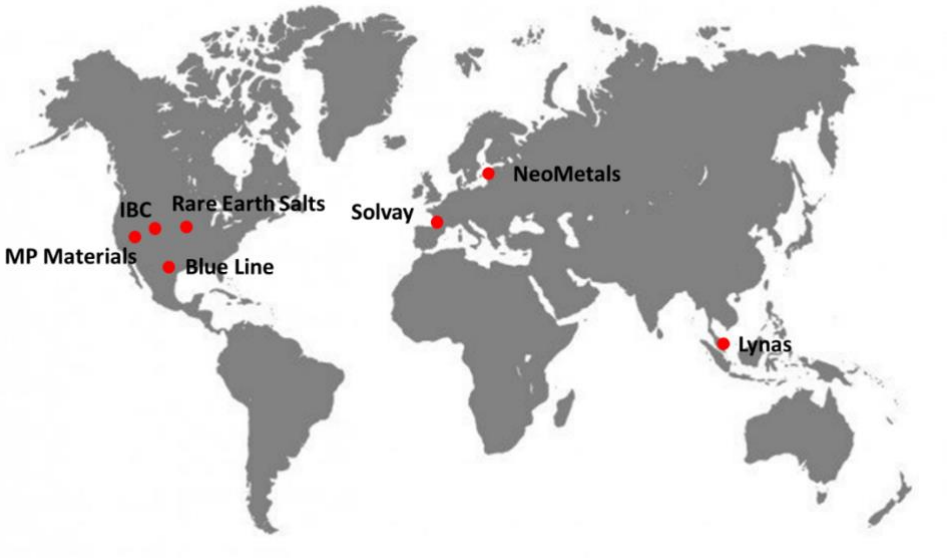


Figure 23. Location of Commercial or Near Commercial Facilities Identified World-Wide.


Figure 24. Neo Performance Materials Global Supply Chain [25].


Figure 25. Neo Performance Materials Separation Facility Utilizing SX [25].


Figure 26. Solvay Rare Earth Facility La Rochelle France [27].

**Solvent Extraction Process Overview:**

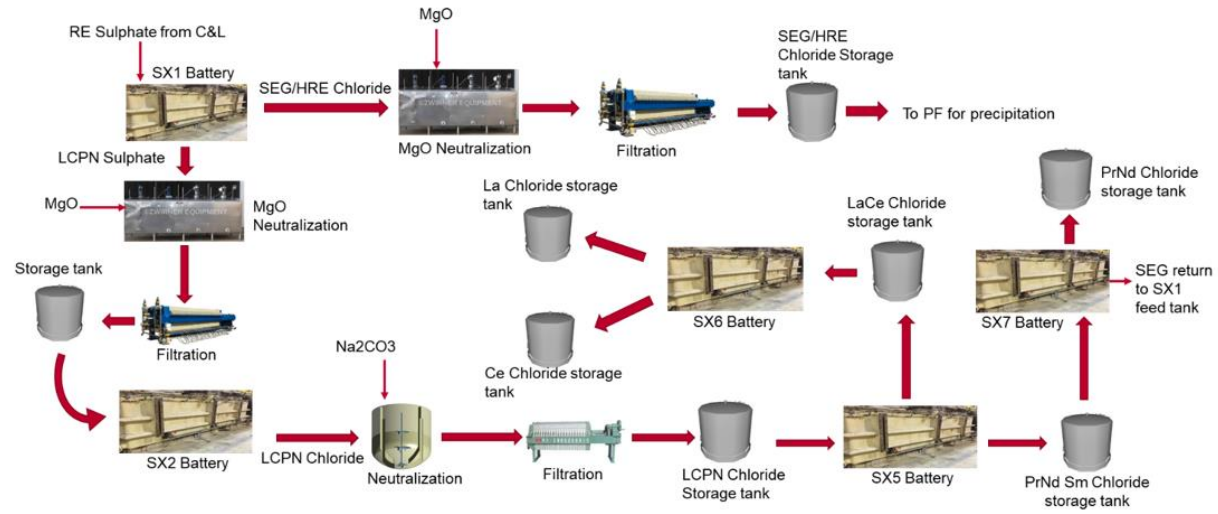


Figure 27. Lynas Malaysia Conceptual Flowsheet [28].


Figure 28. Picture of Lynas SX Facility [29].

To complete the market analysis, a brief review of mining projects was conducted based on the work of Jaroni et al. [38]. A review was performed to refresh the data set to determine recent ownership and an attempt to ascertain the proposed method of REE separation (see Table 27). The overwhelming majority show the contemplation of SX as the method of choice for REE separations currently.

Table 27. Review and Comparison of Mining Projects under consideration based on [38].

| Project | Country | Company | Capacity (mt/Year) | Separation | Reference |
|---|---|---|---|---|---|
| Steenkampskraal | South Africa | Steenkampskraal Monazite Mine (PTY) LTD | 2 | Sale of Concentrate - Feasibility | • https://www.steenkampskraal.com processing/<br>• https://www.steenkampskraal.com media-2/ |
| Mount Weld Phase 1 | Australia | Lynas Corporation Ltd. | 11 | SX (Malaysia) | • https://www.miningmagazine.com chemicals-reagents/news/1364528/lynas-and blue-line-mou-for-rare-earths-separation |
| Ngualla | Tanzania | Peak Resources Ltd. | 10 | SX (UK) - Feasibility | • https://peakrareearths.com/teessid -refinery/<br>• https://wcsecure.weblink.com.au/ df/PEK/02440680.pdf |
| Bear Lodge | USA | Rare Element Resources Ltd. | 7.5 | SX | • https://www.rareelementresource com/bear-lodge-project/proposed operations#.YhUXbujMLAQ |
| Nolans | Australia | Arafura Resources Ltd. | 20 | ??? - FEED Study | • https://www.arultd.com/images/P sentations/20210909_NWM_Cor erence.pdf |
| Zandkopsdrift | Namibia/ South Africa | Frontier Rare Earths Ltd. | 20 | Suspect SX | • http://www.frontierrareearths.com wp-content/uploads/2015/06/Frontier Corporate-Presentation-June-2015.pdf |

| | | | | | |
|---|---|---|---|---|---|
| Nechalacho Basal | Canada | Avalon Rare Metals Inc.<br>Vital Metals | 7 | SX (France) | • https://www.cbc.ca/news/canada/orth/avalon-partners-with-french-company-to-process-rare-earths-1.2572606<br>• https://vitalmetals.com.au/metallu gy/ |
| Browns Range | Australia | Northern Minerals Limited | 3 | Suspect concentrate - Pilot Plant | • https://northernminerals.com.au/t owns-range/browns-range-pilot-plant/ |
| Lofdal | Namibia | Namibia Critical Metals | 1.5 | Mine | • https://www.namibiacriticalmetal com/projects/lofdal-heavy-rare-earths-project |
| Bokan | USA | UCORE | 1.8 | SX | • https://ucore.com/rapidsx/#:~:tex RapidSX%E2%84%A2%20%E2 80%93%20Ucore%20Rare%20M tals%20Inc.&text=The%20Rapid X%E2%84%A2%20platform%2( s,critical%20and%20other%20m al%20feedstocks. |

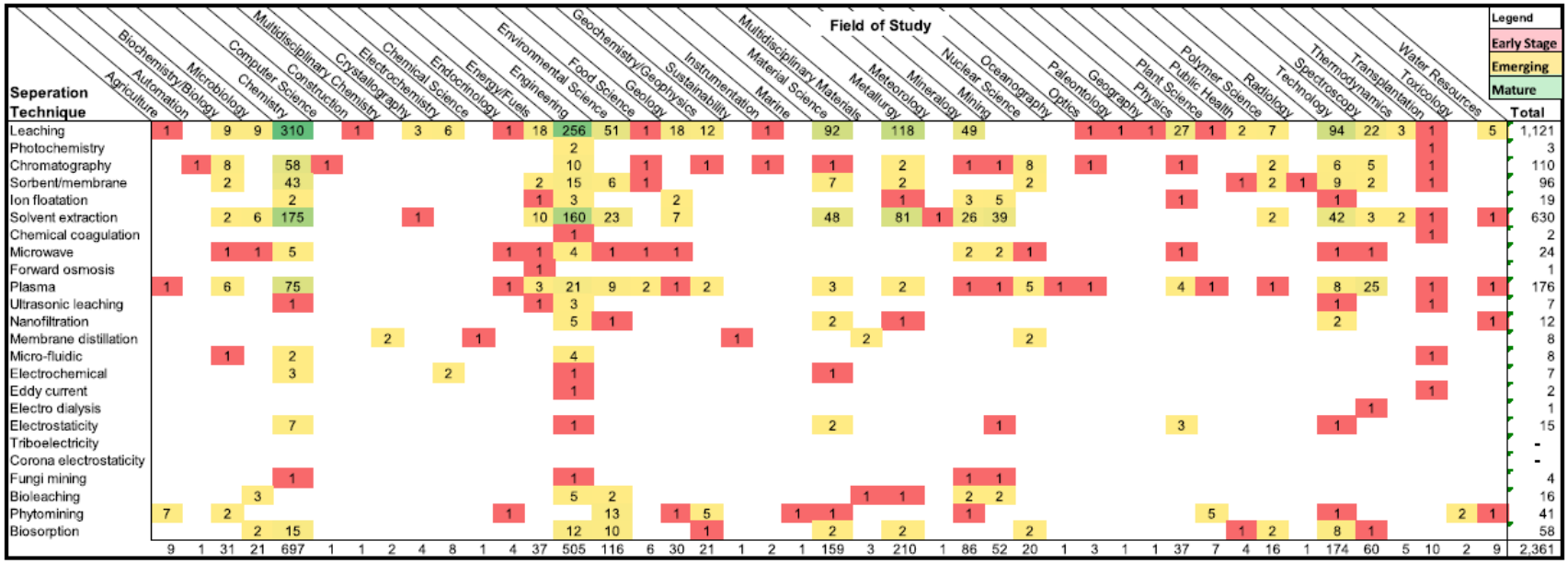


Figure 29. Matrix of Separation Techniques by Field of Study and Publication Quantity [39].

*Additional REE Separation Methods* - To complete the review section an additional reference is shown in Figure 29 depicting the results of a review paper showing the various methods of separation of REEs. Of these, several seem to be less applicable with chromatography, sorbent/membrane, ion flotation, solvent extraction, chemical coagulation, forward osmosis, membrane distillation, micro-fluidic, electrochemical, electrodialysis, phytomining, and biosorption being relevant and of interest to the present study.

### *2.5.2 Subtask 5.2 – Extractant Selection*

Two extractants were selected for SAC modeling, DODGAA and DEHPA. The major benefit of DODGAA is its ability to separate contaminant elements such as calcium, aluminum, and iron from the rare earth elements (REEs). While more popular extractants such as Di-(2-ethylhexyl)phosphoric acid (DEHPA) are better at individually separating REEs, the contaminant elements are often co-extracted in such systems. Therefore, DODGAA was modeled with the intent to remove the impurities before separating the REEs from one another. For this same reason DEHPA is used in the second train. The reasoning is provided in the next sections and based on separability.

### *2.5.3 Subtask 5.3 – Solvent-Assisted Chromatography*

*Principles of Solvent Assisted Chromatography* - By definition, solvent assisted chromatography (SAC) is a select modification solvent extraction (SX) techniques that develops staged based separations that create chromatography-like bands for individual elements. The key to creating these highly selective and efficient separations are the following four principles:

1. Refluxing concentrated aqueous streams.
2. Utilizing pH changes across the system.
3. Controlling the saturation of the organic phase.
4. Manipulating the ion selectivity of the organic phase.

When reviewing at SAC on a stage-by-stage basis, the concentration of elements should resemble the standing waves seen in Figure 30. These peaks can be selectively tapped for individually separated high purity elements.

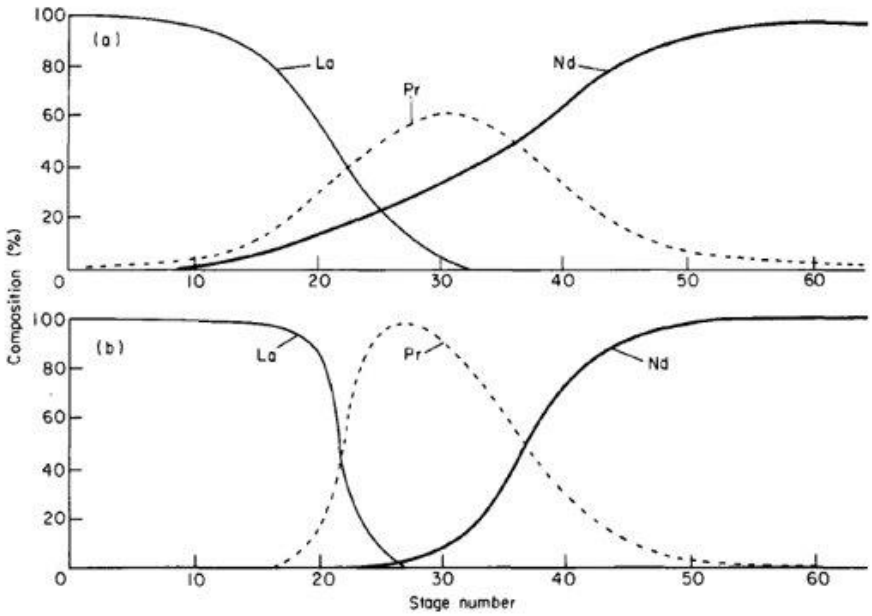


Figure 30. Solvent assisted chromatography stage-based element waves [40].

In standard SX, only binary separations occur. While it is most common for the organic phase to be recycled after stripping, refluxing the aqueous phase brings greater definition to the separations. This principle is demonstrated in Figure 31.

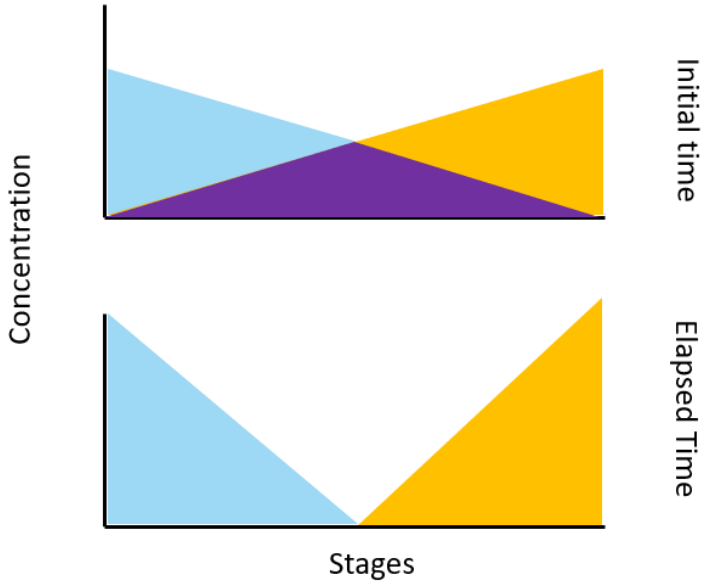


Figure 31**.** The impact of refluxing the aqueous phase on the binary separation of elements in solvent extraction.

The phase in which the elements will be located in is dictated by the pH of the system. This relationship can be seen in Figure 32 for the exractant DODGAA.

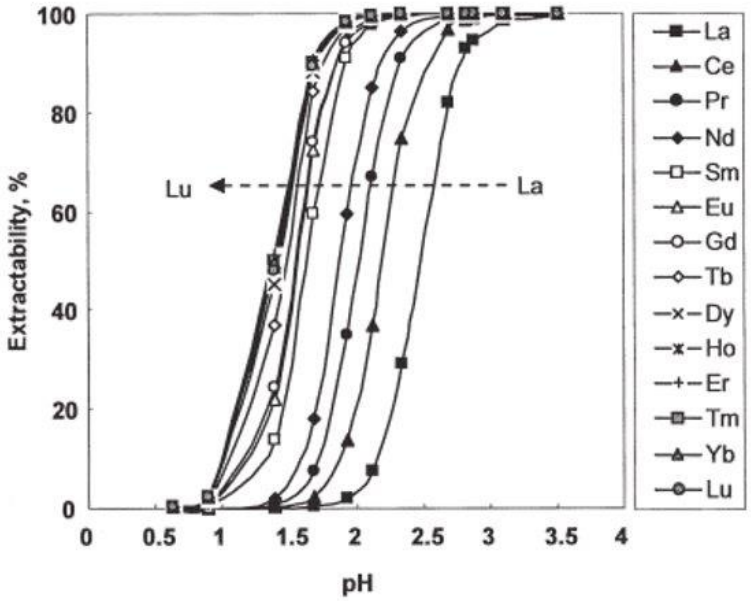


Figure 32. The relationship between pH and percent extraction for DODGAA in solvent extraction [41].

In standard solvent extraction, pH is held constant to selectively load elements into the organic phase. Conversely in solvent asssisted cromatography, the pH changes are implemented throughout the system through manipulating the ionic strength of the aqueious phase and refluxing the remanents. As a result, the pH of the system becomes more of a gradient as the stages progress.

Another deviation from standard SX practices is the intentional saturation of the organic phase. Most SX systems deal with dilute solutions. However, SAC operates by saturating the organic phase in order to contol the number of ions enetering the organic phase. This is specifc principle contributes to the departure from binary seperations. Elements that cannot be loaded into the organic on either ends of the system, can be loaded into the middle stages where the saturation limit has not been reached.

Finally, by manipulating the ion selectivity of the organic phase brings definition to the peaks over time. Because the organic phase will transfer elements into the aqueous phase in preference of other elements, the cromatography like bands will only exist over a specific range of stages. Once the organic finds a more desirable element, it will push all other elements to the aquous phase of to other stages.

While the key principles of SAC mostly relate to the organic phase, the high purity products actually exist in the aqueous phase. Over time, the organic and aqueous phase compositions begin to mirror one another, but the aqueous phase ultimately becomes purer. Therefore, the aqueous phase is the most important to assess and selectively tap for the best quality products.

*Solvent Assisted Chromatography Model Algorithm Design* - Using the aforementioned principles, a MATLAB model was designed to predict the development of the SAC stage-by-stage peaks. The model performs balances based on the following flowsheet seen in Figure 33.

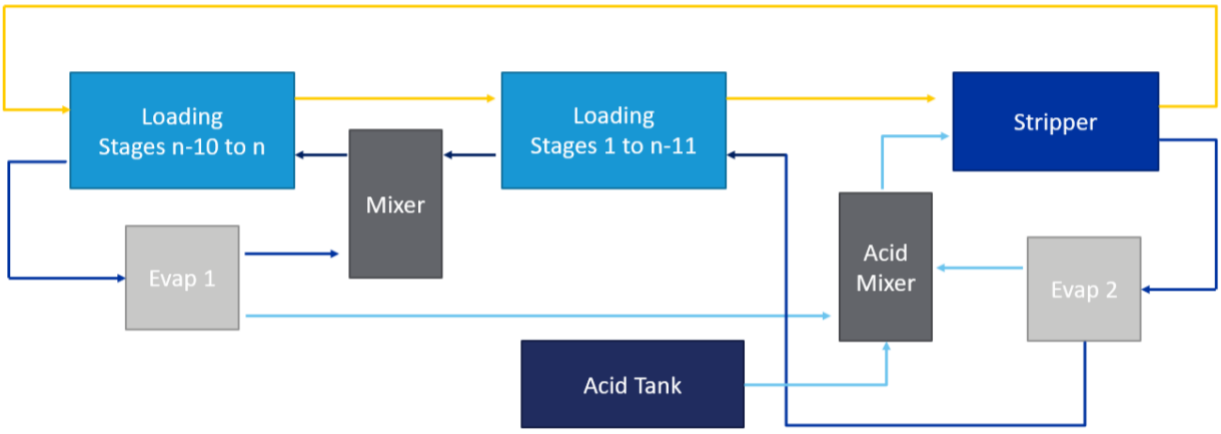


Figure 33. Operations flowsheet for a solvent assisted chromatography system as modeled in MATLAB.

The loading algorithm was constructed to perform calculations on a stage-by-stage basis. For n number of stages, the balances on each stage resemble that of Figure 34.

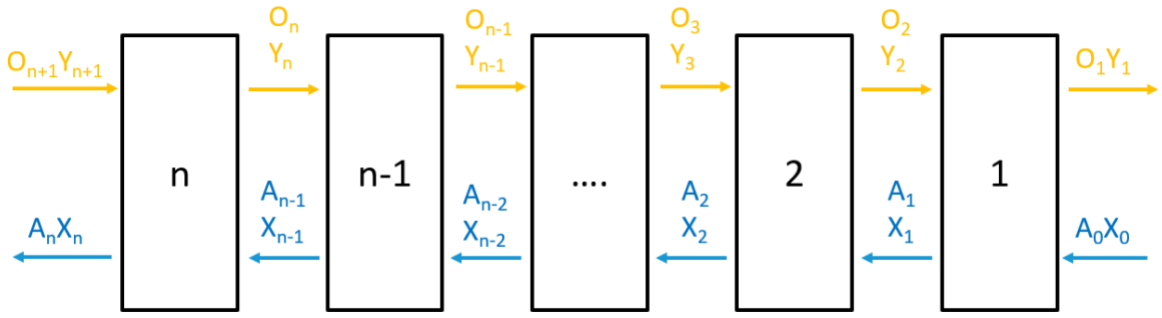


Figure 34. Countercurrent arrangement of flow streams in the loading stages of solvent extraction.

In the above figure, O and A represent the organic and aqueous stream flow rates respectively. Furthermore, Y and X denote the organic and aqueous concentrations respectively. Since the organic and aqueous phases can be assumed to be immiscible, O and A can be written as constant. For an arbitrary stage j, the balance can be simplified to that seen in Figure 35.

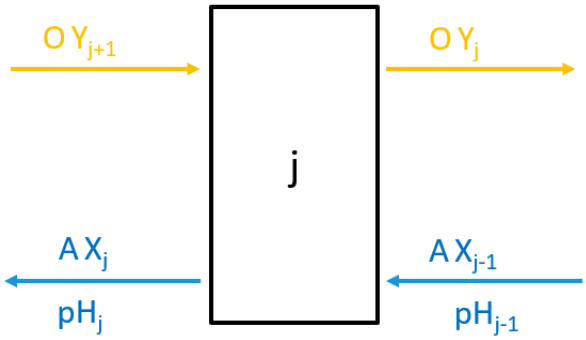


Figure 35. Diagram of the flow streams of a single, arbitrary solvent extraction stage.

Utilizing literature data, percent extraction at each stage can be modeled as a function of pH and curve fit to Equation 1.

$$E_j = \frac{a}{1 + \left(\frac{b}{pH_{j-1}}\right)^c} \tag{1}$$

$E_j$ represents the percent extraction at stage j; $pH_{j-1}$, the pH of the incoming aqueous stream; and a, b, and, c, constants of curve fitting. For example, the fit for yttrium can be seen in Figure 36.

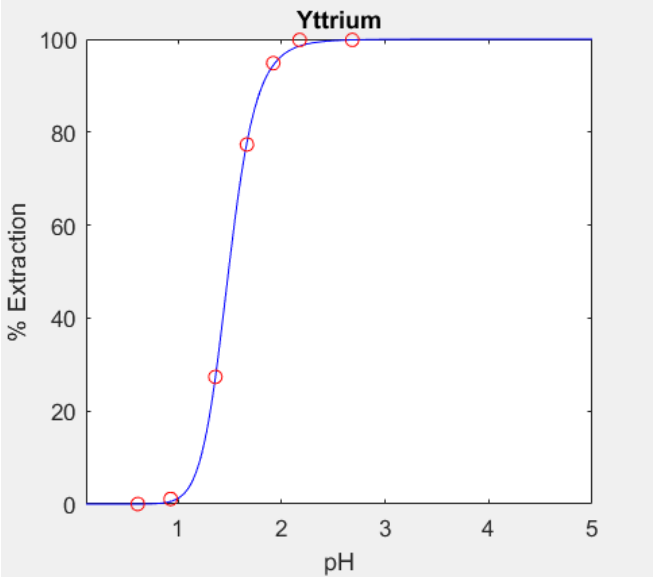


Figure 36. Fitted curve to literature data for the extraction of Yttrium using DODGAA.

After determining the percent extraction, the distribution coefficient is then calculated. Due to SAC principle number 4 (manipulating the ion selectivity of the organic phase), ions can be unloaded into the aqueous phase to make room for more preferable elements. Therefore, it is better to model each stage as a series of equilibriums. This conversion from percent extraction to distribution coefficient, $D_j$, is seen in Equation 2.

$$D_j = \frac{A}{O}\frac{E_j}{\left(100 - E_j\right)} \tag{2}$$

When calculating how many moles of an element are loaded into the organic phase, three limitations must be considered:

1. The number of moles loaded into the organic phase exceeds the saturation limit;
2. The number of moles present in the aqueous phase is less than the number of theoretical moles than can be loaded into the organic phase; and
3. The number of moles to be loaded exceeds the maximum amount as determined by the distribution coefficient.

Using SAC principle number 3 (3.Controlling the saturation of the organic phase), the saturation limit is essential to these separations. This limit can be expressed by controlling the concentration of the ligand, [L]. Since there are multiple elements competing for the same spaces in the organic phase, a ratio of the distribution coefficients is implemented to ensure that elements are loaded in the correct amounts. In other words, if two elements both have a percent extraction of 75% and subsequently the same distribution coefficient, they should have the same number of moles present in the organic phase. However, since the saturation limit must be taken into account, loading 75% of the ions for both elements might not be possible. Furthermore, one element cannot have 75% of its ions loaded and the other have less than 75% loaded. Instead, under these conditions, the percent extraction should be viewed as the strength of the element to load in the organic phase. Therefore, a ratio of the "strengths" of an element k over the sum of all the "strengths" of all the elements present is multiplied by the saturation limit to give a better representation of the number of moles that will be extracted into the organic phase as depicted in Equation 3. It is important to note that method of "strength" is intended to serve as a reasonable approximation to a more rigorous thermodynamic approach.

$$n_{k,ext} = \frac{D_{k,j}}{\sum D_{k,j}}\frac{O[L]}{3} \tag{3}$$

Furthermore, this creates a model for representing SAC principle 4. The elements that are most preferable to the organic will be the elements with the highest distribution coefficients or "strengths." In accordance with loading limitation number 2, the number of moles calculated by Equation 3 must not exceed the number of moles entering the stage. The number of moles entering stage j of an element k can be calculated by Equation 4.

$$n_{k,in} = OY_{k,j+1} + A\,X_{k,j-1} \tag{4}$$

For simplicity, it is easiest to think of the algorithm as stripping everything from the incoming organic phase and combining it with the entering aqueous phase and redistributing the element mass amongst the outgoing two phases. At this point, the loading limitation (based on the extractant concentration) must be checked for and the number of moles calculated accordingly. A flow diagram of this process can be seen in Figure 37.

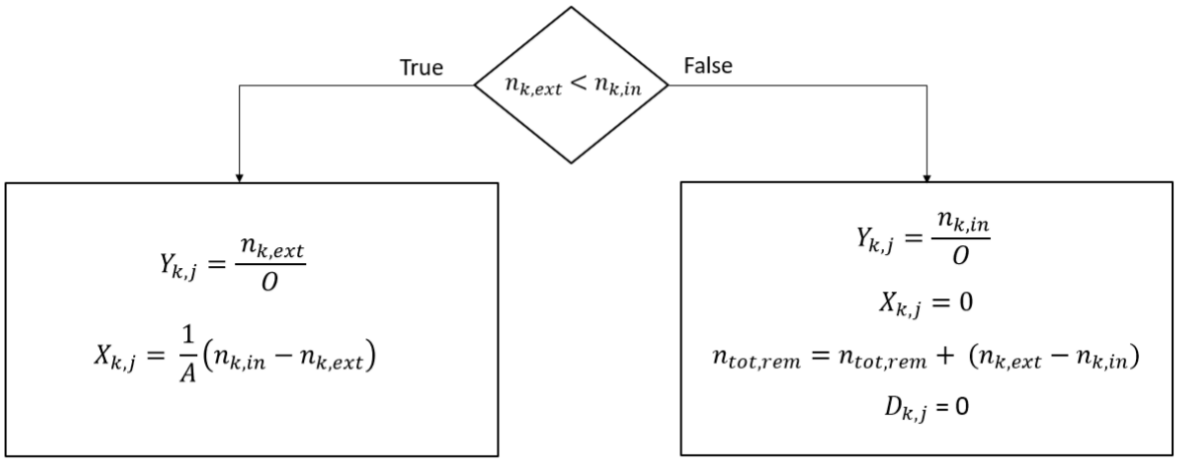


Figure 37. Programming flowsheet for loading algorithm: initial phase.

If the limitation is reached, all the moles available are loaded into the organic phase and a counter on the available moles remaining in the organic phase is started. Also, the distribution coefficient is considered as zero as to update the "strengths" ratio of the remaining elements. If there is remaining space in the organic available, the program will enter a loop. It begins by modifying Equation 3 for the remaining moles as depicted in Equation 5.

$$n_{k,ext} = \frac{D_{k,j}}{\sum D_{k,j}} n_{tot,rem} \tag{5}$$

Next, the algorithm uses Equation 6 to calculate the remaining moles for each element.

$$n_{k,rem} = O\left(Y_{k,j+1} - Y_{k,j}\right) + A\, X_{k,j-1} \tag{6}$$

Then, the maximum number of moles that can be present in the organic phase as determined by the distribution coefficient is computed via Equation 7.

$$n_{k,max} = \frac{O\, n_{k,in}}{\frac{A}{D_{k,j}} + O} \tag{7}$$

Using the results from Equations 5, 6, and 7; All three loading limitations are checked, and the outlet streams are computed accordingly as seen in flowchart in Figure 38.

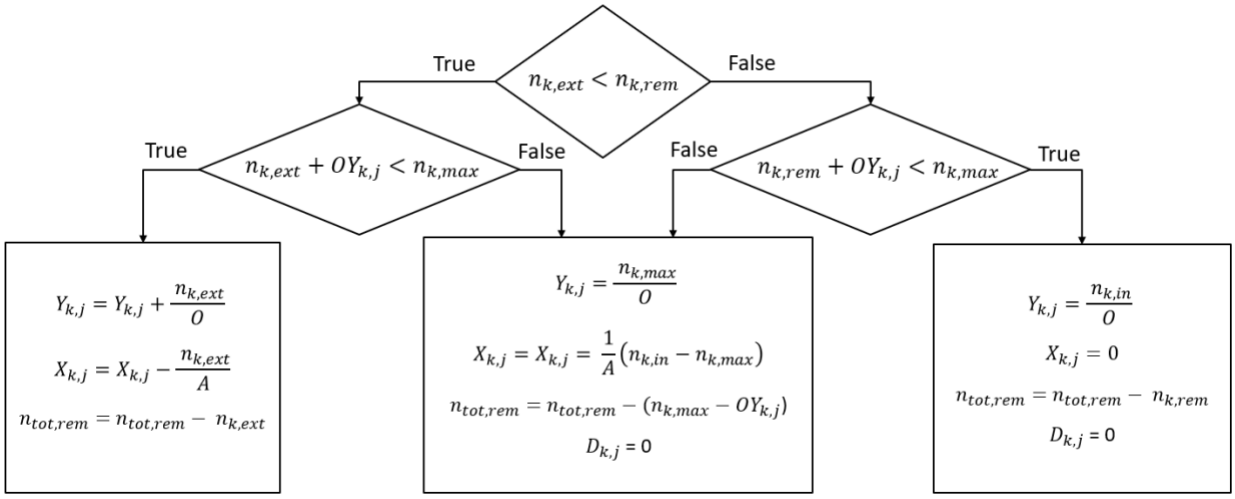


Figure 38. Programming flowsheet for loading algorithm: convergence phase.

Like with the flowchart in Figure 37, this flowchart begins by determining the limiting reagent. Unlike the first flowchart, this one also considers loading limitation number 3 by comparing to the maximum number of moles allowable by the distribution coefficient. This step is repeated until no more moles can be loaded into the organic phase. Finally, the outlet pH calculated using Equation 8.

$$pH_j = -Log\left((10^{-pH_{in}}) + \frac{1}{3}\left(O[L] - n_{tot,rem}\right)\right) \tag{8}$$

This loading algorithm is repeated for each stage until all the outlet streams have been calculated.

*Model Data* - Once the MATLAB model was completed, tests were run to determine the effect of different operating parameters on defining the element peaks and purities. The following variables were considered:

1. pH of the acid used in the stripping section;
2. Saturation concentration of the organic;
3. Total concentration of the elements entering in the aqueous phase;
4. Number of loading stages before and after the reflux stream;
5. Ratio of the acid recovered from the evaporator;
6. Ratio of the flowrates exiting the evaporator;
7. Initial aqueous flowrate; and
8. Organic flowrate.

The first extractant modeled was N,N-dioctyldiglycolamic acid (DODGAA). As discussed in the previous section DODGAA was selected for its elemental selectivity. Table 1 gives a look at the highlights from the DODGAA model tests.

Table 28. DODGAA SAC model test highlights.

| Conditions | Results |
|---|---|
| Stripping pH: 1.5<br>Saturation Limit: 0.003<br>Total Concentration: 0.01<br>Loading Stages: 20 + 10<br>Stripping Stages: 5<br>Acid Recovery Ratio: 0.8<br>Ratio Recovery Flowrate: 0.6<br>Initial Aq. Flowrate: 3<br>Org. Flowrate: 1 | 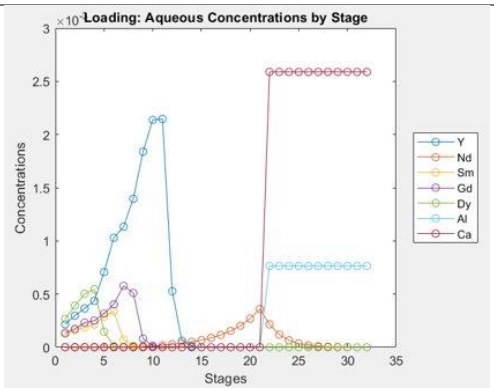 <br> 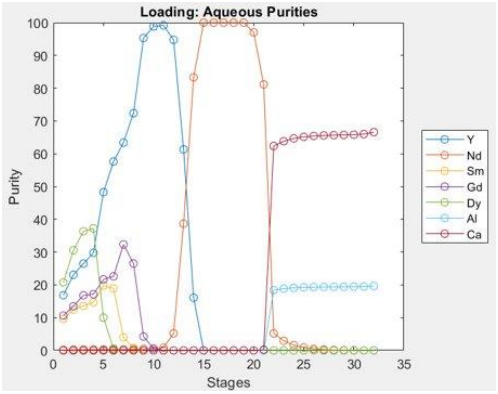 |
| Stripping pH: 1.5<br>Saturation Limit: 0.003<br>Total Concentration: 0.02<br>Loading Stages: 40 + 10<br>Stripping Stages: 5<br>Acid Recovery Ratio: 0.8<br>Ratio Recovery Flowrate: 0.6<br>Initial Aq. Flowrate: 3<br>Org. Flowrate: 1 | 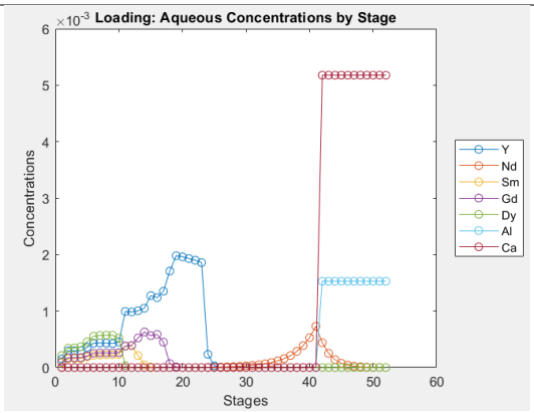 |

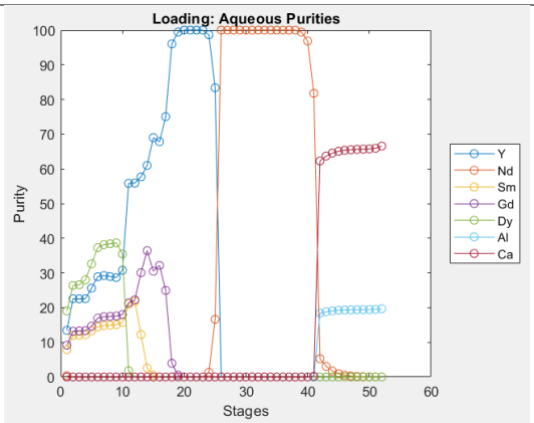


Stripping pH: 1.4

Saturation Limit: 0.003

Total Concentration: 0.02

Loading Stages: 40 + 10

Stripping Stages: 5

Acid Recovery Ratio: 0.8

Ratio Recovery Flowrate: 0.7

Initial Aq. Flowrate: 3

Org. Flowrate: 1

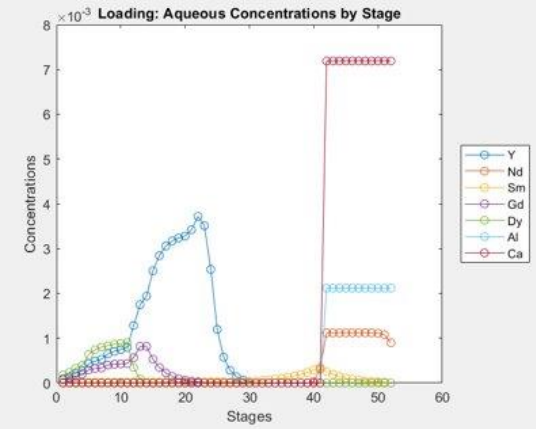


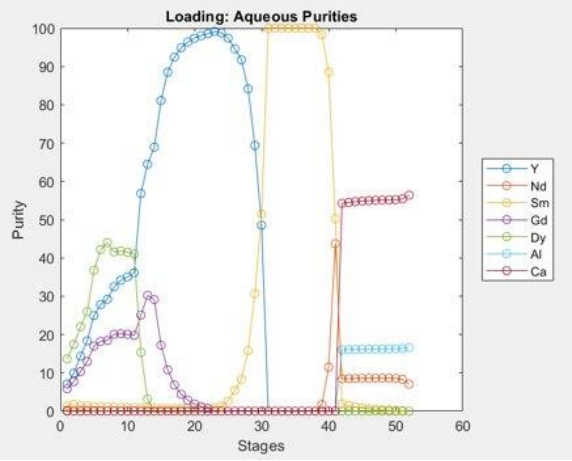

Stripping pH: 1.45

Saturation Limit: 0.003

Total Concentration: 0.02

Loading Stages: 40 + 10

Stripping Stages: 5

Acid Recovery Ratio: 0.8

Ratio Recovery Flowrate: 0.5

Initial Aq. Flowrate: 3

Org. Flowrate: 1

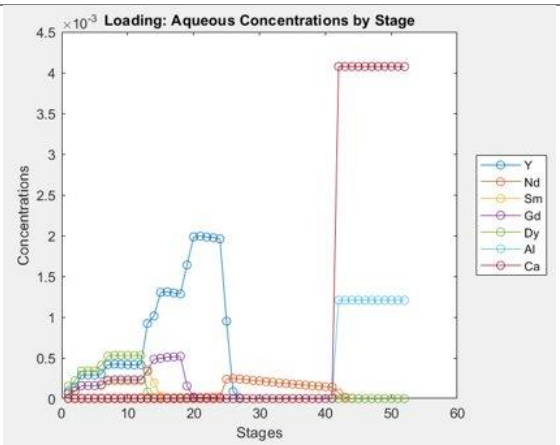


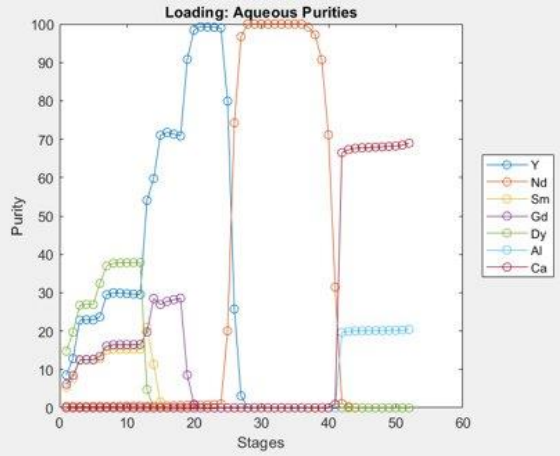


Stripping pH: 1.4

Saturation Limit: 0.0015

Total Concentration: 0.02

Loading Stages: 60 + 10

Stripping Stages: 5

Acid Recovery Ratio: 0.85

Ratio Recovery Flowrate: 0.5

Initial Aq Flowrate: 3

Org Flowrate: 1

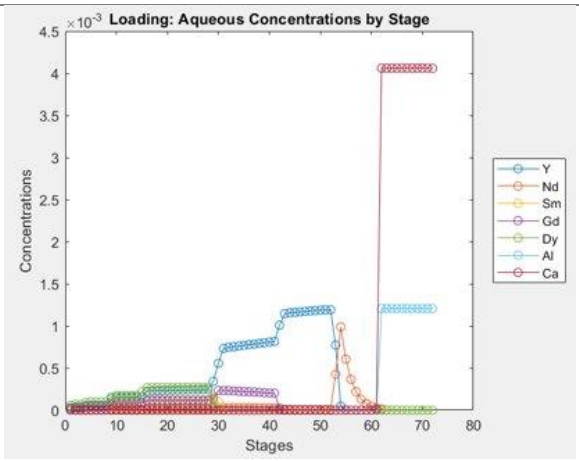

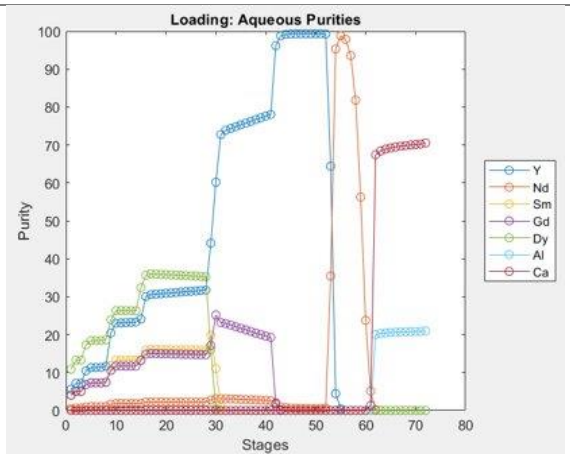


Using the second test in Table 28, four products were determined: a pure Y product, a pure Nd product, a contaminant stream, and an REE mixture. The stages at which these could be tapped as well as their compositions are displayed in Figure 39.

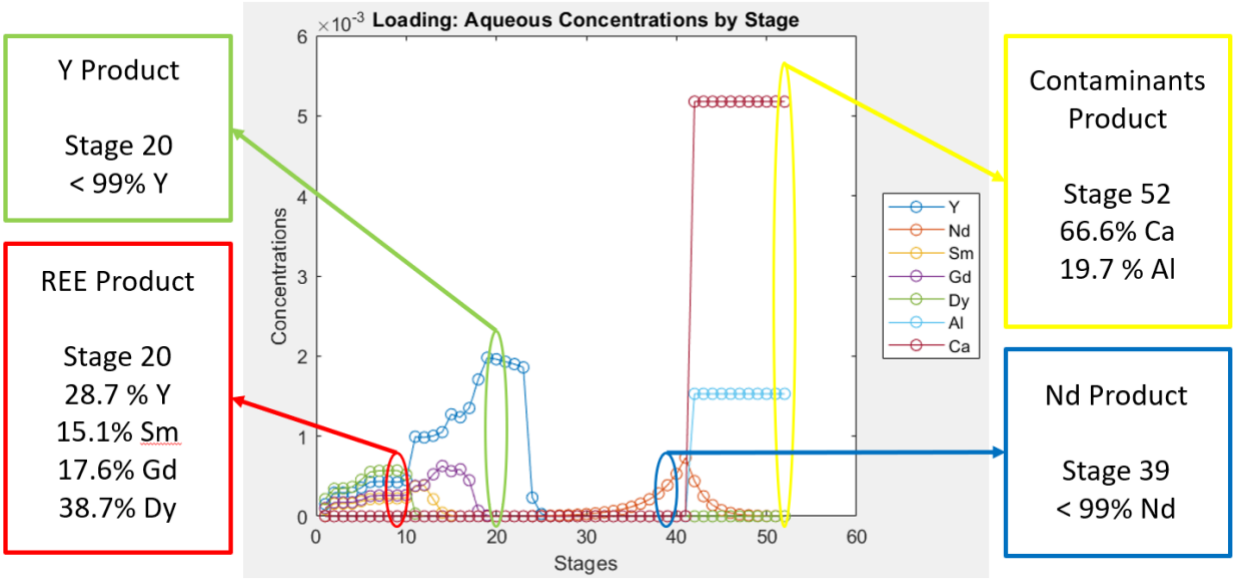


Figure 39. DODGAA SAC model purities and stages for tapping products

Utilizing the REE mixture from stage 20, this product can be taken to second SAC model where it is separated using DEHPA. Table 29 shows the highlights from the DEHPA model tests.

Table 29. DEHPA SAC model test highlights.

| Conditions | Results |
|---|---|
| Stripping pH: 0.4<br>Saturation Limit: 0.015<br>Total Concentration: 0.0739<br>Loading Stages: 40 + 10<br>Stripping Stages: 5<br>Acid Recovery Ratio: 0.9<br>Ratio Recovery Flowrate: 0.5<br>Initial Aq. Flowrate: 3<br>Org. Flowrate: 1 | 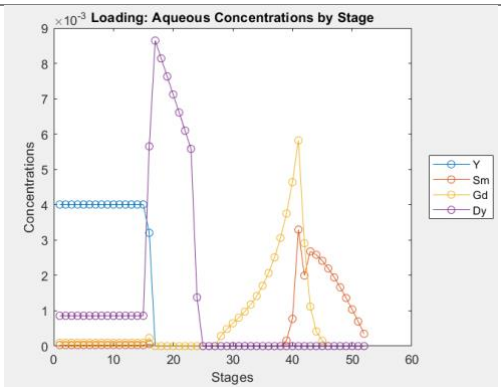 <br> 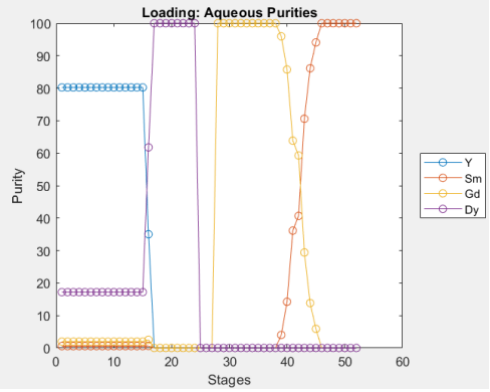 |
| Stripping pH: 0.4<br>Saturation Limit: 0.015<br>Total Concentration: 0.0739<br>Loading Stages: 40 + 10<br>Stripping Stages: 5<br>Acid Recovery Ratio: 0.9<br>Ratio Recovery Flowrate: 0.4<br>Initial Aq. Flowrate: 3<br>Org. Flowrate: 1 | 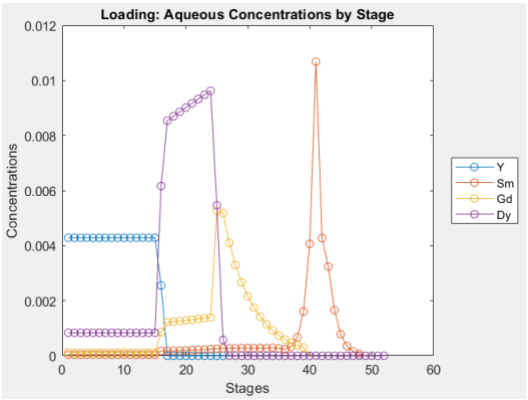 |

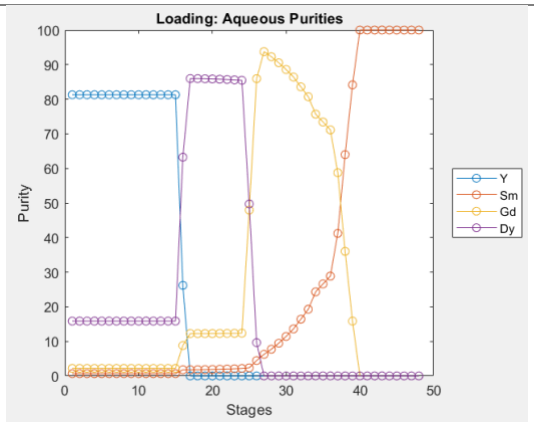


Stripping pH: 0.4

Saturation Limit: 0.012

Total Concentration: 0.0739

Loading Stages: 60 + 10

Stripping Stages: 5

Acid Recovery Ratio: 0.83

Ratio Recovery Flowrate: 0.1

Initial Aq. Flowrate: 3

Org. Flowrate: 1

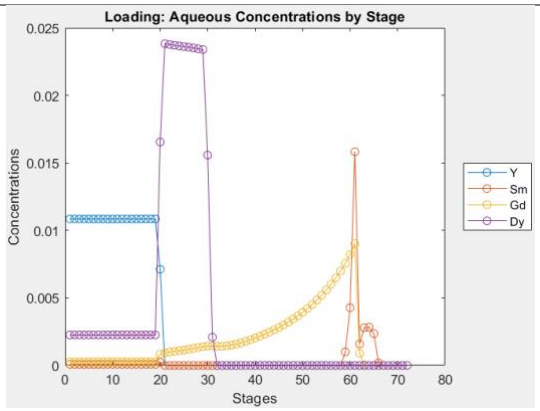


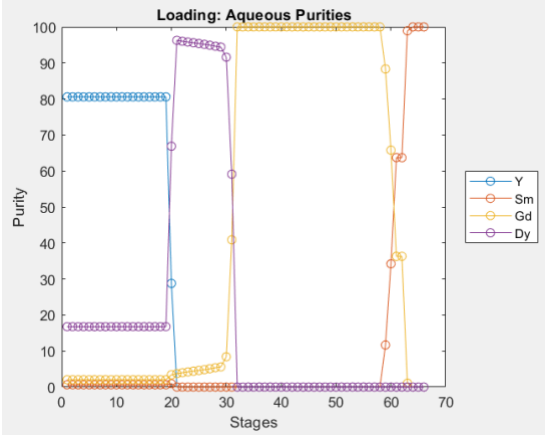

Constant pH: 0.5

Saturation Limit: 0.024

Total Concentration: 0.1478

Loading Stages: 60 + 10

Stripping Stages: 5

Acid Recovery Ratio: 0.855

Ratio Recovery Flowrate: 0.41

Initial Aq. Flowrate: 3

Org. Flowrate: 1

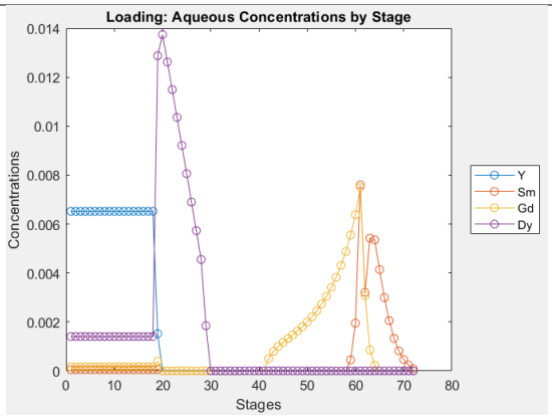


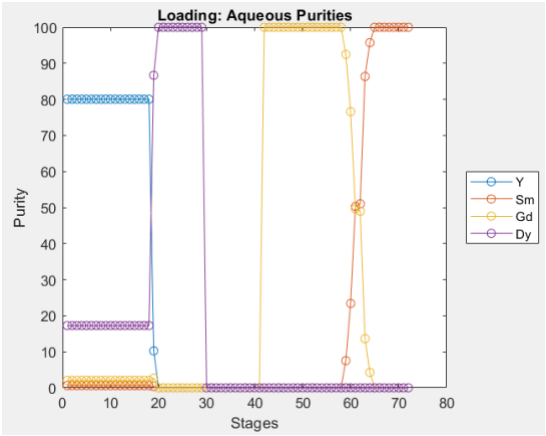


From test 4 of the Table 29, three products can be tapped: pure Dy, Gd, and Sm. The stages and compositions of these products can be found in Figure 40.

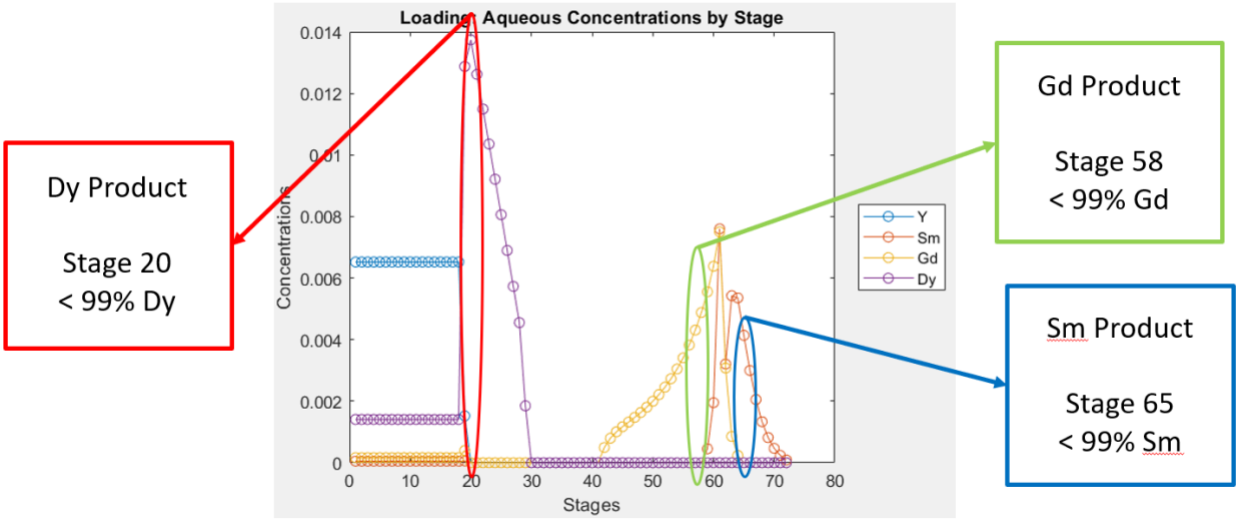


Figure 40. DEHPA SAC model purities and stages for tapping products

When combining the two SAC models, the overall separation tree of elements is represented in Figure 41.

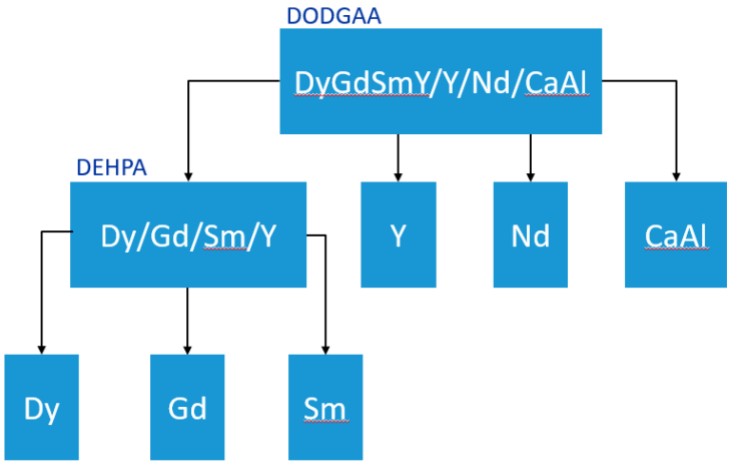


Figure 41. Separation tree of elements based on SAC MATLAB model.

Figure 42 shows the flowsheet for how to create the separations seen in Figure 41 utilizing the learnings from the SAC model tests.

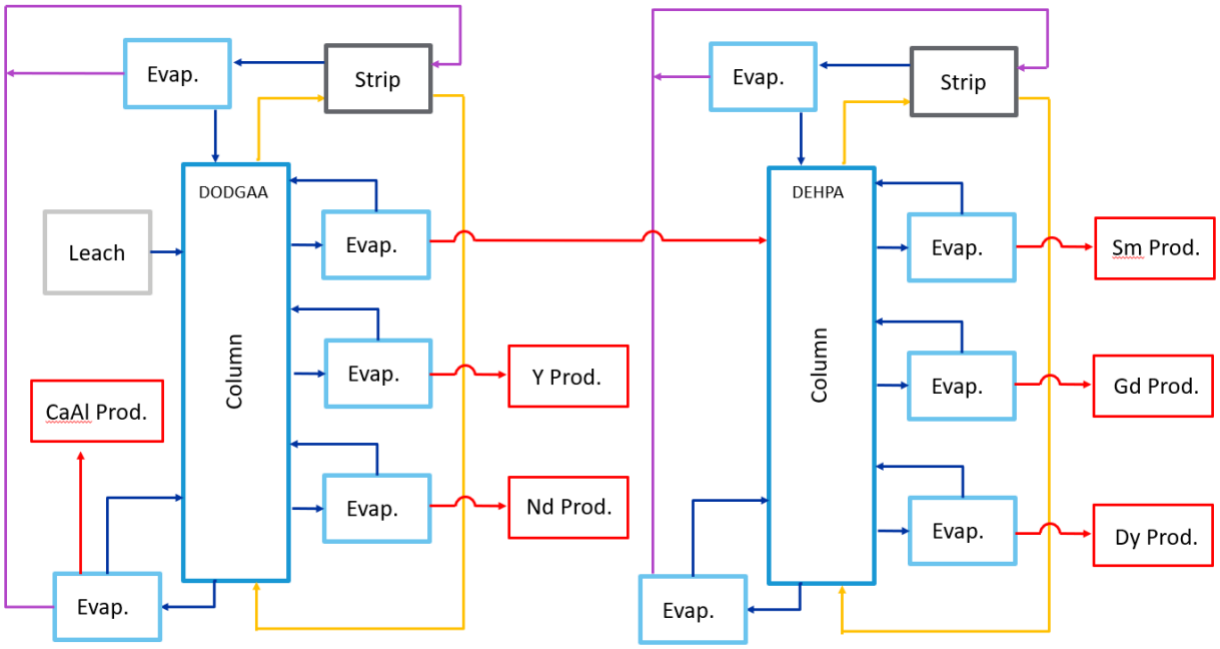


Figure 42. Operations flowsheet for implementing SAC for the separation of the REE mixture.

What proceeded this point was a static demonstration of the SAC concept establishing preliminary modeling capabilities to describe the performance of SAC and will seek to compare this method to several available in the down selection portion of the project. The next sections will be to modify the SAC model in MATLAB has been modified to handle fluid flow into the system rather than batch loading and running to steady state. One of the key questions of the development of the SAC technology is the degree to which new the fresh aqueous phase can be input into the system and

the rate of elemental removal whilst still maintaining the chromatographic behavior. In this implementation the feed enters the aqueous side of the system between stages 10 and 11, or between the loading and scrubbing sections. This can be seen in the diagram below (Figure 43):

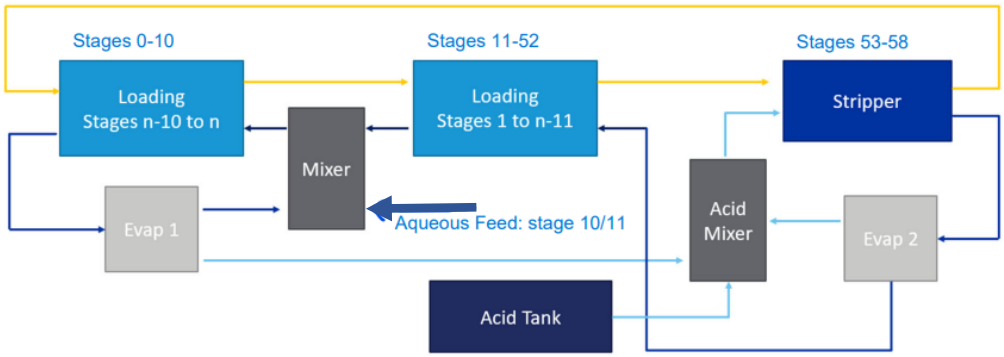


Figure 43. Representation of SAC for testing purposes.

In terms of debugging, the following example is provided. A test of a 58 stage SAC is set up with DODGAA. When the model is run, it begins with no elements in the system. For each loop through the code, the model calculates the concentration of the next stage. For instance, on loop 1, the concentration in stage 10 and 11 being the first stage of aqueous loading. On loop 2 it calculates the concentration on stage 12. This goes on through the system until it reaches the full 58 stages. Once the first 58 loops to initialize the system are completed, graphs like the sets below are generated. These collectively are referred to as Figure 44. Note that the left figures correspond to the aqueous phase and the right figures correspond to the organic phase. The rows correspond to various aqueous phase feed ratios as compared to the flow rates found within the loops. This is defined as the Aqueous Inlet Ratio. This variable is defined as the flowrate of aqueous being fed in divided by the amount of aqueous recirculating through the system. Also in the charts, Stages 0-10 are loading, 10-11 is where feed is added, 11-52 is scrubbing, and 52-58 are stripping. This corresponds to Figure 43. These graphs also show the % purities of each element of interest, defined as the concentration of an element divided by the sum of all element concentrations.

As the Aqueous Inlet Ratio is increased, the system is pushed further away from its steady state with the feed, so lower purities are achieved. On the other hand, as that ratio is decreased, higher purities are achieved while also requiring a much larger system. With the modification of the code to allow for the testing of feed to recirculation ratio a critical performance parameter was tested. However, this cannot be construed to be steady state as additional looping will be required to ensure convergence on a steady state solution.

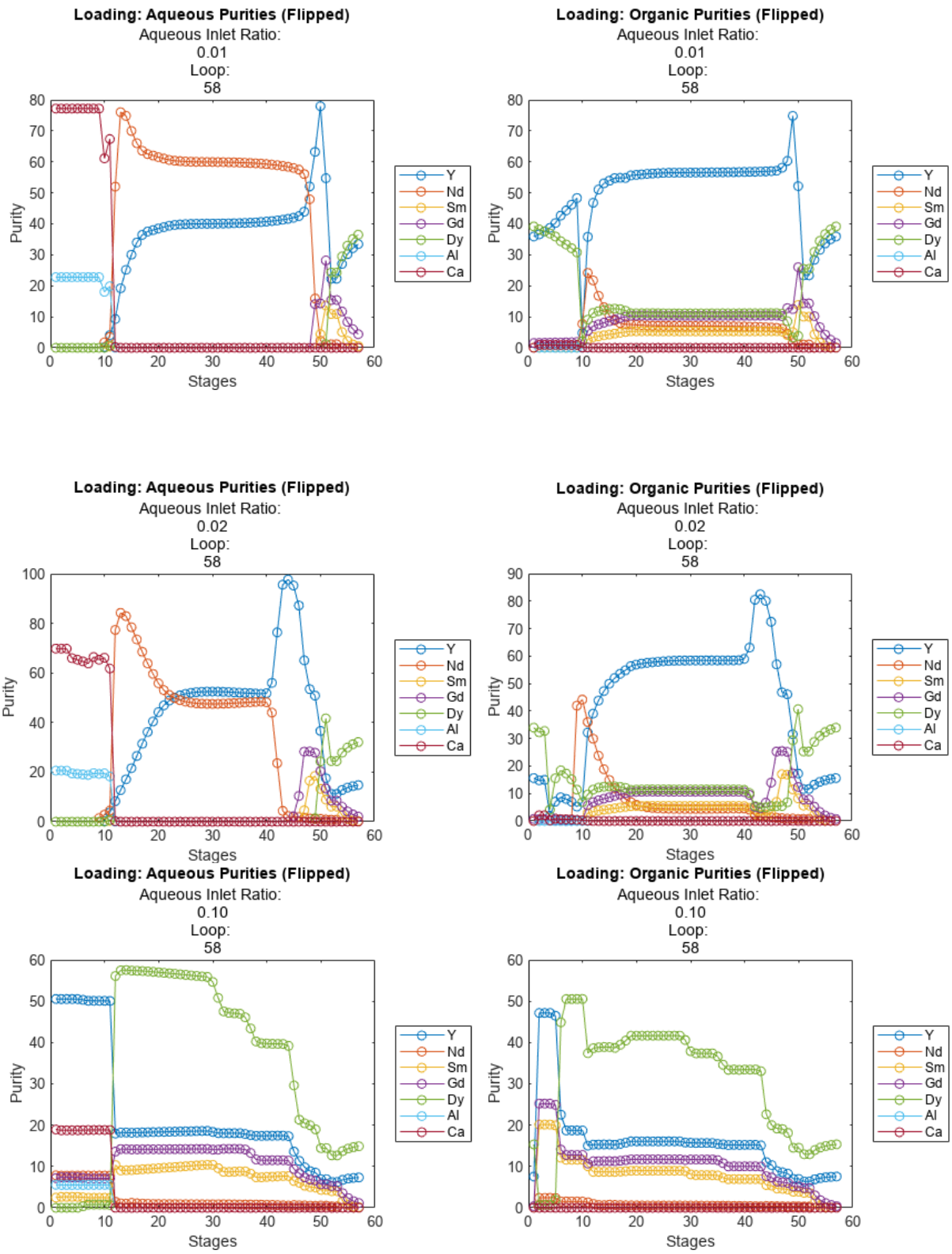

Figure 44. Result of as single initialization run of 58 loops showing different aqueous feed ratios.

As a test of steady state, the number of loops is increased to observe results. In this the next batch of graphs, the Aqueous Inlet Ratio is fixed, and the number of loops is increased (See Figure 45). As the number of loops increased one of the model's larger bugs became visible.

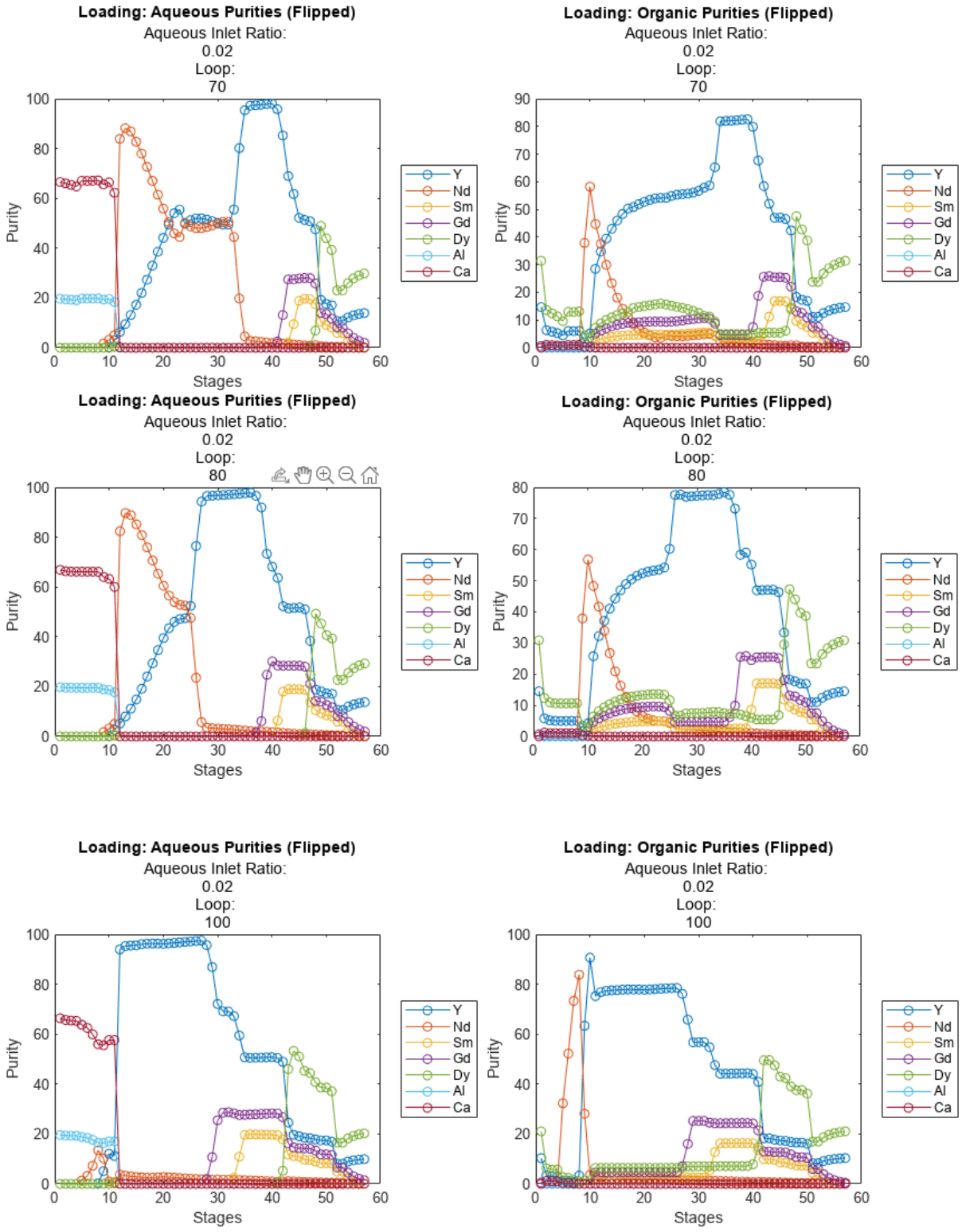

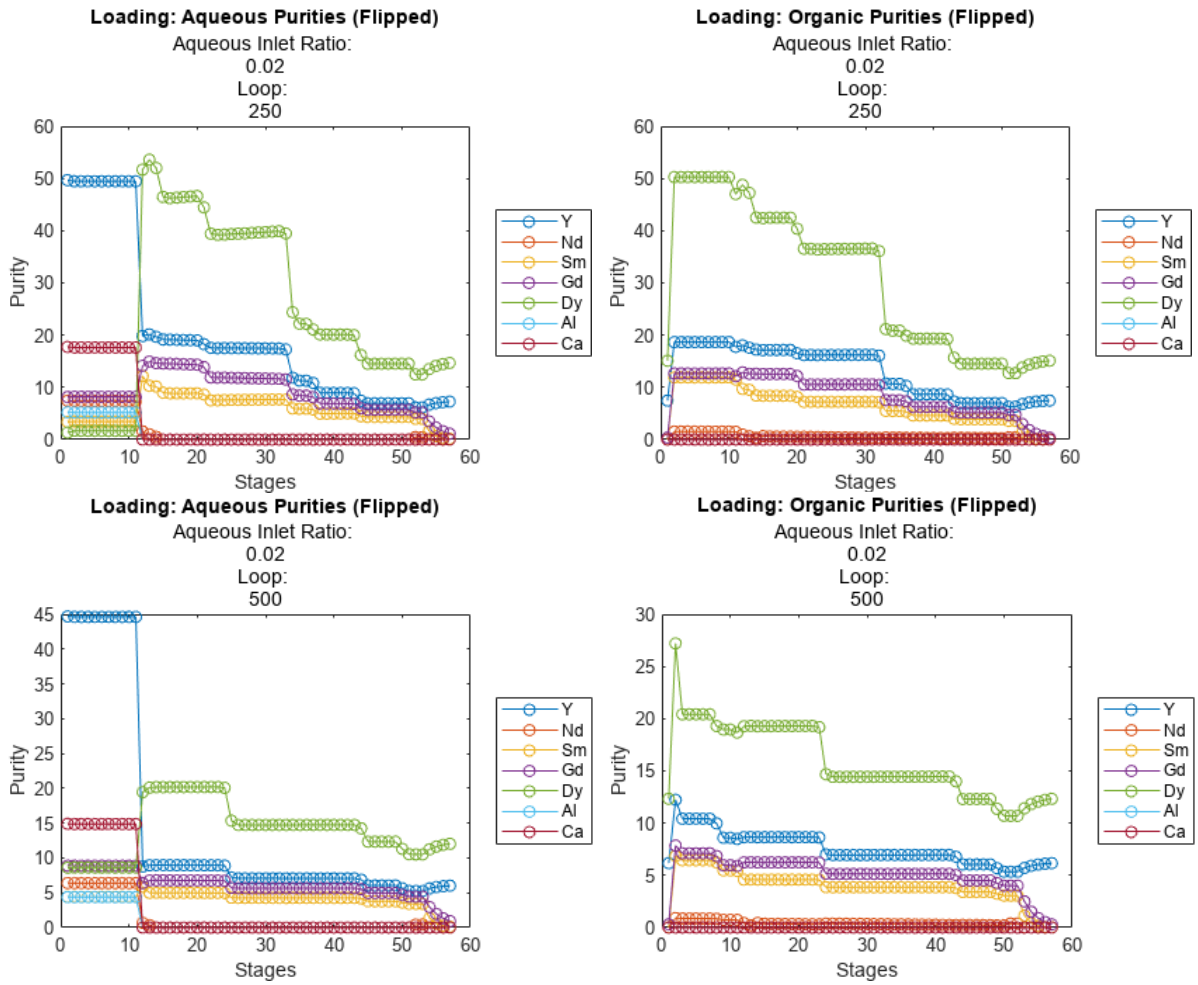


Figure 45. Aqueous feed ratio fixed with the number of loops increased.

The most concerning observation is that as the number of loops increases, the model starts behaving unexpectedly, and begins to look similar to what happens if the Aqueous Inlet Ratio is too high. As each additional loop is calculated aqueous concentrations equal the organic concentrations in the scrubbing and stripping sections. The scrubbing section (Stage 11-52) experiences the largest variation during the loops, and it looks like the purity curves are shifting to the left and widening.

This result is concerning as it appears that as the loops increase, the correct equilibrium condition is not represented by the model. Debugging is seeking to evaluate the cause and determine why this behavior occurs.

In order to evaluate the efficacy of the equilibrium model used as part of the troubleshooting SX equilibria was reexamined from a first principal basis. The first premise in the evaluation of the extraction characteristics of REEs is to determine the occurrence of species in the aqueous solutions. For aqueous solutions, there can exist two different types, namely sulfate and chorine for the salt anion. The sulfate system is an artifact of the extraction circuit and the chorine chosen as a convenient and relatively inexpensive mineral acid chosen for cost and convenience of avoiding certain precipitates such as gypsum and others.

As REEs exist in trivalent forms the following species are considered possible where Ln represents the REE species (Lanthaide) and X the anion in a monovalent chorine type system:

$$Ln^{3+} + X^{-} \rightleftharpoons LnX^{2+} \quad (1)$$

$$LnX^{2+} + X^{-} \rightleftharpoons LnX_2^{+} \quad (2)$$

$$LnX_2^{+} + X^{-} \rightleftharpoons LnX_3 \quad (3)$$

The sulfate system may be more complex seeing as the following species are possible depending on pH: $H_2SO_4$, $HSO_4^{+}$, $SO4^{2-}$. In the case of a monovalent anion, the equilibrium constants which can be also termed as stability constants can be given as:

$$\beta_1 = \frac{|LnX^{2+}|}{|Ln^{3+}||X^{-}|} \quad (4)$$

$$\beta_2 = \frac{|LnX_2^{+}|}{|LnX^{2+}||X^{-}|} \quad (5)$$

$$\beta_3 = \frac{|LnX_3|}{|LnX_2^{+}||X^{-}|} \quad (6)$$

written in terms of activity (denoted by | |). To determine extraction of REEs into the organic phase the nature of the organo-metallic reaction must be defined. From eqns. 1-3 we may see that there are several opportunities for aqueous species.

Moving on to the extractant reactions with the formation of an organo-metallic compound both DODGAA and DEHPA are considered. It appears that the extractant DODGAA exists as a monomer for the purposes of equilibrium evaluation (Shimojo 2014) with the following reaction being proposed:

$$Ln^{3+} + 3HA_{org} \rightleftharpoons LnA_{3,org} + 3H^{+} \quad (7)$$

where Ln represents the lanthanide species and A the organic extractant. DEPHA conversely exists in a dimeric form (Shimojo 2014) with the following reaction being proposed:

$$Ln^{3+} + 3(HA)_{2,org} \rightleftharpoons Ln((HA)_2)_{3,0rg} + 3H^{+} \quad (8)$$

With regard to DODGAA, the following equilibrium expression can then be developed (note that concentrations are assumed and activities are ignored):

$$K_{ex} = \frac{[LnA_3]_{0rg}[H^{+}]^3}{[Ln^{3+}][HA]_{org}^3} \quad (9)$$

where $K_{ex}$ is the equilibrium constant and the [] represent concentrations of the different components. In terms of operating solvent extraction the concentrations of equilibrium will be those streams leaving the stage. Defining the distribution coefficient as

$$D_{DODGAA} = \frac{[LnA_3]_{org}}{[Ln^{3+}]} \tag{10}$$

which simplifies eq 9 to:

$$K_{ex} = D_{DODGAA} \frac{[H^+]^3}{[HA]^3_{org}} \tag{11}$$

and upon further rearrangement produces:

$$\log D_{DODGAA} = 3 \log \frac{[HA]}{[H^+]} + \log K_{ex} \tag{12}$$

However, when the system behaves in a non-ideal way i.e the ionic strength >0.1 M, the solute strongly solvated, or at high concentrations >0.1M (Rydberg 2004) activities must needs be introduced. The remainder was covered previously and is reintroduced here for convenience.

Utilizing literature data, percent extraction at each stage can be modeled as a function of pH and curve fit to Equation 13.

$$E_j = \frac{a}{1 + \left(\frac{b}{pH_{j-1}}\right)^c} \tag{13}$$

$E_j$ represents the percent extraction at stage j; $pH_{j-1}$, the pH of the incoming aqueous stream; and a, b, and, c, constants of curve fitting. For example, the fit for yttrium can be seen in Figure 46.

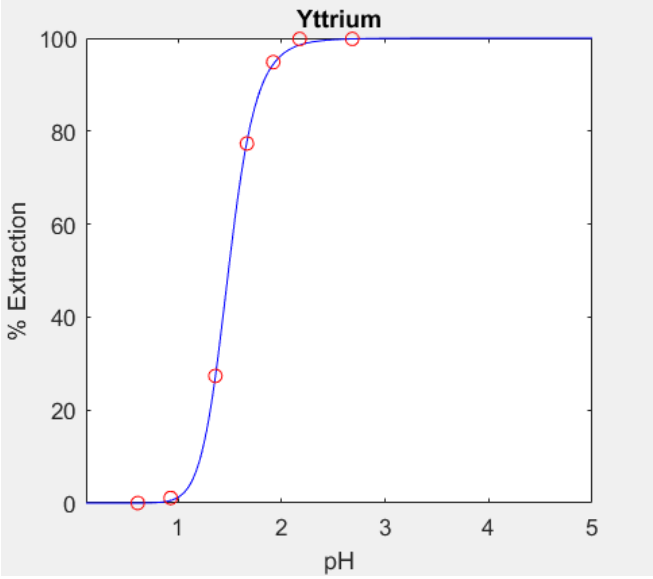


Figure 46. Fitted curve to literature data for the extraction of Yttrium using DODGAA (reproduced form Figure 36 for convenience).

After determining the percent extraction, the distribution coefficient is then calculated.

$$n_{k,ext} = \frac{D_{k,j}}{\sum D_{k,j}} \frac{O[L]}{3} \tag{14}$$

This conversion from percent extraction to distribution coefficient, $D_j$, is seen in Equation 2. Where A corresponds to the aqueous volume or flow rate and O the organic.

$$D_j = \frac{A}{O}\frac{E_j}{\left(100 - E_j\right)} \tag{15}$$

In ratio form:

$$D_j = \frac{A}{O}\frac{E_j}{\left(1 - E_j\right)} \tag{16}$$

In the current model, the limit of loading of and element can be expressed by controlling the concentration of the ligand, [L]. Since there are multiple elements competing for the same spaces in the organic phase, a ratio of the distribution coefficients is implemented to ensure that elements are loaded in the correct amounts. The reader is invited to recall the "strength" discussion surrounding the original occurrence of Eq (3). This strength term is crucial for how the current model defines equilibrium. As the time of project completion, the debugging of the SAC continues and the model was not sufficiently advanced to allow inclusion in the final selection.

### *2.5.4 Subtask 5.4 – Modular Physical Concept Design*

To complete the project requirements, a physical concept design was performed in SolidWorks to be able to explore the concept of SAC. Figure 47 shows this design with a central shaft and mounted impellers with the internal workings needed to maintain separation of the organic and aqueous phases between stages.

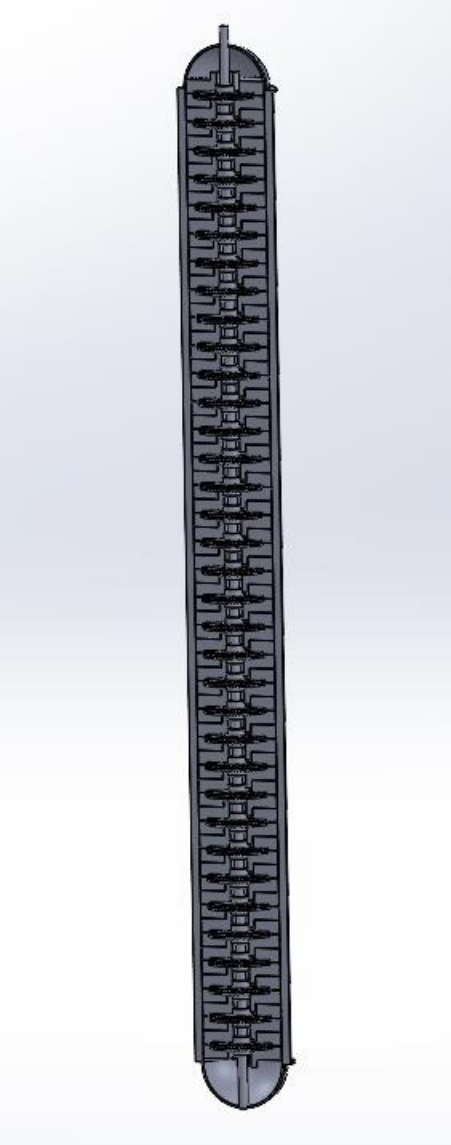

Figure 47. Conceptual model of a multistage SAC.

Figure 48 shows an enhanced view of the internal workings showing the annular space around the shaft where the downward flowing aqueous phase and the upward flowing organic phase are introduced to the next stage mixer. Figure 49 shows the same, but with perspective, perhaps a better view of the spacers, the coalescer shown as a white material to further separate the phases after mixing. The gap on the edge allows for the separated phases to rise or fall as needed to outlet ports near the shaft leading to the next phase impeller. The flow of the liquid phases is further demonstrated in Figure 50.

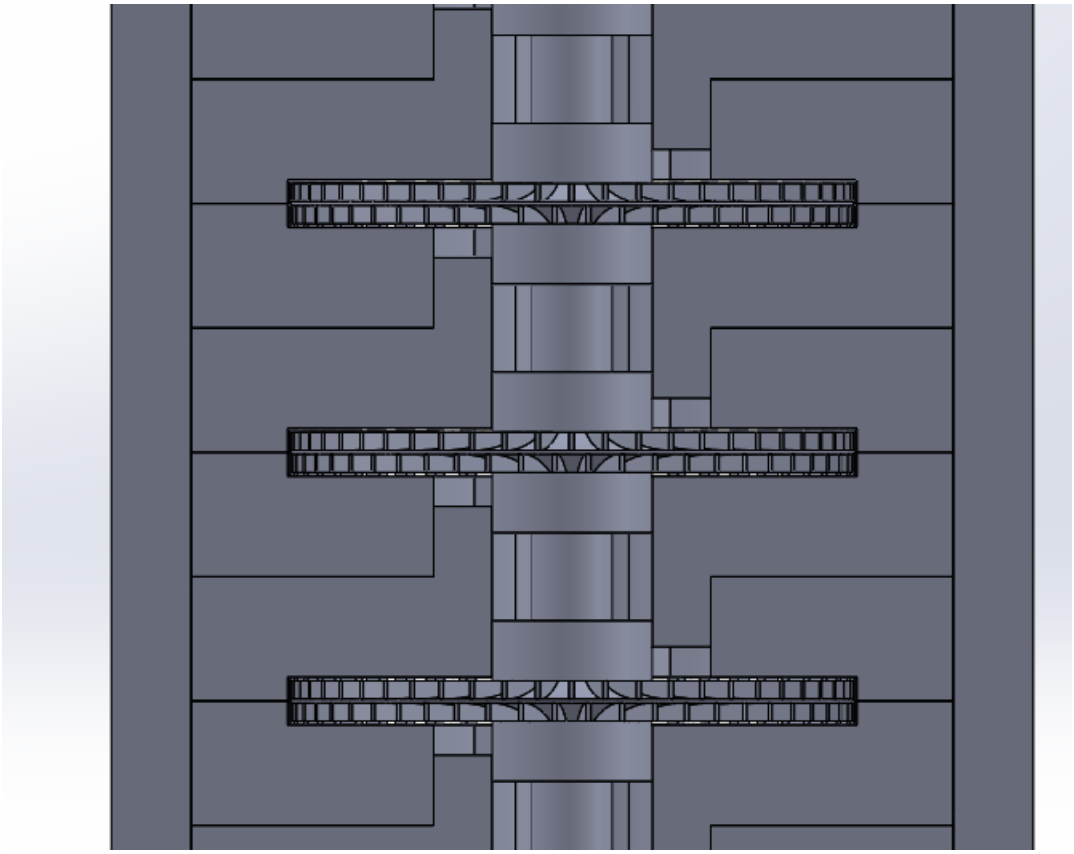

Figure 48. Detail of the internal components of SAC showing rotors and internal components.

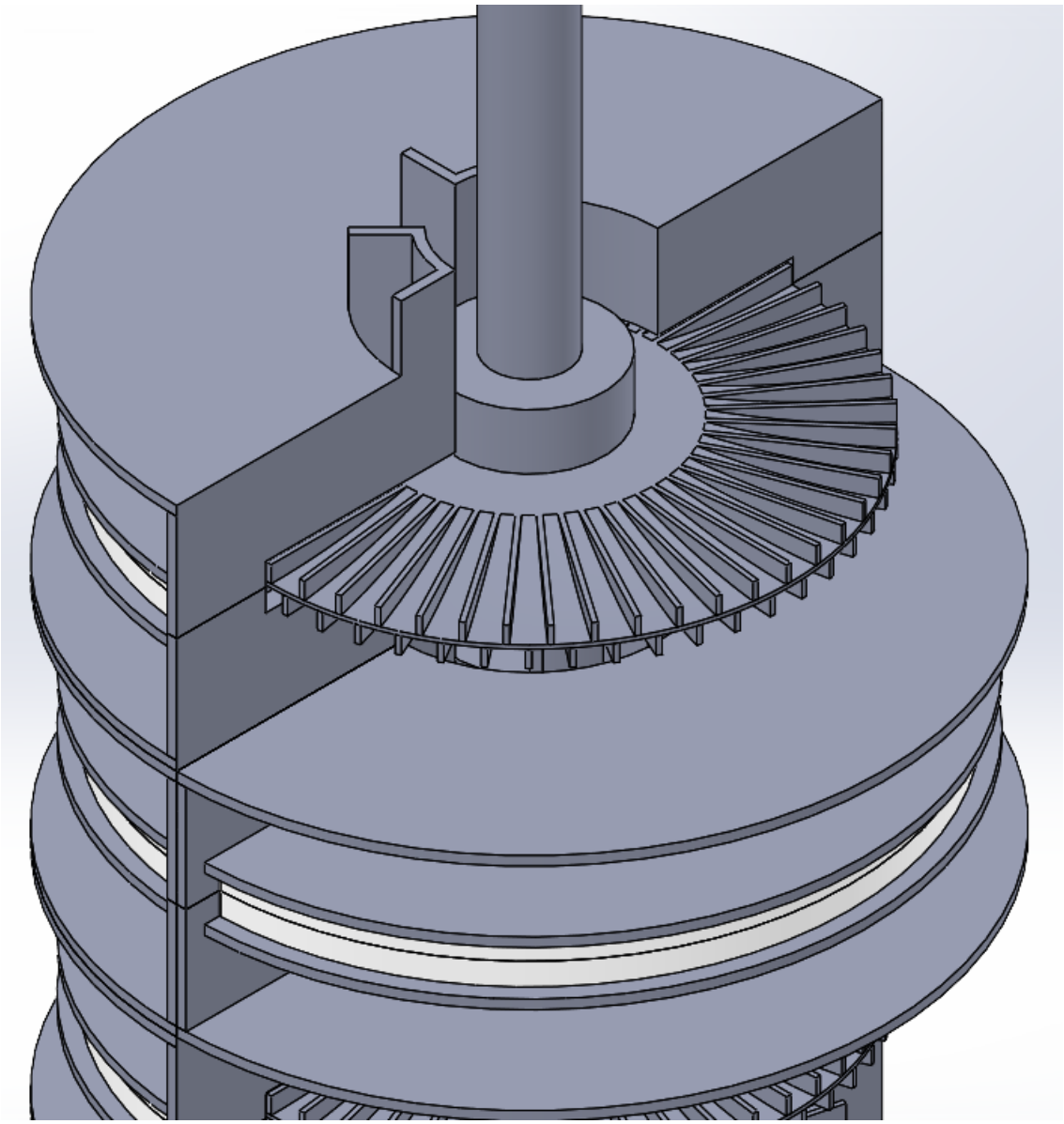

Figure 49. Isometric view of Figure 48.

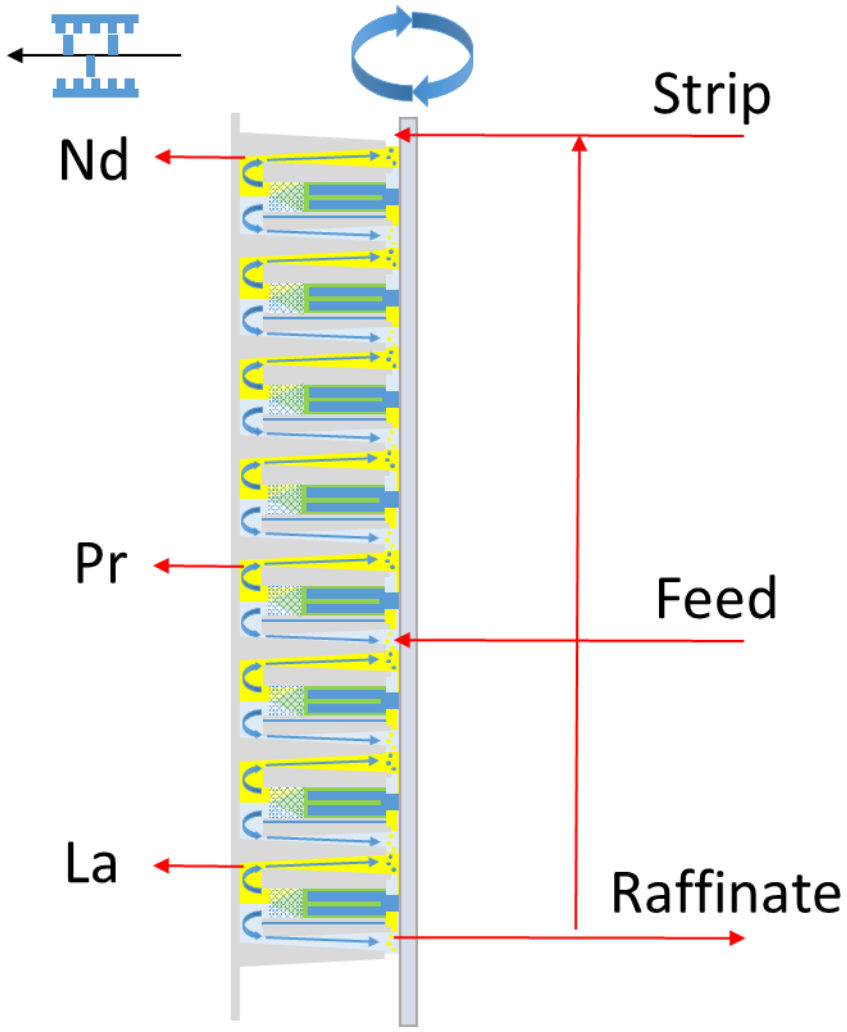


Figure 50. Cross section of proposed SAC apparatus.

### *2.5.5 Section References*

[1] Chandra, Alind. "Thermodynamic Modeling and Equilibrium System Design of a Solvent Extraction Process for Dilute Rare Earth Solutions." (2019).

[2] “Le Chatelier's Principle.” Chemistry LibreTexts, Libretexts, 15 Aug. 2020, https://chem.libretexts.org/Bookshelves/Physical_and_Theoretical_Chemistry_Textbook_Maps/Supplemental_Modules_(Physical_and_Theoretical_Chemistry)/Equilibria/Le_Chateliers_Principle#:~:text=Le%20Ch%C3%A2telier's%20principle%20states%20that,change%20to%20reestablish%20an%20equilibrium.

[3] Sharaf, Maha, et al. "Selective Extraction of Scandium from Other REEs Using Binary Extractant of PC-88A and Versatic 10 from Nitrate Media." Proc. Int. Solvent Ext. Conf. Vol. 2017. 2017.

[4] Mohammadi, Maryam, et al. "Separation of Nd (III), Dy (III) and Y (III) by solvent extraction using D2EHPA and EHEHPA." Hydrometallurgy 156 (2015): 215-224.

[5] Liu, Shushu. Production of High-Grade Mixed Rare Earth Oxides from Acid Mine Drainage via Solvent Extraction: Laboratory-Scale Process Development. Diss. Virginia Tech, 2020.

[6] Zhao, Zhexuan, et al. "Recovery of rare earth elements from spent fluid catalytic cracking catalysts using leaching and solvent extraction techniques." Hydrometallurgy 167 (2017): 183-188.

[7] Kumari, Archana, et al. "Extraction of rare earth metals by organometallic complexation using PC88A." Comptes Rendus Chimie 21.11 (2018): 1029-1034.

[8] Nakamura, Takahide, Syouhei Nishihama, and Kazuharu Yoshizuka. "Separation and recovery process for rare earth metals from fluorescence material wastes using solvent extraction." Solvent Extraction Research and Development 14 (2007): 105-13.

[9] Arellano Ruiz, Verónica Cristina, et al. "Environmentally friendly comprehensive hydrometallurgical method development for neodymium recovery from mixed rare earth aqueous solutions using organo-phosphorus derivatives." Scientific reports 10.1 (2020): 1-13.

[10] Padhan, E., and K. Sarangi. "Recovery of Nd and Pr from NdFeB magnet leachates with bi-functional ionic liquids based on Aliquat 336 and Cyanex 272." Hydrometallurgy 167 (2017): 134-140.

[11] Banda, Raju, Ho Seok Jeon, and Man Seung Lee. "Solvent extraction separation of La from chloride solution containing Pr and Nd with Cyanex 272." Hydrometallurgy 121 (2012): 74-80

[12] Gupta, Chiranjib Kumar, and Nagaiyar Krishnamurthy. "Extractive metallurgy of rare earths." International materials reviews 37.1 (1992): 197-248.

[13] Sharaf, Maha, et al. "Selective Extraction of Scandium from Other REEs Using Binary Extractant of PC-88A and Versatic 10 from Nitrate Media." Proc. Int. Solvent Ext. Conf. Vol. 2017. 2017.

[14] Padhan, E., and K. Sarangi. "Recovery of Nd and Pr from NdFeB magnet leachates with bi-functional ionic liquids based on Aliquat 336 and Cyanex 272." Hydrometallurgy 167 (2017): 134-140.

[15] Lommelen, Rayco, Bieke Onghena, and Koen Binnemans. "Cation effect of chloride salting agents on transition metal ion hydration and solvent extraction by the basic extractant methyltrioctylammonium chloride." Inorganic Chemistry 59.18 (2020): 13442-13452.

[16] Dashti, Somayeh, et al. "Separation and solvent extraction of rare earth elements (Pr, Nd, Sm, Eu, Tb, and Er) using TBP and Cyanex 572 from a chloride medium." Minerals Engineering 161 (2021): 106694.

[17] Soukeur, Abderraouf, et al. "Extraction of rare earth elements from waste products of phosphate industry." Separation and Purification Technology 256 (2021): 117857.

[18] Green, Don W., and Robert H. Perry. Perry's chemical engineers' handbook. McGraw-Hill Education, 2008.

[19] Stichlmair, Chem. Eng. Tech. 52(3) 253-255 1980

[20] Horvath, Milos, and Stanley Hartland. "Mixer-settler-extraction column. Mass transfer efficiency and entrainment." Industrial & Engineering Chemistry Process Design and Development 24.4 (1985): 1220-1225.

[21] "Mixer-Settler Working Principle." Chemical Engineering World, 28 Aug. 2020, https://chemicalengineeringworld.com/mixer-settler-working-principle/.

[22] "Designing of Liquid-Liquid Extraction Columns - Aiche.org." Koch Modular Process Systems, AIChE, https://www.aiche.org/sites/default/files/community/160956/aiche-community-site-files/1720551/liquid-liquidextraction-koch-dec2020.pdf.

[23] Couper, James R., et al. Chemical process equipment: selection and design. Gulf professional publishing, 2005.

[24] "Extraction Column Types: Agitated and Static Columns for Liquid-Liquid Extraction: Koch Modular." Koch Modular Process System, 10 Sept. 2021, https://kochmodular.com/liquid-liquid-extraction/extraction-column-types/.

[25] https://www.neomaterials.com/wp-content/uploads/2021/08/Neo_Investor_Presentation_Q3_2021_FINAL.pdf

[26] https://app.sharelinktechnologies.com/announcement/asx/d46f27b6589727755c4e2a41e0dfd19d

[27] https://ec.europa.eu/docsroom/documents/14043/attachments/1/translations/en/renditions/native

[28] https://lynasrareearths.com/about-us/vtour/

[29] https://www.miningmagazine.com/chemicals-reagents/news/1364528/lynas-and-blue-line-mou-for-rare-earths-separation

[30] https://www.reuters.com/article/us-usa-rareearths-lynas-corp/australias-lynas-wins-funding-for-u-s-heavy-rare-earths-facility-idUSKCN2240UL

[31] https://sanantonioreport.org/hondo-texas-lynas-rare-earths/

[32] https://ucore.com/rapidsx/

[33] Opare, Emmanuel Ohene, Ethan Struhs, and Amin Mirkouei. "A comparative state-of-technology review and future directions for rare earth element separation." Renewable and Sustainable Energy Reviews 143 (2021): 110917.

[34] https://www.miningmagazine.com/chemicals-reagents/news/1364528/lynas-and-blue-line-mou-for-rare-earths-separation

[35] https://www.birdiebreeze.net/facility-location

[36] Brewer, Joseph, Ryan S. Winburn, and Joshua Beaudoin. "Method for extraction and separation of rare earth elements." U.S. Patent No. 10,494,694. 3 Dec. 2019.

[37] Izatt, Steven R., et al. "Molecular recognition technology: a green chemistry process for separation of individual rare earth metals." White Paper on Separation of Rare Earth Elements (2016): 1-13.

[38] Jaroni, Marie Sophie, Bernd Friedrich, and Peter Letmathe. "Economical feasibility of rare earth mining outside China." Minerals 9.10 (2019): 576.

[39] Opare, Emmanuel Ohene, Ethan Struhs, and Amin Mirkouei. "A comparative state-of-technology review and future directions for rare earth element separation." Renewable and Sustainable Energy Reviews 143 (2021): 110917.

[40] Brown, C. G., & Sherrington, L. G. (1979). Solvent extraction used in industrial separation of rare earths. Journal of Chemical Technology and Biotechnology, 29(4), 193-209.

[41] Shimojo, Kojiro, et al. "Extraction behavior and separation of lanthanides with a diglycol amic acid derivative and a nitrogen-donor ligand." _Analytical Sciences_ 23.12 (2007): 1427-1430.

## 2.6 Task 6.0 – Circuit 3 RE Metal Production

### *2.6.1 Subtask 6.1 – SOTA Technology Review*

#### *2.6.1.1 Energy reduction in production of heavy rare earths and yttrium*

The processes for these metals use rare earth fluoride as the starting material with reductions possible with lithium, sodium or calcium metal can be used. Lanthanum can also be used in reduction of dysprosium because dysprosium can be sublimed or distilled to increase the purity. Most reduction processes use calcium as it will reduce fluoride and oxide, whereas sodium is not as effective. Lithium metal can be recycled more easily as it can be electrowon from a chloride salt. Calcium fluoride or chloride from reduction is more difficult to recycle, electrowinning of calcium from a chloride salt was practiced at one time [1], the aluminothermic method replaced it as the metal yields are higher and metal quality is better since electrowinning calcium can have nitrogen contamination.

*Yttrium* - Yttrium chloride and yttrium fluoride have been reduced with calcium metal. The reduction of chloride was found to be more difficult to control than fluoride. In this process, the fluoride reacts with calcium metal gas at temperatures of about 1400 °C [2], which is well below the melting point of yttrium metal, and the byproduct calcium fluoride. From previous work, it was shown that this reaction is very exothermic and self-propagating once the reduction starts to occur. As result, heat savings or energy savings in the process are not possible as the process produces excess heat. Economies in the power supply necessary to heat the calcium metal up so that a high enough vapor pressure is generated would be the best way to improve the energy cost of reduction. This change along with improvements in water chillers used to cool the outside of the vacuum retort would result in some savings.

Once generated, the yttrium fluoride is reduced with calcium metal:

$$2YF_3 + 3Ca_{(g)} = 2Y + 3CaF_{2(s,\,l)}$$

A ratio of 0.9 $CaCl_2/YF_3$ was used [3]. This makes separation of the yttrium from the salt easier. Once produced, the yttrium metal must be remelted to produce ingot forms.

*Gadolinium* - Gadolinium is produced by the metallothermic reaction of gadolinium fluoride. These processes operate below the melting point of the metal. The gadolinium fluoride (50μm) and calcium metal (3 mm) are slowly heated to 1470 °C under vacuum [4]. At this point, the calcium metal reduces the gadolinium fluoride thereby producing calcium fluoride and gadolinium metal. These separate based on density, resulting in a gadolinium ingot. The ingot contains about 0.1% calcium, which is removed by remelting in an arc furnace under vacuum:

$$2GdF_3 + 3Ca_{(g)} = 2Gd + 3CaF_{2(s,\,l)}$$

*Dysprosium* - Dysprosium metal is a high melting point (1405 °C) rare earth. It can be produced by metallothermic reduction of dysprosium fluoride with calcium 1500°C [5]. This process produces pure dysprosium with calcium contamination and can be used to produce ferro dysprosium directly by the following reaction:

$$2DyF_3 + 3Ca_{(g)} = 2Dy_{(l)} + 3CaF_{2(s,\,l)}$$

Further purification by vacuum distillation or sublimation is typically used. This method only produced dysprosium at about 75% yield with some content of oxygen (1000 ppm) and lanthanum at 1%. The oxygen content was reduced with subsequent remelting [6]. The vapor pressure of dysprosium is about 300 times that of lanthanum at the same temperature [7]. Separation by sublimation can be used according to the reaction:

$$Dy_2O_3 + 2La_{(s,l)} = 2Dy_{(s,l)} + La_2O_{3(s,)}$$

A commercial method [8] using a lithium-magnesium alloy as the reductant has been employed to produce dysprosium from chloride. As shown by the flow sheet in Figure 51, this process involves the conversion of chloride to a fluoride salt and subsequent reduction. Magnesium will not reduce dysprosium fluoride. It is used as a vehicle for lithium. This work showed that both tantalum and tungsten boats or crucibles can be used for the distillation process. Tungsten is less reactive with dysprosium than tantalum, resulting in less contamination.

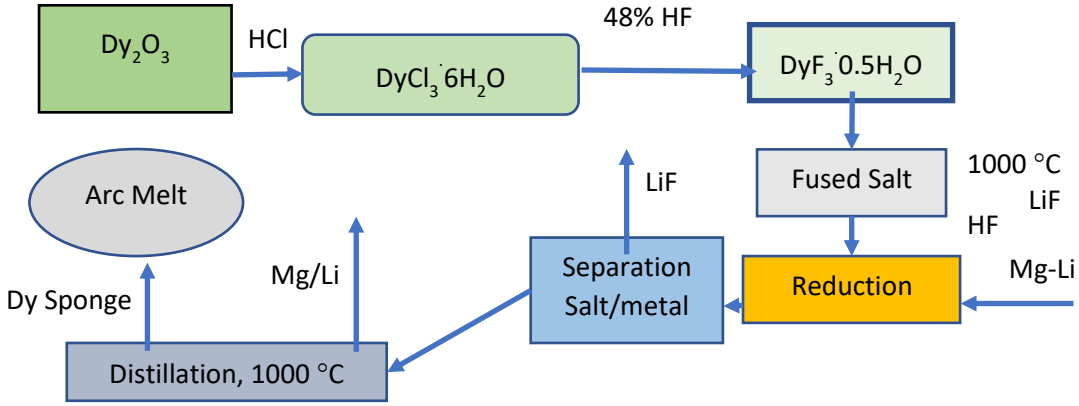


Figure 51. Dysprosium reduction process.

A possible improvement for this process could be using a magnesium-lithium reductant with generation of a lithium fluoride stream as a by product that could be returned to lithium mines for conversion to chloride.

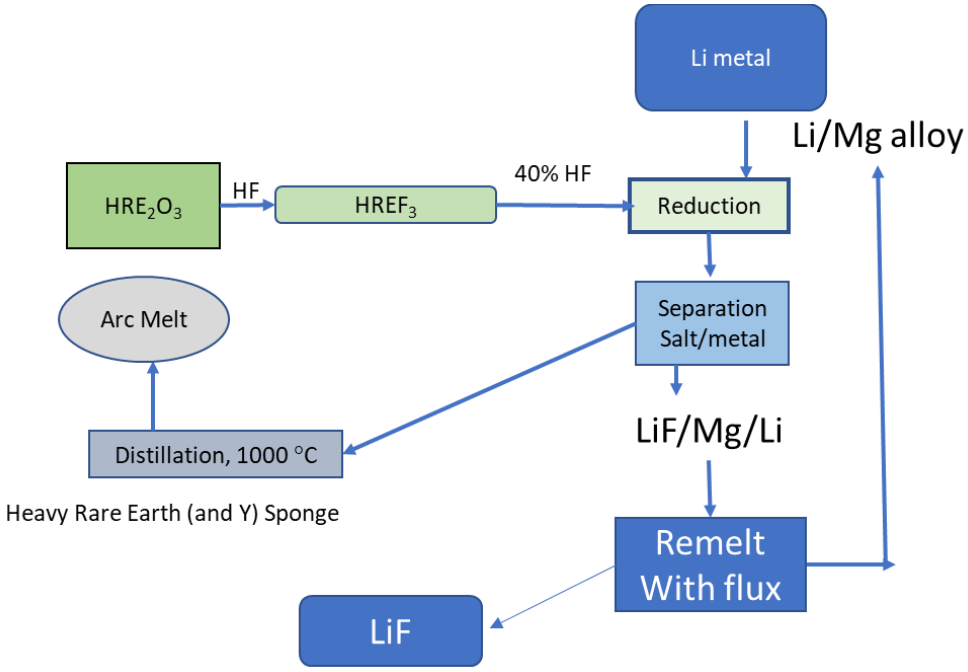


Figure 52. Heavy rare earth reduction process.

The Downs cell, which was first developed in the 1920's, produces sodium metal using a molten sodium chloride in an electrolytic cell. The electrolysis process produces both sodium metal and chlorine gas. This process has a large kW-hr/kg because of the recombination of chlorine and sodium, sodium floats on the electrolyte.

All methods of production of the heavy rare earths using metallothermic reduction are exothermic processes. However, it is difficult to recover the heat for other purposes. The methods of producing the reducing reagents have some room for improvement in terms of current yield. Sodium metal is no longer made in the U.S. Calcium metal is produced by Minteq in Connecticut in various forms The most common is a wire with a steel sheath used for steelmaking.

*2.6.1.2 Section References:*


[1] Mantel, C. L., Hardy, C., Calcium Metallurgy and Technology. Reinhold Publishing, New York, 1945

[2] Daane, A. H., Spedding, F. H. Preparation of Yttrium and Some Heavy Rare Earths. Journal of the Electrochemical society, V 100, (1953), pp442-446

[3] The Rare Earths. Edit by F. H. Spedding and A.H. Daane, Joly Wiley & Sons, New York, 1961 p121.

[4] Rare Earth, Science, Technology, Preparation and Use. Lucas, J., Lucas, P., Lemercier, T., Rollat, A., Davenport, W., Elseiver, 2015 pp116

[5] Schmidt, F. A., Peterson, D. T., Wheelock, J.T., Preparation of rare earth iron alloys by thermite reduction. USP 4,612,047. Sept 16, 1986

[6] A Study of the reduction of dysprosium oxide with lanthanum as a method for producing high purity dysprosium metal. Sanden, B. L., Spedding, F. H., US Atomic Energy commission, W-7405 Feb 1974

[7] Daane, A.H., Dennison, D. H., Spedding, F. H., The Preparation of samarium and ytterbium metals. Journal American Chemical Society, Vol 75, Issue 9, 1953, pp2272

[8] Moriarty, J. L. jr., The Industrial Preparation of the rare earth metals by metallothermic reduction. Journal of Metals, Nov 1968 pp41-45


*2.6.1.3 Ionic Liquid Rare Earth Extraction as it relates to Subtask 6.3*

The following findings from literature were relevant for ionic liquids needed to support membrane-assisted electrowinning.

Rare earth elements were extracted easily with a tri-*n*-butylphosphate with phosphonium ionic liquids. This work was conducted to develop a recycling process for the recovery of rare earths from Nd-Fe-B magnets. The rare earths Pr, Nd, and Dy were extracted by tri-n-butylphosphate (TBP) with ionic liquid triethyl-pentyl-phosphonium bis(trifluoromethyl-sulfornyl)amide ($P_{2225}$[ TFSA]). It was shown that extraction was enhanced significantly with TBP with the $P_{2225}$[TFSA] when extraction of the RE ions was carried out from an aqueous phase. Direct electrodeposition was conducted at 100 °C. The neodymium deposited was found to be metal at the cathode with oxide present at the top of the deposit [1].

Neodymium metal was produced by electrolysis at 100°C using triethyl-pentyl-phosphonium bis(trifluoromethyl-sulfonyl) amide ($P_{2225}$[TFSA]). It was shown that $Nd^{+2}$ can also be stabilized in these solutions. Very small amounts of metallic neodymium metal was produced. The

electrochemical window is very large in these solutions with neodymium metal in 0.05 M to 0.10 M [2].

Dysprosium metal was reduced by electrolysis at 150°C using triethyl-pentyl-phosphonium bis(trifluoromethyl-sulfonyl) amide ($P_{2225}$[TFSA]). A small amount of metal was produced and showed evidence of oxide on the outer layer of the deposit [3]. The dysprosium was deposited on copper foil.

Dysprosium was reduced using dysprosium triflate dissolved in 1-butyl 1-methylpryrrodium triflate at ambient temperature. No metal samples were obtained. Reduction was proved by chronoapermometric electrodeposition. The solution was also studied using NIR methods to determine the structure of the electrolyte [4].

Structural determination and electrochemical work with La, Eu, and Sm were carried out with ionic liquids based on bis(trifluoromethylsulfonyl)amide in a tertiary alkylammonium, pyrrolidinium or methylmorpholium cation. This work has shown that even multivalent rare earths such as Eu and Sm can be solvated with these elements to produce salts. The production method to produce these salts is very complicated [5]. This appears to be the earliest work on non-haloaluminate ionic liquids.

Rare earths Y, Gd, and Yb have been reduced to metal as determined by electrochemical testing, however, no metal was recovered in the process [6]. Electrodeposition was conducted in a butyltrimethylamonium trifate on copper substrate. However, no deposit was shown on platinum. This work was conducted at 100°C.

Neodymium and dysprosium have been deposited using a rare earth metal bis(trifluoromethylsulfonyl)imide or chloride salt dissolved in 1,2 dimethoxyethane or 2-methyltetrahydrofuan. These electrolytes contain a soluble borohydride complex, which allows for deposition of Nd and Dy [7]. The rare earth bis(trifluoromethylsulfonyl)imides tend to leave a layer of fluoride on the surface thereby resulting in passivation. Reduction is conducted at room temperature.

Changing the solvent from 1,2 dimethoxythane to trimethyl phosphate improved the deposit quality, however the deposits were small [8]. Attempts to recycle the solution to a large scale proved not very successful [9]. This work showed that without modification electrowinning of the metal is possible. A membrane or other method is necessary to transfer the metal ion from an aqueous solution to the trimethyl phosphate to deposit metal.

A new lower cost electrolyte is proposed using aluminum chloride additions to 1,3 dimethyl-2-imidazolidinone with neodymium chloride [10]. This solution has been used to deposit neodymium with about 10% oxide content. This work conducted at room temperature.

Water tolerance was improved with change of the base solution to a trihexyltetradecylphosphium bis(trifluoromethylsulfonyl)amide [$P_{666614}$][TFSI]. Water contents of 0.4 weight percent improved the cathode current density to 5 mA/cm$^2$. Metallic deposits of neodymium were produced in this solution [11].

A chloride anode compartment separated by a diaphragm is part of a catholyte process that was developed for the electrowinning of neodymium from neodymium chloride in an ionic fluid. This process generated chlorine gas [12].

In summary, the work reported in this field shows that the use of haloaluminates should be avoided in place of the ionic liquids such as $P_{2225}$ and $P_{66614}$ as these have higher water tolerances than the aluminates. In reviewing the metal samples produced so far, it was revealed that they have been very small and can have significant quantities of impurities. The current densities employed are small (1-5 $mA/cm^2$) compared to conventional electrowinning. However, a significant advantage is that the operating temperatures are much lower than the molten salt process. The work so far is very early in the technology development, and not developed to a point where molten salt electrolysis and ionic liquids can be compared.

*2.6.1.4 Section References:*


[1] Matsumiya, M, Kikuchi, Y., Yamada, T., Kawakami, S., Extraction of rare earth ions by tri-n-butylphosphate/phosphonium ionic liquids and feasibility of recovery by direct electrodeposition. Separation and Purification Technology, Volume 130, Issue 10, June 2014 pp91-101.

[2] Ota, H., Matsumiya, M., Sasaya, N., Nishihata, K., Investigation of electrodeposition behavior for Nd(III) in [$P_{2225}$}TFSA ionic liquid by EQCM methods with elevated temperature. Electrochemica Acta V 222, 2016 pp20-26

[3] Kurchi, A., Mastumiya, M., Tsunashima, K., Kodama, S., Electrochemical behavior and electrodeposition of dysprosium in ionic liquid based on phosphonium cations. J. Applied Electrochemistry, 42 (2012) pp961-968.

[4] Atifi, A., Baek, D. L., Fox, R. B., Electrodeposition of dysprosium in pyrrolidium trifate ionic liquid at ambient temperature: unraveling system efficiency and impact of solvation interplays on the reduction process. Electrochima Acta V378, (2021) 138140

[5] Bhatt, A., I., May, I., Volkovich, V. A., Collison, D., Helliwell, M, Polovov, I. B., Lewin, R. G., Structural characterization of a lanthanum bistriflimide complex, $La(N(SO_2CF_3)_2)_3(H_2O)$, and an investigation of La, Sm, and Eu electrochemistry in room-temperature ionic liquid, $(Me_3N^nBu)[N(SO_2CF_3)_2]$. Inorganic Chemistry V 44, pp4934-4940, 2005

[6] Glukhov, L.M., Greish, A. A., Kustov, L. M., *Electrodeposition of rare earth metals Y, Gd, Yb in ionic liquids.* Russian Journal of Physical Chemistry, A., Vol 84, No 1, 2010, pp104-108.

[7] Gerysens. P., Lin, P-Ch., Fransaer, J., Binnermans, K., *Electrodeposition of neodymium and dysprosium from organic electrolytes*. Physical Chemistry Chemical Physics. V23, 2021, pp9070-9079

[8] Bargi, P. Luo, H., Popovs, I., Thapaliya, B. P., Dehaudt, J., Trimethyl phosphate base neutral ligand room temperature ionic liquids for electrodeposition for rare earth elements. Electrochemistry Communications, 96, 2018, pp88-92.

[9] Sidhu, P., Investigation of the Electrowinning of Neodymium Oxide in Room Temperature Ionic Liquid, Colorado School of Mines MS 2019.

[10] Zhang, B., Wang, L., Liu, Y., Zhang, Y., Zhang, L., Shi, Z., *$AlCl_3$-assisted dissolution of $NdCl_3$ in organic solvents for Nd refining*. Separation and Purification Technology, V 276, 2021, pp 1-8.

[11] Sanchez-Cupido, L., Pringle, J.M., Siriwardana, A. L., Unzurrugzaga, A., Hilder, M., Forsyth, M., Pozo-Gonzalo, C., *Water-Facilitated Electrodeposition of Neodymium in a Phosphonium-Based Ionic Liquid*. Journal of Physical Chemistry Letters, V 10, 2019, pp 289-294

[12] Boubos, E., Giannopoulou, I., Karantonis, A., Paaspaliaris, I., Panias, D., *Reduction of light rare earths and proposed for Nd Electrorecoverery based on Ionic Liquids*. Journal of Sustainable Metallurgy V 4, (2018) pp395-406

### *2.6.2 Subtask 6.2 – High Temperature Molten Salt EW*

For consideration in this project, a new and improved design molten salt EW reactor is proposed incorporating two features: 1) feedback control of the feeder based on demand from the cell, and 2) new heater design that has a lower cold face temperature and the provision to idle the cell, and self-heating for loading solid neodymium and lithium fluoride. Presented is a mass and energy balance required for the determination of the operation and design of a REE molten salt EW reactor. A molten salt siphon was also investigated as a means of improving the quality and safety of the design.

#### *2.6.2.1 Molten Salt EW Cell Design Considerations*

The current cell design is used in Asia, but several factors must be improved. The most obvious is the thermal inefficiency of the design. Half of the joule heat generated in electrolysis is lost, mostly through the open top. Part of reason is the anode design and how they are removed and replaced. Another reason is the method used to remove the rare earth metal from the cell. The electrolytes resistance generates all the heat in the process. To reduce the heat generation, the anode-to-cathode distance must be reduced. The purity for oxide was determined and the siphon method and control system developed.

Section on heavy rare earths and yttrium is added at bottom. These metals are produced by metallothermic reduction and, as a result, do not present an opportunity for heat savings as the reduction process is exothermic.

This a review and mass balance around the production of Nd, Pr, Dy, Gd and Y. Neodymium and praseodymium are electrowon, usually combined as didymium. The market for pure praseodymium is small and it's more difficult to produce than alloyed with neodymium. The light rare earths can be produced by sodium reduction of the chloride. This process is yet to be commercialized; very little data has been published on this topic. It will require very high purity of hygroscopic rare earth chlorides.

*Molten salt electrolysis process for neodymium oxide* - The calculation of the mass and energy balance is constructed with the following assumptions:

- Rate of oxide feed, 1 ton per day;
- Duty cycle is used is 97%;
- Tungsten cathode;
- Tungsten collection well;
- Graphite crucible with stainless steel safety can;
- Cell temperature controlled by resistance heaters on outside of safety can;
- Cell temperature: 1050-1100 °C;
- Cell rated load: 2840 amp;
- Cell count: 9;
- Current yield: 80%;
- Estimated material yield 99.5%;
- Density of the graphite: 1.74 g/cm$^3$;
- Bulk density of oxide: 1.2 g/cm$^3$.

The mass balance will use SI units, with flow rates kg/hr. For this work pure neodymium will work, didymium can be used with correction of didymium molecular weight of 140.9 compared to pure neodymium of 144.24. For design purposes it is important to note the ratio of neodymium: praseodymium varies based on source of the ore, for example the ore body at Mountain Pass is 77:23 compared to didymium sold on Shanghai exchange of 75:25. It is also observed the ratios found in coals vary with each deposit. For design purposes it will be assumed that solubility of the oxide in the electrolyte is about 3.9%. The electrolyte selected is as 87% $NdF_3$: 13% LiF (weight basis). Anode current density is limited to 1 A/cm$^2$. Further considerations include:

- Cell off gas is estimated to contain both CO and $CO_2$ at 3:1 ratio;
- Carbon wear is estimated to be 0.2 #C/#Nd, this is function of electrochemical wear;
- Air burn (oxidation of graphite exposed to air at elevated temperature, >300 °C).

Using Faraday's law, the maximum production rate for electrolysis is 1.794 g Nd/Amp-hr. Neodymium oxide of about 85% metal by weight with an estimated metal production rate of 1 ton per day of oxide is 850 kg/day, or 4.076 kg metal per hour per cell based on 80% current yield. Mass balance around a single cell is shown in Figure 53 and Table 30. The rate of $CF_4$ production is estimated as 9.5 [1] to 27 [2] g/ton. Using the higher measurement, the amount of $CF_4$ generated can be estimated.

Cell count was estimated based on 850 kg metal/day, or 35.4 kg/hr, or 35.4/4.076 = 8-9 cells. A total of 10 cells system should be used for the operation with one or two positions as spared.

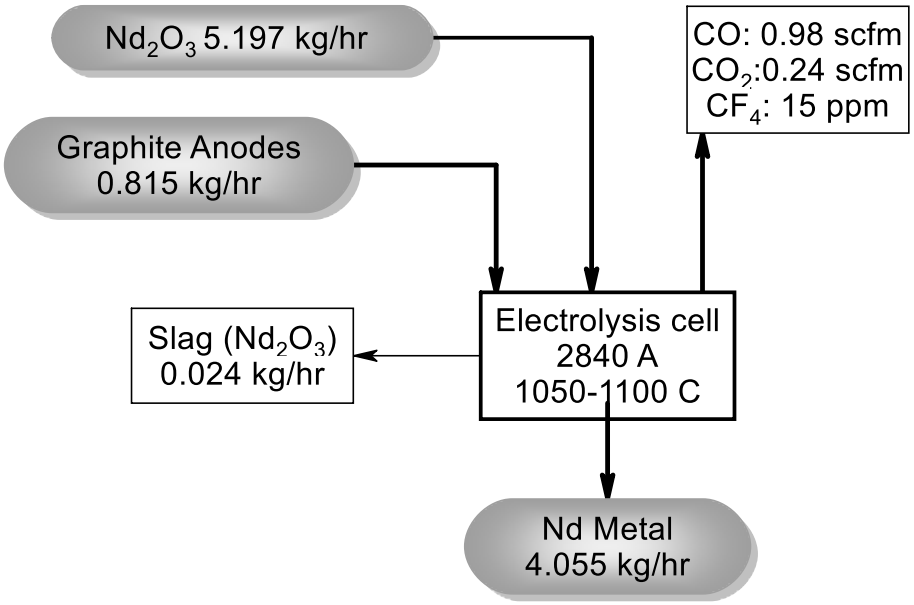


Figure 53. Preliminary molten salt electrolysis cell mass balance.

For the operation of nine cells, the mass balance (kg/min) for one ton per day of oxide is shown in Table 30.

Table 30. Stream table for a 8-9 cell count.

| **Stream chart** | **Feed** | **Anodes feed** | **Nd Metal** | **off Gas $m^3$/min** | **Slag** |
|---|---|---|---|---|---|
| Neodymia | 46.77 | | | | |
| Neodymium | | | 36.50 | | |
| Graphite | | 7.34 | | | |
| $CO_2$ | | | | 0.25 | |
| CO | | | | 0.06 | |
| $CF_4$ | | | | $5.x\ 10^{-6}$ | |
| Slag formation | | | | | 0.22 |

Heat balance of a cell requires the development of the cell design followed by the construction of the heat flow. A similar cell design is reported by Vogel [3] based on industrial practice. The load used in this cell is different for this calculation. Below is the work reported by Vogel [3]. The work presented by Vogel is only reported on previous Chinese work. The heat balance presented does not close (output and inputs do not balance). Other work shows a tremendous heat loss through the open top cell [4].

*Anode and Cathode Reactions:*

The anode reactions for the process result in the production of CO and $CO_2$.

$$Nd_2O_3 + 3C \rightarrow 2Nd + 3CO \qquad E = 1.268V$$

$$Nd_2O_3 + 1.5C \rightarrow 2\ Nd + 1.5CO_2 \qquad E = 1.425\ V$$

For the anode effect, where $CF_4$ is produced:

$$4NdF_3 + 3C \rightarrow 4Nd + 3CF_4 \qquad E = 2.789\ V$$

The oxide feed in the cell forms an oxyfluoride upon dissolution. The oxyfluoride $[NdOF_5]^{-4}$ is the species reduced.

$$3[NdOF_5]^{-4} + 6e^- \rightarrow 3/2O_{2(g)} + 3Nd^{+3} + 15F^-$$

The oxygen subsequently reacts with the carbon anode to produce CO and $CO_2$.

Cathode reaction is:

$$2[NdF6]^{-3} + 6e^- \rightarrow\rightarrow 2Nd + 12F^-$$

*Heat Balance and cell design* - Using the prescribed anode current density of 1 A/cm$^2$, and load of 2840 amps, the anodes may be specified. The design will assume the use of a quarter section of a graphite tube, 30 cm long, with the inside dimeter of the tube being 30.12 cm. The tube can be split into four equal arcs to act as anodes. For ease of use each can be replaced separately. The cathode selected is a 50 mm tungsten rod with is an easily obtainable size and below the diameter where copper is sometimes for manufacturability. This diameter corresponds to a reasonable current density of 6 A/cm$^2$.

The bath density is estimated at 4.7 g/cm$^3$ [5]. Given the electrolyte minimum volume of 30 cm diameter by 30 cm deep, 21,205 cm$^3$, the bath's working mass is 99.67 kg, requiring additional volume for the annular gap between the safety can and the back of the anode. This shown below in Figure 54. Bath composition of 87% $NdF_3$/13% LiF is chosen as the working electrolyte, with estimated solubility of $Nd_2O_3$ of 3.9 % [6]. Carbon wear of 0.2# C/#Nd, with a density of graphite of 1.72 g/cm$^3$.

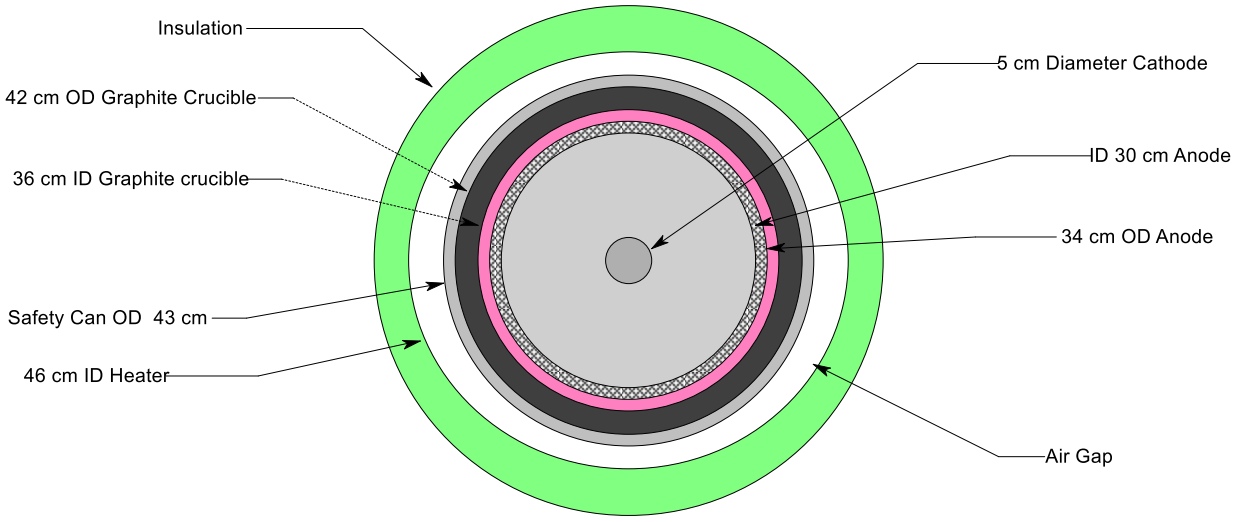


Figure 54. Illustration of the cell (top view).

Assuming the graphite anode will fail once the graphite reaches half its thickness, an estimate of the outside diameter can be made. Using 2840 A (1.79 g/am-hr)(0.2)(0.8), each hour produces 3,998 gr Nd, and consumes 800 gr of carbon for a volume of 460 cm$^3$.

Diameter of the wear line can be determined as:

$$2840 \text{ amp } (.8)(.2)(1/1.74)(\text{ X hours}) = 30\text{cm } (R_{wear}^2 - R_i^2)\pi$$

$$2.77X = R_{wear2} - Ri_2$$

$$2.77X + 225 = R_{wear}^2$$

Using X = 24 hour change cycle, the wear radius is estimated as 17 cm, or about 2 cm per day, giving an anode starting with an outside diameter of 38 cm.

Heating the cell to a temperature sufficient to melt the salt will require external heaters. The cell heat balance is a function of the heat loss through the cell wall and lid. Vogel [3] reports that about 45 % of the heat is loss in current Chinese practice through the top of the cell because no lid is used. Using a cold face temperature of 140 °F, the cell design can then be calculated.

The heat losses in electrolysis cell fall in three categories: 1) the heat loss in heating up the neodymium oxide feed, 2) the loss in replacement of electrolyte, and 3) loss of heat due to evaporation of the electrolyte (assumed to be $NdLiF_4$) and the endothermic reaction at the electrodes. HSC 7.1 was used for the estimates. Table 31 shows the heat capacity data for species of interest. The heat capacity data has the form: $Cp = A + BT + CT^{-2} + DT^2$, HSC used cal/mol for this relation, in the heat balance work kilojoules are used. Additional thermodynamic data is provided in Table 32.

Table 31. Heat Capacity data

| **Parameter** | **A** | **B x10$^3$** | **Cx10$^{-5}$** | **Dx10$^6$** | **Temperature range (k)** |
|---|---|---|---|---|---|
| $Nd_2O_3$ | 29.291 | 10.086 | -2.225 | -1.525 | 298-2333 |
| $NdF_3$ | 22.155 | 5.6 | -1.543 | 0 | 298-1650 (mp) |
| LiF | 12.026 | 0.596 | 1.910 | 3.307 | 298-700 |
| | 10.925 | 2.898 | -2.059 | 0.626 | 700-1121 |
| | 15.340 | | | | 1121(mp)-3000 |
| Nd | 4.374 | 5.402 | 0.509 | 0 | 298-1128 |
| | 10.755 | 0 | 0 | 0 | 1128-1289 |
| | 2.749 | 3.059 | 69.551 | 0 | 1289-1500 |
| $CO_2$ | 7.006 | 9.553 | -0.594 | -3.533 | 298-900 |
| | 13.01 | 1.223 | -10.418 | -0.193 | 900-2700 |
| CO | 6.601 | 1.521 | -0.083 | -0.25 | 298-3600 |
| Ar | 4.968 | 0 | 0 | 0 | 100-8000 |
| $N_2$ | 7.002 | -0.375 | -0.002 | 0.817 | 100=350 |

Table 32. Heat of fusion for fluoride species

| **Species** | **Heat of fusion (kcal/mol)** | **Melting point (mp)** |
|---|---|---|
| LiF | 6.474 | 1121 K (848 °C) |
| $NdF_3$ | 13.1 | 1650 K (1377 °C) |
| Nd | 1.697 | 1289 K (1016 °C) |

For the heat loss by evaporation, a regression line H = A + BT will be used. The data reported in HCH uses W-hr as unit of heat. One W-hr is equal to 3600 joules. The regression was performed over the temperature range of 850°C to 1200°C. The values in Table 33 were found for the three reactions.

Table 33. Heat of evaporation of salts.

| **Reaction** | **A** | **B** |
|---|---|---|
| LiF→LiF(g) | 72.9 | -0.00737 |
| $NdF_3$-→$NdF_{3(g)}$ | 125 | -0.00963 |

There are two endothermic reactions considered being:

$$Nd_2O_3 + 3C = 3CO_{(g)} + 2^{Nd}$$

$$Nd_2O_3 + 1.5C = 1.5CO_{2(g)} + 2^{Nd}$$

While the formation of CO is thermodynamically favored, most of the carbon consumption is from the formation of $CO_2$. Some carbon is lost due to operation of the cell. In practice the anodes might have to be trimmed to fit or some parts removed for electrical or operational reasons. The results of this regression is shown below in Table 34 with the $R^2$ values are 0.999 to 1.0. The values are in W-hr. Molecular weight of $Nd_2O_3$ is 336.40 g/mol.

Table 34. Endothermic reactions at 1050 °C.

| **Reaction** | |
|---|---|
| $Nd_2O_3 + 3C = 3CO_{(g)} + 2Nd$ | 1473.193 kJ |
| $Nd_2O_3 + 1.5\ C = 1.5CO_{2(g)} + 2Nd$ | 1222.319 kJ |
| Overall with 3:1 $CO/CO_2$ ratio | 1410.5 kJ |

*Calculation of heat from the endothermic reaction at 1050 °C* – An assumed feed rate of 4.70 kg/hr, or 13.97 moles/ hour equate to a heat loss of 19,730 kJ/hr. The heat required to raise neodymium oxide from 25 °C to 1050 °C can be estimated from the heat capacity:

$$\Delta H_{Nd2O3} = \int Cp = (29.291(1323\text{-}298)) + 10.086(1323^2\text{-}298^2)(1/2)x10^{-3} + 2.225x10^5 (1/1323\text{-}1/298)\text{-}1.525x10^{-6}(1/3)(1323^3\text{-}298^3) = 30{,}024 + 8380 - 578 - 1164 = 36660 \text{ cal/mole}$$

Assuming a flow rate of 5.197 kg which equates to:

$$5197\text{g/hr}(1/336.4)(36660)(4.18\text{ J/cal}) = 2367\ \underline{\text{kJ/hr}}.$$

The heat of dissolution is not known. Heat loss from metal removal is estimated by the heat capacity of the metal and heat of fusion. Using metal production of 4.051 kg/hr this caluulates to:

$$4051(1/144.24)(1697)(4.18) = 199\text{ kJ/hr}$$

The heat content of the metal released upon cooling is calculated by:

$$\Delta H \text{ Nd} = \int Cp = 4.374(298\text{-}1294) + 5.402(1/2)(298^2\text{-}1294^2)(10^{-3}) + 0.509x10^5(1/298\text{-}1/1294) = \text{-}4356\text{-}4287\text{-}131 = 35 \text{ kJ/mol},$$

Heat loss from 1050° to 1021° mp is evaluated at:

$$(1021\text{-}1050)(10.75) = 1.3 \text{ kJ/mol},$$

The total heat loss from cooling the metal per hour, is then:

$$(4051)(1/144.24)(1.3+35) = 10.1 \text{ kJ/hr}.$$

Heat loss from the emission of $CO_2$ is estimated by:

$\Delta H_{CO2}$ = Heat capacity from 298 to 900 K and 900° to 1323°K

$$\Delta H_{CO2} = (900\text{-}298)7.006 + 9.553x10^{-3}(1/2)(900^2\text{-}298^2) - (\text{-}594x\ 10^5)(1/900\text{-}1/298) - 3.533x10^{-6}(900^3\text{-}298^3) = 4218 + 4338 - 133 - 135 = 34.9 \text{ kJ/mol}$$

$$\Delta H_{CO2} = 13.01(1323\text{-}900) + 1.223(1/2)(10^{-3})(1323^2\text{-}900^2) + 10.418*10^5)(1/1323\text{-}1/900) - 0.193x10^{-6}(1323^3\text{-}900^3) = 5503 + 575 - 370 - 306 = 22.6 \text{ kJ/mol}$$

$$\Delta Hco = 6.601(1323\text{-}298) + 1.521(1/2)(10^{-3})(1323^2\text{-}298^2) + (10^5)(1/1323\text{-}1/298)(\text{-}0.083) - .25x10^{-6}(1323^3\text{-}298^3) = 6766+1264 +21-572 = 36.08 \text{ kJ/mole}$$

Assuming a 3:1 $CO/CO_2$ ratio in the heat balance and total carbon wear rate of 815/gr hour, the heat loss can be determined by:

For $CO_2$: (1/4)(815/12)(22.6 +34.9) = 759 j/hr

For CO: (3/4)(815/12)(36.08) = 1.83kj/hr

Using these values, heat loss calculations were performed and the results presented in Table 35. Most heat loss is a result of the endothermic reaction and heating up of oxide feed from room temperature to operating temperature.

Table 35. Heat loss (chemical process).

| **Species/ process** | **kJ/hr** |
|---|---|
| Neodymium oxide feed | 2,367 |
| Endothermic reactions; | 19,730 |
| Heat loss from $CO/CO_2$ emission | 2.6 |
| Heat loss from metal removal | 199 |
| Total | 22,300 |

Heat is also lost from the sides, top and bottom of the cell. To estimate this heat loss, several assumptions have to be made. For the design of the method of using quarter arcs around the top of

the furnace crucible, this design maximizes the area of the anode so the cell can be operated at 0.5 $A/cm^2$.

The outside anode diameter is 38 cm with a small gap between the crucibles to the anode outside diameter. It will be necessary to isolate the cathode from the cell. Otherwise, safety can become cathodic, resulting in metal deposition on the safety can.

*Heat additions*

*Heat of combustion* – Because graphite will burn in the air at the operating temperature the heat of C combustion must be considered. The heat of combustion to produce $CO_2$ is -395 kJ/mol, and CO is -393 kJ/mol. In the electrolytic process, the assumption is a combustion gas ratio of 3:1 $CO/CO_2$ at the anode. Using the 3:1 ratio, the electrolytic carbon wear can be estimated as:

$$Nd_2O_3 + 3C = 3CO_{(g)} + 2Nd,, \text{ about 36 gC/ 2(144.24) or 0.12g C/gNd,}$$

$$Nd_2O_3 + 1.5C = 1.5CO_{2(g)} + 2Nd, \text{ about 0.06gC/gNd.}$$

$$\text{This sum to } (.75)(0.12) + 0.25(.06) = 0.105.$$

With wear estimate of 0.2 #C/#Nd, air burn fraction equates to 0.095 #C/#Nd. Using this assumption and an average heat of combustion of 393.5 kJ/mol and 4051 g/hr metal produced equates to:

$$4051(.095)(1/12)(\ 393.5)(1/3) = 4207 \text{ kJ/hr added heat.}$$

Since the electrodes are concentric, the solution to estimating the resistance of the cell can be estimated based on the conductivity of the electrolyte. The value of this has been reported [7] as 2.55 $Scm^{-1}$. It has been reported to be in the range of while physical measurement reports a value of [8] 4.9 $Scm^{-1.}$ This difference might be an error in measurement, or the level of oxide dissolved in the bath. Using the diameters found in the sections above and given:

$$¡ = -\kappa\frac{(Va - Vc)}{L}$$

$$¡ = -\kappa\frac{d\phi}{dr}$$

where L is gap between the electrodes and H is length of cylinder:

$$\int_{\phi i}^{\phi o} d\phi = -\frac{I}{2\pi H ¡}\int_{ri}^{ro} dr/r$$

$$\phi_o - \phi_I = \frac{I}{-2\pi H\kappa}\text{In}\frac{ro}{ri}$$

$$\Delta\phi = \frac{I}{2\pi\kappa H}\text{In}\frac{ro}{ri}$$

$$\Omega = \frac{1}{2\kappa\pi H}\text{In}\frac{ro}{ri}$$

Using the $r_o$ of 15 cm and $r_i$ of 2.5 cm, and H of 30 cm, then:

$$\Omega = (2\pi(4.9)(30))^{-1}\ln(15/2.5) = 0.0019 \text{ ohm.}$$

Cell voltage can be estimated by V = IR +E, (0.00190)(2840) +1.4 = 6.9 volts. The heat generated is estimated by:

$$Q = I^2R, (2840)^2(0.0019)(3600) = 55{,}168 \text{ kJ/hr.}$$

The annular gap (15-2.5) is determined at 4.9 inches, which can be reduced by using spaced cathodes. The anode current density must be kept at 1 A/cm$^2$. This will reduce the resistance of the cell. The cell geometry described was shown previously in Figure 54.

Using the heat flow calculator provided by Morgan Technical ceramics, the insulation package is 4 inches of Kaowool 2600 vacuum press board (part of which has the heating elements imbedded, followed by 1/8-inch of Kaowood 3000 paper, followed by 9 inches of insulating fire brick (IFB) insulation. This achieves a cold face of 140 °F with a heat flux of 160 btu/ft$^2$/hr. Giving the outside diameter is 64 inches, and the height with vestibules is about 18 inches, the heat flow per hour is estimated at 18(56)π resulting in 3166 in$^2$, with the bottom section at about 2464 in$^2$, total of about 5370 in$^2$, or 5966 btu/hr, recasting as 6294 kJ/hr. The resulting heat budget is provided in Table 36.

Table 36. Heat budget of NdPr cell.

| **Input** | **Value** | **Output** | **Value** |
|---|---|---|---|
| Joule heating | 55,168 | Neodymium oxide feed | 2367 |
| Air burn of graphite | 4,207 | Endothermic reactions; | 19,730 |
| | | Heat loss from $CO/CO_2$ emission | 2.6 |
| | | Heat loss from metal removal | 199 |
| | | Side and bottom conduction/convection | 6294 |
| **Total kJ/hr** | 59,400 | | 28,600 |

A difference in heat generated and heat loss is about 39,000 kJ/hr. This heat is assumed to be released from the top of the electrolyte surface. The proposed design assumes the use of an external heater. The cell design as reported Vogel [3] has no external heater. A sketch of this design is shown in Figure 55.

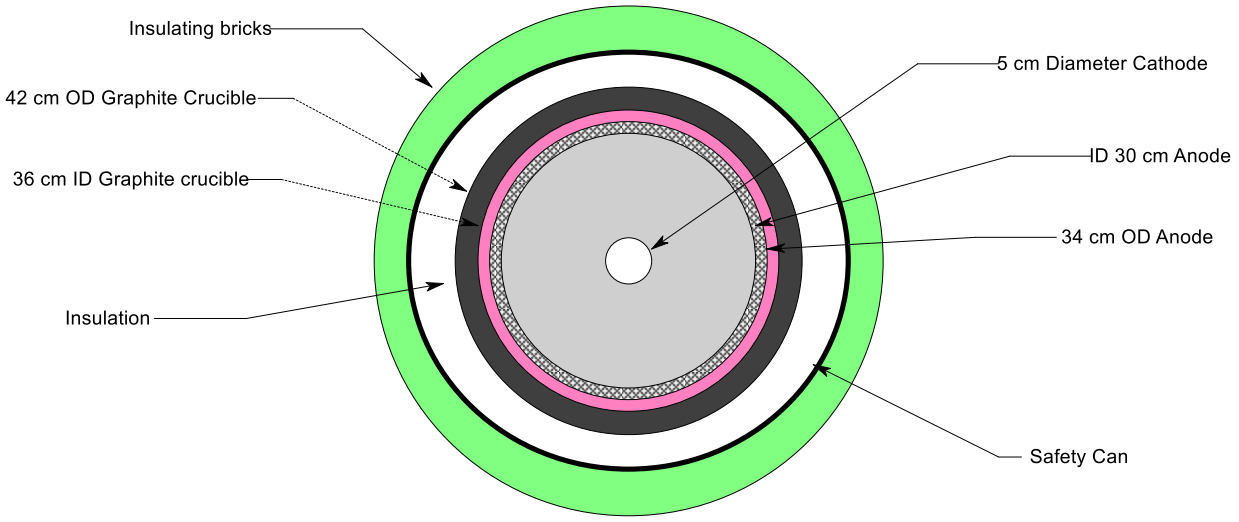


Figure 55. Top view of light rare earth cell with reduced cell voltage.

Based on this design (electrolyte/graphite/insulation/steel safety can/brick), the heat flow can be estimated. This design has no provisions for melting in place of the starting electrolyte, it can either be melted in place by making an arc between the two electrode (replacing the tungsten cathode with carbon) or melted and heated to a sufficient super heat to allow the electrolyte to be poured into the cell without freezing. Immersion heaters might be possible as well, most are not designed to operate at 1050° C. To melt with immersion heaters the bath would be started at a composition near the eutectic and then brought to composition by using alternating current between the electrodes and additions of neodymium fluoride. For insulating the reactor, two inches of Kaowool, with a second layer of 9 inches of insulating fire brick on the outside of the safety can are utilized. This design has a calculated heat flux of 6228 btu//hr, (6566 kJ/hr) assuming a cold face 153 °F. The resulting heat balance is shown below:

Table 37. Reduce cell voltage heat balance.

| **Input** | **Value** | **Output** | **Value** |
|---|---|---|---|
| Joule heating | 55,168 | Neodymium oxide feed | 2367 |
| Air burn of graphite | 4,207 | Endothermic reactions; | 11,461 |
| | | Heat loss from $CO/CO_2$ emission | 2.6 |
| | | Heat loss from metal removal | 199 |
| | | Side and bottom conduction/convection | 6566 |
| Total kJ/hr | 59,375 | | 20,600 |

The improved design has the advantage of lowering the cold face temperature to 140 °F. The heat flow out of the top of the cell is similar between designs, however, the new design presented in

this study is an improvement over the conventional design since the cell can be idled and can be used in the heat up of the electrolyte. These are both improvements in the safe operation of the cell.

The electrical conductivity of the electrolyte is a function of the oxide concentration in the electrolyte in the cerium oxide system [9], this has been reported in the neodymium electrolysis. In Zheng, the conductivity is shown to change with composition. There is a systematic error in the measurement as the reported conductivity is about half that found by Liu, and by analysis of the data presented in Vogel [3]. Increasing the oxide concentration in the electrolyte decreased the conductivity of the electrolyte. This then changes the heat input as shown in the heat balance, where most of the heat input into the cell is the joule heating of the electrolyte.

To mitigate the production of tetrafluoromethane the cells can be operated at potential below that of the decomposition of $NdF_3$ to produce $CF_4$. The control scheme is to operate the cell using voltage control, controlling the current so the potential on the anode does not exceed decomposition ranges. Since the conductivity and Nerst potential on the anode are both function of oxide concentration, the electrical load drops as the oxide is feed to the cell. Typically, batch feeding is used because loss-in-weight feeders are inherently more expensive than volumetric feeders. It is recommended that the feed is controlled so that bath is not over fed as this results oxide falling to the bottom the cell leading to losses.

Since the load is a function of concentration, the heat generated changes with feed cycle, using a supplemental heater in the new design keeps the electrolyte temperature constant making removal easier.

To reduce the energy consumption (by an estimated 20%), the cell voltage must be reduced to 5.52 volts. This corresponds to a decomposition potential of 1.4 volts. From this the resistance of the cell can be estimated as follow:

$$(5.52-1.4)/2840 = 0.00145 \text{ ohms.}$$

The anode/cathode can be estimated as follows:

$$0.00145= = (2\pi(4.9)(30))^{-1}\ln(15/x)$$

$1.339 = \ln(15/x)$, $3.8 = 15/x$, $x$ found as 3.93 cm, With diameter of 7.8 cm, or 3.09 inches.

Heat input is found as 42,100 kJ/hr, still in range to meet heat balance of the cell.

*Feed Control*

As part of the EW cell design, automated feed is considered needful to manage cell voltage to prevent swings in temperature and the generation of deleterious gaseous products. For this reason a process flow diagram for an automation of the feed process is shown in Figure 56. The current practice is to use a manual feeding system, where charges are fed directly to the cell or use of a vibrating feeder. The oxide is usually introduced once per hour. Loss in weight feeders could be used. Feed materials feed clogging the feed pipe to cell are often experienced and considered a design flaw. Alternative methods to consider to prevent interruptions is to have a chain or cable in the feed pipe to break up bridging.

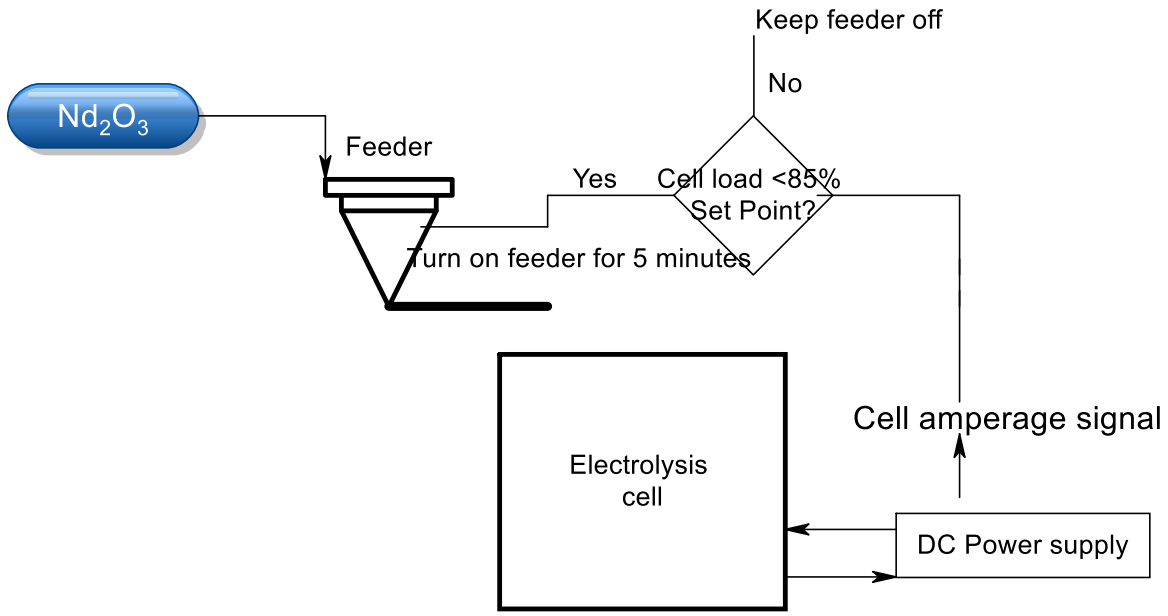


Figure 56. Process flow diagram Nd reduction.

This process eliminates the hand labor used in feeding the cell and results in better cell performance. Understanding the current yield of the cell is also necessary to manage the feeder well. Current yield is measured by the amount of metal removed on a periodic basis.

The composition of the oxide feed for production of neodymium is shown in Table 38. Praseodymium is not typically electrowon in pure form. Some work has been reported on production of praseodymium by electrolysis [10]. Praseodymium oxide is in the form of $Pr_6O_{11}$. This material is not completely soluble in a molten fluoride bath and will flash off some of the oxygen upon addition [11], this has been shown to produce excessive carbon wear. Carbon wear and carbon contamination of the melt is a significant challenge in metal production. One method to overcome it is to use a lid, so that argon or other inert gases can dilute egressed air and slow rate of carbon consumption. Carbon soot generated by the Boudouard reaction and mechanical wear can cause carbon contamination.

*Specification of neodymium oxide* - Specification for the neodymium oxide is based on the material used in electrowinning at Infinium metals. This specification is based on the material that can be purchased, control of rare earths and yttrium present a different problem than transition metals. Rare earths are excluded during production. Iron, chromium, and nickel are the result of scale formation in the cell.

Table 38. Material specification neodymium oxide.

| Species | Concentration | Species | Concentration |
|---|---|---|---|
| $Y_2O_3$ | <500 ppm | $Al_2O_3$ | <400 ppm |
| $Nd_2O_3$ | >99.5% | PbO | <200 ppm |
| $Pr_6O_{11}$ | <450 ppm | $TiO_2$ | <200 ppm |
| $Gd_2O_3$ | <400 ppm | $MnO_2$ | <200 ppm |

| | | | |
|---|---|---|---|
| $Tb_4O_7$ | <400 ppm | $SiO_2$ | <400 ppm |
| $Dy_2O_3$ | <400 ppm | CaO | <200 ppm |
| $Ho_2O_3$ | <400 ppm | $Al_2O_3$ | <400 ppm |
| $Er_2O_3$ | <400 ppm | S | <100 ppm |
| $Y_2O_3$ | <500 ppm | Cl | <100 ppm |
| MgO | <200 ppm | | |

*EW Cell Improvements in cell design and operation*

Current State:

Current practice in the electrowinning space is the operation of a rare earth electrolysis cell at sizes up to about 10kA. These cells are fed with oxide, and metal is tapped out either with a hand ladle or with a mechanical siphon. There are several Chinese patents that used a mechanical ladle similar to a hand ladle, placing the operator further away from the metal and salt. Increasing the distance results in a safer operation for the operator. Metal siphon systems are a technology that is used in the metal collection of magnesium and aluminum and can be adopted for use in rare earth metal production.

Future State:

The innovations in this space are the measurement and control of vacuum (Table 39). Vacuum generation in this project is based on an ejector powered by gas (Venturi effect). This elimination of the mechanical vacuum pump reduces costs, as venturi-based devices have enough vacuum to move metal. It is also easier to break the siphon effect with a gas vacuum break.

Sensor needs:

The issue with these techniques is that the operator requires a "fill gauge" to inform when the tank is full. A level sensor will be used to detect when the tank has reached full. Using a crane scale is also possible and has been used commercially in light metals, however any slags present in the tank render this method problematic as they have mass and reduce the volume of the tank.

Table 39. Comparison of methods of metal removal.

| **Item** | **Delta** | **Positives** |
|---|---|---|
| Hand ladle | Shown to have higher oxygen contamination of the metal harvested | Easy materials of construction. Inexpensive parts |
| | Safety issues with spills | |
| Vacuum assisted siphon | Heat tracing on siphon tube necessary for long runs | Better metal quality by exclusion of oxygen |
| | Siphon tubes must be replaced often. | Commercial method in Al and Mg industries. |
| | Requires a vacuum generator | Drain directly into transport container |

| | | |
|---|---|---|
| Stopper Rod tap | Difficult to start and stop flow | Drain directly into transport container |
| | Material of construction for stopper rod | Metal quality should be good |

*Experiments performed* - During the performance period, a small electrowinning cell was commissioned of the 10-100 A size range. An internal safety review was completed, and cell testing was initiated. This prompted several improvements made in the initial design. Results include: 1) Didymium electrolyte made, and melted, 2) Cell furnace temperature capability verified. Further operational methods were evaluated such as: 1) Metal and electrolyte sample removal method refined, 2) Determined that alumina straws work better than steel or titanium for collection, and 3) Successful in draining of crucible by this method. A picture of the cell is shown in Figure 57.


Figure 57. Lab scale molten salt EW cell used for testing.

*Development of the siphon* - The siphon was developed to remove metal and salt from a cell. It uses a venturi to generate a vacuum to pull the metal into the receiver. For observation, a borescope tube or window can be fitted with a remote camera to observe the fill. The heat tracing of the tube at this scale appears based on experiments not to be necessary. This is a practice is borrowed from industrial magnesium production. The use of hand tools such as ladles results in variability in the quality of the rare earth metal harvested from the cell [20]. Using vacuum transport and casting operation the oxygen level in neodymium is reduced dramatically as in Figure 58 [21]. Figure 59 shows cell and siphon.

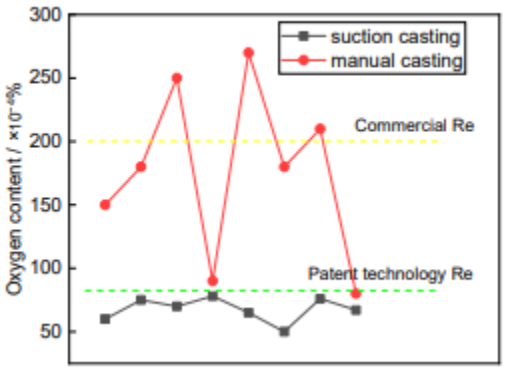


Figure 58. Reduction of oxygen by use of suction device.

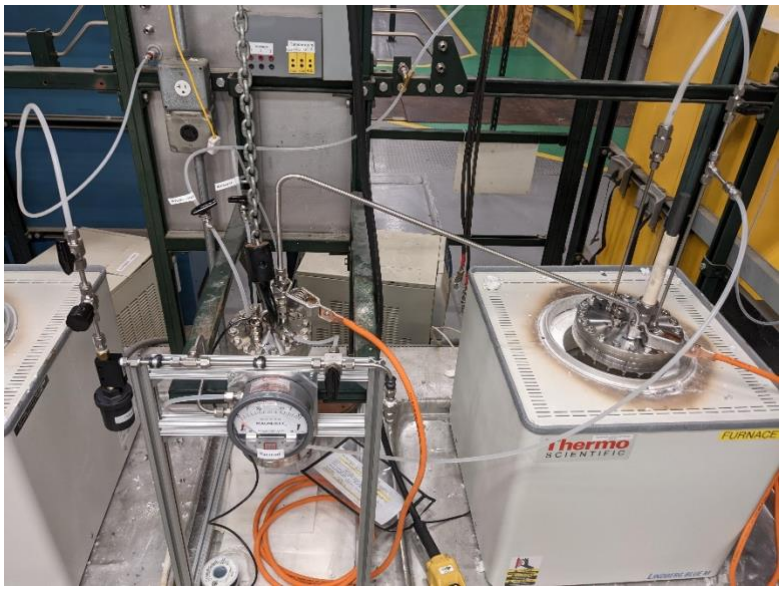


Figure 59. Rare Earth cell with Siphon.

*Heavy rare earth and yttrium reduction*

*Yttrium* - Yttrium metal is produced by the reduction of the halides by lithium, calcium and sodium. The hygroscopic nature of the chloride, bromide and iodine salts makes production of high purity metals. Sodium reduction is a difficult process as yttrium metal can reduce sodium chloride back

to sodium. Lithium metal is the most expensive of the three reductants. The large-scale reduction is performed with calcium metal reaction with yttrium fluoride.

Yttrium fluoride can be produced from the reaction of yttria with ammonium bifluoride, HF or fluoride as shown in Figure 59. Of these, HF and ammonium fluoride is most preferred. Stoichiometric excess of the calcium is necessary to complete the reduction. At 1:7 $Y_2O_3$/ammonium bifluoride is reported as working best [12]. This reaction can be conducted at low temperature (<400 °C). The conversion reaction is shown below:

$$6NH_4(HF_2) + Y_2O_3 = 2YF_3 + 6NH_4F + 3H_2O$$

Once generated the yttrium fluoride is reduced with calcium metal:

$$2YF_3 + 3Ca = 2Y + 3CaF_2.$$

Calcium chloride was added to charge to lower the melting point of the produced salt by making a lower melting point solution. A ratio of 0.9 $CaCl_2/YF_3$ was used [13]. This makes separation of the yttrium from the salt easier. Once produced, the yttrium metal must be remelted to produce ingot forms.

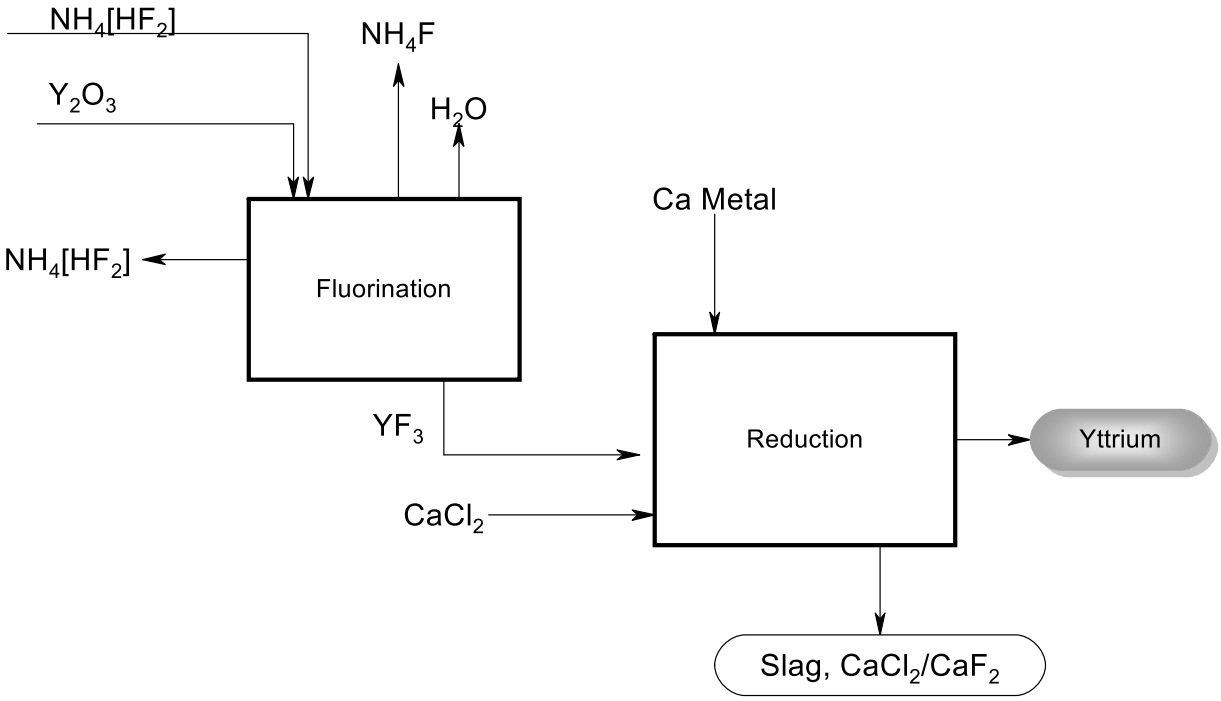


Figure 60. Yttrium metal production from fluoride.

A mass balance table for 1 ton per day supply of yttria is shown in Table 39. The flow rate is in kg/hr using a 23.5-hour day.

Table 40. Yttrium mass balance.

| | **Feed** | **Fluorination** | | **Reduction** | |
|---|---|---|---|---|---|
| | | In | Out | In | Out |
| $Y_2O_3$ | 42.55 | 42.55 | | | |
| $NH_4HF_2$ | | 75.28 | 10.75 | | |
| $NH_4F$ | | | 41.83 | | |
| $YF_3$ | | | 73.59 | 73.59 | |
| $H_2O$ | | | 2.30 | | |
| Ca | | | | 23.97 | 1.44 |
| $CaCl_2$ | | | | 66.23 | 66.23 |
| Y | | | | | 33.51 |
| $CaF_2$ | | | | | 44.09 |

The exhausted ammonium bifluoride and ammonium fluoride must be scrubbed in practice. However, it might be possible to re-fluorinate the ammonium fluoride, dehydrate it and recycle it back using HF is a source of fluorine. This process would be conducted in a tantalum retort for the fluorination process. Cost savings for this process would be based primarily on the materials of construction. As the reduction process is exothermic the heat generated would be used aid in the required heating of the retort. Because of this, it is anticipated the reaction will start and run to completion. The remelting of the yttrium metal to ingot form consumes both energy and tantalum for the crucibles. Reducing the thickness of the crucible wall may decrease the cost. As the project requires a 20% reduction in cost, there appears to be precious little room to make improvement of that magnitude other than a continuous improvement of operations and materials.

*Gadolinium* - Gadolinium metal is used as alloying agent in magnesium, aluminum, and some steel alloys. Only small amounts (1-10%) of the metal is used as an alloying agent. Compounds of gadolinium are used as contrast agent in MRI. The metal can be produced by metallothermic reduction of the fluoride in a similar manner as in yttrium metal production. The reaction with calcium and gadolinium fluoride is not violent. The operating temperature of 1450 °C is used. Reduction of the chloride salt with calcium has proven less successful. Gadolinium has a high melting point of about 1313 °C, making electrolytic production of the metal difficult as most of these processes operate at below the melting point of the metal. Master alloy production can be used with an aluminum cathode. Metallothermic reduction with a magnesium-zinc alloy can also be used to reduce gadolinium fluoride from a mixed salt to an Mg-Zn-Ga alloy [14].

*Dysprosium* - Dysprosium metal is a high melting point (1405 °C) rare earth. It can be produced by metallothermic reduction of fluoride with calcium. Reduction with calcium can make further purification by distillation difficult as dysprosium has high vapor pressure. Calcium metal can be used as the reductant for dysprosium fluoride (using Ta crucibles)[15]. The reduction takes place a high temperature (1750 °C), the yield are low (50%). Subsequent remelting to distill the calcium (4000 ppm) in the dysprosium to lower level (100 ppm) is sued. Further purification by vacuum distillation or sublimation is used [16].

Most commercial dysprosium is used in magnet application is produced by electrowinning dysprosium on to a consumable iron cathode in a molten fluoride salt using oxide feed. This cell

design is very similar to that used in neodymium metal electrowinning. The consumable cathode made of very low carbon steel which is significantly different than the tungsten one used in the lighter rare earths. The eutectic (80% Dy/20%Fe) is produced at the cathode [17]. Additions of iron fluoride or oxide [18] to the bath can be made to adjust the composition at dysprosium will reduce both of these species. An alternative method is to utilize calcium to reduce a combined iron and dysprosium fluoride mixture [19].

*Heat balances- metallothermic reduction of fluorides* - The heat balance of these three fluorides ($YF_3$, $DyF_3$, and $GdF_3$), are reduced with calcium metal. These processes are very similar. Differences are the melting points of the rare earth metal and fluorides. The reduction reactions are more exothermic when calcium vapor is utilized as the reductant. As calcium has a high vapor pressure the reactions start to take place as more calcium additional gas is generated. The produced liquid rare earth metal provides for separation of calcium fluoride from the metal based on density. With the melting point of calcium fluoride is 1417 °C, reactions should have an end point or final temperature above which two-phases are formed (allowing the fluorite and rare earth metal to separate). The reaction is:

$$3Ca_{(g)} + ReF_{3(s,\,l)} = 2Re_{(l)} + 3CaF_{2(l)}$$

These reactions should be conducted at least a few degrees above the melting point of the rare earth and above the melting point of fluorite. The heat of reactions is shown in Figures 60 - 62. The phase transition temperatures for are shown in Table 40.

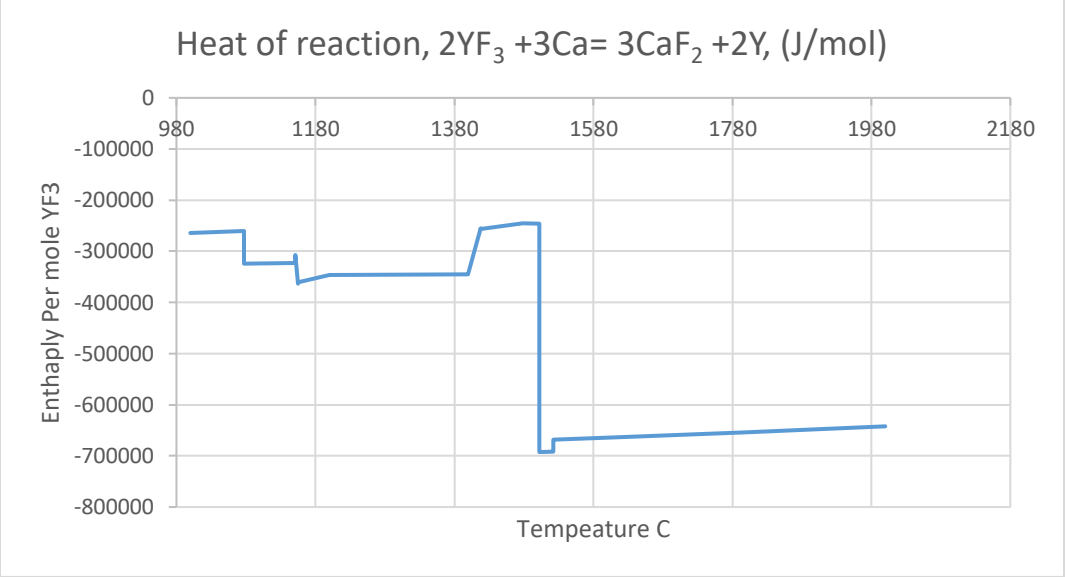


Figure 61. Enthalpy yttrium reduction.

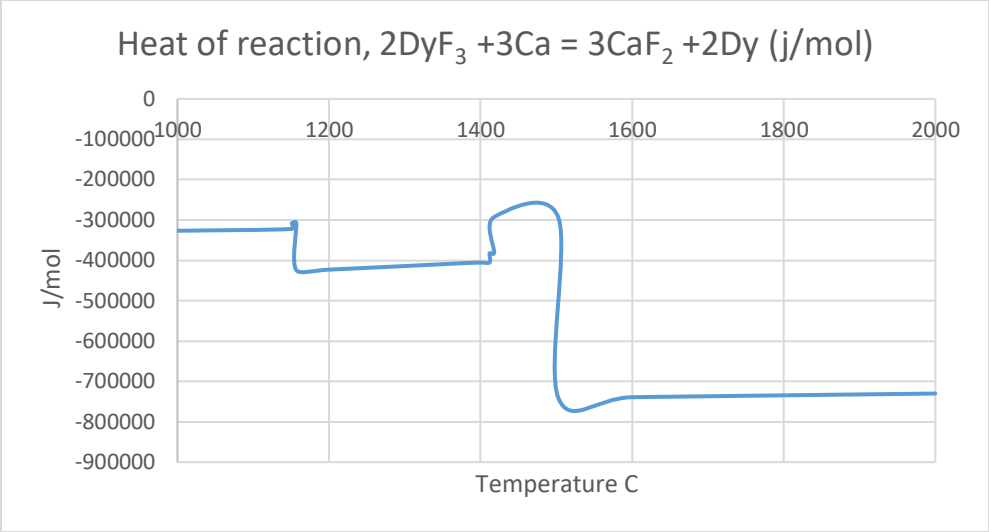


Figure 62. Enthalpy dysprosium reduction.

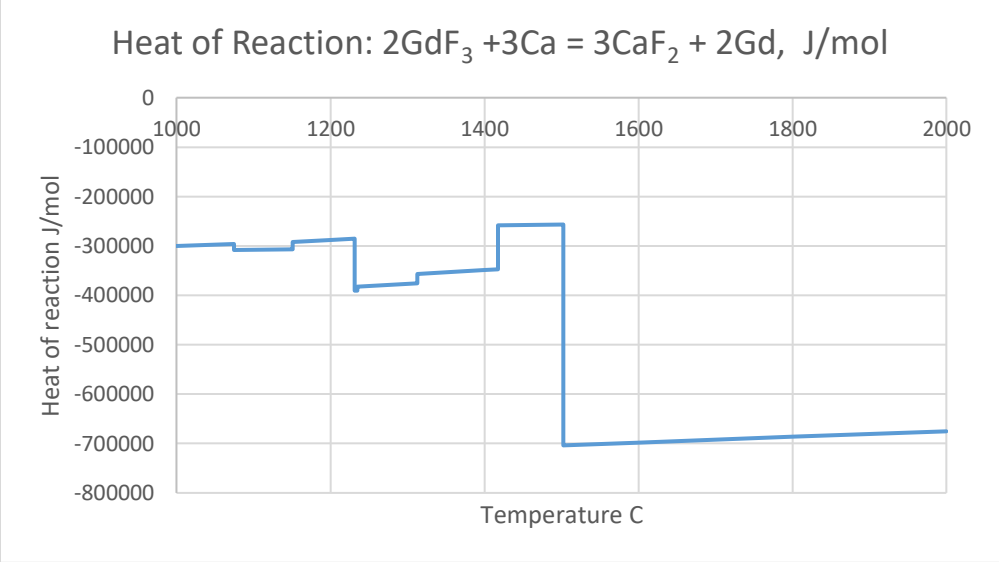


Figure 63. Enthalpy gadolinium reduction.

Table 41. Transition temperatures heavy rare earths and yttrium.

| **Reaction** | **Temperature of transition (°C)** |
|---|---|
| $YF_{3(\beta)} - YF_{3(l)}$ | 1154 |
| $Y_{(s)} - Y_{(l)}$ | 1502 |
| | |
| $DyF_{3(s)} - DyF_{3(l)}$ | 1156 |
| $Dy_{(s)}$-$Dy_{(l)}$ | 1412 |
| | |
| $GdF_{3(\beta)} - GdF_{3(l)}$ | 1231 |
| $Gd_{(s)} - Gd_{(l)}$ | 1312 |

*Samarium* metal is prepared by reducing the oxide with lanthanum. Samarium has the highest vapor pressure of the rare earths. Samarium is prepared by loading samarium oxide and lanthanum metal in tantalum crucibles. The retort is heated in a vacuum furnace to 1100-1400 °C, the lanthanum reduces the samarium, converting to lanthanum oxide [22] and samarium metal and gas. The low vapor pressure of lanthanum allows for separation based on vapor pressure. Other reductants can be used: calcium metal and mischmetal [23] will reduce samarium oxide. Both calcium and cerium have relatively high vapor pressures, and as result are transported into the samarium. Electrolytic methods are less successful because of the two valances of samarium ($Sm^{+3}$ and $Sm^{+2}$) and the high melting point of the metal. Zirconium [24] has also been reported as a reductant, this idea did not lead to a commercial process.

The sublimed samarium then condenses on a colder section of the tantalum retort. Reaction is shown below. Once the reaction is complete the retort is allowed to cool. The retort is removed from the furnace, and the samarium is milled from inside the retort. The samarium in contact with the crucible will be contaminated with tantalum. The milling and erosion of the tantalum by this process results in a limited lifetime of the crucibles, typically about 25 cycles are possible. The cost of tantalum crucibles is one of the drivers of the cost of the process. The economy of metal production is driven by the cost of tantalum as in the current market it's more valuable than samarium.

$$Sm_2O_3 + 2La = 2Sm_{(g)} + La_2O_3$$

Energy reduction in the process is achieved by improvements in the efficiency of the heating elements. The process generates heat when performed.

*Final thoughts* - A review of the physical chemical data from these salts and species show many inconstancies. The melting points of the rare earth fluoride and metals are reported over a range of values. This leads to a conclusion that precise heat balances are difficult in these systems as the values for the enthalpy are only estimates and not direct measurements.

*2.6.2.2 Section References:*


[1] Zhang, L, Wang, X., Gong, B., Perfluorocarbon emissions from electrolytic reduction of rare earth metals in fluoride/oxide system. Atmospheric Pollution Research, Vol 8 2018 pp-61-65

[2] Cai, B,, Liu, H., Kou, F., Yang, Y., Yao, B, Chen, X., Wong, D. S., Zhang, L., Jianzhong, L., Kuang, G., Chen, L., Zheng, J., Gaun, D., Shan, Y,, *Estimating perfluorocarbon emission factors for industrial rare earth metal electrolysis*. Resources, Conservation & Recycling, V 136 (2018) pp315-323

[3] Vogel, H., Friedrich, B., Development and research trends of the Neodymium Electrolysis-A Literature review. Proceedings of the EMC 2015.

[4] Wang, J. Deng, Z-M, Zhang, X-J., The Test Research on Energy balance of 10kA fluoride system in RE Fused-salt electrolysis cell. Jiangxi Non Ferrous Metals, 2004-2

[5] Hu, X, Wang, Z. Gao, B., Shi, Z., Liu, F., Cao, X., *Density and ionic structure of $NdF_3$-LiF Melts*. Journal of Rare Earths, Vol 28, N 4, August 2010 pp 587-590.

[6] Dysinger, D. K., Murphy, J. E., Electrowinning of Neodymium form a molten oxide-fluoride electrolyte. USBM RI9504, 1994

[7] Zheng, X. Zhu, W-h, Peng, G-h., Lange, J, Zhange X-j., *The electrical conductivity of $NdF_3$-LiF-$Nd_2O_3$ molten salt.* China Tungsten Industry.

[8] Liu, F., Fundamental electrochemical study of neodymium molten salt electrolysis in fluoride bath. PhD Dissertation, Colorado School of Mines, 2019.

[9] Thomas, N. B., An Investigation of some aspects of cerium electrowinning. USB MS 1986 Thesis.

[10] Ghandehari, M. H., *Electrolytic production of praseodymium*. USP 4,627,898, Dec 9, 1986

[11] Morrice, E., Henrie, T. A., Electrowinning high purity neodymium, praseodymium, and didymium metals from their oxides. USBM RI 6957, 1967

[12] Walker, J., Olson, E., *Preparation of yttrium fluoride with ammonium bifluoride*. Iowa State University, AEC contact W-7405, 1958.

[13] *The Rare Earths*. Edit by F. H. Spedding and A.H. Daane, Joly Wiley & Sons, New York, 1961 p121.

[14] Sevchenkov, S. A., Bazhin, V. V., Porarov, V. G., Research on the process of gadolinium recovery from the melt of salts of formation of Mg-Zn-Gd master alloys for manufacturing of magnesium and aluminium special purpose alloys. Non-Ferrous Metals No 1, (2020) pp 35-40

[15] Daane, A. H., Spedding, F. H., *Preparation of Yttrium and Some heavy Rare Earth Metals*. Journal of the Electrochemical Society, V 100, 1953, pp442-444

[16] Sandon, B.L. A Study of the reduction of dysprosium oxide with lanthanum as a method for producing high purity dysprosium metal. MS Thesis, Iowa State University, 1973.

[17] Nakamura, E., Itoh, K., Nishio, M., Sakakibara, M., Process and apparatus for producing dysprosium-iron alloy and neodymium-dysprosium-iron alloy. EPA 86309893.5 12/18/1986

[18] 史文范, 黄平, 李雅民, 赖心兰, Method for preparing Dy-Fe alloy through oxide molten salt electrolysis, CN 102140656A, 3/9/2011C02140656

[19] Schmidt, F. A., Peterson, D. T., Wheelock, J.T., *Preparation of rare earth iron alloys by thermite reduction*. USP 4,612,047. Sept 16, 1986

[20] Sun, M., Zhao, Y., Wang, Z., Liang, B., Shao, L-B., Design and dynamic simulation of manipulator. MEMAT 2021, Journal of Physics conference series, 1820 (2012), 012027

[21] Liu, H., Zhang, Y., Luan, Y., Yu, H., Li, D. Research Progress in Preparation and purification of rare earth metals. Metals (2020), 10, 1376.

[22] Daane, A. H., Dennison, D. H., Spedding, F. H., "The preparation of samarium and ytterbium metals". Journal of the American Chemical Society, Vol 7, (1953), pp2272-2273

[23] Ghandehari, M. Samarium metal production. USP 4,439,232, March 1984.

[24] Campbell, T. T., Block, F. E., "Europium and Samarium production"., Journal of Metals Nov (1959), pp744-747

*2.6.2.3 Cost Estimates and Improvements for a Molten Salt EW Cell*

*Cost estimate for 2850 A neodymium cell* - This estimate is based on the design provided in the proceeding section. This comprised of a circular cell with central tungsten cathode surrounded by graphite anodes. The anodes are cut into quarter sections. It appears that the grade of graphite needed is lower than work performed by Argonne. This equates to a value of about $3/kg rather than $21/kg used in the work. This will result in lowering the cost significantly.

The cost of tungsten collection cup is based on:

- harvest frequency of six times per day;
- volume of 4000 $cm^3$
- given base of the crucible, and anode circle for mounting, the cup has a diameter of 8.7 inches (22 cm), with height of 10 cm;

This results in an estimated Cost: $6100 each. For a tungsten cathode:

- 2-inch dimeter;
- 24 inches long;

The estimate Cost is $4650 per cathode. For a graphite crucible:

- 17.8-inch OD, x 16.8-inch ID, height of 20 inches, 1-inch-thick bottom:

Is estimated at $2800 each with a lifetime of about 180 days. In considering the cell itself:

- Safety Can,
- SS310 stainless pipe,

Results in an estimated cost of $5200 per can with flange. Further items considered are:

- Heating furnace: $40,000, with controller;
- DC power supply, $45,000 with six pulse power supply, about $55,000 for a 12 pulse system. These are estimated using an elevation of less than 2000 ft;
- Feeder for each Cell, Schenck Accurate: $4400.

A mechanical convection oven can be used to dry the oxide before use, this usually results in better electrochemical performance.

*Cost estimate for nine cells to operate one ton per day of neodymium oxide* - This cost estimate was made based on bids from vendors for parts and estimates of the cost of graphite. For the single cell operation less engineering is used, for the nine-cell line more engineering and electrical work are needed. The operations of these cells for commercial use the duty cycle is very high (>99%), as result staffing is necessary for the process on a 24-hour basis. For demonstration of the conversion of oxide to metal only single shift operation can be used.

Table 42. Cost item list for molten salt EW cells.

| **Item** | **Count** | **Unit Cost, one cell** | **Total** |
|---|---|---|---|
| Graphite Crucible | 9 | $2,800 | $25,200 |
| Tungsten turn dish | 9 | $6,100 | $54,900 |
| Tungsten Cathode | 9 | $4,650 | $41,850 |
| Safety Can | 9 | $10,000 | $90,000 |
| Graphite Anodes | 36 | $113 | $4,068 |
| Feeder | 9 | $4,400 | $39,600 |
| Lid | 9 | $1,200 | $10,800 |
| Furnace | 9 | $40,000 | $360,000 |
| Power Supply (AC to DC) | 9 | $45,000 | $405,000 |
| Power switch for AC/DC | 1 | | $52,730 |
| AC Power supply for Siphon | 1 | $7,200 | $7,200 |
| Siphon hardware | 2 | $2,000 | $4,000 |
| Controls for power supplies | 1 | $10,000 | $10,000 |
| Duct work | 1 | $44,120 | $44,120 |
| Total | | $177,583 | $1,149,468 |
| Delivery | 5% | $8,879 | $57,473 |
| Tax. Use tax | 0% | | $0 |
| Installation | 20% | $35,517 | $229,894 |
| Piping | 16% | | $183,915 |

| | | | |
|---|---|---|---|
| Electrical | 20% | $35,517 | $229,894 |
| Instrumentation | 7.50% | | $86,210 |
| Engineering | 10- 31% | $17,758 | $356,335 |
| **Total** | | **$275,254** | **$2,293,189** |

The anode wear rate is about 0.2 kg/kg Nd with a 2800 Amp load. The consumption rate of graphite is about 0.8 kg/hr. Each anode set will be replaced about once per day or longer. Running cost is about $120 per day on graphite per cell.

### *2.6.3 Subtask 6.3 – Low Temperature Membrane Organic EW*

Prior to the commencement of this project, Argonne National Labs has been researching ionic liquids and using them with a membrane to electrodeposit lithium metal. For this project a scoping experiment was attempted with two liters of solution provided by the University of Kentucky. The leach liquor was used in the anolyte compartment and ionic liquid with lithium salts was used as the catholyte. A major concern was the high sodium content from the supplied waters. Resolving this concern, the testing demonstrated that the sodium from the leach liquor did not transport across the membrane. The results showed the sodium to lithium ratio was > 200:1. This meant the membrane was effective in excluding sodium. The current efficiency of the deposited lithium could not be determined by mass balance as some of the lithium may have originated from the catholyte. Based on the small sample size further investigation was not possible. For future work, this experiment should be repeated, but for this work was not possible owing to the dismantling of the REE pilot plant where the samples originated from.

The cell voltage was about 6.25volts, with 0.26 g li/amp hour. At 100% current yield the energy cost for reduction is estimated at about 24 kW-hr/kg. Conventional electrowinning of lithium has an energy cost of about 30-40 kW-hr/kg [1]. However, the production of lithium by molten salt electrolysis with a LiCl-KCl bath at 450 °C, electrodeposits will contain some potassium with the lithium that has to be removed by distillation. A benefit to the proposed process is that this does not occur using room temperature ionic liquids.

#### *2.6.3.1 Section References:*

[1] Zhang, X., Han, A., Yang, Y., Review on the production of high purity lithium metal. Journal of Materials Chemistry A. (2020), 8, 22455-22466.

### *2.6.4 Subtask 6.4 – Thermal Plasma Process*

The University of Kentucky pilot plant produced MREO/MRES and CM feed stock materials from coal-based resources and their elemental contents were used in this research project. These feed stocks from circuits 1 and 2 contains rare earth metals including Sc, Y, La, Ce, Pr, Nd, Sm, Eu,

Gd, Tb, Dy, Ho, Er, Tm, Yb and Lu, and critical metals including Al, Ca, Co, Cr, Fe, Li, Sr and Mn. The detailed composition of the above three materials are presented in Table 20 to Table 22.

Based on thermodynamics calculation, oxides concentration of the rare earth elements were reduced completely using $CH_4$ at 2473 K and 1 atm as shown in Figure 64 [1]. As $Sc_2O_3$, $Lu_2O_3$ amounts are very low, they will not be considered. In the first step, the oxides are reduced to their corresponding elements in a plasma reactor by $CH_4$ at 2473 K and 1 atm [2].

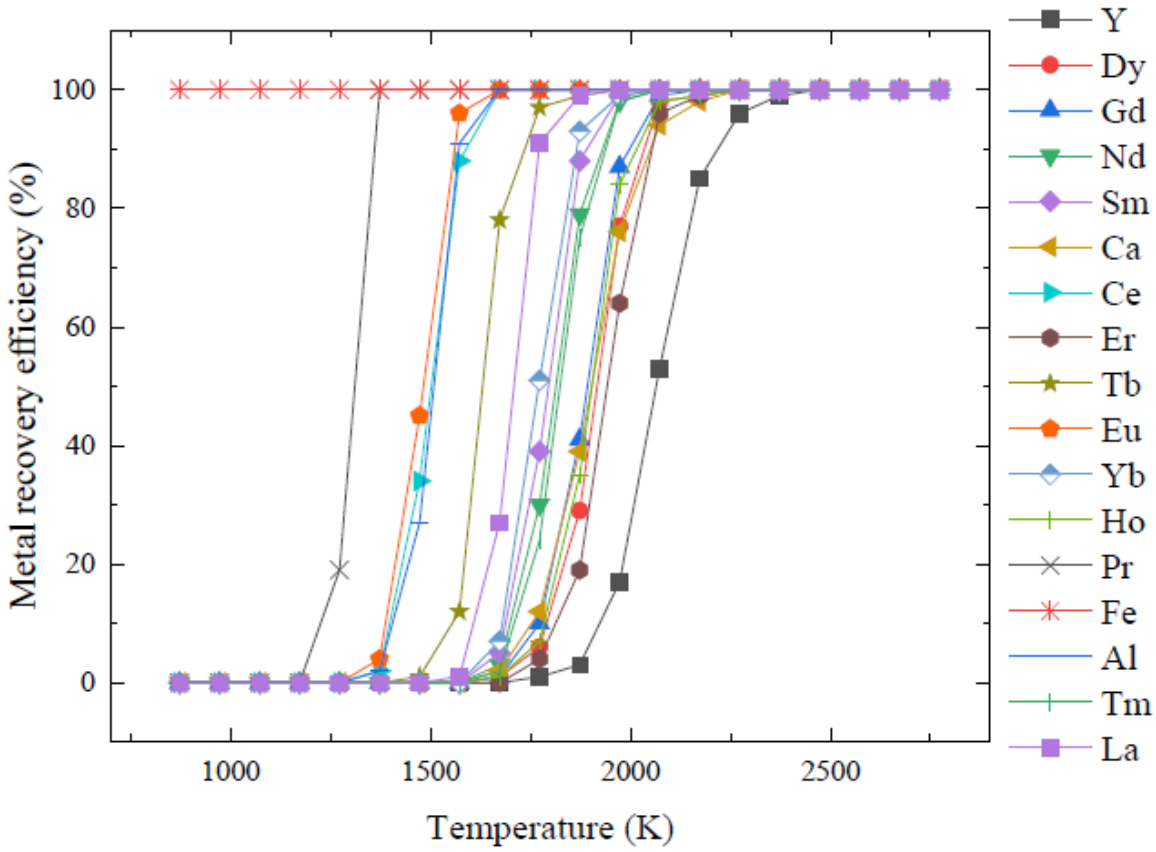


Figure 64. Metal recovery efficiency as a function of temperature (Thermodynamic calculations).

From Figure 65, it is found that the vapor pressures of Sm, Eu, Dy, Tm, Yb and Ca are higher than 1.01 bar at 2473 K. In the second step, they are separated as vapor phase from the rest of the elements (Nd, Y, Gd, Al, Fe….). Based on the properties and prior work cited in the next section, the proposed flowsheet was developed as shown in Figure 66.

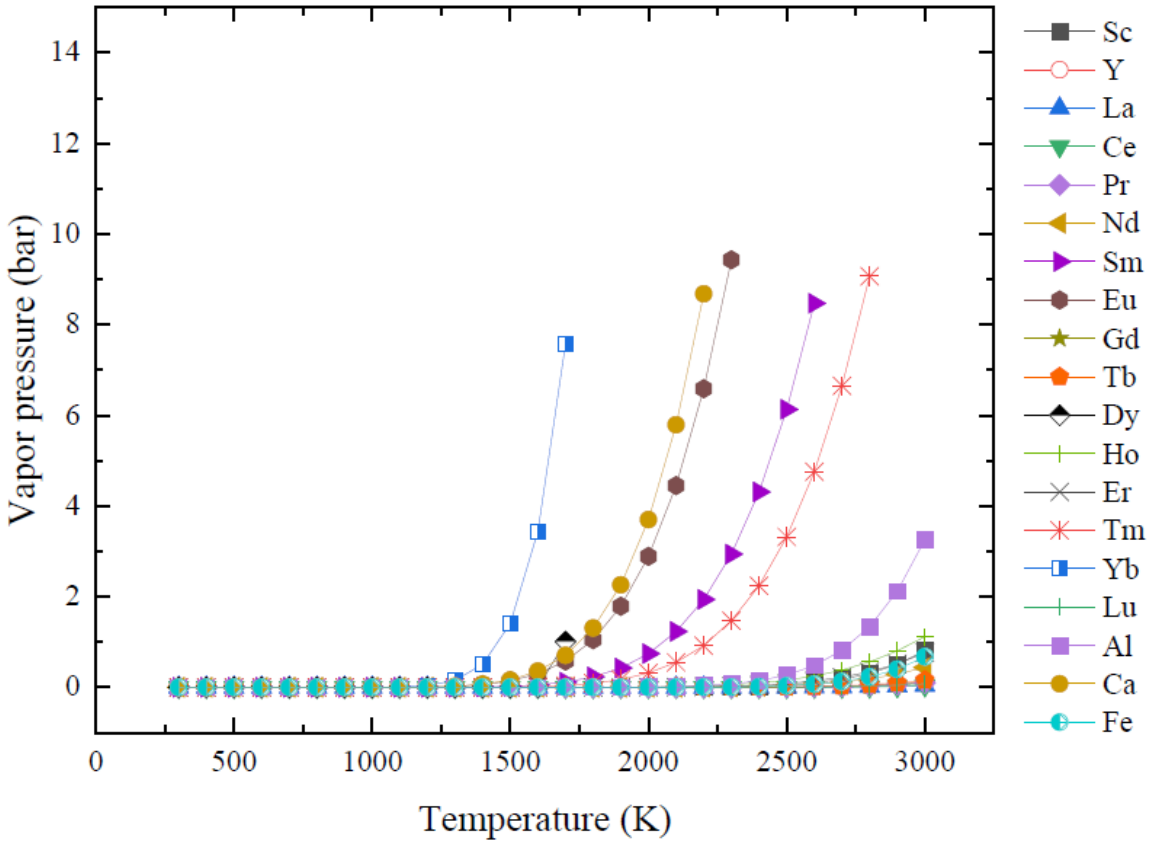


Figure 65. Vapor pressure vs temperature for different elements.

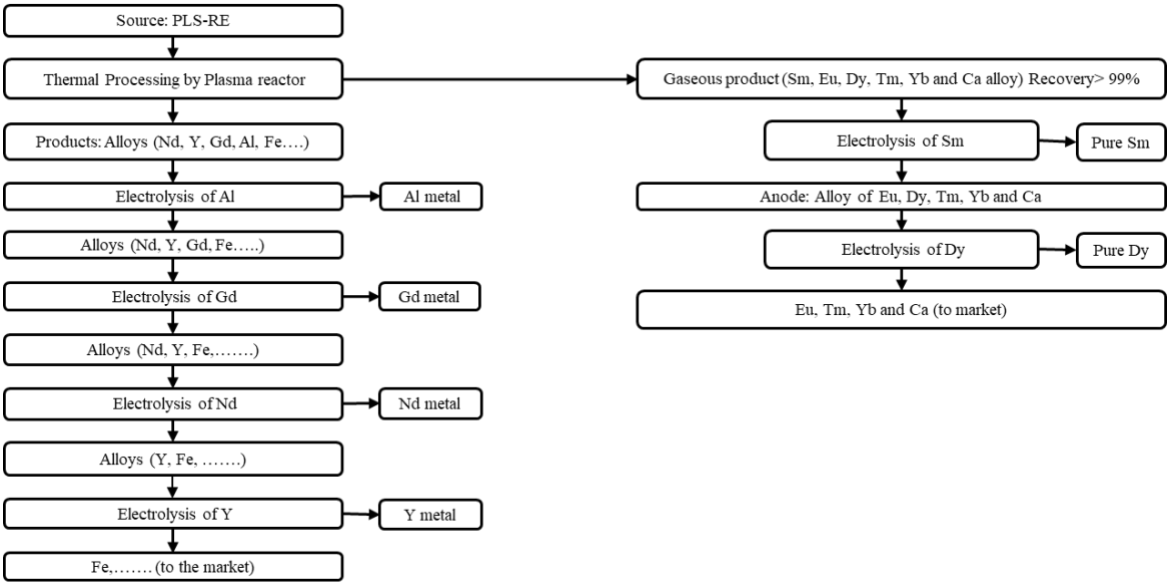


Figure 66. Combined plasma distillation and ionic liquid circuit for the purification and reduction to metal of REEs.

*2.6.4.1 Section References:*

[1] HSC Chemistry Software, V 5.11, Copyright Outokumpu Research.

[2] S. W. White and R. G. Reddy, Waste Processing of MgO Bag house Dust Using Plasma Arc Technology, EPD Congress, ed. by B. Mishra, TMS, pp. 687-697, 1999.

[3] E. Gómez, P. Cojocaru, L. Magagnin, and E. Valles, Electrodeposition of Co, Sm and Sm-Co from a deep eutectic solvent, Journal of Electroanalytical Chemistry. 658 (2011) 18–24. doi:10.1016/j.jelechem.2011.04.015.

*2.6.5 Subtask 6.5 – Carrier-Based Ionic Liquid EW.*

From the plasma process outline in the previous section and the flow sheet depicted in Figure 66. For convenience the following abbreviations are provided:

- Dy(OTf)3: dysprosium triflate
- CMPOTf: 1-Butyl-1-metylpyrrolidinium triflate
- CMIC: 1-Butyl-3-methylimidazolium chloride
- Gd(NTf2)3: gadolinium bis(trifluoromethane)sulfonimide
- TMP: trimethyl phosphate
- Nd(CF3SO3)3: neodymium(III) trifluoromethanesulfonate
- DMI: 1,3-dimethyl-2-imidazolidinone
- Y(OTf)3: Yttrium trifluoromethanesulfonate/ Yttrium triflate

Starting with the initial split created by the plasma reactor the distilled vapor phase of Sm, Eu, Dy, Tm, Yb and Ca can be used as an anode to extract Sm. Tungsten (W) is used as cathode. The electrolyte is a mixture of Sm(NO3)3 and Urea-Choline chloride (2:1). The optimum temperature and voltage of this process are 343 K and -1.9 V respectively [3]. Sm is deposited on the tungsten cathode and rest of the elements (Eu, Dy, Tm, Yb and Ca) are in the anode.

This anode (alloy of Eu, Dy, Tm, Yb and Ca) is used further to deposit Dy using dysprosium triflate on a tungsten substrate. The electrolyte is dysprosium triflate containing 1-butyl-1-metylpyrrolidinium triflate electrolyte. The temperature and potential are starting 298 K and -3.2 V respectively [4].

The rest of the elements which are not in the gaseous phase (Nd, Y, Gd, Al, Fe….) in the second step form an alloy. This alloy is used as an anode to separate Al. In this case, the electrolyte is a mixture of AlCl3 and CMIC at 2:1 molar ratio. Cu is used as a cathode. Temperature and voltage are starting 373 K and -1.5 V respectively. The current density and energy consumption of this process are estimated as 427 A/m2 and 5.3 kWh/kg [5].

After extracting Al, the alloy (Nd, Y, Gd, Fe….) is used as an anode to deposit Gd. The electrolyte is the starting 2.52 mol% Gd (NTf2)3 in TMP. Tungsten is used as cathode [6]. Dy deposition is carried out at starting 298 K and -1.75 V. Black precipitation reported is observed on the cathode surface which indicates the presence of Dy.

After Al deposition, the remaining alloy (Nd, Y, Fe….) is used to extract Nd using Nd (CF3SO3)3 + LiNO3+DMI as electrolyte. Temperature and potential of deposition are starting 323 K and -2.5

V, respectively [7]. The deposition rate is hindered by the slow reduction kinetics of Nd cations. Because of this reason additives such as LiNO3 is used to improve the kinetics and conductivity.

Finally, Y is extracted from the rest of the alloy (Y, Fe….) at starting 373 K and -2.6 V. Electrolyte is Y(OTf)3 solution in CMPOTf. CMPOTf ionic liquid is needed to be synthesized. Tungsten is used as a cathode. The deposition process occurs in a single step (Y3+ to Y0). Tenuous black precipitation of yttrium is reported in the cathode.

*2.6.5.1 Section References:*


[4] A. Atifi, D.L. Baek, R.V. Fox, Electrodeposition of dysprosium in pyrrolidinium triflate ionic liquid at ambient temperature: Unraveling System Efficiency and impact of solvation interplays on the reduction process, Electrochimica Acta, 378 (2021) 138140. doi:10.1016/j.electacta.2021.138140.

[5] Y. Wang, R.G. Reddy, R. Wang, Dendrite-free al recycling via electrodeposition using Ionic liquid electrolytes: The effects of deposition temperature and cathode surface roughness, Journal of Cleaner Production. 287 (2021) 125043. doi:10.1016/j.jclepro.2020.125043.

[6] P. Bagri, H. Luo, I. Popovs, B.P. Thapaliya, J. Dehaudt, and S. Dai, Trimethyl phosphate based neutral ligand room temperature ionic liquids for electrodeposition of rare earth elements, Electrochemistry Communications. 96 (2018) 88–92. doi:10.1016/j.elecom.2018.10.001.

[7] B. Zhang, L. Wang, K. Pan, W. Zhang, Y. Liu, Y. Zhang, L. Zhang, and Z. Shi, LiNO3-supported electrodeposition of metallic Nd from Nd-containing solvate Ionic liquid, The Journal of Physical Chemistry C. 125 (2021) 20798–20805. doi:10.1021/acs.jpcc.1c06335.

[8] L.M. Glukhov, A.A. Greish, and L.M. Kustov, Electrodeposition of rare earth metals Y, Gd, Yb in Ionic Liquids, Russian Journal


## 2.7 Task 7.0 – Circuit 4 CM Product Production

### *2.7.1 Subtask 7.1 – State-of-the-Art Technology Review*

A comprehensive literature survey was conducted to identify potential chemical separation technologies to produce eight CMs, namely lithium, manganese, cobalt, gallium, and strontium, germanium, zinc, and nickel. Many papers have been identified representing a diverse range of feedstock materials, target and contaminant metals, and separation approaches. While the review primarily focused on the chemical separation technologies, other process operations, including beneficiation and extraction, have also been noted in the database.

The feedstocks for the separation technologies included in the literature reviewed range from concentrated ores to E-waste and other recycled components to synthetic solutions. Particular focus was placed on low concentration and highly contaminated solutions as those data will be most relevant to the Circuit 4 being developed in the current project. In addition, some papers include data on beneficiation and leaching with operations with common beneficiation processes being roasting, crushing, and physical separation. Likewise, common leaching operations include mineral acid leaching using sulfuric, nitric, or hydrochloric acid.

Chemical separation technologies identified in the review generally fall into the following categories and sub-categories:

- Solvent extraction
  - conventional extractants and circuits
  - novel extractants and circuits
  - room temperature ionic liquids
- Selective precipitation
  - pH controlled precipitation
  - redox controlled precipitation
  - ligand assisted precipitation
  - carrier precipitation
- Selective adsorption
  - gels and resins
  - ion exchange
  - ion chromatography
- Membrane separations
  - supported liquid membranes
  - solvent impregnated membranes
  - reverse osmosis;
- Ion flotation and foam separation
- Electrochemical separation
  - Electrowinning
  - Electrolysis cells
- Combinatory and other methods.

*2.7.1.1 Lithium*

Table 43 shows the methods reported in the literature for lithium purification, including solvent extraction, membrane-based methods, reverse osmosis/precipitation, carbonate precipitation, etc. All these methods have merits and demerits, and a process flowsheet integrating multiple methods is required to achieve the efficient extraction of lithium of low concentrations.

Table 43. Purification methods of lithium reported in the literature.

| Feedstock | Beneficiation | Extraction /Leaching | Chemical Separation | Other Elements | Article Year | Ref |
|---|---|---|---|---|---|---|
| Brines and leachates | N/A | N/A | solvent extraction with commercial extractants | N/A | 2018 | [1] |
| LIB, brine, high grade ore | N/A | N/A | supported liquid membrane and solvent extraction | N/A | 2016 | [2] |
| Geothermal water | N/A | N/A | solvent extraction (adsorption and reaction) | Na, K, Mg, Ca | 2007 | [3] |
| Waste water that contains Li | N/A | N/A | reverse osmosis and precipitation | Na | 2018 | [4] |

| | | | | | | |
|---|---|---|---|---|---|---|
| Lithium bromine solution | N/A | N/A | ion-selective cation exchange membrane by electrodialysis process | N/A | 2020 | [5] |
| Salt Lake brine | N/A | N/A | room temperature ionic liquid in tributyl phosphate | N/A | 2015 | [6] |
| Dilute synthetic solution | N/A | N/A | liquid membrane of KIX54 and TOPO in kerosene | N/A | 2005 | [7] |
| Lithium ion batteries | N/A | Sulfuric acid leach | carbonate precipitation (SX for other elements) | Co, Mn, Ni | 2015 | [8] |

*2.7.1.1.1 Section References:*


[1] Nguyen, T., & Lee, M. (2018). A review on the separation of lithium ion from leach liquors of primary and secondary resources by solvent extraction with commercial extractants. Processes, 6(5), 55. https://doi.org/10.3390/pr6050055

[2] Swain, B. (2016). Separation and purification of lithium by solvent extraction and supported liquid membrane, analysis of their mechanism: A Review. Journal of Chemical Technology & Biotechnology, 91(10), 2549–2562. https://doi.org/10.1002/jctb.4976

[3] T. Hano, M. Matsumoto, T. Ohtake, N. Egashir & F. Hori (1992) Recovery of Lithium from Geothermal Water by Solvent Extraction Technique, Solvent Extraction and Ion Exchange, 10:2, 195-206, DOI: 10.1080/07366299208918100

[3] Swain, B. (2018), Cost effective recovery of lithium from lithium ion battery by reverse osmosis and precipitation: a perspective. J. Chem. Technol. Biotechnol, 93: 311-319. https://doi.org/10.1002/jctb.5332.

[4] Majid Bazrgar Bajestani, Ahmad Moheb, Mohammad Dinari, Preparation of lithium ion-selective cation exchange membrane for lithium recovery from sodium contaminated lithium bromide solution by electrodialysis process, Desalination, Volume 486, 2020, 114476, ISSN 0011-9164, https://doi.org/10.1016/j.desal.2020.114476.

[5] Chenglong Shi, Yongzhong Jia, Chao Zhang, Hong Liu, Yan Jing,Extraction of lithium from salt lake brine using room temperature ionic liquid in tributyl phosphate, Fusion Engineering and Design, Volume 90, 2015, Pages 1-6, ISSN 0920-3796, https://doi.org/10.1016/j.fusengdes.2014.09.021.

[6] Bipan Bansal, Xiao Dong Chen, Md. Monwar Hossain, Transport of lithium through a supported liquid membrane of LIX54 and TOPO in kerosene, Chemical Engineering and Processing: Process Intensification, Volume 44, Issue 12, 2005, Pages 1327-1336, ISSN 0255-2701, https://doi.org/10.1016/j.cep.2005.05.003.

[7] Xiangping Chen, Yongbin Chen, Tao Zhou, Depei Liu, Hang Hu, Shaoyun Fan, Hydrometallurgical recovery of metal values from sulfuric acid leaching liquor of spent

lithium-ion batteries, Waste Management, Volume 38, 2015, Pages 349-356, ISSN 0956-053X, https://doi.org/10.1016/j.wasman.2014.12.023.

*2.7.1.2 Manganese*

Table 44 shows the methods reported in the literature for manganese purification, including solvent extraction, solvent extraction, electrowinning, precipitation, etc. The performance of the different technologies is shown in
Table 45.

Table 44. Purification methods of manganese reported in the literature.

| **Feedstock** | **Beneficiation** | **Extraction /Leaching** | **Chemical Separation** | **Other Elements** | **Article Year** | **Ref.** |
|---|---|---|---|---|---|---|
| Ores, soil, waters | magnetic separation and froth flotation | chemical leaching | hydrometallurgical processing | N/A | 2014 | [9] |
| Manganese ore | crushing | sulfuric acid leaching | cane molasses as reductant | Al, Fe | 2008 | [10] |
| Coarse manganese concentrate | roasting and magnetic separation | N/A | N/A | Fe | 2021 | [11] |
| Ferruginous manganese ores: | washing, gravity, floatation, magnetic | reductive leaching | N/A | Fe | 2019 | [12] |
| Ammonium chloride solutions | N/A | heptanoic acid | N/A | N/A | 1988 | [13] |
| Low grade ore | N/A | bioleaching | N/A | N/A | 2017 | [14] |
| Waste solutions | N/A | bioleaching | N/A | N/A | 2018 | [15] |
| On-site manganese-bearing wastewater | N/A | $CO_2$ leaching | precipitation | Mg, Ca | 2019 | [16] |
| Electrolytic manganese residue | crushing | toxicity leaching | low temp roasting and water washing | N/A | 2021 | [17] |
| Lithium ion batteries | N/A | sulfuric acid leaching | solvent extraction with $D_2EHPA$ | Ni, Co, Li | 2020 | [18] |
| Electrolytic manganese residue | ball grinding | acidic leaching | water as extractant under mechanochemical ball grinding | Fe | 2020 | [19] |
| Alkaline batteries | N/A | acidic leaching | electrowinning | Zn | 2004 | [20] |

Table 45. Performance of the different technologies shown in Table 44.

| Ref. | Technology Description | Performance | Disadvantage |
|---|---|---|---|
| [9] | Review article: precipitation (hydroxide, oxidative, sulfide, and ammonium/carbonate), electrolysis, ion exchange, solvent extraction | N/A | N/A |
| [10] | Reductive leaching to dissolve manganese from ores | 97% Mn was leached under the optimum conditions | Used for leaching instead of purification |
| [11] | Roasting with calcium chloride, calcium hypochlorite, and coke | Mn and Fe were effectively separated through magnetic separation after roasting | High energy consumption |
| [12] | Review about Mn separation from Fe: physical separation, reductive leaching, acid leaching | N/A | N/A |
| [13] | Solvent extraction from ammonium chloride solution with heptanoic acid | Satisfactory recovery was obtained in synthetic solutions | N/A |
| [14] | Bioleaching of Mn | Around 80% Mn can be leached | The technology was not used for Mn purification |
| [15] | Review of biotechnology processes applied for Mn recovery from waste | N/A | Mainly used to leach Mn from ores |
| [16] | Carbonate precipitation with the flue gas generated from the leaching of rhodochrosite ore ($MnCO_3$) | 99.99% $Mn^{2+}$ was selectively recovery from $Ca^{2+}$, $Mg^{2+}$, and $Mn^{2+}$ containing solutions | N/A |
| [17] | Roasting followed by water leaching | Electrolytic Mn residue was roasted at 600C followed by water leaching to recovery Mn | High temperature was used |
| [18] | Solvent extraction to recover Mn from leach solutions of lithium-ion batteries | 70% Mn was extracted in a single stage, while the coextraction of Co was less than 5% | N/A |
| [19] | Waster leaching under mechanochemical ball grinding | 98% Mn was leached from electrolytic Mn residue, while the recovery of Fe was less than 2% | The technology was developed for electrolytic Mn residue |
| [20] | Acid leaching followed by electrowinning of Mn and Zn (recovery from alkaline batteries) | 100% Zn and 40% Mn were leached, Zn and Mn were then recovered by simultaneous electrowinning | |

*2.7.1.2.1 Section References:*

[9] Baba, A. , Ibrahim, L. , Adekola, F. , Bale, R. , Ghosh, M. , Sheik, A. , Pradhan, S. , Ayanda, O. and Folorunsho, I. (2014) Hydrometallurgical Processing of Manganese Ores: A Review. Journal of Minerals and Materials Characterization and Engineering, 2, 230-247. doi: 10.4236/jmmce.2014.23028.

[10] Haifeng Su, Yanxuan Wen, Fan Wang, Yingyun Sun, Zhangfa Tong, Reductive leaching of manganese from low-grade manganese ore in H2SO4 using cane molasses as reductant, Hydrometallurgy, Volume 93, Issues 3–4, 2008, Pages 136-139, ISSN 0304-386X, https://doi.org/10.1016/j.hydromet.2008.01.001.

[11] Xiao, J.; Zou, K.; Chen, T.; Xiong, W.; Deng, B. Extraction of Manganese and Iron from a Refractory Coarse Manganese Concentrate. Metals 2021, 11, 563. https://doi.org/10.3390/met11040563

[12] Liu, B., Zhang, Y., Lu, M., Su, Z., Li, G., & Jiang, T. (2019). Extraction and separation of manganese and iron from ferruginous manganese ores: A Review. Minerals Engineering, 131, 286–303. https://doi.org/10.1016/j.mineng.2018.11.016

[13] Apostoluk W. Extraction of manganese(II) from ammonium chloride solutions with heptanoic acid
Hydrometallurgy, 21 (3) (1989), pp. 345-357

[14] S. Ghosh, B. Bal & A. P. Das (2018) Enhancing Manganese Recovery from Low-Grade Ores by Using Mixed Culture of Indigenously Isolated Bacterial Strains, Geomicrobiology Journal, 35:3, 242-246, DOI: 10.1080/01490451.2017.1362080

[15] Mohanty, S., Ghosh, S., Bal, B. et al. A review of biotechnology processes applied for manganese recovery from wastes. Rev Environ Sci Biotechnol 17, 791–811 (2018). https://doi.org/10.1007/s11157-018-9482-1

[16] Chen Yu, Ying Mei, Yuhua Xue, Chenjie Wu, Hengpeng Ye, Jinlin Li, Dongyun Du, A novel approach for recovery of manganese from on-site manganese-bearing wastewater, Journal of Cleaner Production, Volume 227, 2019, pages 675-682, ISSN 0959-6526, https://doi.org/10.1016/j.jclepro.2019.04.085.

[17] He, S., Wilson, B. P., Lundström, M., & Liu, Z. (2021). Hazard-free treatment of electrolytic manganese residue and recovery of manganese using low temperature roasting-water washing process. Journal of Hazardous Materials, 402, 123561.

[18] Vieceli, N., Reinhardt, N., Ekberg, C., & Petranikova, M. (2020). Optimization of manganese recovery from a solution based on lithium-ion batteries by solvent extraction with D2EHPA. Metals, 11(1), 54.

[19] Lan, J., Dong, Y., Xiang, Y., Zhang, S., Mei, T., & Hou, H. (2021). Selective recovery of manganese from electrolytic manganese residue by using water as extractant under mechanochemical ball grinding: Mechanism and kinetics. Journal of Hazardous Materials, 415, 125556.

[20] De Souza, C. C. B. M., & Tenório, J. A. S. (2004). Simultaneous recovery of zinc and manganese dioxide from household alkaline batteries through hydrometallurgical processing. Journal of Power Sources, 136(1), 191-196.

*2.7.1.3 Cobalt*

Table 46 shows the methods reported in the literature for cobalt purification, including precipitation, solvent extraction, electrochemical methods, selective adsorption, etc. The performance of the different technologies is shown in
Table 47.

Table 46. Purification methods of cobalt reported in the literature.

| **Feedstock** | **Beneficiation** | **Extraction/Leaching** | **Chemical Separation** | **Other Elements** | **Article Year** | **Ref.** |
|---|---|---|---|---|---|---|
| Cobalt ore | crushing | sulfuric acid | precipitation | Ni | 2014 | [21] |
| Aqueous solution | N/A | N/A | extraction with Nitrobenzoylpr azolone-5 | N/A | 2013 | [22] |
| Batteries | N/A | N/A | extraction with deep eutectic solvent | Fe | 2017 | [23] |
| Aqueous solution | N/A | N/A | Biocathode microbial electrolysis cells | N/A | 2014 | [24] |
| Lithium ion batteries | N/A | acid leaching | electrochemica l techniques | C, Al | 2007 | [25] |
| Synthetic aqueous media | N/A | N/A | biopolymer gel | Cu | 1991 | [26] |
| Lithium ion batteries | N/A | organic citric acid and hydrogen peroxide | hydrometallurg y | Li | 2010 | [27] |
| Waste cathodic active material | N/A | H2O2 leaching | solvent extractions with Cyanex 272 | N/A | 2007 | [28] |
| Lithium cobalt oxide | N/A | microbial fuel Cell | microbial electrolysis cell | Li | 2014 | [29] |
| Copper-cobalt ore | grinding, ammonium salt roasting | leaching | filtration and precipitation | Cu | 2012 | [30] |
| Zinc plant residue | sulfation roasting | sulfuric acid | hydrometallurg ical separation | N/A | 2002 | [31] |

Table 47. Performance of the different technologies shown in Table 46.

| Ref. | Technology Description | Performance | Disadvantage |
|---|---|---|---|
| [21] | Co/Ni solvent extraction does not remove impurities, e.g., Fe, As, Pb, Mn, Ca. It only divides them between its Ni-rich and Co-rich products. Thus, these impurities if present must be removed before and/or after solvent | This is the practice of Ni/Co mining industry | Ni/Co ores are completely different from coal-based materials |

| | | | |
|---|---|---|---|
| | extraction. Precipitation and/or ion exchange are used to remove impurities. | | |
| [22] | Solvent extraction with nitrobenzoylprazolone-5 | Optimum conditions: pH range 5.5 - 7.0 and extractant concentration of 0.02 M | Separations from other metal ions were not conducted |
| [23] | A novel solvent extraction system for the recovery of both cobalt and nickel from acidic (lactic acid) media is used | Satisfactory separation among Co, Fe, Nd, and Ni was achieved | No noticeable disadvantage |
| [24] | Use biocathode microbial electrolysis cells | At an applied voltage of 0.2 V, 88.1% of Co(II) was reduced; CO2 was converted into acetate and methane | Contaminant metal ions that are easier to be electrochemically reduced will impair the performance |
| [25] | Electrochemical recycling of cobalt from a leach solution of the cathodes of spent lithium-ion batteries | Cobalt was deposited | Cobalt concentration should be high, and contaminant concentration should be low |
| [26] | Direct dispensing of sodium alginate to adsorb the bulk of metals followed by the addition of partially coagulated calcium alginate spheres to "polish" the leachate | Metals in the cobalt ore leachate can be removed by algin using the two-stage approach described in this work | The feed leachate contained much more Co than Fe and Al |
| [27] | Cobalt recovery from waste cathodic material: citric acid leaching | No separation was investigated in this article | NA |
| [28] | Cobalt recovery from waste cathodic material: leaching with sulfuric acid followed by solvent extraction with Cyanex 272 | Cobalt sulfate solution with a purity 99.99% was obtained from the cobalt-loaded organic | The matrix of the solution is much simpler than coal-based solutions |
| [29] | Cobalt recovery from lithium cobalt oxide: self-driven microbial fuel cell-microbial electrolysis cell system | Cobalt dissolution from lithium cobalt and reduction to metal occur in the same system | No noticeable disadvantage |
| [30] | Cobalt recovery from an ore: ammonium roasting, water leaching, ammonium bicarbonate precipitation | Copper and cobalt mixed carbonate was obtained | The flowsheet is complex |
| [31] | Cobalt recovery from zinc plant residue: washing, roasting and leaching, precipitation of iron and manganese, separation of zinc, cadmium, and copper by anion-exchange resin, separation of nickel by selective extraction of cobalt, precipitation of cobalt | The total recovery of cobalt was about 93.5%. | The flowsheet is complex |

*2.7.1.3.1 Section References:*


[21] Michael S. Moats, William G. Davenport, Chapter 2.2 - Nickel and Cobalt Production, Editor(s): Seshadri Seetharaman, Treatise on Process Metallurgy, Elsevier,2014, Pages 625-669, ISBN 9780080969886, https://doi.org/10.1016/B978-0-08-096988-6.00026-2.

[22] O. Gerald, A. Judith and O. Martin, "Studies on Extraction Behaviour of Cobalt(II) with Nitrobenzoylprazolone-5," Journal of Minerals and Materials Characterization and Engineering, Vol. 1 No. 3, 2013, pp. 90-94. doi: 10.4236/jmmce.2013.13017.

[23] Franziska-Jane Albler, Katharina Bica, Mark R.StJ. Foreman, Stellan Holgersson, Mikhail S. Tyumentsev, A comparison of two methods of recovering cobalt from a deep eutectic solvent: Implications for battery recycling, Journal of Cleaner Production, Volume 167, 2017, Pages 806-814, ISSN 0959-6526, https://doi.org/10.1016/j.jclepro.2017.08.135.

[24] Huang, L., Jiang, L., Wang, Q., Quan, X., Yang, J., & Chen, L. (2014). Cobalt recovery with simultaneous methane and acetate production in biocathode microbial electrolysis cells. Chemical Engineering Journal, 253, 281-290.

[25] Freitas, M. B. J. G., & Garcia, E. M. (2007). Electrochemical recycling of cobalt from cathodes of spent lithium-ion batteries. Journal of Power Sources, 171(2), 953-959.

[26] Jang, L. K., Lopez, S. L., Eastman, S. L., & Pryfogle, P. (1991). Recovery of copper and cobalt by biopolymer gels. Biotechnology and bioengineering, 37(3), 266-273.

[27] Li, L., Ge, J., Wu, F., Chen, R., Chen, S., & Wu, B. (2010). Recovery of cobalt and lithium from spent lithium ion batteries using organic citric acid as leachant. Journal of hazardous materials, 176(1-3), 288-293.

[28] Swain, B., Jeong, J., Lee, J. C., Lee, G. H., & Sohn, J. S. (2007). Hydrometallurgical process for recovery of cobalt from waste cathodic active material generated during manufacturing of lithium ion batteries. Journal of Power Sources, 167(2), 536-544.

[29] Huang, L., Yao, B., Wu, D., & Quan, X. (2014). Complete cobalt recovery from lithium cobalt oxide in self-driven microbial fuel cell–microbial electrolysis cell systems. Journal of Power Sources, 259, 54-64.

[30] Zhang, M., Zhu, G., Zhao, Y., & Feng, X. (2012). A study of recovery of copper and cobalt from copper–cobalt oxide ores by ammonium salt roasting. Hydrometallurgy, 129, 140-144.

[31] Wang, Y., & Zhou, C. (2002). Hydrometallurgical process for recovery of cobalt from zinc plant residue. Hydrometallurgy, 63(3), 225-234.


*2.7.1.4 Gallium*

Table 48 shows the methods reported in the literature for gallium purification, including selective precipitation, solvent extraction, ion exchange, selective adsorption, ion flotation, membrane

technologies, vacuum metallurgy, etc. The performance of the different technologies is shown in Table 49.

Table 48. Purification methods of gallium reported in the literature.

| Feedstock | Beneficiation | Extraction/ Leaching | Chemical Separation | Other Elements | Article Year | Ref. |
|---|---|---|---|---|---|---|
| Coal fly ash | N/A | acid leaching and alkaline leaching | solution extraction. | N/A | 2017 | [32] |
| Red mud | N/A | auto clave leaching | tricalcium hydroaluminate precipitation and carbonization. | $VO_5$ | 2015 | [33] |
| Leach liquors | N/A | N/A | solvent extraction, ion exchange, and solvent-impregnated resins/gels | In | 2018 | [34] |
| N/A | N/A | N/A | solvent extraction with an open cell polyurethane foam | N/A | 1977 | [35] |
| Iron, zinc ores | N/A | Ether extraction | gallium separation from iron through NaOH precipitation | Al, Au | 1924 | [36] |
| Gallium nitrate hydrate | N/A | acid leaching | ion flotation | Zn | 2016 | [37] |
| Gallium standard solution | N/A | N/A | supercritical $CO_2$ extraction | N/A | 2008 | [38] |
| Zinc target | N/A | weak acid | thermal diffusion | N/A | 1996 | [39] |
| Acidic leach solution | N/A | N/A | emulsion type of liquid membranes | Fe, Al | 2004 | [40] |
| N/A | N/A | N/A | supported liquid membranes | In | 1997 | [41] |
| Stock solutions | N/A | N/A | adsorption | In | 2000 | [42] |
| N/A | N/A | acidic leaching | separation by cation-exchange chromatography | Al, Fe | 1983 | [43] |
| GaAs-based e-wastes (LED) | N/A | N/A | pyrolysis-vacuum metallurgy separation | N/A | 2018 | [44] |
| Hydrochloric acid solutions | N/A | acidic leaching | selective recovery with a continuous counter-current foam separation | Zn, Al, Cu, In, As | 2011 | [45] |

Table 49. Performance of the different technologies shown in Table 48.

| Ref. | Technology Description | Performance | Disadvantage |
|---|---|---|---|
| [32] | A review article about Gallium extraction: Ion-exchange resin adsorption, acid desorption, precipitation, purification, electrolysis | The purity of Ga product was improved from 99.9% to 99.99% | The process was developed to recover Ga from the Bayer process |

| | | | |
|---|---|---|---|
| [33] | Autoclave leaching for its conversion into ferrous hydrogarnet product and extraction of valuable components (i.e. Na2O, Al2O3, Ga and V2O5) | This allowed the generation of alkaline solutions suitable for recycling back to leaching stage and recovery of a concentrate (30% AI2O3) that is rich in Ga (0.32%) and V2O5 (3.7%) | The process is complex |
| [34] | Review article: Solvent extraction and ion exchange | Compared to common commercial extractants such as D2EHPA, PC88A, Cyanex 272, and Cyanex 301, synthetic extractants offer higher extraction and separation efficiency, but extraction kinetics and stripping efficiency in these systems should be improved in the future. | The content of Ga in the leach solution of coal refuse is much lower |
| [35] | Open cell polyurethane foam sponge as a solvent extractor | Not available | Not available |
| [36] | Gallium trichloride is extracted almost completely by ether from 5 to 6 N hydrochloric acid solutions; Sodium hydroxide precipitation to separate Ga and Fe | Can be used to separate Ga from complex solution matrix | A high concentration of HCl is required |
| [37] | Ionic flotation using sodium dodecyl sulfate as the collector | Around 90% of Ga was recovered at pH 3, while only 3% Zn was recovered | Chemical cost may be high |
| [38] | Extraction of Ga from acidic aqueous solution with sCO2 | 80-90% recovery was obtained using the PySH chelating agent under the conditions of 70 °C, 3000 psi, pH 2.0-3.0 | Only tested on a Ga standard solution |
| [39] | Irradiated target foils were heated up to 400°C, that is close to the melting point of zinc. At this temperature the gallium isotopes became movable in the zinc matrix and were concentrated on the surface of the target. | By dipping the foils into a weak acid, more than 60% of the radioactivity was etched off the target and with less than 0.5% loss of the target material. | Only tested for Ga and Zn, and seems to be only valid for metals |
| [40] | PIMs entrap an extractant within a polymer matrix, often with the addition of plasticizer and/or modifier to improve their extraction characteristics. | The separation factors of gallium over Zn, Co, and Ni, at the optimum conditions, were found to be of 963, 702, and 514, respectively, for the feed solution of 100mg/dm3 Ga, 1,000mg/dm3 Zn, 600mg/dm3 Co, and 600mg/dm3 Ni. | No noticeable disadvantage |
| [41] | A supported membrane containing diisostearylphosphoric acid diluted by heptane | In can be preferentially extracted prior to Ga | Only tested for Ga and In |
| [42] | A chelating sorbent was used | The retention of Ga was nearly 100% between pH 4-7, while for In, the maximum was between pH 6-12 | Only tested for Ga and In |

| | | | |
|---|---|---|---|
| [43] | Cation exchange chromatography at high HCl concentration with AG 50W-X4 resin | Trace amounts and up to 1.5 mg of gallium can be separated from up to gram amounts of Al, Cd, Cu, In, Mn, Ni, Pb, U(VI) and many other elements | The elements need to be eluted in high concentration (8 M) HCl |
| [44] | Processing under vacuum, the boiling points of metals can be reduced a lot, which means less energy consumption. | This indicated that gallium and arsenic can be recycled efficiently at the heating temperature of 1273 K, the holding time of 60 min, and the vacuum pressure of ~20 Pa, and the total recovery efficiency can reach 95 wt % | No noticeable disadvantage |
| [45] | Counter-current foam separation with simultaneous injections of metal and surfactant solutions into rising foam bed | The separation factor of gallium(III) was 67 over iron(III) and more than 1000 over the other metals | Recovery increases with the acidity of solution, and 6 M HCl is required to achieve 100% recovery |

*2.7.1.4.1 Section References:*


[32] Fanghai Lu, Tangfu Xiao, Jian Lin, Zengping Ning, Qiong Long, Lihua Xiao, Fang Huang, Wankun Wang, Qingxiang Xiao, Xiaolong Lan, Haiyan Chen, Resources and extraction of gallium: A review, Hydrometallurgy, Volume 174, 2017, Pages 105-115, ISSN 0304-386X, https://doi.org/10.1016/j.hydromet.2017.10.010.

[33] R.A. Abdulvaliyev, A. Akcil, S.V. Gladyshev, E.A. Tastanov, K.O. Beisembekova, N.K. Akhmadiyeva, H. Deveci, Gallium and vanadium extraction from red mud of Turkish alumina refinery plant: Hydrogarnet process, Hydrometallurgy, Volume 157, 2015, Pages 72-77, ISSN 0304-386X, https://doi.org/10.1016/j.hydromet.2015.07.007.

[34] Nguyen, T. H., & Lee, M. S. (2018). A review on separation of gallium and indium from leach liquors by solvent extraction and ion exchange. Mineral Processing and Extractive Metallurgy Review.

[35] Gesser, H. D., & Horsfall, G. A. (1977). The separation and concentration of gallium by polyurethane. Journal de Chimie Physique, 74, 1072-1076.

[36] Swift, E. H. (1924). A new method for the separation of gallium from other elements. Journal of the American Chemical Society, 46(11), 2375-2381.

[37] Bahri, Z., Rezai, B., & Kowsari, E. (2016). Selective separation of gallium from zinc using flotation: Effect of solution pH value and the separation mechanism. Minerals Engineering, 86, 104-113.

[38] Chou, W. L., Wang, C. T., Yang, K. C., & Huang, Y. H. (2008). Removal of gallium (III) ions from acidic aqueous solution by supercritical carbon dioxide extraction in the green separation process. Journal of hazardous materials, 160(1), 6-12.

[39] Tolmachev, V., & Lundqvist, H. (1996). Rapid separation of gallium from zinc targets by thermal diffusion. Applied radiation and isotopes, 47(3), 297-299.

[40] Kumbasar, R. A., & Tutkun, O. (2004). Separation and concentration of gallium from acidic leach solutions containing various metal ions by emulsion type of liquid membranes using TOPO as mobile carrier. Hydrometallurgy, 75(1-4), 111-121.

[41] Kondo, K., Yamamoto, Y., & Matsumoto, M. (1997). Separation of indium (III) and gallium (III) by a supported liquid membrane containing diisostearylphosphoric acid as a carrier. Journal of membrane science, 137(1-2), 9-15.

[42] Bermejo-Barrera, P., Martinez-Alfonso, N., & Bermejo-Barrera, A. (2001). Separation of gallium and indium from ores matrix by sorption on Amberlite XAD-2 coated with PAN. Fresenius' journal of analytical chemistry, 369(2), 191-194.

[43] Van der Walt, T. N., & Strelow, F. W. (1983). Quantitative separation of gallium from elements by cation-exchange chromatography. Analytical Chemistry, 55(2), 212-216.

[44] Zhan, L., Xia, F., Xia, Y., & Xie, B. (2018). Recycle gallium and arsenic from gas-based E-wastes via pyrolysis–vacuum metallurgy separation: theory and feasibility. ACS Sustainable Chemistry & Engineering, 6(1), 1336-1342.

[45] Kinoshita, T., Ishigaki, Y., Shibata, N., Yamaguchi, K., Akita, S., Kitagawa, S., ... & Nii, S. (2011). Selective recovery of gallium with continuous counter-current foam separation and its application to leaching solution of zinc refinery residues. Separation and purification technology, 78(2), 181-188.

#### *2.7.1.5 Strontium*

Table 50 shows the methods reported in the literature for strontium purification, including solvent extraction, selective adsorption, carrier precipitation, membrane technologies, etc. The performance of the different technologies is shown in Table 51.

Table 50. Purification methods of gallium reported in the literature.

| Feedstock | Beneficiation | Extraction/ Leaching | Chemical Separation | Other Elements | Article Year | Ref. |
|---|---|---|---|---|---|---|
| Acidic nuclear waste streams | N/A | N/A | solvent extraction with crown ether | N/A | 2007 | [46] |

| | | | | | | |
|---|---|---|---|---|---|---|
| Loaded solutions | N/A | nitric acid | solvent extraction with BOC8A/NO | N/A | 2020 | [47] |
| Organic and aqueous solution | N/A | N/A | the Universal Solvent Extraction (UNEX) process | Cs, LN, AN | 2007 | [48] |
| Synthetic mixed fission product solutions | N/A | N/A | the PUREX process (TBP and kerosene) | Cs, Zr, Ru | 2010 | [49] |
| Seawater | N/A | auto clave leeching | selective adsorption with titanate nanotubes | N/A | 2016 | [50] |
| Oil-filled water | N/A | HCL | selective adsorption with adsorption beads | N/A | 2013, 2021 | [51] |
| Seawater | magnetic separation | N/A | selective adsorption with nanocomposites | Ca, Mg, Na, K Mn, Fe | 2019 | [52] |
| Ca-rich composite | N/A | $HNO_3$ | recovery using a strontium-specific extraction chromatographic resin | N/A | 2009 | [53] |
| Simulated feeds (PUREX waste) | N/A | acidic leaching | strontium recovery through carrier precipitation | N/A | 1961 | [54] |
| Combination with calcium | N/A | N/A | strontium separation from calcium with potassium rhodizonate (precipitation) | Ca | 1957 | [55] |
| High level waste | N/A | $HNO_3$ | strontium recovery using supported liquid membrane | N/A | 2012 | [56] |

Table 51. Performance of the different technologies shown in Table 50.

| Ref. | Technology Description | Performance | Disadvantage |
|---|---|---|---|
| [46] | Strontium is extracted from acidic (>1 M HNO3) solution using a 0.20 M solution of di-t-butylcyclohexano-18-crown-6 in 1-octanol | Tests of the process on a synthetic dissolved sludge waste solution show that only strontium, barium, and technetium are appreciably extracted by the crown ether. | The extraction selectivity is excellent at high acidity |
| [47] | Solvent extraction with a novel BOC8A extractant in nitro alkalines | A very small concentration of BOC8A (0.01 M) in NO is sufficient for quantitative extraction of Sr2+ from 3.0 to 4.0M HNO3 medium. | The extraction ability of BOC8A increases with increasing feed acid concentration. |
| [48] | Solvent extraction with a synergistic extraction mixture | The synergistic extraction mixture of CCD–REG–CMPO in a polar diluent enables the effective separation of Cs, Sr, RE, and AN elements | Tested on highly acidic solutions |

| | | | |
|---|---|---|---|
| | | simultaneously from highly acidic HAW. | |
| [49] | Two new crown compounds used in conjunction with a cation exchanger in a matrix solution of TPB and kerosene | Allow the removal of both cesium and strontium from mixed fission products dissolved in 3 M HNO3 | The feed solution contained high concentrations of Sr |
| [50] | Titanate nanotubes synthesized through a simple hydrothermal reaction | Demonstrated a maximum adsorption capacity of 97 mg/g | Ca2+ significantly hindered Sr2+ sorption on TiNTs; how to apply these nanofibers in pilot and industrial scales is an issue |
| [51] | Ca-alginate beads | Showed certain adsorption capacity for Sr, Li, and La; Can use different pH to separate the metal ions | Stronger adsorption capacity for Al(III) and Fe(III) |
| [52] | Selective adsorption by Fe3O4/MnO2/fulvic acid nanocomposite | Demonstrated an excellent adsorption capacity of 227.3 mg/g for Sr(II) | Adsorption capacity reduced from 49.1 mg/g after 4 stages of regeneration/reuse; Optimum performance achieved at pH > 8 |
| [53] | Strontium-specific extraction chromatographic resin based on a crown ether | Very efficient for the separation of Sr from other metal ions | The elements need to be dissolved in 7 M HNO3 |
| [54] | Use lead carriers to improve the sulfate precipitation of Sr | 95-100% of Sr can be recovered | The investigated solution did not contain Ca and Mg; Pb is toxic |
| [55] | Precipitation with potassium rhodizonate | Very selective in the separation between Sr and Ca | The separation of Sr from other elements has not been tested |
| [56] | Liquid membrane based separation methods, particularly those involving supported liquid membranes (SLM) have significantly low solvent inventory which are relevant not only from environmental point of view but also are preferred for separation methods involving expensive reagents such as crown ethers. Moreover, SLM based separation methods are efficient due to the | 100% Sr was extracted from a feed solution containing 3 M HNO3 | High acid concentration, the selectivity was not studies |

simultaneous extraction and stripping. Additionally, due to the non-dispersive mass transfer, SLM based methods do not have limitations such as third phase formation and slow phase separation.

*2.7.1.5.1 Section References:*


[46] Horwitz, E. P., Dietz, M. L., & Fisher, D. E. (1991). SREX: a new process for the extraction and recovery of strontium from acidic nuclear waste streams. Solvent Extraction and Ion Exchange, 9(1), 1-25.

[47] Khan, P. N., Bhattacharyya, A., Sharma, J. N., & Manohar, S. (2020). The recovery of strontium from acidic medium using novel strontium selective extractant: An experimental and DFT study. Journal of Hazardous Materials, 397, 122476.

[48] Romanovskiy, V. N., Smirnov, I. V., Babain, V. A., Todd, T. A., Herbst, R. S., Law, J. D., & Brewer, K. N. (2001). The universal solvent extraction (UNEX) process. I. Development of the UNEX process solvent for the separation of cesium, strontium, and the actinides from acidic radioactive waste. Solvent Extraction and Ion Exchange, 19(1), 1-21.

[49] Shuler, R. G., Bowers Jr, C. B., Smith Jr, J. E., Van Brunt, V., & Davis Jr, M. W. (1985). The extraction of cesium and strontium from acidic high activity nuclear waste using a PUREX process compatible organic extractant. Solvent Extraction and Ion Exchange, 3(5), 567-604.

[50] Ryu, J., Kim, S., Hong, H. J., Hong, J., Kim, M., Ryu, T., ... & Kim, B. G. (2016). Strontium ion (Sr2+) separation from seawater by hydrothermally structured titanate nanotubes: removal vs. recovery. Chemical Engineering Journal, 304, 503-510.

[51] Song, D., Park, S. J., Kang, H. W., Park, S. B., & Han, J. I. (2013). Recovery of lithium (I), strontium (II), and lanthanum (III) using Ca–alginate beads. Journal of Chemical & Engineering Data, 58(9), 2455-2464. Liu, C., Yu, X., Ma, C., Guo, Y., & Deng, T. (2021). Selective recovery of strontium from oilfield water by ion-imprinted alginate microspheres modified with thioglycollic acid. Chemical Engineering Journal, 410, 128267.

[52] Ghaeni, N., Taleshi, M. S., & Elmi, F. (2019). Removal and recovery of strontium (Sr (II)) from seawater by Fe3O4/MnO2/fulvic acid nanocomposite. Marine Chemistry, 213, 33-39.

[53] De Muynck, D., Huelga-Suarez, G., Van Heghe, L., Degryse, P., & Vanhaecke, F. (2009). Systematic evaluation of a strontium-specific extraction chromatographic resin for obtaining a purified Sr fraction with quantitative recovery from complex and Ca-rich matrices. Journal of Analytical Atomic Spectrometry, 24(11), 1498-1510.

[54] Bray, L. A., & Van Tuyl, H. H. (1961). Laboratory Development of a Carrier-Precipitation Process for the Recovery of Strontium from Purex Wastes (No. HW-69534). General Electric Co. Hanford Atomic Products Operation, Richland.

[55] Weiss, H. V., & Shipman, W. H. (1957). Separation of Strontium from Calcium with Potassium Rhodizonate... Application to Radiochemistry. Analytical Chemistry, 29(12), 1764-1766.

[56] Kandwal, P., Ansari, S. A., & Mohapatra, P. K. (2012). A highly efficient supported liquid membrane system for near quantitative recovery of radio-strontium from acidic feeds. Part II: Scale up and mass transfer modeling in hollow fiber configuration. Journal of membrane science, 405, 85-91.

*2.7.1.6 Germanium*

*Solution Chemistry:* The most important forms of Ge in aqueous solution are $Ge(OH)_4$ and its dissolution products such as $GeO(OH)_3^-$ and $GeO_2(OH)_2^{2-}$ [16], [41]. The predominant species of Ge at pH < 10 are $Ge(OH)_4$ and $GeO(OH)_3^-$, while $GeO_2(OH)_2^{2-}$ exists only at pH greater than 11 (Figure 67).

$$GeO_2 + 2H_2O = Ge(OH)_4 \qquad \log K = -1.38$$

$$GeO(OH)_3^- + H^+ = Ge(OH)_4 \qquad \log K = 6.92 - 9.32$$

$$GeO_2(OH)_2^{2-} + H^+ = GeO(OH)_3^- \qquad \log K = 11.7 - 12.7$$

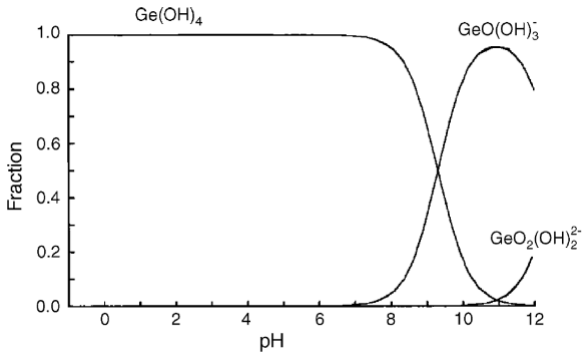


Figure 67. Species distribution of Ge as a function of pH [16].

The replacement of oxygen from the coordination sphere of Ge(IV) with chloride is very difficult; therefore, Ge(IV)-chloride complexes do not become important until the concentration of HCl exceeds 4 M [41]. However, in the presence of citric, oxalic and tartaric acid and catechol, Ge(IV) forms stable complexes with organic ligands at ambient conditions. For example, stable Ge-catechol complexes like $Ge(C_6H_4O_2)_3^{2-}$ are formed in aqueous solution at pH < 9, stable Ge-citrate complexes like $Ge(OH)_4(H_3C_6H_4O_7)_2^{2-}$ at pH < 7, stable Ce(IV)-oxalic complexes in pH range 3-6, and stable Ce(IV)-tartaric complexes in pH range 3-4.

*Germanium Leaching from Coal Fly Ash:* Water, acid, and alkaline leaching have been used to extraction Ge(IV) from coal fly ash. In the process of critical elements recovery from the leachate of coal refuse, a preconcentrate of critical elements is first obtained by collecting the precipitates

formed in a certain pH range (e.g., 5-9). Thus, all the critical elements in the preconcentrate are water insoluble; therefore, acid or alkaline leaching is more suitable to dissolve Ge(IV) from the preconcentrate.

Leaching with different acids, such as HCl, $H_2SO_4$, and HF, has been frequently used to extract Ge(IV) from coal fly ash. Since stable Ge(IV)-Cl complexes are difficult to form at low HCl concentrations, Ge(IV) extraction from coal fly ash with HCl is inefficient. Similar to HCl, low concentrations of $H_2SO_4$ normally provide unsatisfactory leaching recovery values of Ge(IV). The Ge(IV) in coal fly ash can be easily dissolved in HF, but this method is difficult to commercialize due to the toxicity of HF. Unlike mineral acids, catechol organic acids, such as citric, oxalic and tartaric acids, show a strong ability to extract Ge(IV) from coal fly ash, which is attributable to the formation of stable organic complexes. In addition to acid leaching, alkaline leaching has also been used to extract Ge(IV) from coal fly ash. However, the leaching recovery of Ge is unsatisfactory with low concentrations of NaOH due to the formation of Na-Al-Si gel.

Based on the leaching results reported in the literature, it can be inferred that Ge in the critical element preconcentrate is difficult to extract using water and mineral acids, while satisfactory leaching performance can be obtained using catechol, organic acids, and bases. This inference can be used to design proper flowsheets for Ge extraction and purification from the preconcentrate.

*Germanium Leaching from Zinc Residues:* Zinc residues are generated from the conventional zinc refinery process consisting of ZnS roasting to obtain ZnO followed by leaching with weak $H_2SO_4$ to dissolve and recover Zn [3],[38], leaving Ge and other metals in zinc residues that contain oxides of Fe, Cu, Pb, and Si [23],[24]. Ge(IV) leaching from zinc residues is normally carried out in two different ways: single-stage leaching and stepwise leaching. $H_2SO_4$ and HCl are normally used as the lixiviant in the single-stage leaching process; however, the leaching performance of single-stage leaching is unsatisfactory due to two factors: (1) silica gel formed in the acid leaching process adsorbs Ge(IV) from solution to form germanium gel $SiO_2$-$GeO_2$; and (2) Ge(IV) sulfate and chloride are unstable and hydrolyze to insoluble $GeO_2$ at low acid concentration and temperature. To improve the leaching performance, a number of measures have been applied, such as control of leaching time and temperature, addition of oxidants and salts of chlorides/nitrates [22][42], addition of HF to $H_2SO_4$ and HCl solutions [15]. In addition, replacing mineral acids with organic acids represents a promising solution due to the formation of stable Ge(IV)-organic acid complexes which are soluble in water. The dissolution of impurities from zinc residues is also low by using organic acids due to the formation of oxalate precipitates of other metal ions.

Taking advantage of the low leaching recovery of Ge(IV) by using mineral acids, stepwise leaching has been developed to selectively extracted Ge(IV) from zinc residues. For example, Liu et al. [24] leached a zinc residue with $H_2SO_4$ first to dissolve Zn(II) and Cu(II), and then used oxalic acid to leach Ge(IV) from the first step leaching residue. Rao et al. [33] leached the majority of Zn(II) from a zinc residue first using $H_2SO_4$, and then used NaOH to leach the Ge(IV) remained in the first step leaching residue. In the second step leaching with NaOH, due to the high concentration of Si(IV) and Pb(II), the separation and purification of Ge(IV) from the leachate are challenging.

Based on the leaching results of Ge(IV) recovery from zinc residues, it can be inferred that Ge(IV) in the critical element preconcentrate can be extracted through single-stage leaching with organic acids or stepwise leaching with mineral acids first followed by organic acids.

*Germanium Leaching from Solar Panel and Optical Fibers*: A mixture waste of $GeO_2$ and $SiO_2$ can be obtained from the recycling of solar panel. Leaching of Ge(IV) from the mixture can be proceeded through two ways: alkaline leaching and acid leaching. In the alkaline leaching process [18], the mixture is reacted with a NaOH solution to obtain a leachate rich in Ge, and then catechol is added into the leachate to solubilize Ge(IV). The leaching recovery is low when using HCl, $HNO_3$, and $H_2SO_4$ [5]. This finding is consistent with the phenomenon observed from coal fly ash and zinc residues. To resolve this issue, the mixture of HF with other mineral acids was used [5]; however, this method is difficult to be used in the industry due to the toxicity and environmental hazards of HF. Roasting with NaOH has been applied prior to acid leaching to improve the leaching efficiency of Ge(IV) [4].

*Germanium Leaching Summary and Promising Flowsheets for Germanium Leaching from the Critical Element Preconcentrate:* Based on discussions in the above paragraphs, Ge(IV) has the following leaching characteristics: (1) mineral acids except HF cannot effectively leach Ge(IV); (2) catechol and organic acids, such as citric, oxalic and tartaric acids, can effectively leach Ge(IV); (3) selective leaching of Ge(IV) can be achieved through stepwise leaching using appropriate lixiviants; (4) alkaline leaching is ineffective in the present of large amounts of Si; and (5) certain issues that cannot be addressed through hydrometallurgical approaches can be solved by combining roasting with leaching. Based on these leaching characteristics, several potential flowsheets that can be used to leach Ge(IV) from the critical element preconcentrated obtained from coal refuse leachate are developed. As Figure 68 shows, REEs and critical elements (CMs) except Ge are preferentially leached in Flowsheet I using mineral acids, while Ge (VI) is leached prior to REEs and other CMs in Flowsheet II and III using organic acids and bases, respectively.

Based on findings reported in the literature, Flowsheet I is the most promising flowsheet. The success of Flowsheet II depends on the selection of appropriate organic acids that will not interfere with the downstream separation and purification of REEs and other CMs. In addition, the leaching recovery of Ge(IV) using Flowsheet III will be low if large amounts of Si exist in the preconcentrate. Laboratory experimental tests need to be performed to optimize each flowsheet and select the best flowsheet.

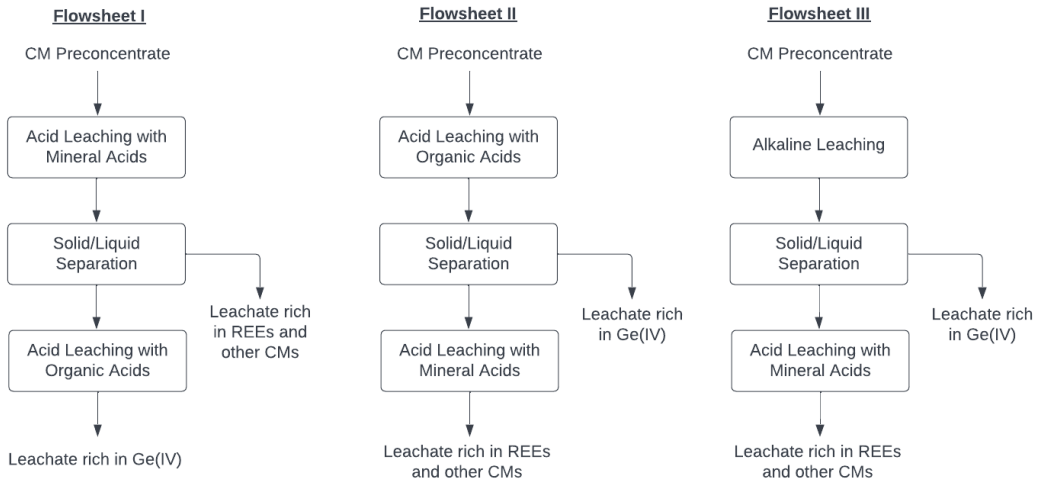


Figure 68. Promising flowsheets for Ge(IV) leaching from the critical element (CM) preconcentrate.

*Purification of Germanium from Leach Solutions*: Many different methods of Ge(IV) recovery and purification from leach solutions have been reported in the literature. A critical review of the methods is presented as follows:

Cementation

Mechanisms**:** $Ge(OHJ)_4 + 4H^+ + 2Fe = Ge_{(s)} + 2Fe^{2+} + 4H_2O$

Applications: Cementation of Ge(VI) and Cu(II) from vitriol supernatant in zinc hydrometallurgy plant, and both Ge(IV) and Cu(II) are cemented by iron powder [44].

Precipitation

Mechanisms: Precipitation with tannins

Applications: Precipitation of Ge(IV) from a sulfate solution that contains 6.0 g/L Ge, 1.7 g/L In, and 4.4 g/L Sn [10]; commercial uses on large scale (Zhang et al., 2019).

Advantages: Tannins can effectively precipitate Ge(IV) from leach solutions with a certain degree of selectivity [20]; Ge(IV) precipitation with tannins has been commercialized [ 43].

Disadvantages: The consumption of tannins is high, particularly in the presence of large amounts of contaminants; depending on the concentration of Ge(IV) and contaminant elements in the leach solution, other methods may be required prior to tannin precipitation to concentrate Ge(IV) and remove contaminants.

Solvent Extraction

Mechanisms: Different types of extractants, such as neutral extractants, acidic extractants, and amines, have been used to extract and purify Ge(IV) from leach solutions, and a systematic review of the extractants has published in a review article [27].

Applications: As Table 52 shows, solvent extraction has been used to extract Ge(IV) from different media using different extractants.

Advantages: Solvent extraction has been widely used in the industry; using appropriate extractions, solvent extraction can be used to recover and purify Ge(IV) from leach solutions of different matrixes.

Disadvantages: Conventional solvent extraction using mixers and settlers is inefficient for extracting targe elements of low concentrations.

Supported Ionic Liquid Phase and Membrane

Mechanisms: Ionic liquids supported on solids or membranes for Ge(IV) extraction.

Applications: Adsorption of Ge(IV)-citrate complexes from $HCl/H_2SO_4/HNO_3$ medium using Aliquat 336 supported on Amberlite XAD-16 N beads (Van Roosendael et al., 2019); Adsorption of Ge(IV)-tartrate complexes from a sulfate medium using Aliquat 336 supported on a membrane [13].

Advantages: Suitable for the extraction of low-concentration metal ions.

Disadvantages: Lower technology readiness level compared with solvent extraction; the lifetime and maintenance cost of supported ionic liquid phase and membranes are unclear.

Ion Exchange

Mechanisms: Chelating reaction and anion exchange.

Applications: Ge(IV) adsorption from sulfate solutions at pH 3 using Chelating resins (Amberlite IRA-743, WP-2 and Lewatit TP-260) and a weak anion exchanger (Amberlite IRA-67) (Virolainen et al., 2013); Ge(IV)-catechol complexes adsorption using anionic-exchange resins, such as Amberlite IRA-900 and IRA-958 [37].

Advantages: Ion exchange has been commercialized.

Disadvantages: Lower processing capacity compared with solvent extraction.

Table 52. Solvent extraction of Ge(IV) from different media [27].

| **Extractants** | **Media** | **Remarks** | **References** |
|---|---|---|---|
| Cyanex 301 (R) | 8 M HCl: Ge(IV), Al(III) | Extraction: ~95% Ge IV)<br>Extracted species: $GeCl_4$.2 R<br>Strippant: 0.5 M HCl | [11] |
| Cyanex 923 (R) | 8 M HCl: Ge(IV), Al(III), Cu(II) | Extraction: ~95% Ge(IV)<br>Extracted species: $GeCl_4$.2 R<br>Strippant: 0.3 M $NH_4SCN$ | |
| Cyanex 923 (R) | 0.1 M oxalic acid, pH = 3-3.2: Ge(IV), Zn(II), Cd(II), Co(II), Ni(II) | Extraction: ~90% Ge (IV)<br>Extracted species: $H_2Ge(C_2O_4)_3$.4 R<br>Strippant: 0.1 M NaOH | [13] |
| Aliquat 336 ($R_4NCl$) | 0.001 M tartaric acid, pH = 3-3.2: Ge(IV), Zn(II), Cd(II), Co(II), Ni(II) | Extraction: ~100% Ge(IV)<br>Extracted species: $(R_4N)_2.Ge(OH)_2C_4H_4O_6$<br>Strippant: 2 M HCl | [13] |
| N-*n*-Octylaniline (RR'NH) | 9 M HCl, Ge(IV), | Extraction: > 90% Ge(IV)<br>Extracted species: $(RR'NH_2)_2.Ge(OH)_nCl_{6-n}$<br>Strippant: 7 M $NH_4OH$ | [34] |
| TOA ($R_3N$) | 0.016 M catechol, pH = 2-3, Ge(IV), Ga(III), As(III), Sb(II), V(IV), Ni(II) | Extraction: > 90% Ge(IV)<br>Extracted species: $(R_3NH)_2.Ge(C_6H_4O_2)_3$<br>Strippant: 1 M NaOH | [2] |
| TOA + TBP | 0.005 M tartaric acid, 0.1 M $H_2SO_4$ + 5% v/v HF, pH = 2, Ge(IV), Si(IV) | Extraction: 91.3% Ge(IV)<br>Extracted species: $(R_3NH)_2.Ge(C_4H_6O_6)_3$<br>Strippant: 1.5 M NaOH | [5] |
| | 0.008-0.01 M tartaric acid + $H_2SO_4$, pH = 2, Ge(IV), Zn(II) | Extraction: 97% Ge(IV)<br>Extracted species: $(R_3NH)_2.Ge(C_4H_6O_6)_3$<br>Strippant: 7.5 M NaOH | [21] |
| N235 + TOP | 0.004 M tartaric acid, pH = 1.2, Ge(IV), Zn(II), As(III), Fe(III), Si(IV), Cd(II) | Extraction: 93% Ge(IV)<br>Extracted species: $R_3NH.Ge(OH)_2C_4H_5O_6/(R_3NH)_2.Ge(OH)_2C_4H_4O_6$<br>Strippant: 0.5 M NaOH | [43] |

| | | | |
|---|---|---|---|
| N235 + TBP | 0.67 M oxalic acid, $H_2SO_4$, pH = 0.5: Ge(IV), Ga(III), Fe(III) | Extraction: 99.8% Ge(IV)<br>Extracted species: $(R_3NH)_2.(TBP)_{0.25}.Ge(C_2O_4)_3$<br>Strippant: 4 M NaOH | [23] |
| D2EHPA + TBP | 80 g/L $H_2SO_4$, Ge(IV), Ga(III), Zn(II), Fe(III) | Extraction: 94.3% Ge(IV)<br>Strippant: NaOH | [25] |
| HGS98 (HL) + D2EHPA (HA) | 0.041 g/L Ge(IV), 25 g/L $H_2SO_4$ | Extraction: 99% Ge(IV)<br>Extracted species: $GeL_3(HA_2)$<br>Strippant: 2 M $NH_4F$ | [36] |
| LIX 63 (HA) | 1.1 M $H_2SO_4$, Ge(IV), Cu(II), As(III) | Extraction: 99% Ge(IV) in four stages<br>Extracted species: $HA.GeO_3.2H_2SO_4.H_2O$<br>Strippant: 3.8 M NaOH | [9] |
| LIX 63 (HA) + Ionquest 801 (HB) | 1 M $H_2SO_4$, Ge(IV), Cd(II), Zn(II), Co(II), Ni(II), Al(III), Fe(III), In(III), Ga(III) | Extraction: > 68% Ge(IV)<br>Extracted species: $Ge(SO_4)_2.(HA)_2.(HB).H_2SO_4$<br>Strippant: 0.5 M NaOH + 1 M $Na_2SO_4$ | [28] |
| LIX 63 + OPAP | 0.5 M $H_2SO_4$, Ge(IV), Ga(III) | Extraction: 73% Ge(IV)<br>Strippant: $H_2O$ at 75 °C | [14] |
| Kelex 100 (L) | 1.5 M $H_2SO_4$, Ge(IV), Zn(II) | Extraction: 87% Ge(IV)<br>Extracted species: $GeL_2(OH)_2/GeL_3HSO_4$<br>Strippant: 3 M NaOH | [6] |

*Purification of Germanium from the Leach Solution of Critical Element Preconcentrate:* Based on the discussions in the above section, potential flowsheets to produce high-purity germanium products from the critical element preconcentrate are developed. As Figure 69 shows, Flowsheet I shown in Figure 69 is used to generate a leachate rich in Ge(IV) from the preconcentrate. After that, solvent extraction and ion exchange are used, respectively, to concentrate and purify the Ge(IV). Finally, tannic acid is used as a precipitant to selectively precipitate Ge(IV). The capability of the two process to produce high-purity Ge(IV) has been confirmed for other materials, such as gasification fly ash [1],[2].

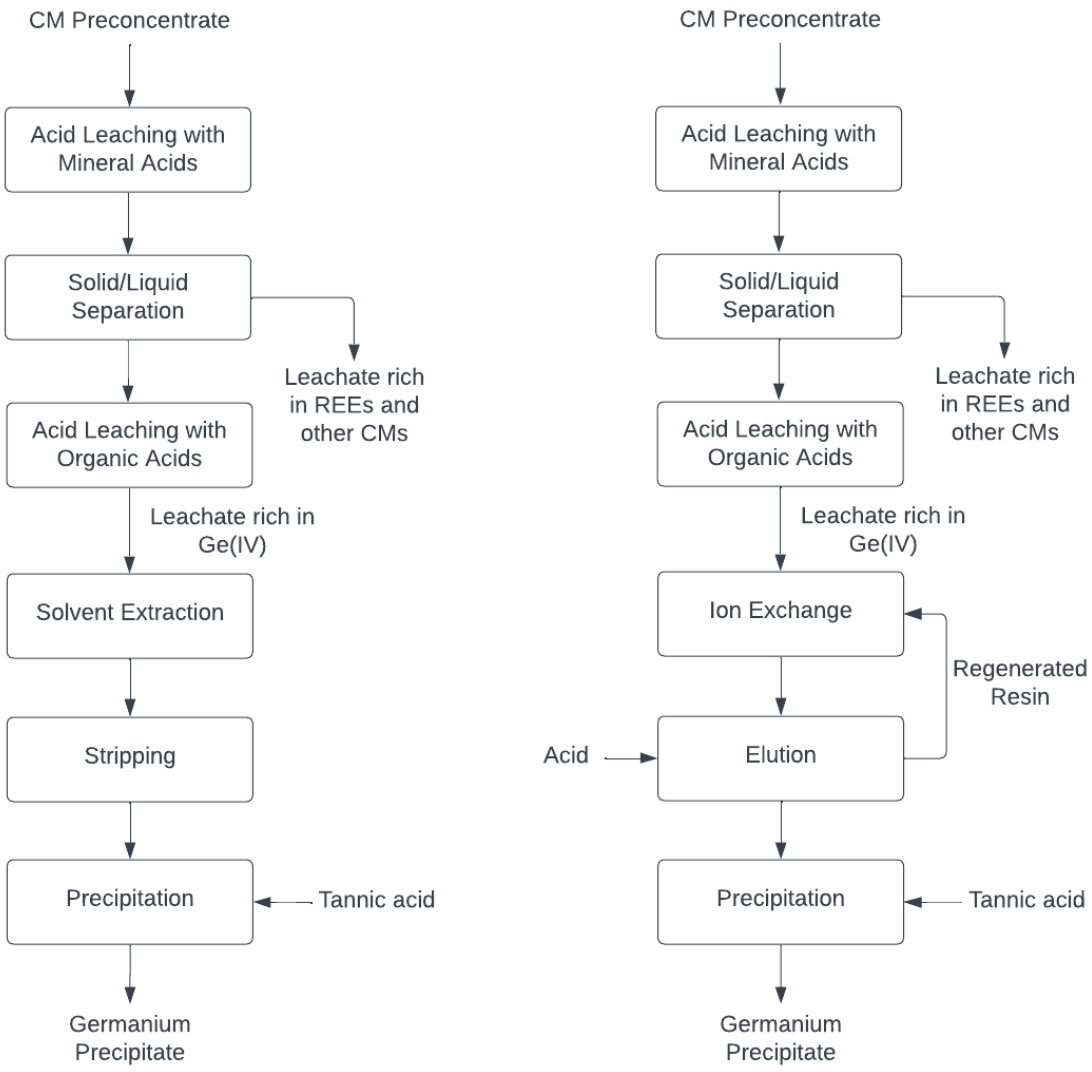


Figure 69. Promising flowsheets for high-purity Ge(IV) production from the critical element preconcentrate obtained from coal refuse leachate.

*Other Methods Used for Germanium Recovery and Purification:* In addition to the hydrometallurgical methods, some other methods have also been used for germanium recovery and purification. For example, as Figure 70 shows, a chlorination process with HCl is used to convert $GeO_2$ to $GeCl_4$. Since $GeCl_4$ has a higher boiling point than most of the impurities, an ultrapure $GeCl_4$ can be obtained from this step. Then, the $GeCl_4$ is hydrolyzed in pure deionized water at high temperature and pressure to obtained ultrapure $GeO_2$. Compared with the hydrometallurgical methods, chlorination and distillation require high pressure and temperature, suggesting high carbon emissions. Ultrapure $GeO_2$ can be reduced to Ge metal using $H_2$, and then, impurities in the metal can be further removed through fractional crystallization (zone refining) [7] (Figure 71). After zone refining, Ge metal is ultrapure and can be used to produce single crystals.

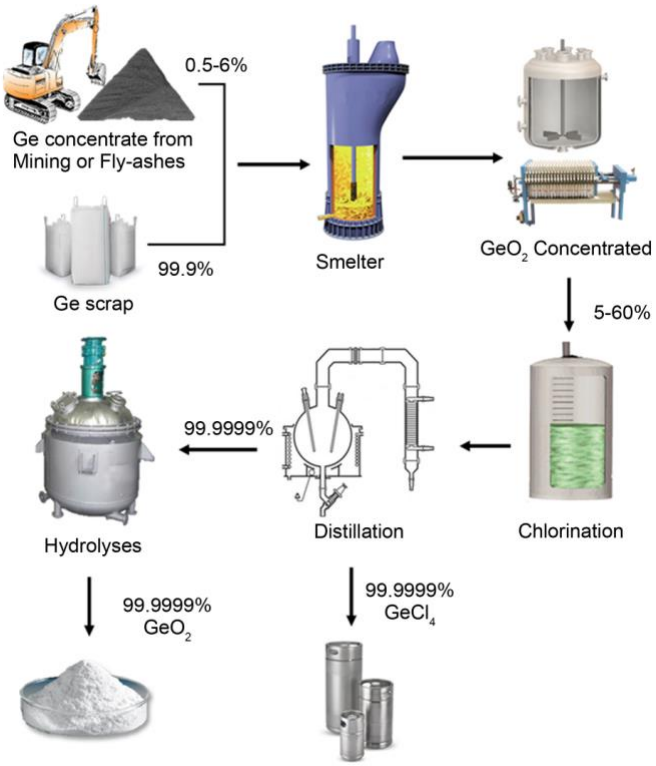


Figure 70. Germanium recovery via pyrometallurgical route [7].

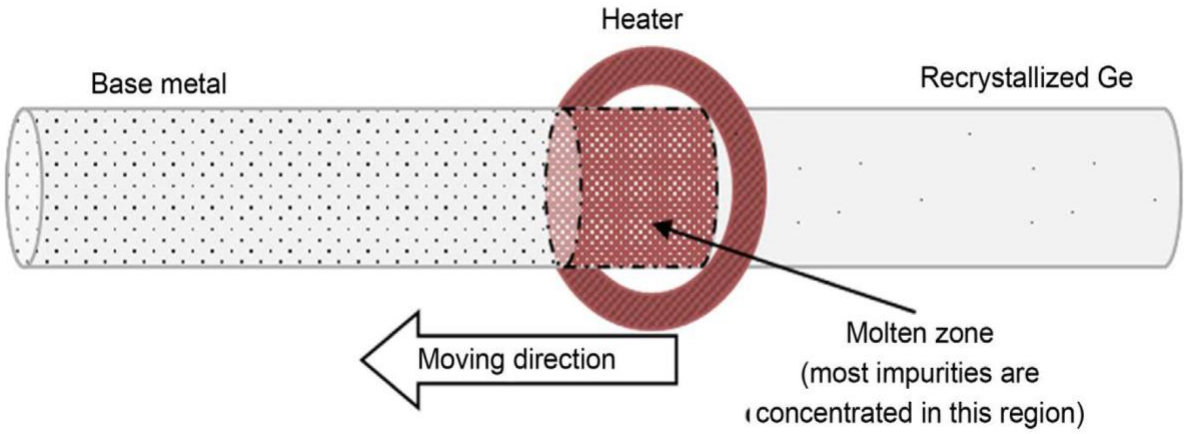


Figure 71. Schematic representation of the zone melting process.

*2.7.1.6.1 Section References:*

[1] Arroyo, F., & Ferna´ndez-Pereira, C. (2008). Hydrometallurgical recovery of germanium from coal gasification fly ash. Solvent extraction method. Ind. Eng. Chem. Res., 47, 3186-3191.

[2] Arroyo Torralvo, F., Fernández-Pereira, C., García Villard, E., Luna, Y., Leiva, C., Vilches, L., & Villegas, R. (2018). Low environmental impact process for germanium

recovery from an industrial residue. Minerals Engineering, 128, 106-114. https://doi.org/10.1016/j.mineng.2018.07.022

[3] Boisvert, L., Turgeon, K., Boulanger, J.-F., Bazin, C., & Houlachi, G. (2020). Recovery of Cobalt from the Residues of an Industrial Zinc Refinery. Metals, 10(11). https://doi.org/10.3390/met10111553

[4] Chen, W.-S., Chang, B.-C., & Chen, Y.-J. (2018). Using ion-exchange to recovery of germanium from waste optical fibers by adding citric acid. IOP Conf. Ser.: Earth Environ. Sci., 159, 012008.

[5] Chen, W.-S., Chang, B.-C., & Chiu, K.-L. (2017). Recovery of germanium from waste Optical Fibers by hydrometallurgical method. Journal of Environmental Chemical Engineering, 5(5), 5215-5221. https://doi.org/10.1016/j.jece.2017.09.048

[6] Cote, G., & Bauer, D. (1980). Liquid-liquid extraction of germanium with oxine derivatives. Hydrometallurgy, 5, 149-160.

[7] Curtolo, D. C., Friedrich, S., & Friedrich, B. (2017). High Purity Germanium, a Review on Principle Theories and Technical Production Methodologies. Journal of Crystallization Process and Technology, 07(04), 65-84. https://doi.org/10.4236/jcpt.2017.74005

[8] Darvishi, D., Haghshenas, D. F., Alamdari, E. K., Sadrnezhaad, S. K., & Halali, M. (2005). Synergistic effect of Cyanex 272 and Cyanex 302 on separation of cobalt and nickel by D2EHPA. Hydrometallurgy, 77(3-4), 227-238. https://doi.org/10.1016/j.hydromet.2005.02.002

[9] De Schepper, A. (1976). Liquid-liquid extraction of germanium by LIX 63. Hydrometallurgy, 1, 291-298.

[10] Drzazga, M., Chmielarz, A., Benke, G., Leszczyńska-Sejda, K., Knapik, M., Kowalik, P., & Ciszewski, M. (2019). Precipitation of Germanium from Sulphate Solutions Containing Tin and Indium Using Tannic Acid. Applied Sciences, 9(5). https://doi.org/10.3390/app9050966

[11] Gupta, B., & Mudhar, N. (2006). Extraction and Separation of Germanium Using Cyanex 301/Cyanex 923. Its Recovery from Transistor Waste. Separation Science and Technology, 41(3), 549-572. https://doi.org/10.1080/01496390500525021

[12] Haghighi, H. K., Irannajad, M., Fortuny, A., & Sastre, A. M. (2019). Selective separation of Germanium(IV) from simulated industrial leachates containing heavy metals by non-dispersive ionic extraction. Minerals Engineering, 137, 344-353. https://doi.org/10.1016/j.mineng.2019.04.021

[13] Haghighi, H. K., Irannajad, M., & Sastre, A. M. (2019). Germanium transport across supported liquid membrane with Cyanex 923: Mathematical modeling. Transactions of

Nonferrous Metals Society of China, 29(9), 1956-1966. https://doi.org/10.1016/s1003-6326(19)65103-4

[14] Harbuck, D. D. (1992). Gallium and germanium recovery from domestic sources.

[15] Harbuck, D. D., Judd, J. C., & Behunin, D. V. (1991). Germanium Solvent Extraction from Sulfuric Acid Solutions (and Co-Extraction of Germanium and Gallium). Solvent Extraction and Ion Exchange, 9(3), 383-401. https://doi.org/10.1080/07366299108918060

[16] Hernández-Expósito, A., Chimenos, J. M., Fernández, A. I., Font, O., Querol, X., Coca, P., & García Peña, F. (2006). Ion flotation of germanium from fly ash aqueous leachates. Chemical Engineering Journal, 118(1-2), 69-75. https://doi.org/10.1016/j.cej.2006.01.012

[17] Kim, Y. S., & Zeitlin, H. (1972). The Separation of Zinc and Copper from Seawater by Adsorption Colloid Flotation. Separation Science, 7(1), 1-12. https://doi.org/10.1080/00372367208058967

[18] Kuroiwa, K., Ohura, S.-i., Morisada, S., Ohto, K., Kawakita, H., Matsuo, Y., & Fukuda, D. (2014). Recovery of germanium from waste solar panels using ion-exchange membrane and solvent extraction. Minerals Engineering, 55, 181-185. https://doi.org/10.1016/j.mineng.2013.10.002

[19] Li, Q., & Zhang, W. (2022). Process development for recovering critical elements from acid mine drainage. Resources, Conservation and Recycling, 180. https://doi.org/10.1016/j.resconrec.2022.106214

[20] Liang, D., Wang, J., Wang, Y., Wang, F., & Jiang, J. (2008). Behavior of tannins in germanium recovery by tannin process. Hydrometallurgy, 93(3-4), 140-142. https://doi.org/10.1016/j.hydromet.2008.03.006

[21] Liang, J., Fan, L., Xu, K., & Huang, Y. (2012). Study on Extracting of Germanium with Trioctylamine. Energy Procedia, 17, 1965-1973. https://doi.org/10.1016/j.egypro.2012.02.340

[22] Liu, F., Liu, Z., Li, Y., Liu, Z., Li, Q., & Zeng, L. (2016). Extraction of gallium and germanium from zinc refinery residues by pressure acid leaching. Hydrometallurgy, 164, 313-320. https://doi.org/10.1016/j.hydromet.2016.06.006

[23] Liu, F., Liu, Z., Li, Y., Wilson, B. P., Liu, Z., Zeng, L., & Lundström, M. (2017). Recovery and separation of gallium(III) and germanium(IV) from zinc refinery residues : Part II: Solvent extraction. Hydrometallurgy, 171, 149-156. https://doi.org/10.1016/j.hydromet.2017.05.009

[24] Liu, F., Liu, Z., Li, Y., Wilson, B. P., & Lundström, M. (2017). Recovery and separation of gallium(III) and germanium(IV) from zinc refinery residues: Part I: Leaching and

iron(III) removal. Hydrometallurgy, 169, 564-570. https://doi.org/10.1016/j.hydromet.2017.03.006

[25] Ma, X.-h., Qin, W.-q., & Wu, X.-l. (2013). Extraction of germanium(IV) from acid leaching solution with mixtures of P204 and TBP. Journal of Central South University, 20(7), 1978-1984. https://doi.org/10.1007/s11771-013-1698-1

[26] Mubarok, M. Z., & Hanif, L. I. (2016). Cobalt and Nickel Separation in Nitric Acid Solution by Solvent Extraction Using Cyanex 272 and Versatic 10. Procedia Chemistry, 19, 743-750. https://doi.org/10.1016/j.proche.2016.03.079

[27] Nguyen, T. H., & Lee, M. S. (2020). A Review on Germanium Resources and its Extraction by Hydrometallurgical Method. Mineral Processing and Extractive Metallurgy Review, 42(6), 406-426. https://doi.org/10.1080/08827508.2020.1756795

[28] Nusen, S., Zhu, Z., Chairuangsri, T., & Cheng, C. Y. (2015). Recovery of germanium from synthetic leach solution of zinc refinery residues by synergistic solvent extraction using LIX 63 and Ionquest 801. Hydrometallurgy, 151, 122-132. https://doi.org/10.1016/j.hydromet.2014.11.016

[29] Otrembska, P., & Gęga, J. (2012). Separation of Nickel(II) and Cadmium(II) with Ion-Exchange Process. Separation Science and Technology, 47(9), 1345-1349. https://doi.org/10.1080/01496395.2012.672520

[30] Parhi, P., & Sarangi, K. (2008). Separation of copper, zinc, cobalt and nickel ions by supported liquid membrane technique using LIX 84I, TOPS-99 and Cyanex 272. Separation and Purification Technology, 59(2), 169-174. https://doi.org/10.1016/j.seppur.2007.06.008

[31] Pariga, C., & P.V.R., S. B. (2000). Separation of nickel and copper from ammoniacal solutions through co-extraction and selective stripping using LIX84 as the extractant. Hydrometallurgy, 54, 195-204.

[32] Pospiech, B., & Walkowiak, W. (2007). Separation of copper(II), cobalt(II) and nickel(II) from chloride solutions by polymer inclusion membranes. Separation and Purification Technology, 57(3), 461-465. https://doi.org/10.1016/j.seppur.2006.07.005

[33] Rao, S., Wang, D., Liu, Z., Zhang, K., Cao, H., & Tao, J. (2019). Selective extraction of zinc, gallium, and germanium from zinc refinery residue using two stage acid and alkaline leaching. Hydrometallurgy, 183, 38-44. https://doi.org/10.1016/j.hydromet.2018.11.007

[34] Sargar, B. M., & Anuse, M. A. (2005). Solvent extraction separation of germanium(IV) with N-n-octylaniline as an extractant. Journal of Analytical Chemistry, 60, 404-408.

[35] Tait, B. K. (1993). Cobalt-nickel separation: the extraction of cobalt(II) and nickel(II) by Cyanex 301, Cyanex 302 and Cyanex 272. Hydrometallurgy, 32, 365-372.

[36] Tang, S.-f., Zhou, C.-s., Jiang, X.-y., & Zhao, C.-l. (2000). Extraction separation of germanium with hydroxamic acid HGS98. Journal of Central South University, 7(1), 40-42.

[37] Torralvo, F. A., & Fernández-Pereira, C. (2011). Recovery of germanium from real fly ash leachates by ion-exchange extraction. Minerals Engineering, 24(1), 35-41. https://doi.org/10.1016/j.mineng.2010.09.004

[38] Turan, M. D., Altundoğan, H. S., & Tümen, F. (2004). Recovery of zinc and lead from zinc plant residue. Hydrometallurgy, 75(1-4), 169-176. https://doi.org/10.1016/j.hydromet.2004.07.008

[39] Van Roosendael, S., Regadío, M., Roosen, J., & Binnemans, K. (2019). Selective recovery of indium from iron-rich solutions using an Aliquat 336 iodide supported ionic liquid phase (SILP). Separation and Purification Technology, 212, 843-853. https://doi.org/10.1016/j.seppur.2018.11.092

[40] Virolainen, S., Heinonen, J., & Paatero, E. (2013). Selective recovery of germanium with N-methylglucamine functional resin from sulfate solutions. Separation and Purification Technology, 104, 193-199. https://doi.org/10.1016/j.seppur.2012.11.023

[41] Wood, S. A., & Samson, I. M. (2006). The aqueous geochemistry of gallium, germanium, indium and scandium. Ore Geology Reviews, 28(1), 57-102. https://doi.org/10.1016/j.oregeorev.2003.06.002

[42] Zhang, L., Guo, W., Peng, J., Li, J., Lin, G., & Yu, X. (2016). Comparison of ultrasonic-assisted and regular leaching of germanium from by-product of zinc metallurgy. Ultrason Sonochem, 31, 143-149. https://doi.org/10.1016/j.ultsonch.2015.12.006

[43] Zhang, T., Jiang, T., & Liu, Z. (2019). Recovery of Ge(IV) from synthetic leaching solution of secondary zinc oxide by solvent extraction using tertiary amine (N235) as extractant and trioctyl phosphate (TOP) as modifier. Minerals Engineering, 136, 155-160. https://doi.org/10.1016/j.mineng.2019.03.011

[44] Zhou, Z.-a., Chu, G., Gan, H.-x., Yang, T.-z., & Chen, L. (2013). Ge and Cu recovery from precipitating vitriol supernatant in zinc plant. Transactions of Nonferrous Metals Society of China, 23(5), 1506-1511. https://doi.org/10.1016/s1003-6326(13)62623-0

*2.7.1.7 Zinc*

Table 53 and

Table 54 summarize the literature on zinc purification. As shown, solvent extraction with D2EPHA, LIX 841, and TBP were shown to be the most common methods of zinc recovery and separation. Other methods included supported liquid membrane and adsorption colloid flotation.

Table 53. Literature review for zinc solvent extraction separations.

| **Solution matrix** | **Extractants** | **Procedure** | **Remarks** | **References** |
|---|---|---|---|---|
| A mixed sulfate/chloride leachate containing 11.8 g/L Fe, 24.8 g/L Cu, 0.23 g/L Zn, 3.8 g/L Co, 35.2 g/L Ni, 176.3 g/L Cl, and 48.9 g/L sulfate | TBP, MIBK, LIX 841, Cyanex 923 | Extracted Fe first with TBP and MIBK, followed by Cu with LIX 841, and finally Zn with Cyanex923. Ni and Co stayed in the raffinate. | Co-extraction of Co and Ni with Zn was nil; 99.1% of Zn was extracted with three-stage counter-current extraction | [5] |
| A stock sulfate solution containing 0.1 M Cu, Ni, and Zn, respectively | LIX 84 I | Extracted Cu first at pH 4.0, followed by Ni at pH 7.5, finally Zn at pH 9.0 | >99% Zn was extracted with two-stage counter current extraction | [4] |
| A sulfate leachate containing 28.8 g/L Zn, 11.21 mg/L Pb, 0.21 g/L Fe, 0.16 g/L Mn, 60.18 mg/L Ni, 0.11 g/L Co, and 35.81 mg/L Ca | D2EHPA with TBP as a phase modifier | Extracted Zn under appropriate conditions | Zn concentration in the aqueous phase was reduced from 4.69 g/L to around 40 mg/L | [8] |
| A sulfate leachate containing 1.99 g/L Cu, 1.04 g/L Co, 12.58 g/L Zn, 8.39 g/L Fe, 1.57 g/L Al, 0.53 g/L Ca, and 0.03 g/L Si | LIX 984, D2EHPA | Cu extraction with LIX 984 first, followed by iron removal through, and then Co/Zn co-extraction with D2EHPA, finally Co/Zn separation through selective stripping | 99% Cu was extracted with <1% co-extraction of Co, Ni, and Fe; 99% Fe was removed with 3% and 5% loss of Co and Zn, respectively; 96% and 99% Zn were extracted, and 100% of Co was selectively stripped at pH 2.5 | [2] |
| A spent pickle liquor that contains 90-100 g/L HCl, 100-120 g/L Zn, 30-32 g/L Fe(II), 1-2 g/L Fe(III), and 230-250 g/L $Cl^-$ | TiOA or TEHA, in the absence and presence of D2EHPA, Versatic 10 acid | Fe(III) extraction first with TiOA/TEHA+D2EHPA at O/A <1:5, then Zn(II) extraction with the same extractants at O/A 7.5:1, finally bio-oxidation of Fe(II) and solvent extraction with Versatic 10 acid | Nearly 100% Zn was extracted | [7] |

Table 54. Other zinc purification technologies.

| Technology | Solution matrix | Remarks | References |
|---|---|---|---|
| Supported liquid membrane (use LIX 84I and TOPS-99 as Cu and Zn extractants, respectively) | A solution containing 8.97 $mol/m^3$ Cu, 8.97 $mol/m^3$ Zn, 8.97 $mol/m^3$ Co, 8.97 $mol/m^3$ Ni and 8.97 $mol/m^3$ ammonium sulfate | Cu was first extracted with LIX 84I supported liquid membrane, and then, Zn was extracted with TOPS-99 supported liquid membrane | [3] |
| Adsorption colloid flotation (use negatively charged ferric hydroxide as the collector, a cationic surfactant, dodecylammine, and air) | Two synthetic solutions prepared by dissolving Zn metal in hydrochloric solution and Cu sulfate in hydrochloric acid, respectively | 100% recovery of Zn was obtained | [6] |
| Electrodialysis with cation-exchange and anion-exchange membranes | Electroplating waste waters | Zn was successfully separated from Fe with the help of complexing agent. | [1] |

*2.7.1.7.1 Section References:*


[1] Babilas, D., & Dydo, P. (2018). Selective zinc recovery from electroplating wastewaters by electrodialysis enhanced with complex formation. Separation and Purification Technology, 192(June 2017), 419–428. https://doi.org/10.1016/j.seppur.2017.10.013

[2] Kongolo, K., Mwema, M. D., Banza, A. N., & Gock, E. (2003). Cobalt and zinc recovery from copper sulphate solution by solvent extraction. Minerals Engineering, 16(12), 1371–1374. https://doi.org/10.1016/j.mineng.2003.09.001

[3] Ramesh, A., Hasegawa, H., Maki, T., & Ueda, K. (2007). Adsorption of inorganic and organic arsenic from aqueous solutions by polymeric Al/Fe modified montmorillonite. Separation and Purification Technology, 56(1), 90–100. https://doi.org/10.1016/j.seppur.2007.01.025

[4] Reddy, B. R., & Priya, D. N. (2005). Process development for the separation of copper(II), nickel(II) and zinc(II) from sulphate solutions by solvent extraction using LIX 84 I. Separation and Purification Technology, 45(2), 163–167. https://doi.org/10.1016/j.seppur.2005.02.014

[5] Sarangi, K., Parhi, P. K., Padhan, E., Palai, A. K., Nathsarma, K. C., & Park, K. H. (2007). Separation of iron(III), copper(II) and zinc(II) from a mixed sulphate/chloride solution using TBP, LIX 84I and Cyanex 923. Separation and Purification Technology, 55(1), 44–49.

[6] Sik Kim, Y., & Zeitlin, H. (1972). The Separation of Zinc and Copper from Seawater by Adsorption Colloid Flotation. Separation Science, 7(1), 1–12. https://doi.org/10.1080/00372367208058967

[7] Sinha, M. K., Sahu, S. K., Meshram, P., & Pandey, B. D. (2014). Solvent extraction and separation of zinc and iron from spent pickle liquor. Hydrometallurgy, 147–148, 103–111. https://doi.org/10.1016/j.hydromet.2014.05.006

[8] Vahidi, E., Rashchi, F., & Moradkhani, D. (2009). Recovery of zinc from an industrial zinc leach residue by solvent extraction using D2EHPA. Minerals Engineering, 22(2), 204–206. https://doi.org/10.1016/j.mineng.2008.05.002

*2.7.1.8 Nickel*

Table 55 shows the methods reported in the literature for nickel purification, including solvent extraction, ion exchange, membrane technologies, etc.

Table 55. Nickel purification technologies.

| **Method** | **Solution matrix** | **Details** | **Remarks** | **References** |
|---|---|---|---|---|
| Solvent extraction | A solution containing 100 g/L $NiSO_4 \cdot 6H_20$ and 2 g/L $COSO_4 \cdot 7H_20$ | Cyanex 301, Cyanex 302 and Cyanex 272 were compared. Cyanex 302 showed better separation performance | N/A | [6] |
| Solvent extraction | A leach liquor containing ( in $kg/m^3$) 13.8 Cu, 10.7 Ni, 90 $NH_4 \cdot OH$ and 45 $(NH_4)_2SO_4$ | Ni and Cu were co-extracted using LIX84, and then Ni was selectively stripped. | N/A | [4] |
| Solvent extraction | A synthetic solution containing Ni and Co | A mixture of Cyanex 302 and D2EHPA was performed. | The synergistic effect of the two extractant occurred. | [1] |
| Solvent extraction | A nitric acid solution of Ni and Co | Cyanex 272 was used to separate Ni and Co. | Ni and Co were effectively separated using Cyanex 272. | [2] |
| Ion exchange | A synthetic solution of Ni and Cd | Lewatit OC-1026, Lewatit TP-207, and Lewatit MonoPlus SP 112 resins were used. | The best separation of metal ions was obtained for the | [3] |

| | | | | |
|---|---|---|---|---|
| | | | ion-exchange process with Lewatit OC 1026 | |
| Polymer inclusion membranes | An aqueous HCl solution containing Cu(II), Co(II) and Ni(II) | Tertiary amines, i.e. tri-n-octylamine (TOA) and triisooctylamine (TIOA) have been applied as the ion carriers in membrane | Cu(II) and Co(II) ions were effectively removed from the source phase by transport through PIMs with TOA and TIOA as the ionic carriers into 0.1M NaOH as the receiving phase. Ni(II) was not detected in the receiving phase | [5] |

*2.7.1.8.1 Section References:*


[1] Darvishi, D., Haghshenas, D. F., Alamdari, E. K., Sadrnezhaad, S. K., & Halali, M. (2005). Synergistic effect of Cyanex 272 and Cyanex 302 on separation of cobalt and nickel by D2EHPA. Hydrometallurgy, 77(3–4), 227–238. https://doi.org/10.1016/j.hydromet.2005.02.002

[2] Mubarok, M. Z., & Hanif, L. I. (2016). Cobalt and Nickel Separation in Nitric Acid Solution by Solvent Extraction Using Cyanex 272 and Versatic 10. Procedia Chemistry, 19, 743–750. https://doi.org/10.1016/j.proche.2016.03.079

[3] Otrembska, P., & Gega, J. (2012). Separation of Nickel(II) and Cadmium(II) with Ion-Exchange Process. Separation Science and Technology (Philadelphia), 47(9), 1345–1349. https://doi.org/10.1080/01496395.2012.672520

[4] Parija, C., & Bhaskara Sarma, P. V. R. (2000). Separation of nickel and copper from ammoniacal solutions through co-extraction and selective stripping using LIX84 as the extractant. Hydrometallurgy, 54(2), 195–204. https://doi.org/10.1016/S0304-386X(99)00069-9

[5] Pospiech, B. (2015). Separation of cadmium(II), cobalt(II) and nickel(II) by transport through polymer inclusion membranes with phosphonium ionic liquid as ion carrier. Archives of Metallurgy and Materials, 60(4), 2933–2938. https://doi.org/10.1515/amm-2015-0468

[6] Tait, B. K. (1993). Cobalt-nickel separation: the extraction of cobalt(II) and nickel(II) by Cyanex 301, Cyanex 302 and Cyanex 272. Hydrometallurgy, 32(3), 365–372. https://doi.org/10.1016/0304-386X(93)90047-H

### *2.7.2 Subtask 7.2 – St-Li Adsorption Process*

*Staged Precipitation* - Staged precipitation tests were conducted to evaluate the precipitation characteristics of selected critical elements and contaminant elements as a function of pH. As Figure 72 shows, by raising the pH of a leachate from coal to around 4.5, nearly all Fe and most Al were precipitated, while most of the critical elements still existed in the solution. Therefore, Fe and Al in the leachate can be largely removed by removing the precipitate formed at 4.5. After that, critical elements started to precipitate with the increase in the pH. When the pH reached around 9.0, REEs, Co, Mn, Ge, and Ga were precipitated, while Li and Sr remained in the solution. Although the precipitation curve of Zn and Ni is not presented in the figure, the prior study of the team has confirmed that Zn and Ni precipitated in a similar pH range as Co and Mn. Therefore, after staged precipitation, the critical elements contained in the leachate were separated into two material streams: precipitate rich in REEs, Co, Mn, Ge, Ga, Zn, and Ni, as well as a solution rich in Li and Sr with some contentment elements, such as Ca and Mg. A flowsheet describing the staged precipitation process is shown in Figure 73.

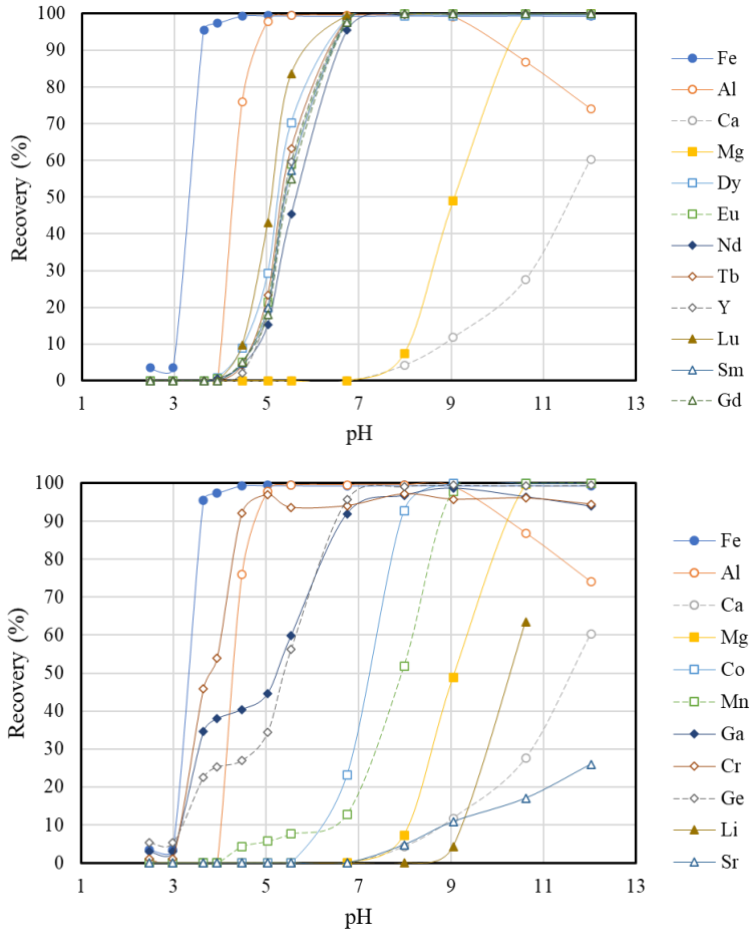


Figure 72. Precipitation recovery of selected critical elements and contaminant elements as a function of pH.

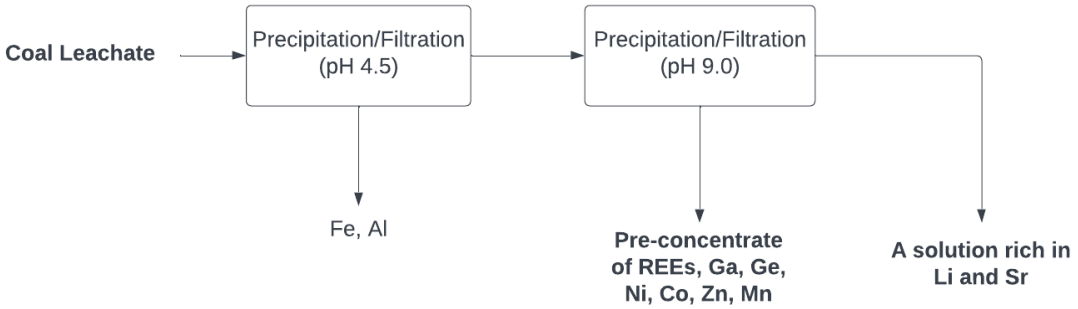


Figure 73. Staged precipitation flowsheet.

*Li and Sr Recovery* - After staged precipitation, Li and Sr remained in the solution together with some contaminant elements, such as Ca and Mg. An exhaustive review on the recovery and purification of Li and Sr has been conducted by the team. The potential technologies that can be used for the recovery of Li and Sr from the solution after staged precipitation include adsorption, solvent extraction, membrane-based technologies, electrodialysis, etc. Based on these technologies, two flowsheets were developed to produce high-grade Li and Sr products (>99% pure) from the leachate.

*Flowsheet I:* Flowsheet I (Figure 74) was developed based on selective adsorption and solvent extraction. In this process, Li existing in the leachate is first adsorbed using appropriate adsorbents (e.g., Al-, Mn-, and Ti-series). After adsorption, Li is desorbed, leading to a solution rich in Li with minor contaminants. Then, the solution is fed to solvent extraction to selectively extract Li by remaining the contaminants in the aqueous phase. Stripping of the loaded organic phase will generate a concentrated Li solution, from which commercial grade lithium carbonate can be obtained through carbonate precipitation. After Li adsorption from the solution of staged precipitation, Sr can also be selectively adsorbed using selective adsorbents, such as strontium alginate. In addition, after selective adsorption, Sr can also be purified through solvent extraction. Finally, commercial-grade strontium carbonate can be obtained through carbonate precipitation.

*Flowsheet II:* Flowsheet II (Figure 75) uses reverse osmosis to concentrate metal ions existing in the solution obtained from staged precipitation. Then, monovalent and divalent metal ions in the concentrated solution are separated using nanofiltration. The separation of Li from other monovalent metal ions is realized through supported liquid membranes. Finally, commercial-grade lithium carbonate is produced through carbonate precipitation. Sr is separated from other divalent metal ions following the same process as the Flowsheet I: selective adsorption, desorption, solvent extraction, and carbonate precipitation. Based on the results reported in the literature, commercial-grade strontium carbonate can be produced using this process.

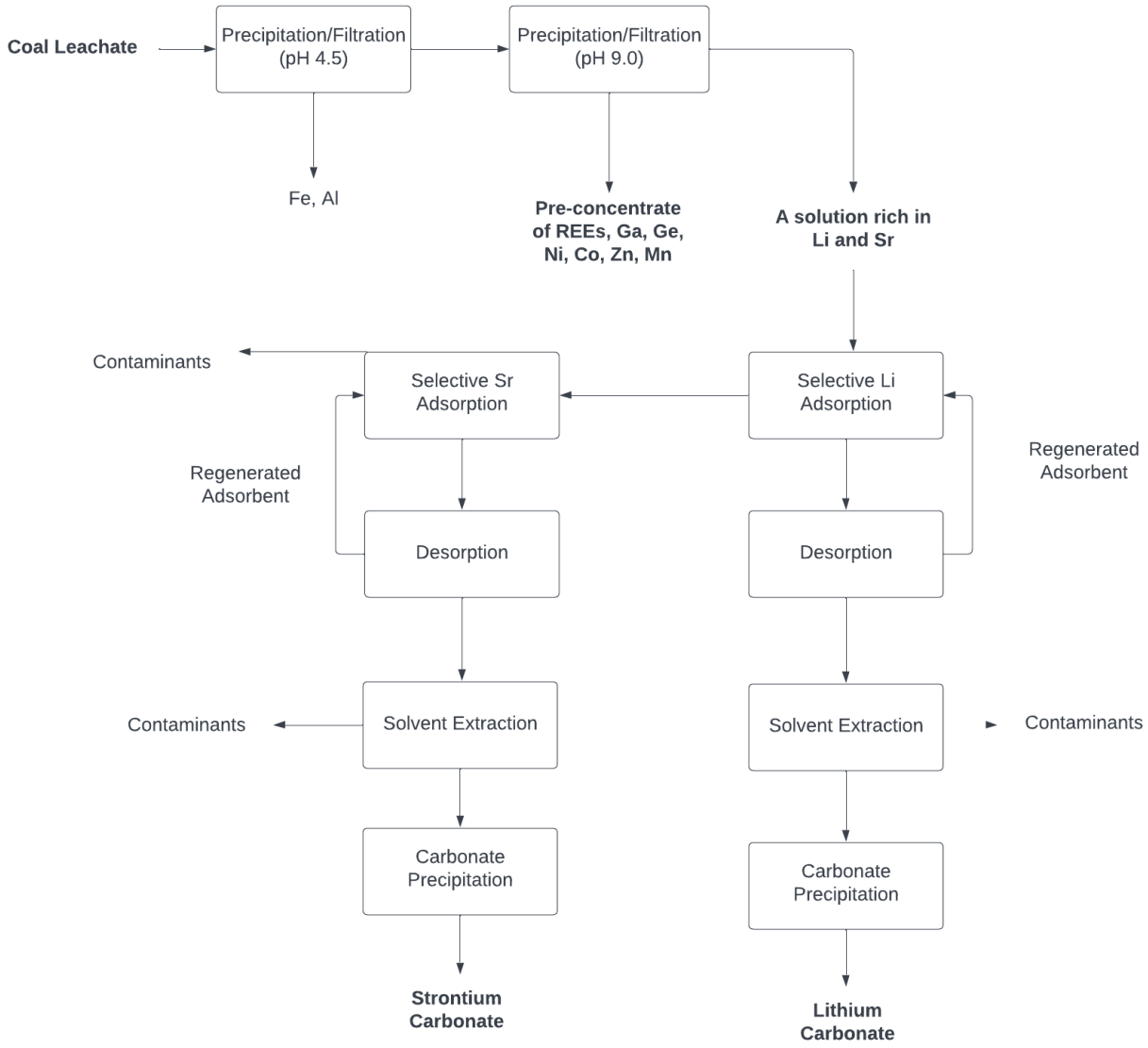


Figure 74. Flowsheet I for Li and Sr recovery and purification.

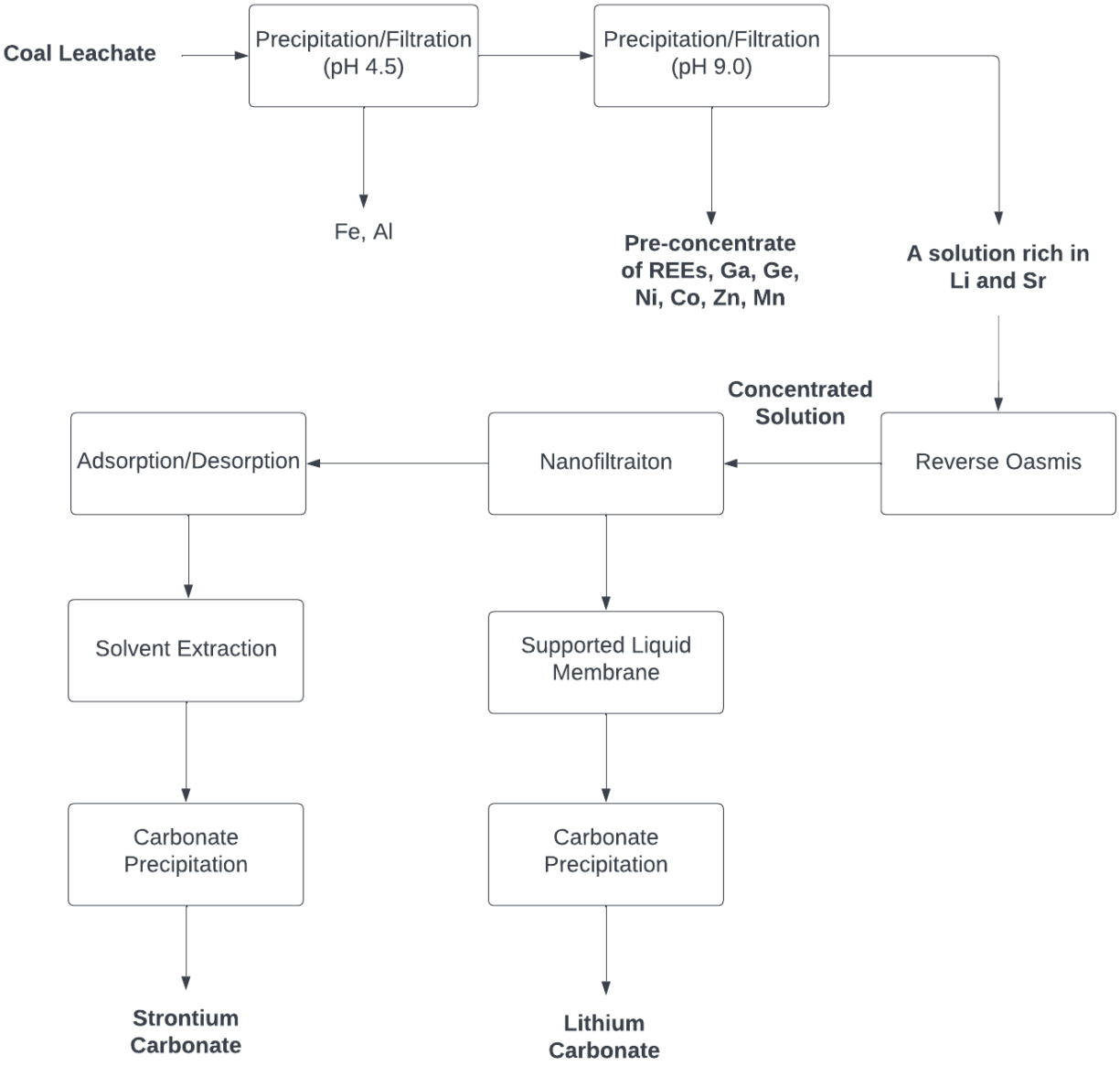


Figure 75. Flowsheet II for Li and Sr recovery and purification.

### *2.7.3 Subtask 7.3 – Reduction/Ionic Liquid/Plasma Distillation Circuit*

*Thermal and electrochemical methods to produce Zn, Ni, Co, Mn* – A CM concentrate given in

Table 56 produced from  circuit 1 provides the bases for a CM product and provided as the assumed feedstock for the CM Thermal and electrochemical system.

Table 56. Oxides concentration for the base metals - Heap leach PLS Co-Ni-Zn product (sulfide converted to oxides by roasting).

| Elements | Elemental Concentration | | Elemental MW | Oxide Form | Oxides Concentration |
|---|---|---|---|---|---|
| | mg/kg | % dry weight | g/mol | | % dry weight |
| **TREE** | 2768.3 | 0.3 | | | **0.33** |
| Al | 5960.3 | 0.6 | 13 | $Al_2O_3$ | 1.70 |
| Ca | 1427.9 | 0.1 | 40 | CaO | 0.20 |
| Co | 56371.3 | 5.6 | 28 | CoO | 8.86 |
| Cu | 9724.6 | 1.0 | 64 | CuO | 1.22 |
| Fe | 10556.5 | 1.1 | 56 | $Fe_2O_3$ | 1.51 |
| Mg | 26914.2 | 2.7 | 24 | MgO | 4.49 |
| Mn | 17784.4 | 1.8 | 55 | MnO | 2.81 |
| Na | 33888.2 | 3.4 | 23 | $Na_2O$ | 4.57 |
| Ni | 187197.6 | 18.7 | 59 | NiO | 28.93 |
| Se | 251.1 | 0.0 | 79 | $SeO_2$ | 0.04 |
| Sr | 78.2 | 0.0 | 88 | SrO | 0.01 |
| Zn | 136566.9 | 13.7 | 65 | ZnO | 17.02 |

*Thermodynamic Calculations* - Thermodynamic equilibrium calculations are performed using a computer program based on the Gibbs energy minimization method to determine the condensed metal recovery efficiency of PLS Co-Ni-Zn product-$CH_4$ system as a function of temperature. This method is based on the fact that systems will achieve equilibrium at the lowest possible energy level. Hence, the total Gibbs energy for a system is at a minimum at equilibrium. This method is represented by Eqs. 1, 2, and 3.

$$G = \sum_{gas} n_i (g_i^o + RT\ln P_i) + \sum_{\substack{pure\\condensed\\phase}} n_i g_i^o + \sum_{solution-1} n_i (g_i^o + RT\ln X_i + RT\ln \gamma_i) + \sum_{solution-2} n_i (g_i^o + RT\ln X_i + RT\ln \gamma_i) + \cdots \quad (1)$$

$$P_i = (n_i / n) P_{total} \quad (2)$$

$$\gamma_i = \frac{a_i}{X_i} \quad (3)$$

where G is total Gibbs energy of the system; $g_i^o$ is standard molar Gibbs energy of species i at T and P; $n_i$ is number of moles of species i; $P_i$ is partial pressure of species i; $X_i$ is the mole fraction of species i; and $\gamma_i$ is the activity coefficient of species i. The software used in this study is from HSC Chemistry [1], which chooses the $n_i$ to minimize G subject to mass balance constraints.

The calculations are performed for the heap leach PLS Co-Ni-Zn product and methane gas as the reductant is used to reduce the products to metals. The REE oxides, because of their low

concentration (0.33wt%) are not considered for these calculations. The results are shown in Figure 76 which shows the condensed metal recovery efficiency of critical metals (wt.%) as a function of temperature.

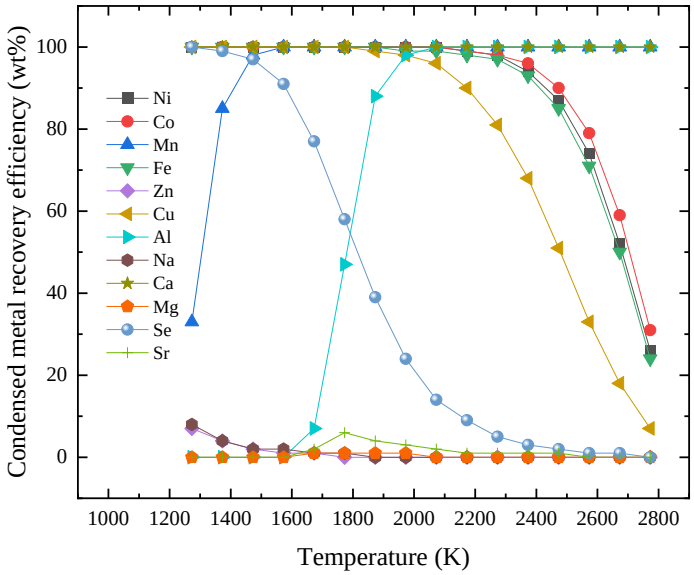


Figure 76. Condensed critical metal recovery efficiency vs. temperature.

Table 56 shows the heap leach PLS Co-Ni-Zn product composition. Thermal processing and electrochemical production of critical metals from PLS Co-Ni-Zn product in low temperature ionic liquid are studied [2, 3]. The proposed flowsheet for pure critical metals production from heap leach Co-Ni-Zn product is shown in Figure 77Figure 77. Proposed flow sheet for the production of critical metals from heap leach PLS Co-Ni-Zn products.. The process steps in the production of pure critical metals and generated products are discussed below.

*2.7.3.1 Proposed CM process for Mn Co, Ni, Zn*

*A. Thermal processing of heap leach PLS Co-Ni-Zn product* - The first step is the production of Zn and Na alloy powders which is done by the thermal reduction of Heap leach PLS Co-Ni-Zn product using $CH_4$ gas. The gaseous product composition is 80 wt.% Zn and 20 wt.% Na. The reduced product is mainly consisted of Ni, Co, Fe, Zn, Cu and Mn alloy and slag consists of mainly MgO and $Al_2O_3$.

*B. Production of pure Zn* - The produced gaseous product from process A is an Zn and Na alloy powder. This powder is water leached at room temperature. The yield of pure Zn from Heap leach PLS Co-Ni-Zn product is 92 wt. %. The Na is produced as NaOH byproduct which is marketable.

*C. Production of Pure Ni* - Condensed product from process A is converted into anodes. These anodes are used for electrochemical production of pure Ni using nickel chloride electrolytes containing eutectic based ionic liquid (2:1-Urea:ChCl) at low temperature (343K)[2], The expected yield of pure Ni is 100 wt. %.

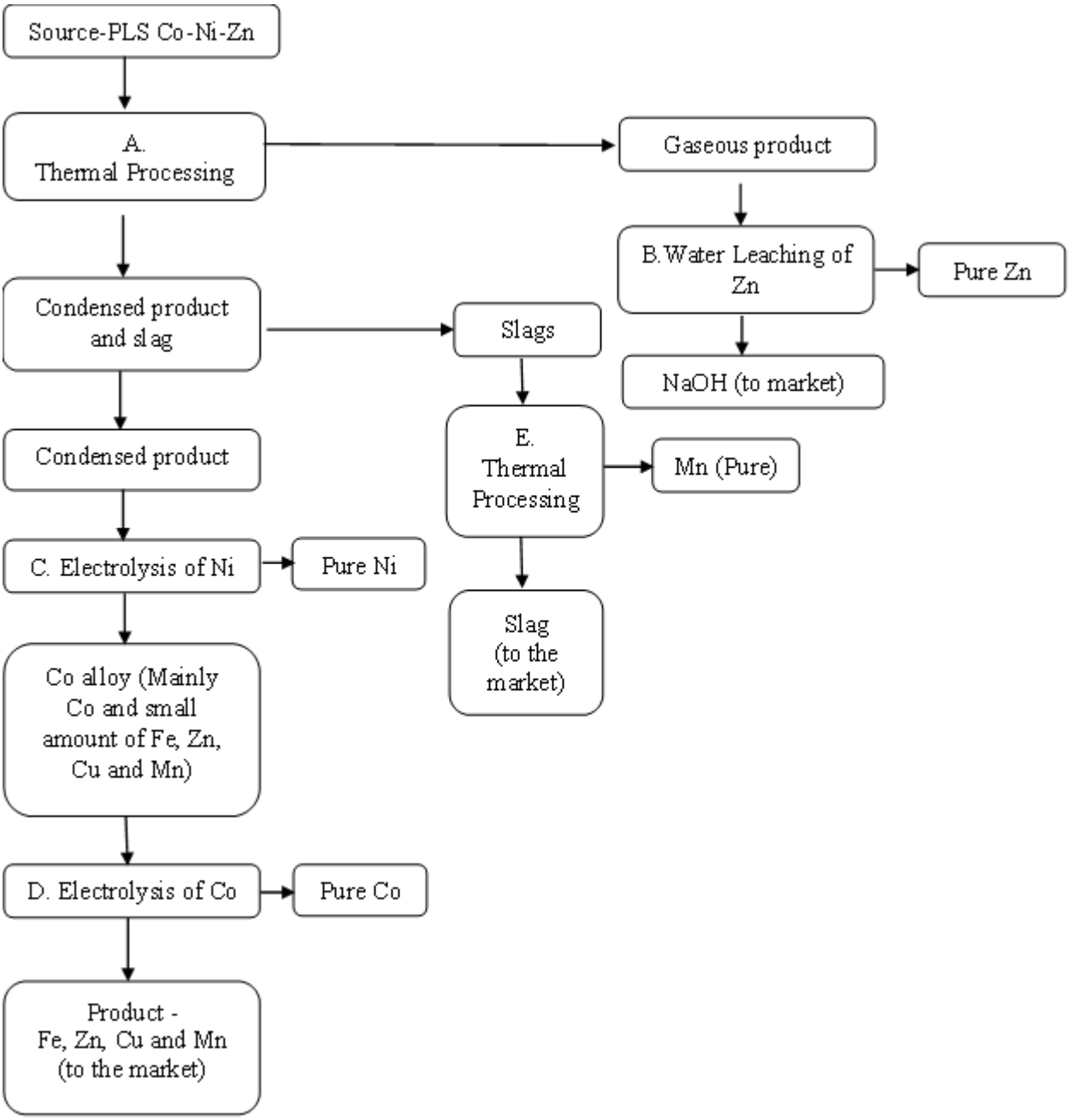


Figure 77. Proposed flow sheet for the production of critical metals from heap leach PLS Co-Ni-Zn products.

*Production of pure Co* - The Remaining anode from process B containing Co, Fe, Cu and Mn is further treated using the electrolytic process to produce pure Co. The electrolyte used is $CoCl_2$ containing Urea: ChCl (2:1) at a low temperature of 323 K [2]. The expected yield of Co using this process is 100 wt. %.

*Production of pure Mn* - Slag from process A containing MgO, MnO and $Al_2O_3$ are reduced by $CH_4$ at 1473 K and 1 atm. Pure Mn metal is produced in this process step. The residues slag

contains MgO, and $Al_2O_3$, which can be marketable to refractory industry. The expected Mn yield is 65.4 wt. %.

Thermal processing analysis of heap leach PLS Co-Ni-Zn products is conducted to produce a condensed and gaseous product. The gaseous product subjected to water leaching to produce pure zinc and NaOH. The slag produced is further thermal processed to produce pure Mn. Electrochemical production of pure nickel and cobalt using low temperature ionic liquids is proposed. The anode residue containing mainly Fe and Cu which can be marketable to copper industry.

*2.7.3.2 Section References:*


[1] HSC Chemistry Software, V 10, Copyright Outokumpu Research, (2021).

[2] Y. Yang, X.W. Guo, X.B. Chen, S.H. Wang, G.H. Wu, W.J. Ding, and N. Birbilis, On the electrodeposition of nickel–zinc alloys from a eutectic-based Ionic liquid, Electrochimica Acta. 63 (2012) 131–138.

[ 3] A. R. Kim, and R. G. Reddy, Cobalt electrodeposition from cobalt chloride using urea and choline chloride ionic liquid: Effect of temperature, applied voltage, and cobalt chloride concentration on current efficiency and energy consumption. The Minerals, Metals & Series (2017) 97–114.


*2.7.3.3 Heap leach PLS Mn product (hydroxide converted to oxides by roasting)*

Table 57 shows the heap leach PLS Mn product. This is the feed materials from which pure magnesium and manganese are extracted. Figure 3.1 shows the flow sheet for the production of Mg and Mn.

Table 57. Oxides concentration for the base metals - Heap leach PLS Mn product (hydroxide converted to oxides by roasting).

| **Elements** | **Elemental Concentration** | | **Elemental MW** | **Oxide Form** | **Oxides Concentration** |
|---|---|---|---|---|---|
| | mg/kg | % dry weight | g/mol | | % dry weight |
| **TREE** | 8465.0 | 0.8 | | | **1.03** |
| Al | 67481.9 | 6.7 | 13 | $Al_2O_3$ | 19.21 |
| Ca | 1046.7 | 0.1 | 40 | CaO | 0.15 |
| Co | 200.6 | 0.0 | 28 | CoO | 0.03 |
| Fe | 2530.3 | 0.3 | 56 | $Fe_2O_3$ | 0.36 |
| Mg | 217721.9 | 21.8 | 24 | MgO | 36.29 |
| Mn | 142053.3 | 14.2 | 55 | MnO | 22.47 |
| Na | 57405.7 | 5.7 | 23 | $Na_2O$ | 7.74 |
| Ni | 1095.8 | 0.1 | 59 | NiO | 0.17 |
| Se | 643.2 | 0.1 | 79 | $SeO_2$ | 0.09 |

The assessment of the heap leach PLS Mn product Table 57 for the production of CMs is discussed. As seen from the Table 57, the main components are oxides of Mn, Mg, Al, Na, Ni, and Fe. A critical literature review on the production of CMs from feed stock was made. The reduction of magnesium oxide to magnesium using thermal plasma processing with methane as a reducing gas is proposed. The high energy densities which plasma systems can achieve (gas enthalpies of 3-8 kWh per normal $m^3$) could usefully be harnessed for the production of metals from their oxides when the reduction reactions are highly endothermic [1]. This is not only true for primary production but is also applied to the secondary recovery of metals from oxide materials. The carbothermic reduction of MgO can be operated at or near atmospheric pressure using a plasma reactor whereas conventional methods must be operated in a vacuum [2]. Plasma also allows for improved energy efficiency over conventional methods. In this research, the natural gas will be used as the reducing agent. A water-cooled heat exchanger will be used for the shock quenching of the gaseous magnesium. The effects of natural gas to MgO ratio and power input on production of magnesium is discussed below.

*Thermodynamic Calculations* - The standard Gibbs energy change ($\Delta G^o$ ) as a function of temperature (T) diagram for several oxides is shown in Figure 78[3]. From this graph, an element can reduce the oxide of any element with a $\Delta G^o$ line appearing above it at a given temperature. The negative slope for the carbon monoxide formation means the increased stability of carbon monoxide at higher temperatures. The fact that carbon has an increasing affinity for oxygen as temperatures increase indicates the effectiveness for carbon based source to be used as a reducing agent especially for metallic oxides. Extrapolation of the corresponding lines gives that at about 1700°C the MgO line intercepts the carbon monoxide line. This means that at temperatures greater than 1700°C, carbon can be used to reduce MgO to Mg using thermal plasma technology [4,5].

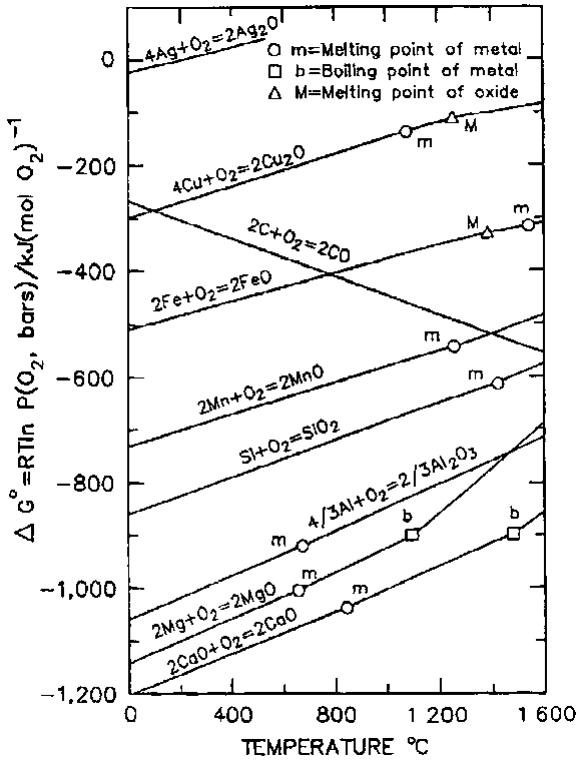


Figure 78. $\Delta G^o$ vs. T diagram for the formation of oxides [3]

Thermodynamic equilibrium calculations were performed using a computer program based on the Gibbs energy minimization method to determine the most stable compositions of the MgO-$CH_4$ system as a function of temperature. This method is based on the fact that systems will achieve equilibrium at the lowest possible energy level. Hence, the total Gibbs energy for a system is at a minimum at equilibrium. This method is represented by Eqs. 1, 2, and 3.

$$G = \sum_{gas} n_i (g_i^o + RT\ln P_i) + \sum_{\substack{pure\\ condensed\\ phase}} n_i g_i^o + \sum_{solution-1} n_i (g_i^o + RT\ln X_i + RT\ln \gamma_i) + \sum_{solution-2} n_i (g_i^o + RT\ln X_i + RT\ln \gamma_i) + \cdots \quad (1)$$

$$P_i = (n_i / n) P_{total} \quad (2)$$

$$\gamma_i = \frac{a_i}{X_i} \quad (3)$$

where G is total Gibbs energy of the system; $g_i^o$ is standard molar Gibbs energy of species i at T and P; $n_i$ is number of moles of species i; $P_i$ is partial pressure of species i; $X_i$ is the mole fraction of species i; and $\gamma_i$ is the activity coefficient of species i. The software used in this study is from HSC Chemistry[6], which chooses the $n_i$ to minimize G subject to mass balance constraints.

The calculations were performed for the ratio of 50% MgO / 50% $CH_4$ system. For simplicity, ideal solutions were assumed. The results are shown in Figure 79. At above 1700°C, magnesium gas is formed. If the gas is shock quenched from this temperature, then magnesium powder is produced. The thermodynamic calculation showed a yield of pure Mg at 1700°C.

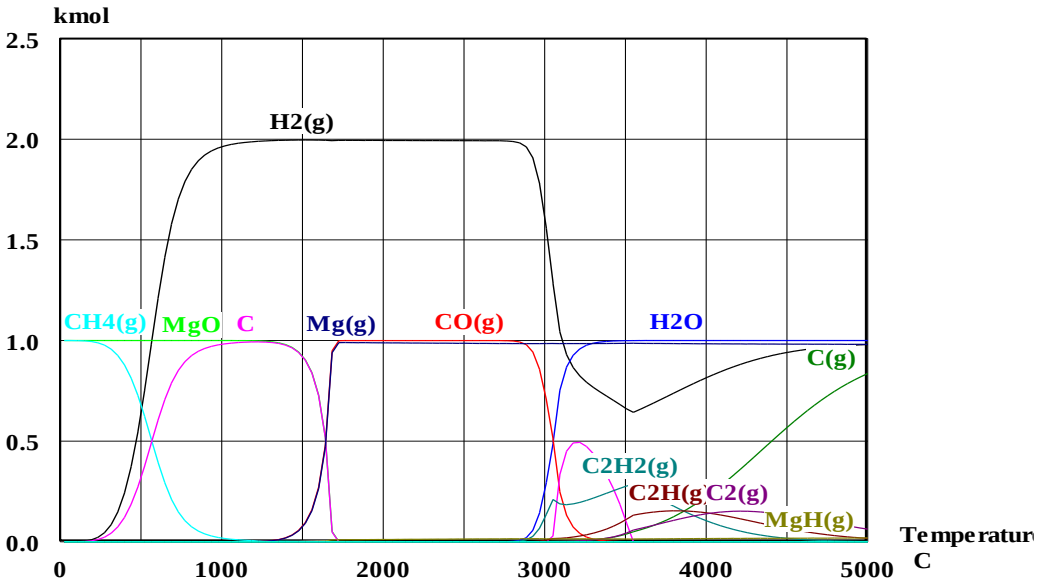


Figure 79. Reduction of magnesium oxide to magnesium reactions with natural gas ($CH_4$)

The experiments conducted in our laboratory using thermal plasma reactor showed a complete reduction of magnesium oxide to magnesium occurs at a temperature above 1700°C and at a molar ratio of MgO:$CH_4$=1:1. The pure Mg (>99%) was collected from the condensed gas phase. The other reaction products are liquid alloy and slag. The slag mostly contains alumina with small amount of sodium and other oxides. The alloy contains manganese, aluminum and small amount of other metals.

The electrochemical process of alloy is proposed for the production of pure manganese metal. The alloy produced will be used as an anode material for electrochemical deposition of Mn. The electrodeposition of manganese and alloys in low temperature ionic liquid electrolytes were studied [7-15]. At a constant potential of about 2 V and 323 K, pure Mn can be deposited. The obtained current efficiency is greater than 99%. The anode residue containing mostly Al will be marketed.

The proposed flow sheet for the production of critical metals from heap leach - PLS-Mn product is shown in Figure 80.

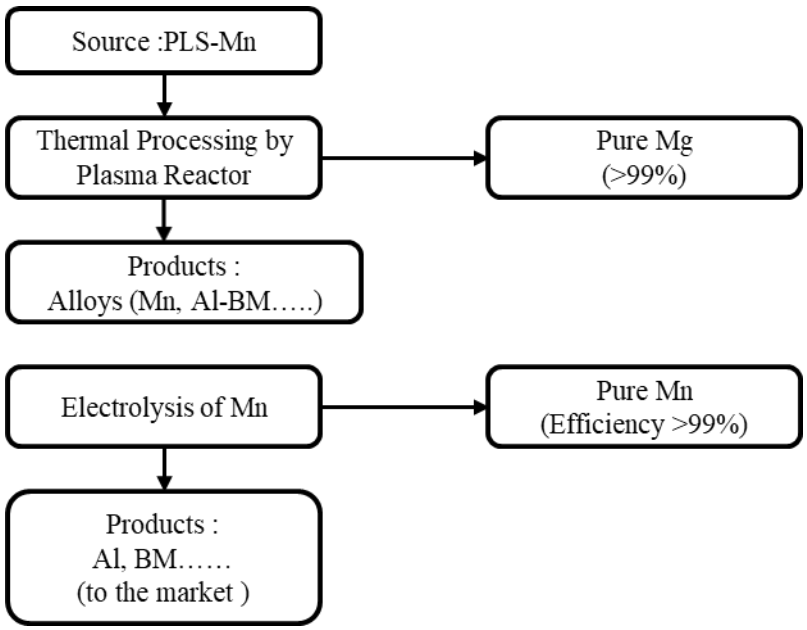

Figure 80. Flow sheet for production of critical metals from the heap leach PLS Mn product

The pathways to assess the process technologies for the production of IREEs and CMs for the feed sources heap leach PLS Rare earth product (oxalate converted to oxides by roasting) and heap leach PLS Co-Ni-Zn product (sulfide converted to oxides by roasting) are in progress and results will be reported in the next reports.

*2.7.3.4 Section References:*

[1] G.K. Bhat, "Potential, Problems, and innovations of Plasma Heat Applications in the Metallurgical Industry," *Pure and Applied Chemistry*, v.56 (2), (1984), pp. 209-214.
[2] A.M. Cameron, D.L. Canham, and V.G. Aurich, "Magnesium Production by Plasma-Powered Processing," *Journal of Metals*, (April 1990), pp. 46-48.
[3] N.A. Gokcen and R.G. Reddy, *Thermodynamics*, 2nd Ed, (1996), Plenum Press, New York, NY, USA.
[4] M. Ramachandran and R.G. Reddy, Direct reduction of magnesium oxide to magnesium using thermal plasma technology, SME Transactions, 32 (2015), 30–37
[5] S. W. White and R. G. Reddy, Waste Processing of MgO Bag house Dust Using Plasma Arc Technology, EPD Congress, TMS, (1999), pp. 687-697.
[6] HSC Chemistry Software, V 10, Copyright Outokumpu Research, (2021).
[7] J. K. Chang, C. H. Huang, W. T. Tsai, M. J. Deng, I. W. Sun, and P. Y. Chen, Manganese films electrodeposited at different potentials and temperatures in ionic liquid and their application as electrode materials for supercapacitors, Electrochimica Acta. 53 (2008) 4447–4453.
[8] Y. Wang, R.G. Reddy and R. Wang, Dendrite-free Al recycling via electrodeposition using Ionic liquid electrolytes: The effects of deposition temperature and cathode surface roughness, Journal of Cleaner Production. 287 (2021) 125043.
[9] P. P. Chung, P. A. Cantwell, G. D. Wilcox, and G.W. Critchlow, Electrodeposition of zinc–manganese alloy coatings from ionic liquid electrolytes, Transactions of the IMF. 86 (2008) 211–219.

[10] P. Y. Chen, and C.L. Hussey, The electrodeposition of Mn and Zn–Mn alloys from the room-temperature tri-1-butylmethylammonium bis((trifluoromethane)sulfonyl)imide ionic liquid, Electrochimica Acta. 52 (2007) 1857–1864.
[11] M. Li, Z. Wang and R.G. Reddy, Cobalt electrodeposition using urea and choline chloride, Electrochimica Acta. 123 (2014) 325–331.
[12] M. Li, Z. Wang and R. G. Reddy, "Electrodeposition of Nickel in 1-Butyl-3-Methylimidazolium Tetrafluoroborate ionic liquids", *Journal of the electrochemical society*, Vol. 161, (2014), D150-D153.
[13] A. Liu, Z. Shi and R. G. Reddy, "Mechanism study of Cu-Zn alloys electrodeposition in deep eutectic solvents", *Ionics*, Vol 26 (6), (2020), 3161-3172.
[14] A. Liu, Z. Shi and R.G. Reddy, Electrochemical Synthesis of Co-Nd Films in Urea and Choline Chloride Deep Eutectic Solvents, Metallurgical and Materials Transactions B, 51B, (2020), 1162-1168.
[15] Yuxiang Peng, Pravin. S. Shinde, and Ramana G. Reddy, "Diffusion coefficient and nucleation density studies electrochemical deposition of Aluminum from chloroaluminate ionic liquid electrolytes", *Journal of Electroanalytical Chemistry*, Vol 895, (2021), 115363.

### *2.7.4 Subtask 7.4 – Other CMs*

A comprehensive flowsheet to produce high-purity (>99% pure) REEs, Ni, Co, Mn, Zn, Ga, and Ge products from the pre-concentrate obtained through staged precipitation is shown in Figure 81. As the figure shows, selective dissolution is first applied to dissolve REEs, Ni, Co, Mn, Zn, and Ga, while leaving Ge in the undissolved solid. The undissolved Ge is then dissolved using correct lixiviants, which are primarily organic acids. After dissolution, Ge is purified through solvent extraction or ion-exchange, and finally precipitated with tannic acid to generate high-purity Ge tannate. The REEs, Ni, Co, Zn, Ga, and Mn dissolved into solution in the selective dissolution step is subjected to oxalic acid precipitation to selectively precipitate REEs. The precipitate is then washed and roasted to generate high-purity rare earth oxides. The solution after oxalic acid precipitation can be processed using several different technologies, such as solvent extraction, ionic flotation, chromatography, ion exchange, and membrane-based technologies, in order to separate the critical elements. After being separated, high-purity products of the critical elements are obtained through precipitation or evaporative crystallization.

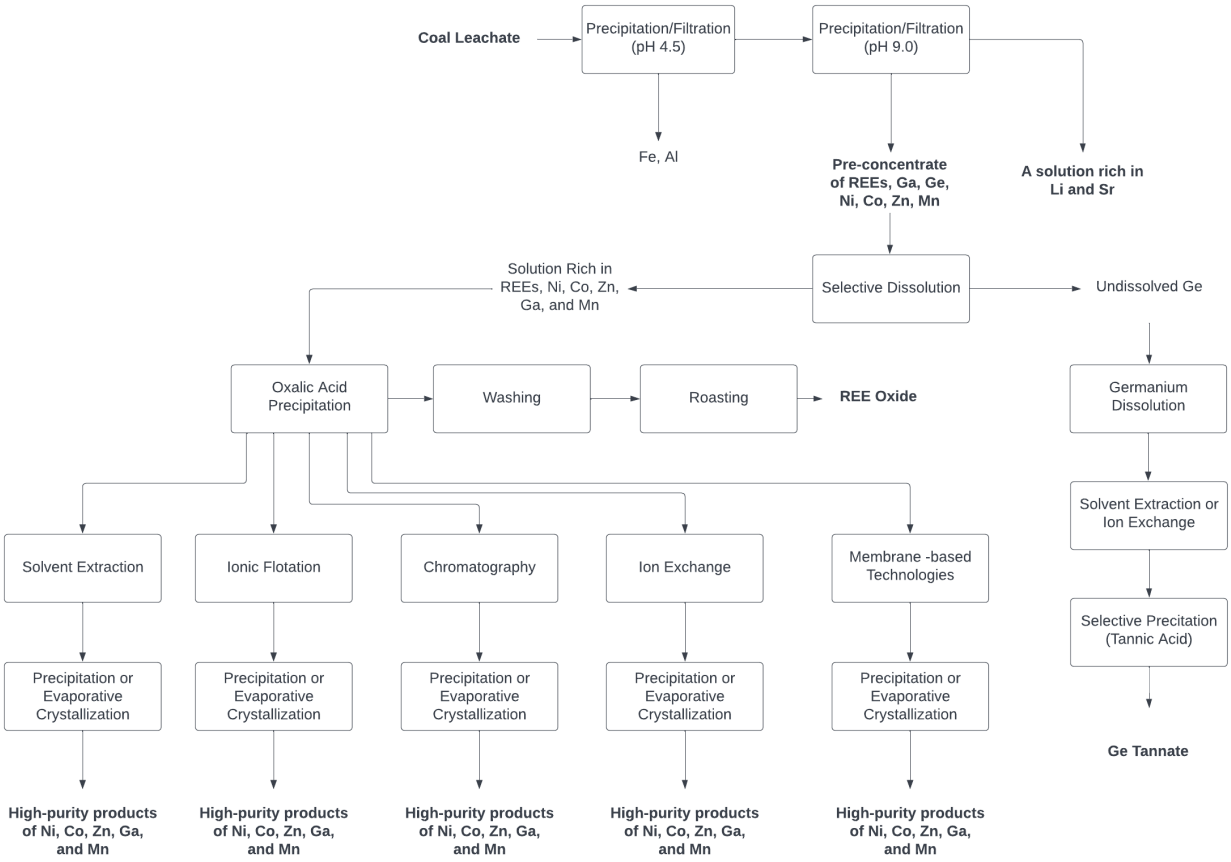


Figure 81. Flowsheet for REEs, Ni, Co, Mn, Zn, Ga, and Ge recovery.

## 2.8 Task 8.0 – Process Integration & Technology Downselect

As part of the project, a downselect was required to identify the technology set most likely to succeed in meeting the project deliverables. In this project, the technologies were largely self-selecting. In this the modeling of the SAC did not reach sufficient maturity to be considered against the combined Circuit 2-3-4 combination that the plasma/ionic liquid offering. With successful thermodynamic modeling and evidences from literature available, this technology is anticipated to meet the capacity and purity specifications for the project. For these reasons, it was selected as the technology for the proposal. Please reference the following sections for the technical details of the selected technology and flowsheet.

## 2.9 Task 9.0 – Process Flow Diagram Development

*Process Description and Process Flow Diagram* - To describe the proposed flowsheet, it is necessary to provide context for the reasons in deciding upon certain configurations. For Circuit 1, staged precipitation tests conducted by VT prior to the start of this project were conducted to evaluate the precipitation characteristics of selected critical elements and contaminant elements as a function of pH. As Figure 82 shows, by raising the pH of a leachate from coal to around 4.5, nearly all Fe and most Al were precipitated, while the majority of the critical elements remained in the solution. Therefore, Fe and Al in the leachate can be largely removed by removing the precipitate formed at pH 4.5. After that, critical elements begin to precipitate with an increase in

the pH of the solution. When the pH of the solution reached around 9.0, rare earth elements (REEs), Co, Mn, Ge, and Ga were precipitated, while Li and Sr remained in solution. Although the precipitation curve of Zn and Ni is not presented in the figure, the prior study of the project team has confirmed that Zn and Ni precipitate in a similar pH range as Co and Mn. Therefore, after staged precipitation, the critical elements contained in the leachate were separated into two material streams: a precipitate rich in REEs, Co, Mn, Ge, Ga, Zn, and Ni, and a solution rich in Li and Sr with some contaminate elements, such as Ca and Mg.

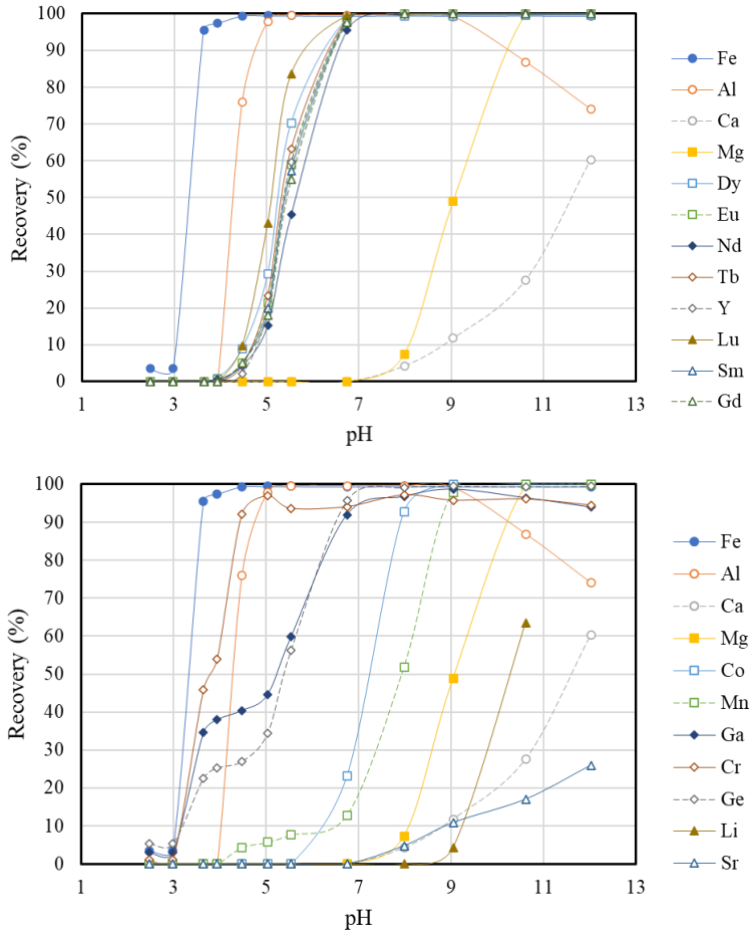


Figure 82. Precipitation recovery of selected critical elements and contaminant elements as a function of pH.

To make use of the REE and critical mineral (CM) characteristics and produce useful products, including rare earth metals (REMs), the following flow sheet is proposed to produce four (4) product streams to meet the requirements of the project (see

Figure 83 and

Figure 84). At this time, staged precipitation, which creates several distinct products is favored owing to the downstream selection of pyrometallurgical methods. The products include a REE product containing Ga and Ge, a CM product containing Co, Ni, and Zn, a Mn and Mg product,

and waters containing Sr and Li. These intermediate products have been formed as precipitates previously in another DOE sponsored project (Demonstration of Scaled-Production of Rare Earth Oxides and Critical Materials from Coal-Based Sources using Innovative, Low Cost Process Technologies and Circuits - DE-FE0031827) as shown in Table 58 to

Table 60.

Table 58. Heap leach pregnant leach solution rare earth product*

| Elements | Elemental Concentration | | Elemental MW | Oxide Form | Oxides Concentration |
|---|---|---|---|---|---|
| | mg/kg | % dry weight | g/mol | | % dry weight |
| Sc | 287 | 0.0 | 45 | Sc2O3 | 0.04 |
| Y | 303804 | 30.4 | 89 | Y2O3 | 38.58 |
| La | 2889 | 0.3 | 139 | La2O3 | 0.34 |
| Ce | 28337 | 2.8 | 140 | CeO2 | 3.48 |
| Pr | 9080 | 0.9 | 141 | Pr6O11 | 1.10 |
| Nd | 69877 | 7.0 | 144 | Nd2O3 | 8.15 |
| Sm | 54613 | 5.5 | 150 | Sm2O3 | 6.33 |
| Eu | 16037 | 1.6 | 152 | Eu2O3 | 1.86 |
| Gd | 111411 | 11.1 | 157 | Gd2O3 | 12.84 |
| Tb | 16656 | 1.7 | 159 | Tb4O7 | 1.96 |
| Dy | 123926 | 12.4 | 163 | Dy2O3 | 14.22 |
| Ho | 12564 | 1.3 | 165 | Ho2O3 | 1.44 |
| Er | 27816 | 2.8 | 167 | Er2O3 | 3.18 |
| Tm | 3192 | 0.3 | 169 | Tm2O3 | 0.36 |
| Yb | 15534 | 1.6 | 173 | Yb2O3 | 1.77 |
| Lu | 2067 | 0.2 | 175 | Lu2O3 | 0.24 |
| **TREE** | 798091 | 79.8 | | **∑REO** | **95.89** |
| **Al** | 4294 | 0.4 | 13 | Al2O3 | 1.22 |
| **Ca** | 44847 | 4.5 | 40 | CaO | 6.28 |
| **Fe** | 8865 | 0.9 | 56 | Fe2O3 | 1.27 |

*Note: Oxalates converted to oxides by roasting.

Table 59. Heap leach pregnant leach solution Co, Ni, and Zn product*

| Elements | Elemental Concentration | | Elemental MW | Oxide Form | Oxides Concentration |
|---|---|---|---|---|---|
| | mg/kg | % dry weight | g/mol | | % dry weight |
| **TREE** | 2768.3 | 0.3 | | | **0.33** |
| Al | 5960.3 | 0.6 | 13 | Al2O3 | 1.70 |
| Ca | 1427.9 | 0.1 | 40 | CaO | 0.20 |
| Co | 56371.3 | 5.6 | 28 | CoO | 8.86 |
| Cu | 9724.6 | 1.0 | 64 | CuO | 1.22 |
| Fe | 10556.5 | 1.1 | 56 | Fe2O3 | 1.51 |
| Mg | 26914.2 | 2.7 | 24 | MgO | 4.49 |
| Mn | 17784.4 | 1.8 | 55 | MnO2 | 2.81 |
| Na | 33888.2 | 3.4 | 23 | Na2O | 4.57 |
| Ni | 187197.6 | 18.7 | 59 | NiO | 28.93 |
| Se | 251.1 | 0.0 | 79 | SeO2 | 0.04 |
| Sr | 78.2 | 0.0 | 88 | SrO | 0.01 |
| Zn | 136566.9 | 13.7 | 65 | ZnO | 17.02 |

*Note: Sulfides converted to oxides by roasting.

Table 60. Heap leach pregnant leach solution Mg/Mn product*

| Elements | Elemental Concentration | | Elemental MW | Oxide Form | Oxides Concentration |
|---|---|---|---|---|---|
| | mg/kg | % dry weight | g/mol | | % dry weight |
| **TREE** | 8465.0 | 0.8 | | | **1.03** |
| Al | 67481.9 | 6.7 | 13 | Al2O3 | 19.21 |
| Ca | 1046.7 | 0.1 | 40 | CaO | 0.15 |
| Co | 200.6 | 0.0 | 28 | CoO | 0.03 |
| Cu | 26.9 | 0.0 | 64 | CuO | 0.00 |
| Fe | 2530.3 | 0.3 | 56 | Fe2O3 | 0.36 |
| Mg | 217721.9 | 21.8 | 24 | MgO | 36.29 |
| Mn | 142053.3 | 14.2 | 55 | MnO2 | 22.47 |
| Na | 57405.7 | 5.7 | 23 | Na2O | 7.74 |
| Ni | 1095.8 | 0.1 | 59 | NiO | 0.17 |
| Se | 643.2 | 0.1 | 79 | SeO2 | 0.09 |
| Sr | 0.0 | 0.0 | 88 | SrO | 0.00 |
| Zn | 365.1 | 0.0 | 65 | ZnO | 0.05 |

*Note: Hydroxides converted to oxides by roasting.

The process depicted in
Figure 83 begins with the representation of the heap leach. It is important to note that the heap leach concept depends on the Dotiki coarse refuse propensity to autogenerate sulfuric acid ($H_2SO_4$) from the oxidation of contained pyrite ($FeS_2$). To account for the variation of seasonal temperature and rainfall effects on the generation of the appropriate amount of acid, a controlled pyrite bio-oxidation step is added as a potential mitigation method. As conceived, the heap leach receives liquid in the forms of make-up water, or water recycled back from the primary precipitation stage. Following leaching, iron precipitation is performed by raising the solution pH. An important option of this process is the use or blending of lignite sources for additional REE recovery. Iron precipitate derived from the process will be returned to coarse refuse impoundment from whence it originated or incorporated into areas of spent heap leach material for disposal. Techniques for rendering these refuses inert at closure make them ideal for containing this material. Increasing the pH further will result in an Al/Sc rich precipitate that will be settled in much the same manner via pond.

Following Al/Sc precipitation, further pH adjustment induces the precipitation of REEs. A thickener is utilized to decrease the volume reporting to the filter press for the recovery of this precipitate. The REEs are captured via an additional precipitation step and releached and precipitated via an oxalic acid precipitation step. The resulting precipitate is then roasted into an oxide form. For additional recovery the lixiviant is further processed by the introduction of $Na_2S$ which will selectively induce a CoS precipitate. The pH of the lixiviant is then adjusted to produce an a Mn rich concentrate for recovery. The remaining liquid is then sent for additional processing to recover Li and Sr.

As shown in
Figure 83, a blended pyrometallurgical method utilizing a plasma reactor and electrowinning using various ionic liquids is proposed for reduction and purification of REEs to metals/REMs. The difference between vaporization of several REEs allows for a preliminary split of REEs to be

accomplished. More detailed information about this circuit (circuits 2/3) was provided in past reports and will be included in the final project report. Of particular note is the treatment of Ga and Ge. As can be seen from
Figure 83, it appears that Ga and Ge will report to this stream and owing to the lower vaporization temperature of Ga and Ge than the REEs, it is anticipated that these elements will report to the Eu, Tm, Yb, and Ca product. In consideration of this, it is envisioned that the plasma reactor may be run at a lower initial temperature to split the lower volatility elements off first or methods described with releaching and recovery will be suitable for additional processing. It is important to note that this will be further investigated and included as part of the technical economic analysis (TEA). Investigations of hydrometallurgical methods for these elements to date make it difficult to implement in view of the proposed pyrometallurgical technique and require additional considerations.

The CM refining circuit (Circuit 4) is shown in
Figure 84. This circuit embodies the progressive electrolysis of the CM precipitate into Zn, Ni, Mn, and Co. It is important to note the Mn is removed during this stage owing to the imperfect split from selective precipitation. The 3$^{rd}$ precipitate processed is the Mg/Mn precipitate as shown in
Figure 84. Utilizing plasma processing, a pure Mg condensate will be created along with a Mn oxide which will be reduced to metal via electrochemical means. The residual materials derived from these processes will be evaluated as part of the Technical Research Plan to determine their potential value. The remaining waters containing Li and Sr could be processed to lithium and strontium carbonate products. As indicated in
Figure 84, a process integrating adsorptive technology, solvent extraction (SX), and precipitation is included as a place holder as a final process determination cannot be made at this time owing to lack of data.

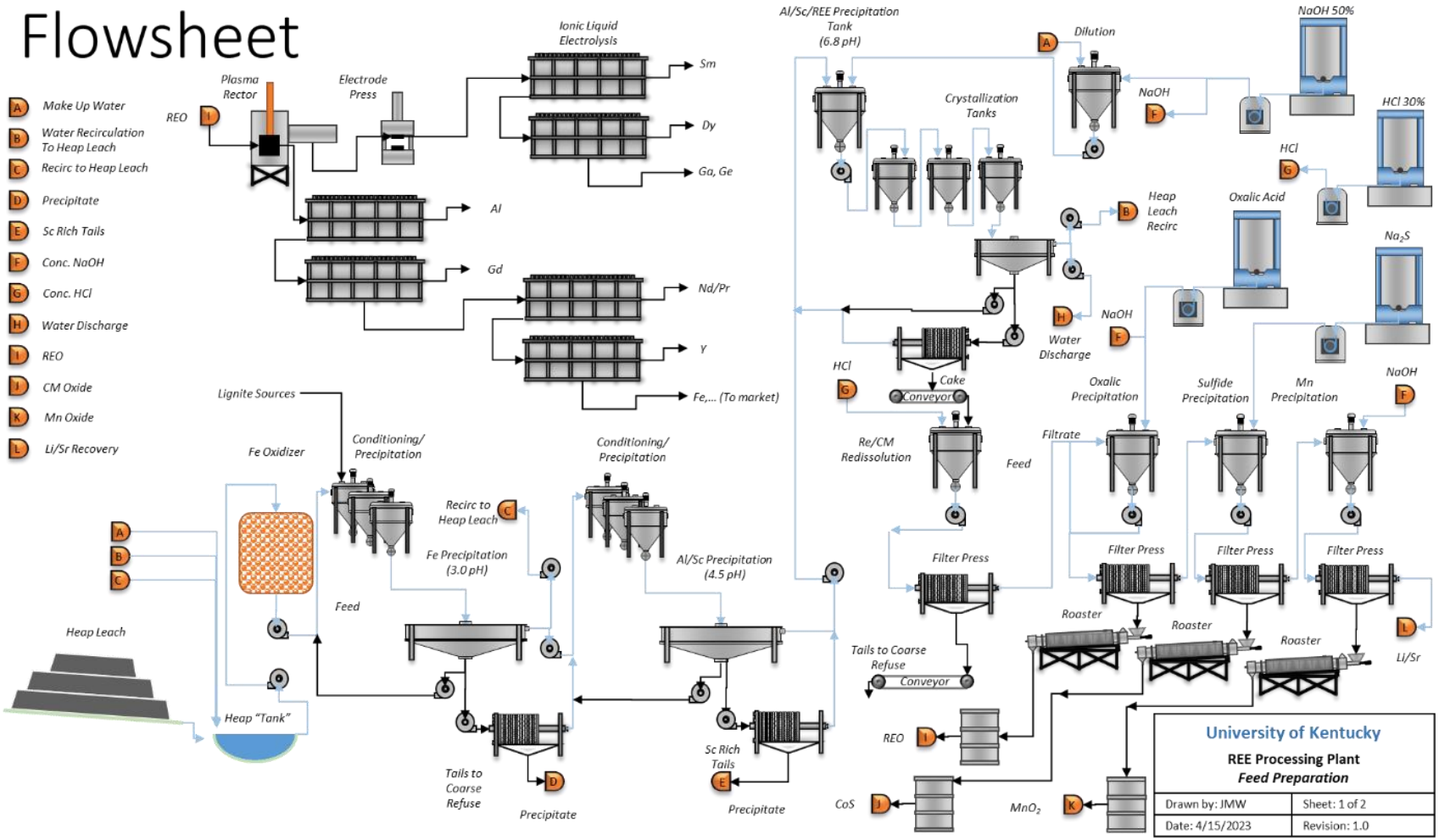


Figure 83. Proposed conceptual flow sheet showing the combined Circuit 1 (extraction and concentration of REEs) and a combined Circuit 2 and 3 (REE separation and purification and production of REMs). The associated REEs and CMs are Y, Pr, Nd, Gd, Dy, Sm, Ga, and Ge.

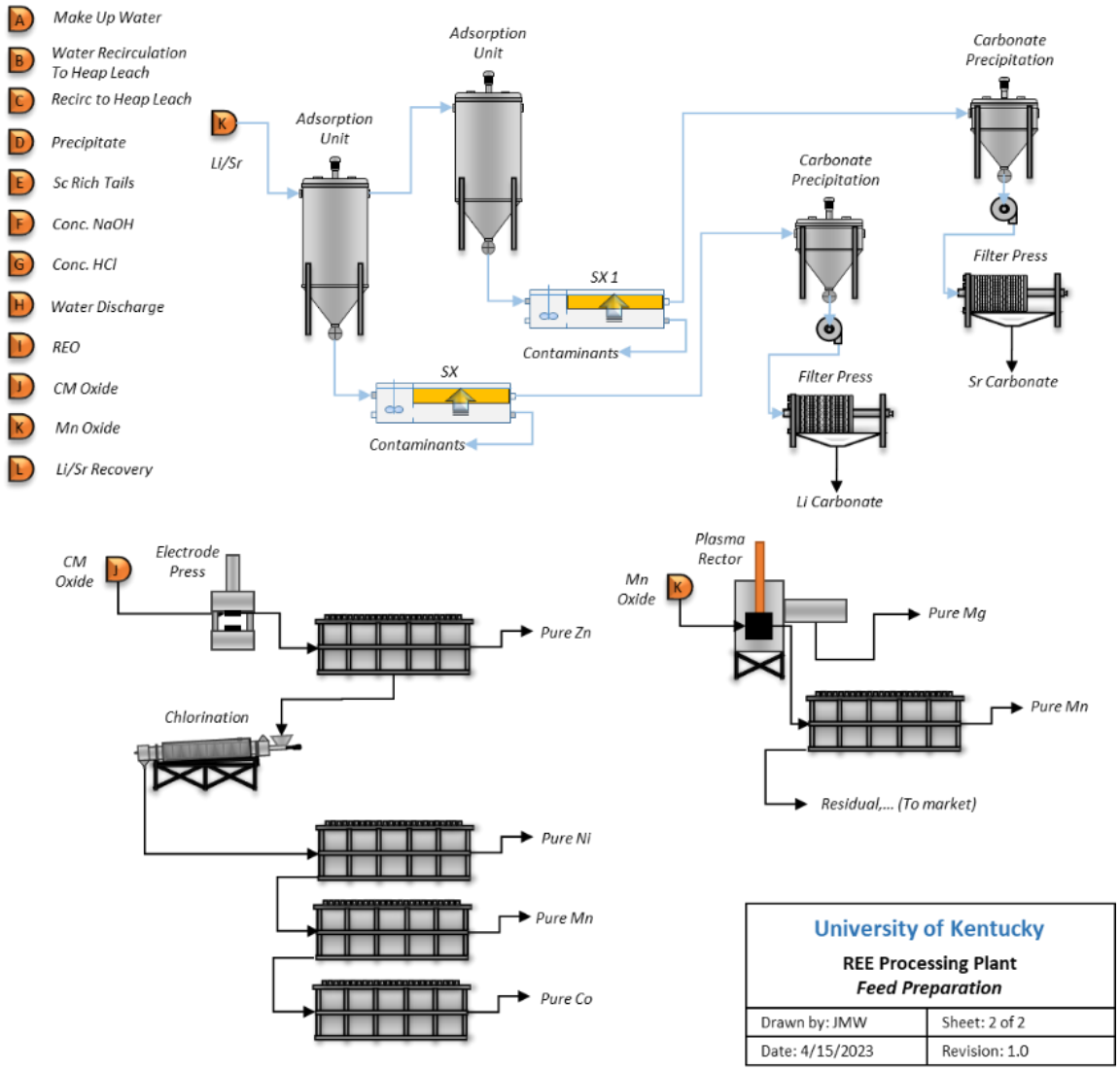


Figure 84. Proposed conceptual flow sheet for Circuit 4, CM production. The associated CM are Co, Mn, Ga, Sr, Li, Ni, and Zn.

*Mass and Energy Balance* - The mass balance was performed on the metal equivalent of each element provided as a mass yield across each process step. The resulting summary mass balance is shown in
Figure 85 and

Figure 86. As this model is contained in the excel file "DOE_FE0032119_TEA", contained therein are the process step yields, masses, and capital and operational expenditures.

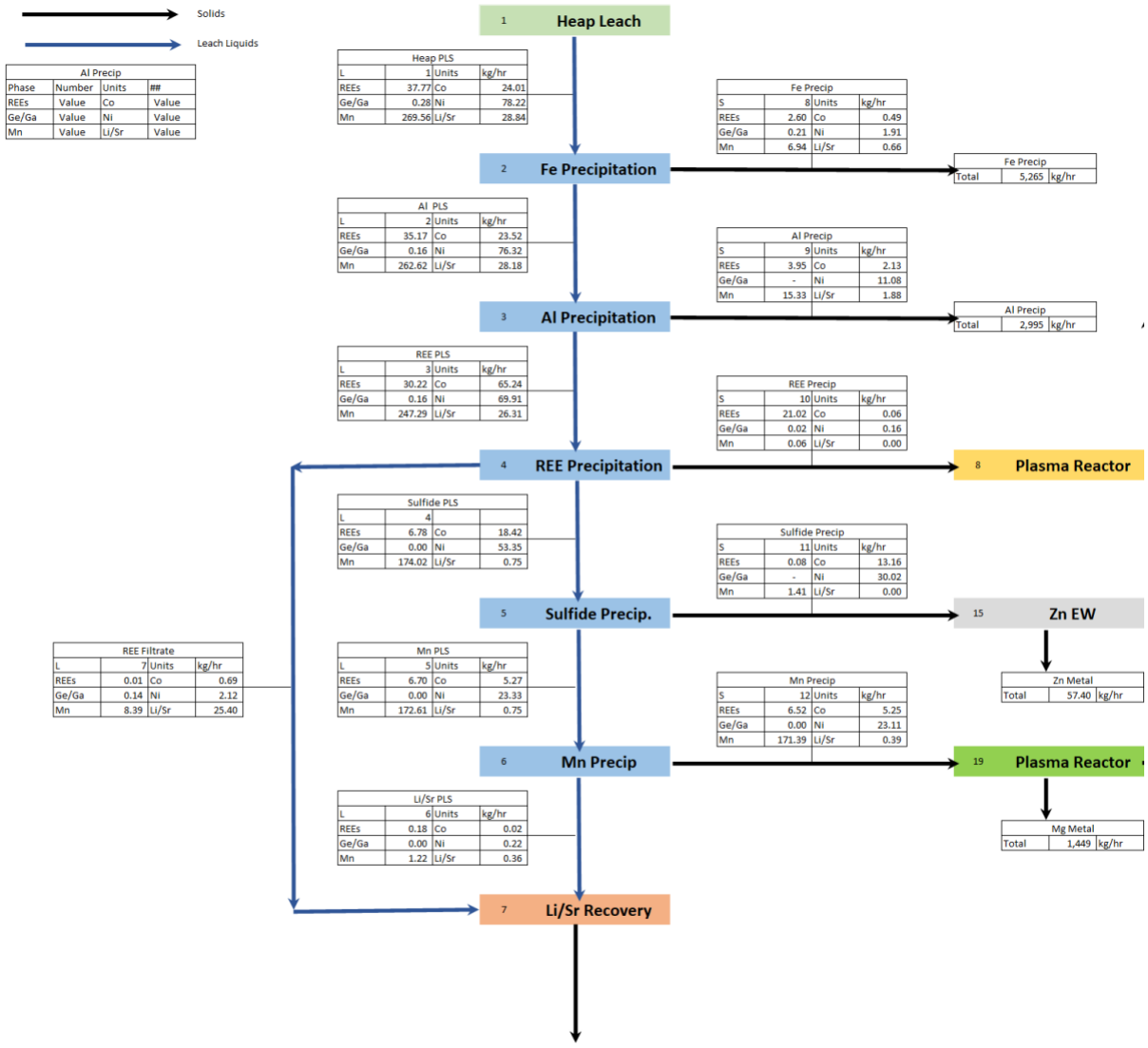


Figure 85. Process mass balance showing heap leaching, precipitation, and Li/Sr recovery. Also shown are the preliminary stages of the purification and metal making processes.

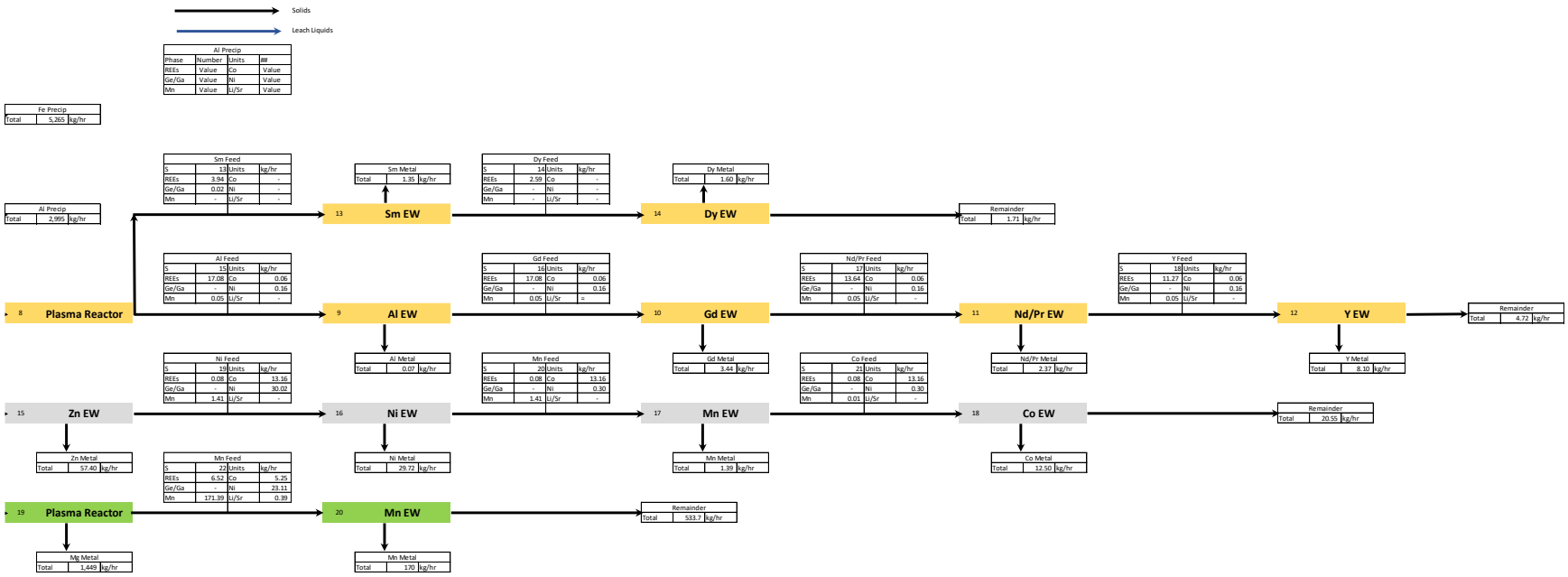


Figure 86. The downstream stages of the purification and metal making processes. These processes include the REEs, metal sulfide precipitates, and the Mg/Mn process.

The process power requirements/balance are shown in
Figure 87. These power requirements are based specifically on power inputs such as electricity for electrowinning or lances for the plasma furnaces. It is anticipated that this represents the majority of the process energy required for the chemical operation of the process. Process energy requirements for heating, pumping, roasting, and facilities (HVAC, lighting, etc.) are not provided at this time due to the difficulty of estimation at this level of detail. It is suspected that the energy listed below represents 80-90% of the total energy requirements of the process.

| Variable | Quantity | Units |
|---|---|---|
| RE Metal Making | 238 | Kw |
| Sulfide Metal Making | 367 | Kw |
| MgMn Metal Making | 4182 | Kw |

Figure 87. Process power input (excluding pumping, heating, and roasting).

The products generated are shown in Figure 92 with the required elements highlighted in yellow. Note that for Ge and Sr, assay data did not exist in the experimental data sets and therefore could not be estimated. Of note is that while the anticipated mass of REEs being leached is equivalent to 1 metric tonne per day of rare earth oxide (REO) equivalent, the recovered REMs equate to 0.405 tonne per day because not all REEs are required to be recovered (elements not recovered Sc, La, Ce, Eu, Tb, Ho, Er, Tm, Yb, Lu). Nor should they be owing to the great difference in respective value.

| Product Constituents | | | | |
|---|---|---|---|---|
| **Composition** | | | | |
| Description | Value Units | Value Units | Value Units | Value Units |
| | | RE Metal Making | | |
| Sc | | | | |
| Y | 8.10 Kg/hr | 194.5127 Kg/Day | 70.99714 mt/year | $ 564,427.24 $/Year |
| La | | | | |
| Ce | | | | |
| Pr | 0.32 Kg/hr | 7.760442 Kg/Day | 2.832561 mt/year | $ 293,170.10 $/Year |
| Nd | 2.05 Kg/hr | 49.13907 Kg/Day | 17.93576 mt/year | $ 2,031,225.08 $/Year |
| Sm | 1.35 Kg/hr | 32.45655 Kg/Day | 11.84664 mt/year | $ 26,654.94 $/Year |
| Eu | | | | |
| Gd | 3.44 Kg/hr | 82.56072 Kg/Day | 30.13466 mt/year | $ 1,706,525.98 $/Year |
| Tb | | | | |
| Dy | 1.60 Kg/hr | 38.28553 Kg/Day | 13.97422 mt/year | $ 4,632,453.65 $/Year |
| Ho | | | | |
| Er | | | | |
| Tm | | | | |
| Yb | | | | |
| Lu | | | | |
| | | | | |
| Ge | | | | |
| Ga | 0.02 Kg/hr | 0.537082 Kg/Day | 0.196035 mt/year | $59,545.57 $/Year |
| | | | | |
| | | Sulfide Metal Making | | |
| Mg | 0.00 Kg/hr | 0 Kg/Day | 0 mt/year | $ - $/Year |
| Mn | 1.39 Kg/hr | 33.40629 Kg/Day | 12.1933 mt/year | $ 59,015.56 $/Year |
| Co | 12.50 Kg/hr | 300.0138 Kg/Day | 109.5051 mt/year | $ 3,805,848.02 $/Year |
| Ni | 29.72 Kg/hr | 713.2501 Kg/Day | 260.3363 mt/year | $ 6,911,928.07 $/Year |
| Zn | 57.40 Kg/hr | 1377.526 Kg/Day | 502.7969 mt/year | $ 1,588,838.13 $/Year |
| Cu | | | | |
| | | | | |
| | | Sulfide Metal Making | | |
| Mg | 1449.05 | 34777.31 Kg/Day | 12693.72 mt/year | $ 48,870,819.73 $/Year |
| Mn | 169.68 | 4072.225 Kg/Day | 1486.362 mt/year | $ 7,193,992.84 $/Year |
| | | | | |
| | | Li/Sr Recovery | | |
| Sr | | | | |
| Li | 24.47 Kg/hr | 587.2356 Kg/Day | 214.341 mt/year | $13,181,971.34 $/Year |
| | | | | |
| Al | 0.07 Kg/hr | 1.611594 Kg/Day | 0.588232 mt/year | |
| Ca | | | | |
| Fe | | | | |
| | | | | |
| REE metal | 16.86 Kg/hr | 404.715 Kg/Day | 147.721 mt/year | $ 9,254,457.00 $/Year |
| All Others | 1744.27 Kg/hr | 41862.58 Kg/Day | 15279.84 mt/year | $ 81,612,413.68 $/Year |
| | | | | |
| Total | | | | $ 90,866,870.68 |

Figure 88. Summary of produced products.

## 2.10 Task 10.0 – Technical Research Plan Development

*Teaming Arrangement* - The project team will include the University of Kentucky (UK) as the Prime Contractor, the University of Alabama (UA), Argonne National Laboratory (ANL), Virginia Tech (VT), MP Materials Corp. (MP), and Alliance Coal. The project team will be led by Dr. Rick Honaker as Principal Investigator (PI) and Dr. Josh Werner as the Technical Lead. Drs. Honaker and Werner have led a research team over the past several years in the design, construction, and testing of the UK rare earth and critical material pilot plant. Dr. Honaker has been awarded and managed over $30 million in project funds over his 30 year career from which he has reported his

findings in over 250 peer-reviewed articles and other publications in the area of extractive metallurgy. Dr. Werner served seven years as a practicing materials engineer for Honeywell before pursuing a PhD degree in extractive metallurgy. Drs. Honaker and Werner will be assisted by a project manager.

MP is the United States' largest producer of rare earth materials and one of the largest integrated rare earth operations in the world. MP's stated mission is to reestablish a complete, vertically integrated supply chain for rare earth permanent magnets in the U.S. MP has laid out a three-stage development program, with Stage 1 having been completed in 2020 and with Stage 2 currently underway. MP has commenced plans for Stage 3, which is called "Vertical Integration of Magnet Making". MP will provide process engineering support under the direction of Michael Rosenthal, Chief Operating Officer, that will include experts in metal and magnet production. Dr. Alan Lund, Executive Vice President of Magnetics, who has 37 U.S. patents in metal production and Dr. Judson Marte, Vice President of Magnetics, who has 22 U.S. patents will participate extensively in the evaluation of the proposed advanced metal production processes and flowsheet diagram development as well as technoeconomic analysis (TEA).

Dr. Ramana Reddy is a world-renowned expert in metal production and a Professor at UA with over 452 refereed journal and conference articles and five patents. Dr. Reddy's research has recently focused on the use of low temperature ionic liquid and thermal plasma technology for reduction to metals, including select rare earth elements (REEs) and cobalt. Dr. Reddy and UA will be principally involved with efforts associated with process Circuits 3 (rare earth metal making) and 4 (critical material products).

Dr. John Hryne and Mr. Matthew Earlam will lead the ANL project team. Metal reduction processes to be advanced by ANL will include high temperature electrolysis and an innovative low-temperature membrane technology. ANL will lead the effort in developing advanced concepts for the reduction of rare earth oxides (REOs)/rare earth salts (RES) to rare earth metals (REMs). ANL staff members associated with this project have extensive industrial experience in high temperature fused salt electrowinning (EW).

VT researchers have developed processes for the recovery and purification of critical minerals (CMs) such as Co and Mn from coal-based materials. VT researchers will develop advanced technologies and flowsheets for production of high purity CMs and provide technical data needed for Circuit 4.

Alliance Coal is the coal-based resource owner and host of the UK rare earth plant. Their role is associated with resource assessment, sample collection, and general engineering activities.

*Research Plan* - Where Phase 2 is anticipated to contain "Laboratory/Bench-Scale Testing of Advanced Concepts for Production of Rare Earth Elements (REE) and Production of Critical Minerals (CM) from Coal-Based or Alternate Resources" the following is recommended for experimental consideration.

*2.10.1 Production of Mixed Rare Earth Oxides/Salts (MREO/MRES) and Critical Minerals (CM) in Pilot-Scale Facilities*

*2.10.1.1 – Refit of Pilot Plant* - The Recipient will reassemble and upgrade the existing plant circuitry to include the required operations and circuit configurations. To the largest extent possible, the Recipient will repurpose and reuse existing plant equipment; however, modifications may be required to replace, and refit worn equipment. The Recipient will prepare and solicit

competitive bid packages for major purchases of replacement equipment, materials, fabricated components, and services necessary to complete the installation of the proposed circuitry. Upon receipt, the bid packages will be reviewed, and appropriate vendors will be selected on the basis of cost, availability, and suitability.

Fabrication and construction activities will be performed as major equipment is delivered to the Recipient's facilities. These activities will include both internal fabrication work conducted within the shops/facilities operated by the project partners as well as off-site fabrication work carried out by equipment vendors and contract service providers. Upon receipt at the pilot plant, final components will be inspected to ensure they are of suitable workmanship, and are structurally, mechanically, and/or electrically operational. Lastly, all units will be assembled and installed into the existing pilot plant. In addition to the actual process equipment, this work will include all the installation of piping, electrical wiring, and control systems needed for plant operations.

*2.10.1.2 – Acquisition of feed material* - The Recipient will collect, prepare, and characterize representative batches/lots of plant feedstock. For each solid sample, all pertinent geographic/stratigraphic information will be documented including location, site description, etc. Each sample will be subjected to proximate, ultimate, and rare earth element (REE) analyses. Field sampling based on ASTM standards will be used to ensure that representative samples are collected. For planning purposes, it is expected that work under this task will at a minimum include the acquisition of coarse refuse samples from Alliance Mining in western Kentucky where the West Kentucky No. 13 seam is processed. The samples of coarse refuse collected from each site will be collected, sized using a vibrating screen, and pre-concentrated using a dual scan x-ray sorter. The upgraded feedstock will then be passed through an impact (hammer) mill to reduce the top size to below 1 mm. The pulverized feedstock will then be placed into 55 gallon drums and transported to the pilot-scale test facility. Additional lignite samples will be collected and processed under this task as deemed appropriate by the project partners. Prior to REE analysis, solid samples will be digested using the appropriate material containing >300 ppm total rare earth elements (dry whole-sample basis).

*2.10.1.3 – Pilot plant shakedown* - At the completion of construction, startup tests will be conducted to resolve operational problems that often arise during the commissioning of new pilot-scale processes. Mock operator training exercises will be conducted to ensure that all parties are familiar with standard operating and emergency shutdown procedures. Initial "water only" test runs will be conducted to ensure that pumping capacities, pipe/tubing sizes, electrical supplies, control systems, instrumentation, etc., are adequate. After completing start-up activities, shakedown tests will be initiated using actual feedstocks and staged dosing of reagents/acids/bases to validate the structural integrity of the process circuitry and to confirm the design capacities of the various unit operations used in the pilot-plant circuitry are within established norms.

Coincident with startup and shakedown, the Recipient will update the existing documentation for process operation, maintenance, and safety. In particular, the Recipient will conduct a systems safety analysis to identify and eliminate any new hazards resulting from the modified plant circuitry. Hazards will be classified according to severity and likelihood, and a control strategy will be developed for any hazards that cannot be effectively eliminated with engineering controls.

*2.10.1.4 – Lignite leaching and REE generation* – In order to provide REEs suitable for the testing of downstream processes, the Recipient will perform a series of leaching exercises to produce a

quantity of REEs needed for testing. It is anticipated that the majority of the REEs will be from lignite sources.

*2.10.1.5 – Heap leaching testing* – As part of the experimentation, the Recipient will test heap leaching kinetics to evaluate on/off leaching pads for suitability. Based on the gaps identified, task for heap leaching will evaluate the impact of varying recycle vs. fresh pregnant leach solution (PLS) rates, overall irrigation rates, and application rates on the maximum concentration of REEs in PLS possible, as well as the rate of REE generation and leaching recovery. The design of experiments (DOE) would also explore the effect of counter current PLS on maximizing REE recovery and PLS concentration, as well as the impact of material preparation type and age on permeability and irrigation rate. Additionally, the Recipient will investigate the natural acid generation potential of heap material and evaluate the strength and properties of heap material for optimized heap leach pad design. This task would provide valuable insights for optimizing heap leaching and increasing the recovery of REEs.

*2.10.2 Proof-of-Concept Laboratory/Bench-Scale Testing for Production of Individually Separated, High Purity (ISHP) Rare Earth Oxides/Salts (REO) and CM (Circuit 2) & Rare Earth Metals REM (Circuit 3)*

2.10.2.1 – *Plasma reactor testing and evaluation* – The Recipient will evaluate the use of advanced thermal plasma processing technology for the reduction of rare earth oxides/rare earth salts (REOs/RESs) to rare earth metals (REMs). Thermal plasma technology provides very high processing temperatures, at which all materials are in the monoatomic gas state, and very high quenching velocities that allow for nucleation directly from the gaseous state for the formation of fine-grained metals. A typical design of experiments will be conducted on such parameters as, duration, feed material, power, and temperature to develop needed demonstration data for purity validations. Further specific testing will be used to evaluate Ge and Ga proclivity to report to the vapor phase.

2.10.2.2 – *Rare Earth metal ionic liquid testing and evaluation* – The Recipient will evaluate a low temperature, high efficiency metal reduction via electrolysis using ionic liquids that will eliminate the production of $CO_2$ and other greenhouse gases (GHGs). The effect of electrorefining parameters on the current density, current efficiency, and energy consumption values of all the refining processes will be determined. The refined product will be characterized using X-ray diffraction (XRD) and scanning electron microscopy (SEM) energy dispersive X-ray spectroscopy (EDS) techniques for determining the phases and composition. In addition, the modeling and simulation of electrorefining processes will be performed. The work will include determining acceptable aluminum contamination, designing a cell for feed material, producing cathode for composition analysis, estimating electrolyte life and maintenance, and conducting tails washing and characterization.

*2.10.3 Proof-of-Concept Laboratory/Bench-Scale Testing for Production of Individually Separated Critical Minerals (Circuit 4)*

2.10.3.1 – *Plasma reactor testing and evaluation* – This task is an intended duplication of task 5.2.1 intended to encompass the critical elements identified in the flowsheet.

2.10.3.2 – *RE metal ionic liquid testing and evaluation* – This task is an intended duplication of task 5.2.2 intended to encompass the critical elements identified in the flowsheet.

2.10.3.3 *–Recovery of Sr and Li–* The Recipient will evaluate, demonstrate, and select the technologies identified in this grant. It is anticipated that the adsorptive/Solvent Extraction (SX)/precipitation process will likely be the ideal process, but scooping experiments will be conducted to validate this hypothesis. The Li process developed by Argonne National Laboratory (ANL) will also be considered in the scoping studies. Upon data-based selection a design of experiments (DOE) will be performed to determine the optimum operation parameters. Specific research and development activities should include bench-scale testing of the selective adsorption and reverse osmosis processes in both synthetic and real solutions. These tests should screen for the appropriate range of various operating parameters (e.g. reagent/adsorbent selection, operational pH, lithium concentration, and lithium to contaminant ratios) while evaluating process yield, selectivity, robustness, and scalability. Pending these results, higher fidelity cost models should be developed using predicted mass and energy balances and bottom-up cost models. Evaluation and analysis of the model results can then be the basis for more detailed pilot testing campaigns on real product materials.

This task will encompass all needed testing to provide 1) initial evaluation of Li and Sr process for final selection, 2) optimization of process, 3) validation of operation parameters for technoeconomic analysis (TEA).

*2.10.4 Re-evaluation of the TEA report for Phase 2 and initialized in Phase 1.*

The Recipient will develop and provide NETL a techno-economic analysis (TEA) based on testing and operation of the REE/CM recovery system. The Recipient will develop a detailed TEA that estimates the cost and performance for scale-up to a commercial demonstration.

## 2.11 Task 11.0 - Techno-Economic Analysis

*2.11.1 Main TEA*

*Introduction* - This report presents the findings of a conceptual technical economic analysis (TEA) of rare earth metal (REM) and critical mineral production to determine the conceptual feasibility of the project for the Department of Energy (DOE). The study focused on assessing the technical feasibility and economic viability of a proposed REM and critical mineral production process. The analysis considered various factors such as raw material costs and energy consumption, among others, to estimate capital and operational expenses. This report provides an overview of the proposed production process, a detailed analysis of the estimated costs, and recommendations for the DOE to support the development of domestic REM and critical mineral production.

*Summary and Scope* - A techno-economic analysis (TEA) was conducted to evaluate the conceptual feasibility of an extraction, purification, and metal making facility for rare earth metals (REM) and other critical metals. The scope of the TEA conducted in this report was to evaluate the proposed REM production process, covering both operational and capital costs. To perform this analysis, the process flow sheet presented in Task 9.0 was utilized as the technical scope of the evaluation. The TEA focused on individual components of the proposed process to provide a detailed resolution for each. These components included Heap Leaching, Precipitation, Rare Earth Metal (REM) Making, Sulfide Metal Making, Mg/Mn Metal Making, Li/Sr Recovery, Tax & Insurance, Site Services, Facilities and Buildings, General & Administrative, and Mobile Equipment. The analysis evaluated each of these categories individually to estimate their

respective costs, including both operational and capital expenses. The results were then combined to provide an overall economic evaluation of the proposed process.

The results of the TEA are shown

Figure 89 and include a $737,294,920 capital expense (CapEx) and a per year operation expense (OpEx) of $220,836,421. The determination of these figures is contained in the following sections of the report and in the TEA model (Microsoft Excel file). Of note is the sustaining CapEx per year. This represents the amortized capital replacement cost of equipment over its useful life and is not to be confused with maintenance costs. The revenue by stage is also included to provide insights into the incremental benefit of each stage. Per the requirements of DE-FOA-0002404, under which this cooperative agreement was made, new and unique processing methods are required for evaluation, and as such the sulfide metal making, Mg/Mn production, and other steps may be less expensive based on conventional technologies. As presently constituted, the OpEx is greater than the revenue per year. The costs are further broken down graphically in

Figure 90 and

Figure 91 for OpEx and CapEx, respectively. The top 3 expenses in both categories are the heap leach, Mg/Mn production, and precipitation. The large expense of the Mg/Mn production has to do with the significant mass processed by the plasma reactors.

The products generated are shown in Figure 92 with the project's required elements highlighted in yellow. Note that for Ge and Sr, assay data did not exist in the experimental data sets and therefore could not be estimated. However, an error was discovered which significantly decreased the Ga contribution. Of note is that while the anticipated mass of rare earth elements (REEs) being leached is equivalent to 1 metric tonne per day of rare earth oxide (REO) equivalent, the recovered REMs equate to 0.405 tonne per day (tpd) because not all REEs are required to be recovered (elements not recovered Sc, La, Ce, Eu, Tb, Ho, Er, Tm, Yb, Lu). Nor should they be, owing to their great difference in respective value. In summary, even though the project did not show profitability, there exists a significant margin for additional cost cutting and process replacement (Mg/Mn production) to lower the overall cost of the project.

| ID | Sector | CapEx | Sustaining CapEx/Year | OpEx/Year | Revenue By Stage |
|---|---|---|---|---|---|
| 1HL | HeapLeaching | $ 310,449,832 | $ 62,089,966 | $ 24,812,951 | |
| 2PC | Precipitation | $ 166,685,158 | $ 6,364,642 | $ 100,977,724 | |
| 3RE | RE Metal Making | $ 5,433,694 | $ 1,086,739 | $ 5,361,167 | $ 9,314,003 |
| 4SU | Sulfide Metal Making | $ 12,038,146 | $ 2,273,493 | $ 16,585,277 | $ 12,365,630 |
| 5MM | MgMn Metal Making | $ 232,707,293 | $ 46,541,459 | $ 67,332,813 | $ 56,064,813 |
| 6WW | Li Sr Recovery | TBD | TBD | TBD | $ 13,181,971 |
| 8TI | TAX & INSURANCE | $ - | $ - | | |
| 9SS | SITE SERVICES | $ 3,466,599 | $ 167,262 | $ - | |
| 10FB | FACILITIES AND BUILDINGS | $ 5,503,237 | $ 202,144 | $ 267,182 | |
| 11GA | GENERAL & ADMINISTRATIVE | $ 51,360 | $ 12,465 | $ 5,410,582 | |
| 12ME | MOBILE EQUIPMENT | $ 959,600 | $ 156,800 | $ 88,724 | |
| Total | | $ 737,294,920 | $ 118,894,970 | $ 220,836,421 | $ 90,926,416 |
| Yearly Total (OpEx + Sustaining Capital) | | | | $ 339,731,390.49 | |

Figure 89. Cost summaries by process module for the TEA.

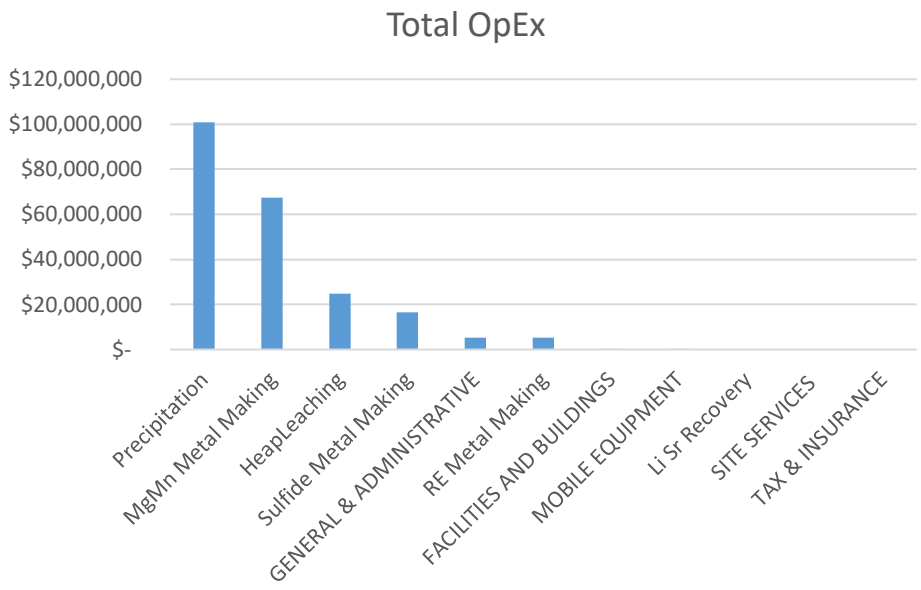


Figure 90. Pareto Chart of OpEx Expenses.

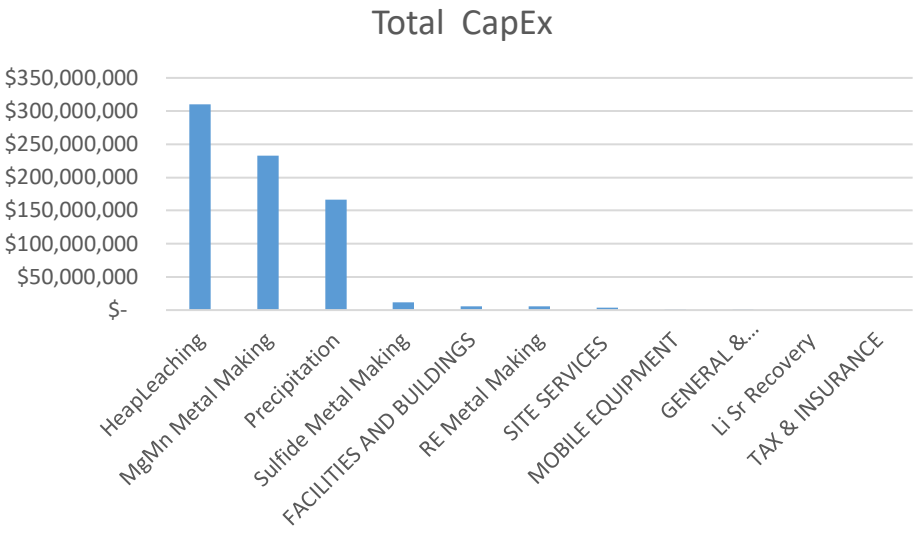


Figure 91. Pareto Chart of CapEx Expenses.

| Product Constituents | | | | |
|---|---|---|---|---|
| **Composition** | | | | |
| Description | Value Units | Value Units | Value Units | Value Units |
| | | RE Metal Making | | |
| Sc | | | | |
| Y | 8.10 Kg/hr | 194.5127 Kg/Day | 70.99714 mt/year | $ 564,427.24 $/Year |
| La | | | | |
| Ce | | | | |
| Pr | 0.32 Kg/hr | 7.760442 Kg/Day | 2.832561 mt/year | $ 293,170.10 $/Year |
| Nd | 2.05 Kg/hr | 49.13907 Kg/Day | 17.93576 mt/year | $ 2,031,225.08 $/Year |
| Sm | 1.35 Kg/hr | 32.45655 Kg/Day | 11.84664 mt/year | $ 26,654.94 $/Year |
| Eu | | | | |
| Gd | 3.44 Kg/hr | 82.56072 Kg/Day | 30.13466 mt/year | $ 1,706,525.98 $/Year |
| Tb | | | | |
| Dy | 1.60 Kg/hr | 38.28553 Kg/Day | 13.97422 mt/year | $ 4,632,453.65 $/Year |
| Ho | | | | |
| Er | | | | |
| Tm | | | | |
| Yb | | | | |
| Lu | | | | |
| | | | | |
| Ge | | | | |
| Ga | 0.02 Kg/hr | 0.537082 Kg/Day | 0.196035 mt/year | $59,545.57 $/Year |
| | | Sulfide Metal Making | | |
| Mg | 0.00 Kg/hr | 0 Kg/Day | 0 mt/year | $ - $/Year |
| Mn | 1.39 Kg/hr | 33.40629 Kg/Day | 12.1933 mt/year | $ 59,015.56 $/Year |
| Co | 12.50 Kg/hr | 300.0138 Kg/Day | 109.5051 mt/year | $ 3,805,848.02 $/Year |
| Ni | 29.72 Kg/hr | 713.2501 Kg/Day | 260.3363 mt/year | $ 6,911,928.07 $/Year |
| Zn | 57.40 Kg/hr | 1377.526 Kg/Day | 502.7969 mt/year | $ 1,588,838.13 $/Year |
| Cu | | | | |
| | | Sulfide Metal Making | | |
| Mg | 1449.05 | 34777.31 Kg/Day | 12693.72 mt/year | $ 48,870,819.73 $/Year |
| Mn | 169.68 | 4072.225 Kg/Day | 1486.362 mt/year | $ 7,193,992.84 $/Year |
| | | Li/Sr Recovery | | |
| Sr | | | | |
| Li | 24.47 Kg/hr | 587.2356 Kg/Day | 214.341 mt/year | $13,181,971.34 $/Year |
| | | | | |
| Al | 0.07 Kg/hr | 1.611594 Kg/Day | 0.588232 mt/year | |
| Ca | | | | |
| Fe | | | | |
| | | | | |
| REE metal | 16.86 Kg/hr | 404.715 Kg/Day | 147.721 mt/year | $ 9,254,457.00 $/Year |
| All Others | 1744.27 Kg/hr | 41862.58 Kg/Day | 15279.84 mt/year | $ 81,612,413.68 $/Year |
| | | | | |
| Total | | | | $ 90,866,870.68 |

Figure 92. Summary of produced products.

*Process Definition and Analysis Extents* – To describe the proposed flowsheet, it is necessary to provide context for the reasons in deciding upon certain configurations. For Circuit 1, staged precipitation tests were conducted prior to the start of this project to evaluate the precipitation characteristics of selected critical elements and contaminant elements as a function of pH. As Figure 93 shows, by raising the pH of a leachate from coal to around 4.5, nearly all Fe and most Al were precipitated, while the majority of the critical elements remained in the solution. Therefore, Fe and Al in the leachate can be largely removed by removing the precipitate formed at pH 4.5. After that, critical elements started to precipitate with an increase in the pH of the solution. When the pH of the solution reached around 9.0, rare earth elements (REEs), Co, Mn, Ge, and Ga were precipitated, while Li and Sr remained in the solution. Although the precipitation curve of Zn and Ni is not presented in the figure, the prior study of the team has confirmed that Zn and Ni precipitated in a similar pH range as Co and Mn (DE-FE0031827) (See also Table 62

herein). Therefore, after staged precipitation, the critical elements contained in the leachate were separated into two material streams: a precipitate rich in REEs, Co, Mn, Ge, Ga, Zn, and Ni, and a solution rich in Li and Sr with some contaminant elements, such as Ca and Mg.

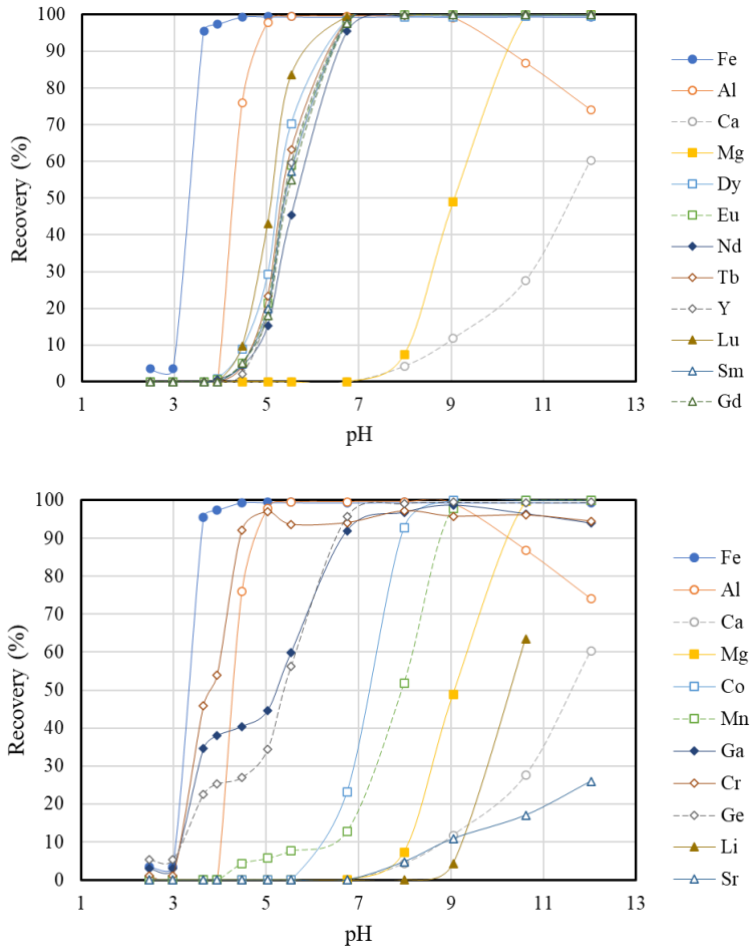


Figure 93. Precipitation recovery of selected critical elements and contaminant elements as a function of pH.

To make use of the rare earth element (REE) and critical mineral (CM) characteristics and produce useful products, the following flow sheet is proposed to produce 4 product streams to meet the requirements of the project (see Figure 94 and Figure 95). At this time, staged precipitation which creates several distinct products is favored owing to the downstream selection of pyrometallurgical methods. The products include a REE product containing Ga and Ge, a CM product containing Co, Ni, and Zn, a Mn and Mg product, and waters containing Sr and Li. It is noted that these products have been produced previously in other DOE sponsored projects (DE-FE0031827). Table 61 through

Table 63 show the various intermediate products that have been formed as precipitates from a pregnant leach solution (PLS) derived from a test heap leach pad (DE-FE000053) and processed in a REE pilot facility (DE-FE0031827).

A blended pyrometallurgical method utilizing a plasma reactor and electrowinning using various ionic liquids is proposed for the reduction to metals of REEs and various CMs. As demonstrated in Figure 94, the difference between the vaporization of several REEs allows for a preliminary split of REEs to be accomplished. More detailed information about this circuit (circuit 2/3) was provided in past quarterly reports and will be included in the final project report. Of particular note is the treatment of Ga and Ge. As shown in Figure 93, it appears that Ga and Ge will report to this stream and owing to the lower vaporization temperature of Ga and Ge than the REEs, it is anticipated that these elements will report to the Eu, Tm, Yb, and Ca product. In light of this, it is envisioned that the plasma reactor may be run at a lower initial temperature to split the lower volatility elements off first or the methods described with releaching and recovery will be suitable for additional processing. This will be further investigated and included as part of the TEA. Additionally, it is noted that investigations of hydrometallurgical methods for these elements to date make it difficult to implement in view of the proposed pyrometallurgical technique and require additional considerations.

The CM refining circuit (Circuit 4) is shown in Figure 94. This circuit embodies the progressive electrolysis of the CM precipitate into Zn, Ni, Mn, and Co. It is important to note the Mn is removed during this stage owing to the imperfect split from selective precipitation. The 3$^{rd}$ precipitate processed is the Mg/Mn precipitate as shown in Figure 95. Utilizing plasma processing, a pure Mg condensate will be created and a Mn metal via additional processing via electrochemical means. The residual materials derived from these circuit 4 processes will be evaluated as part of the Technical Research Plan to determine their potential value. The remaining waters containing Li and Sr could be processed to lithium and strontium carbonate products, as indicated in Figure 95. However, a final determination cannot be made at this time owing to a lack of data.

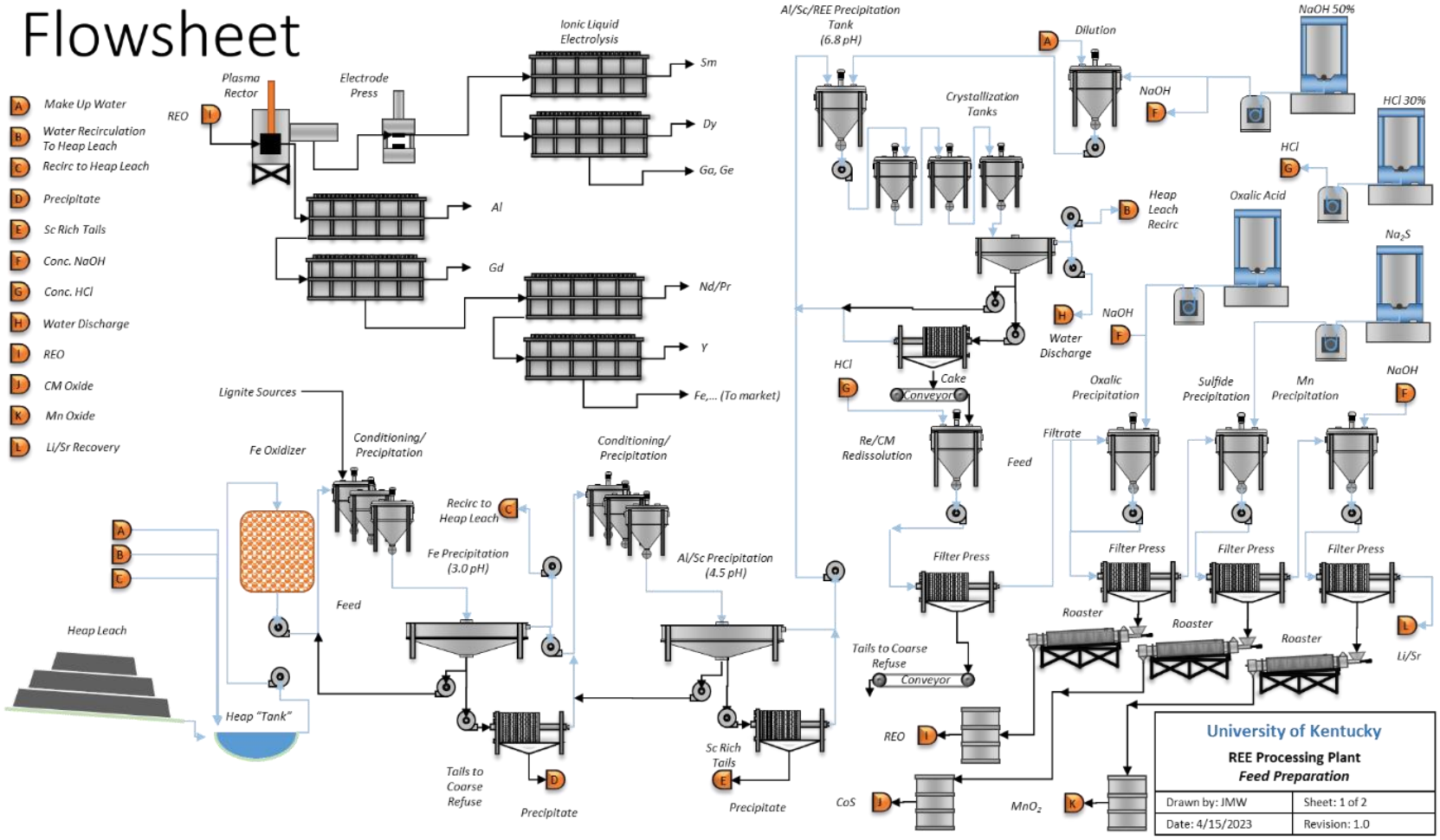


Figure 94. Circuits 1, 2, & 3 of the proposed pilot plant process showing selective precipitation and REM production via plasma reactor and electrochemical methods.

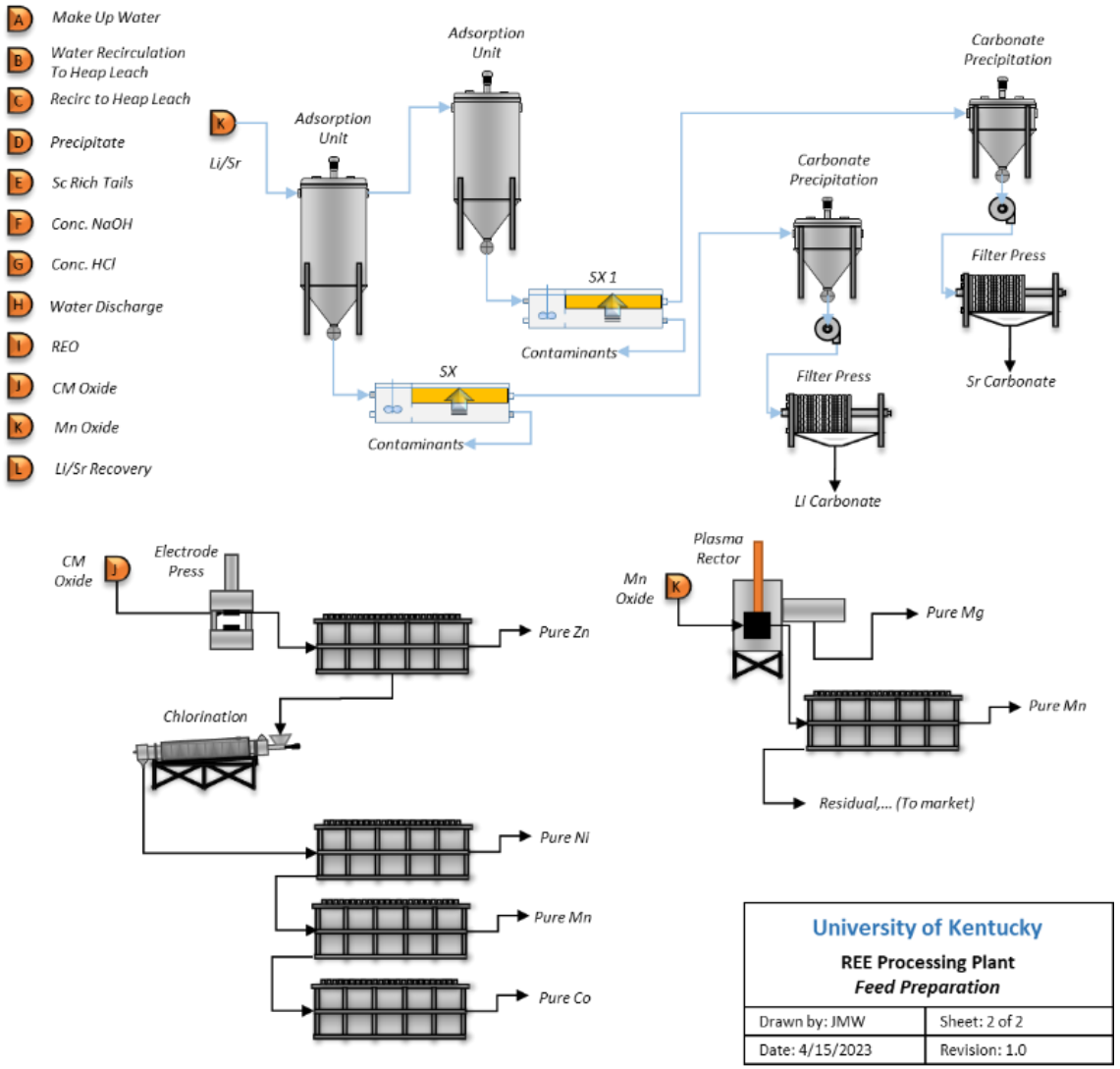


Figure 95. Circuit 4 of the proposed pilot plant process showing electrochemical methods to recover Zn, Ni, Mn, Co, Li, and Sr via plasma reactor and electrochemical methods.

Table 61. Heap leach pregnant leach solution rare earth product*

| Elements | Elemental Concentration | | Elemental MW | Oxide Form | Oxides Concentration |
|---|---|---|---|---|---|
| | mg/kg | % dry weight | g/mol | | % dry weight |
| Sc | 287 | 0.0 | 45 | Sc2O3 | 0.04 |
| Y | 303804 | 30.4 | 89 | Y2O3 | 38.58 |
| La | 2889 | 0.3 | 139 | La2O3 | 0.34 |
| Ce | 28337 | 2.8 | 140 | CeO2 | 3.48 |
| Pr | 9080 | 0.9 | 141 | Pr6O11 | 1.10 |
| Nd | 69877 | 7.0 | 144 | Nd2O3 | 8.15 |
| Sm | 54613 | 5.5 | 150 | Sm2O3 | 6.33 |
| Eu | 16037 | 1.6 | 152 | Eu2O3 | 1.86 |
| Gd | 111411 | 11.1 | 157 | Gd2O3 | 12.84 |
| Tb | 16656 | 1.7 | 159 | Tb4O7 | 1.96 |
| Dy | 123926 | 12.4 | 163 | Dy2O3 | 14.22 |
| Ho | 12564 | 1.3 | 165 | Ho2O3 | 1.44 |
| Er | 27816 | 2.8 | 167 | Er2O3 | 3.18 |
| Tm | 3192 | 0.3 | 169 | Tm2O3 | 0.36 |
| Yb | 15534 | 1.6 | 173 | Yb2O3 | 1.77 |
| Lu | 2067 | 0.2 | 175 | Lu2O3 | 0.24 |
| **TREE** | 798091 | 79.8 | | **∑REO** | **95.89** |
| **Al** | 4294 | 0.4 | 13 | Al2O3 | 1.22 |
| **Ca** | 44847 | 4.5 | 40 | CaO | 6.28 |
| **Fe** | 8865 | 0.9 | 56 | Fe2O3 | 1.27 |

*****Note: Oxalates converted to oxides by roasting.

Table 62. Heap leach pregnant leach solution Co, Ni, and Zn product*

| Elements | Elemental Concentration | | Elemental MW | Oxide Form | Oxides Concentration |
|---|---|---|---|---|---|
| | mg/kg | % dry weight | g/mol | | % dry weight |
| **TREE** | 2768.3 | 0.3 | | | **0.33** |
| Al | 5960.3 | 0.6 | 13 | Al2O3 | 1.70 |
| Ca | 1427.9 | 0.1 | 40 | CaO | 0.20 |
| Co | 56371.3 | 5.6 | 28 | CoO | 8.86 |
| Cu | 9724.6 | 1.0 | 64 | CuO | 1.22 |
| Fe | 10556.5 | 1.1 | 56 | Fe2O3 | 1.51 |
| Mg | 26914.2 | 2.7 | 24 | MgO | 4.49 |
| Mn | 17784.4 | 1.8 | 55 | MnO2 | 2.81 |
| Na | 33888.2 | 3.4 | 23 | Na2O | 4.57 |
| Ni | 187197.6 | 18.7 | 59 | NiO | 28.93 |
| Se | 251.1 | 0.0 | 79 | SeO2 | 0.04 |
| Sr | 78.2 | 0.0 | 88 | SrO | 0.01 |
| Zn | 136566.9 | 13.7 | 65 | ZnO | 17.02 |

*Note: Sulfides converted to oxides by roasting.

Table 63. Heap leach pregnant leach solution Mg/Mn product*

| Elements | Elemental Concentration | | Elemental MW | Oxide Form | Oxides Concentration |
|---|---|---|---|---|---|
| | mg/kg | % dry weight | g/mol | | % dry weight |
| **TREE** | 8465.0 | 0.8 | | | **1.03** |
| Al | 67481.9 | 6.7 | 13 | Al2O3 | 19.21 |
| Ca | 1046.7 | 0.1 | 40 | CaO | 0.15 |
| Co | 200.6 | 0.0 | 28 | CoO | 0.03 |
| Cu | 26.9 | 0.0 | 64 | CuO | 0.00 |
| Fe | 2530.3 | 0.3 | 56 | Fe2O3 | 0.36 |
| Mg | 217721.9 | 21.8 | 24 | MgO | 36.29 |
| Mn | 142053.3 | 14.2 | 55 | MnO2 | 22.47 |
| Na | 57405.7 | 5.7 | 23 | Na2O | 7.74 |
| Ni | 1095.8 | 0.1 | 59 | NiO | 0.17 |
| Se | 643.2 | 0.1 | 79 | SeO2 | 0.09 |
| Sr | 0.0 | 0.0 | 88 | SrO | 0.00 |
| Zn | 365.1 | 0.0 | 65 | ZnO | 0.05 |

*Note: Hydroxides converted to oxides by roasting.

*Methodology* - The technoeconomic analysis (TEA) conducted in this report evaluates the proposed rare earth metal (REM) and critical material (CM) metal production process from both CapEx and OpEx perspectives. The CapEx component of the TEA covers equipment costs, transportation and erection, first fill and critical spare parts, and yearly equivalent CapEx. Equipment costs include the purchase of machinery and materials required for the process. Transportation and erection costs are the expenses associated with moving equipment to the site and assembling it. First fill and critical spare parts cover the cost of necessary initial supplies, and the yearly equivalent CapEx is the annualized cost of the equipment over its useful life for a replacement place holder. On the other hand, the OpEx component of the TEA covers power and utilities, maintenance costs, consumables and reagents, and labor. Power and utilities expenses refer to the electricity, water, and gas necessary for the operation. Maintenance costs include the expenses for repairs and replacement of equipment and parts. Consumables and reagents are the materials used in the process, and labor costs include wages and salaries for the workforce. The TEA combines these costs to estimate the total cost of the proposed process and determine its economic feasibility. An important distinction for the TEA is the anticipated level of accuracy. As this is a concept study and the project was not scoped to provide for experimental work, data and results from several previous and concurrent DOE studies were leveraged (DE-FE000053, DE-FE0031827) in order to enhance this analysis.

The specific domains of the analysis are based on the flowsheet (Figures 6 and 7) and scope of analysis were defined as follows with corresponding worksheet designations. Heap Leaching (1HL) refers to the process of extracting rare earth elements (REEs) from ores via heap leaching based upon the pilot heap leach test conducted in project DE-FE000053 titled “A Unique Collaboration of Coal-based REEs and the U.S.’s Largest Rare Earth Producer”. This domain was evaluated to estimate the cost of this module and with the costs determined from the previous project utilized for inclusion into this study. Precipitation (2PC) refers to the process of precipitating rare earth elements (REEs) from the pregnant leaching solution (PLS) obtained from the heap leach. Costs for this process were assumed and modified from the same project as the

heap leach. Rare Earth Metal (REM) Making (3RE) and Sulfide Metal Making (4SU) refer to the processes of beginning with a sulfide precipitate, converting to and oxide, removing Zn, chlorinating and then ionic liquid reduction to critical metals. Although short form used throughout this document, it is not proposed that sulfides directly be made into metals. These domains were evaluated to estimate the cost of the necessary equipment, energy consumption, and reagents. Moreover, this process module was evaluated for costs utilizing first principles such as throughput, specific capacity, and energy consumption to establish needed equipment sizing. MgMn Metal Making (5MM) refers to the process of making magnesium and manganese alloy. This domain was evaluated to estimate the cost of the necessary equipment and energy consumption. LiSr Recovery (6Li) refers to the recovery of lithium and strontium. This domain was evaluated to estimate the cost of the necessary equipment and energy consumption and largely serves as a place holder at the time of writing as sufficient information does not exist to provide a cost estimate. Tax & Insurance (7TI) covers the taxes and insurance associated with the operation, Site Services (8SS) covers the cost of site-related expenses, Facilities and Buildings (9FB) covers the cost of building the facilities, General & Administrative (10GA) covers the general administration costs, and Mobile Equipment (11MA) covers the cost of mobile equipment. Additionally, the worksheet model and components include personnel and equipment availability and CapEx and OpEx rollup to estimate the total cost of the proposed process. For this concept study the personnel and equipment availability are set to 100% for simplicity. The reader is strongly encouraged to review the accompanying Microsoft Excel TEA model as the breath of many assumptions are prohibitive from documenting succinctly in report form.

*TEA Detailed Components*

*Feed and Materials Yield Methodology for TEA* – As previously mentioned, this study makes use of data and experimentation out of scope for the current project by leveraging the value of previous studies funded by DOE. For example, in determining the feed and materials yield for this project, heap leach data from DOE contract DE-FE000053 and data from the processing of the pregnant leach solution (PLS) from the test heap leach pad from project DE-FE0031827 titled "Demonstration of Scaled-Production of Rare Earth Oxides and Critical Materials from Coal-Based Sources using Innovative, Low Cost Process Technologies and Circuits" were utilized. For convenience, the following are figures provided to show the source data from these reference projects.

Figure 96 shows the test heap leach pad used to extract REEs from coal refuse constructed in Western Kentucky for the generation of test heap leach solution. Associated with the pilot heap test are the response data presented in Figure 97 which shows the time dependency of the total rare earth elements (TREEs) in the PLS over the course of a year, including both summer and winter months. The associated contaminants vs. runtime are shown in Figure 98. From project DE-FE000053 a flow rate of 5800 gpm of PLS was selected as needed to produce 1 metric tonne of REO equivalents per day.

Figure 96. Test heap leach pad used to extract REEs from coal refuse.

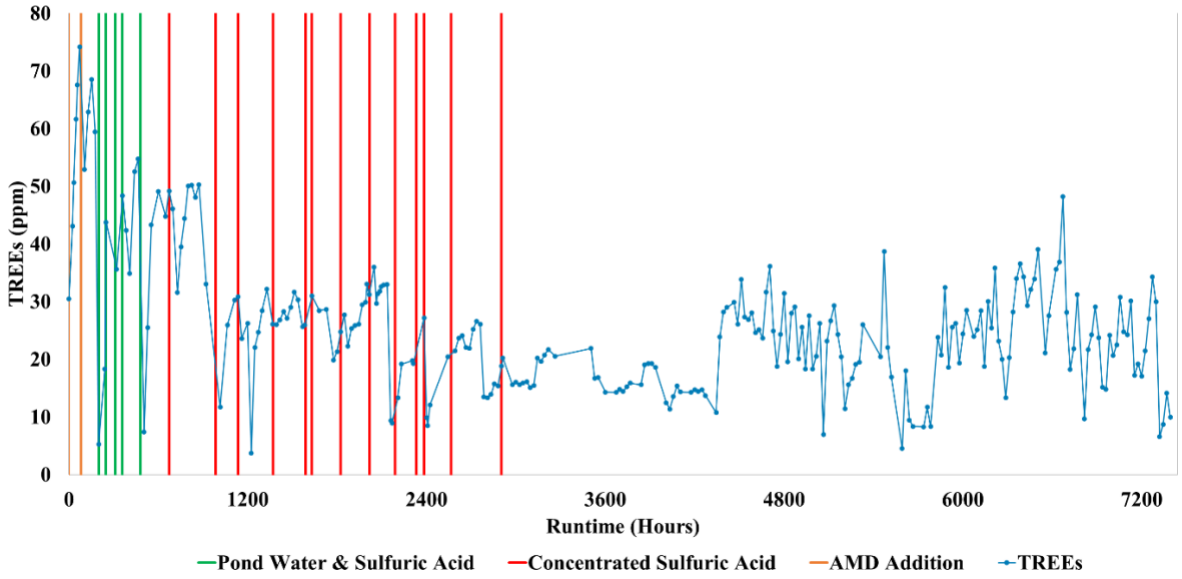


Figure 97. Time dependency of the TREEs in the PLS.

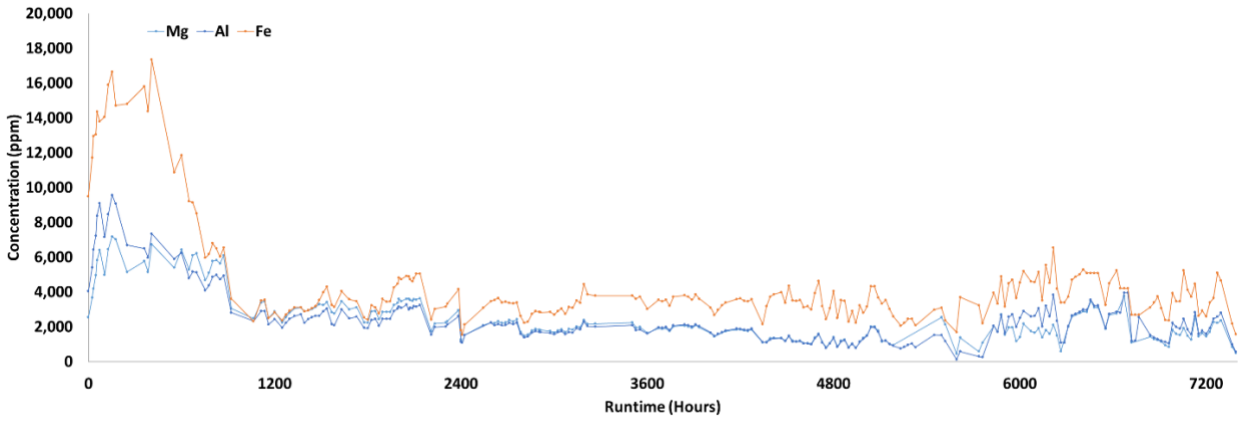


Figure 98. Select contaminant response vs. runtime.

From project DE-FE0031827, a test to treat the PLS titled “PLS 4” was conducted to evaluate the efficacy of the production of precipitates from the heap leach pad PLS. In this manner the reagent consumptions were determined, and corresponding yields and reagent amounts are covered in the associated Microsoft Excel TEA model as well as subsequent sections of this TEA report specific to each process module. For the purposes of this TEA, the composition of the “PLS 4” feed was used to determine the specific consumptions based on concentration and then extrapolated to the average feed shown in

Table 64. In this manner the PLS 4 feed concentration which was taken during colder months could be used to provide what may be termed a more representative data set.

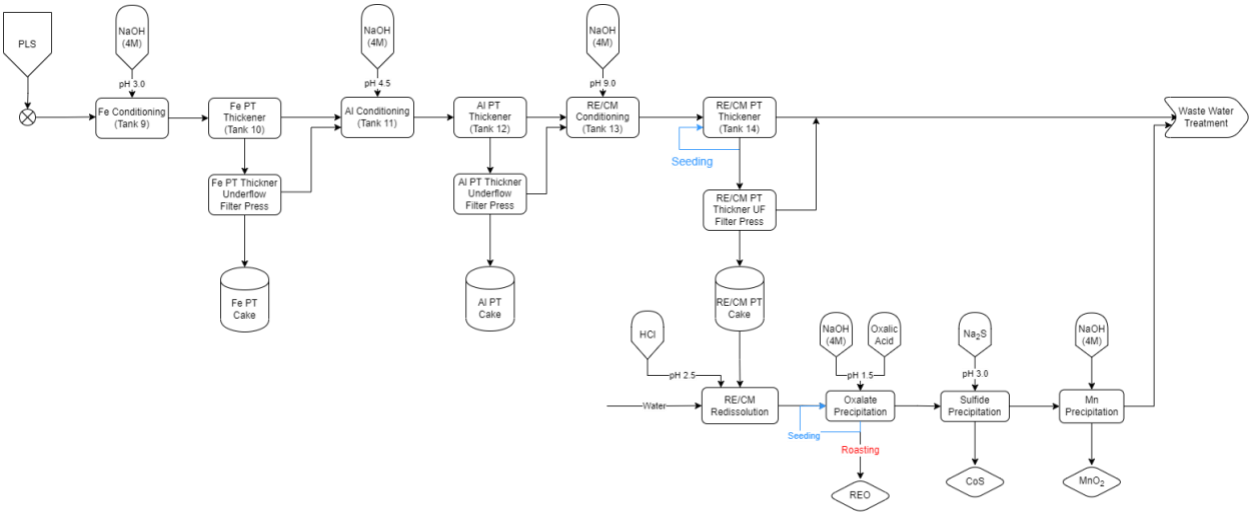


Figure 99. Experimental flowsheet for consumption data provided for precipitation testing in DE-FE0031827.

For the TEA a full mass balance was not considered, but rather the product mass yield for various experiments sources listed was provided to estimate the reagent consumptions and hypothetical yields between various process steps. Further details are provided in the following module sections.

*Heap Leaching (1HL)* – The heap leaching module converts the feed concentrations and summarizes the costing provided in DOE award DE-FE000053. The values provided were based on work in that project report provided by Golder and provided to the DOE final report package for DE-FE000053 and utilize a 1.036 factor to account for inflation to bring them to today's dollars. The HLF: Trucking and Placement of Refuse (HLF stands for heap leach facility) are covered in the OpEx portion of the workbook (See Figure 100). The reader is encouraged to revisit the final report of DE-FE000053 for further discussion about this process module. The CapEx is calculated at $310,449,832 and OpEx at $24,812,950/yr. These values include the assumption that interlift liners are required for the heap leach owing to the permeability issues discovered during the heap leach pad operation.

Table 64. Comparison to the average PLS heap data to the specific PLS 4 data.

| Element | Average PLS Value (mg/L) | PLS 4 Values (mg/L) |
|---|---|---|
| **Sc** | 0.99 | 0.35 |
| **Y** | 12.02 | 4.91 |
| **La** | 0.26 | 0.13 |
| **Ce** | 1.82 | 0.99 |
| **Pr** | 0.44 | 0.18 |
| **Nd** | 2.17 | 1.20 |
| **Sm** | 1.80 | 0.80 |
| **Eu** | 0.49 | 0.22 |
| **Gd** | 3.57 | 1.40 |
| **Tb** | 0.49 | 0.21 |
| **Dy** | 2.08 | 1.19 |
| **Ho** | 0.53 | 0.20 |
| **Er** | 1.00 | 0.49 |
| **Tm** | 0.15 | 0.06 |

| | | |
|---|---|---|
| **Yb** | 0.70 | 0.31 |
| **Lu** | 0.16 | 0.05 |
| **Mg** | 2415.55 | 877.79 |
| **Mn** | 204.63 | 68.85 |
| **Co** | 18.23 | 7.21 |
| **Ni** | 59.38 | 20.16 |
| **Zn** | 61.01 | 20.48 |
| **Cu** | 10.76 | 4.35 |
| **Se** | 8.95 | 9.37 |
| **Sr** | - | - |
| **Ge** | 0.10 | - |
| **Ga** | 0.18 | 0.07 |
| **Li** | 21.90 | 7.13 |
| **Al** | 2419.78 | 1038.90 |
| **Ca** | 432.13 | 322.35 |
| **Fe** | 4352.67 | 2079.23 |

**Equipment Cost (CapEX)**

| ID | Unit Equipment | No. of Units | Capacity of Unit | Units | Installed Capacity | Utilization | Utilized Capacity | Unit Cost | Total | Notes/Description |
|---|---|---|---|---|---|---|---|---|---|---|
| 1 | HLF: Pad | 1 | 1 | each | 1 | 100% | 1 | $ 152,370,736 | $ 152,370,736 | |
| 2 | HLF: Geomembrane Liner | 1 | 1 | each | 1 | 100% | 1 | $ 25,406,864 | $ 25,406,864 | |
| 3 | PLS Pond & Overflow Pond | 1 | 1 | each | 1 | 100% | 1 | $ 6,039,880 | $ 6,039,880 | |
| 4 | Misc. Roads and Surface Water Controls | 1 | 1 | each | 1 | 100% | 1 | $ 51,800 | $ 51,800 | |
| 5 | HLF: Indirect, EPCM | 1 | 1 | each | 1 | 100% | 1 | $ 34,813,744 | $ 34,813,744 | |
| 6 | HLF:Owners Costs | 1 | 1 | each | 1 | 100% | 1 | $ 9,193,464 | $ 9,193,464 | |
| 7 | HLF: Contingency | 1 | 1 | each | 1 | 100% | 1 | $ 78,984,640 | $ 78,984,640 | |
| 8 | HLF: Closure | 1 | 1 | each | 1 | 100% | 1 | $ 3,578,344 | $ 3,578,344 | |
| 9 | HLF: Trucking and Placement of Refuse | 0 | 1 | $/Each/year | 0 | 100% | 0 | $ 16,808,064 | $ - | |
| 10 | HLF: OPEX Contingency | 0 | 1 | $/Each/year | 0 | 100% | 0 | $ 5,688,883 | $ - | |
| 11 | | | | | 0 | | 0 | | | |
| 12 | | | | | 0 | | 0 | | | |
| 13 | | | | | 0 | | 0 | | | |
| 14 | | | | | 0 | | 0 | | | |
| 15 | | | | | 0 | | 0 | | | |
| 16 | | | | | 0 | | 0 | | | |
| 17 | | | | | 0 | | 0 | | | |
| 18 | | | | | 0 | | 0 | | | |
| 19 | | | | | 0 | | 0 | | | |
| 20 | | | | | 0 | | 0 | | | |
| 21 | | | | | 0 | | 0 | | | |
| | | | | | | | | | $ 310,439,472 | |

Figure 100. 1HL (Heap Leaching) Equipment Cost tab.

*Precipitation (2PC)* – The precipitation module utilized a blend of data from DOE contract DE-FE000053 and updated OpEx information derived from DE-FE0031827. The derived yield model is shown below in Figure 101 for documentation purposes. The reader is encouraged to evaluate the provided Microsoft Excel TEA model for a clear, navigable example. Nevertheless, the model is provided to communicate mass yields of important elements and contaminants corresponding to

the major states of the precipitation circuit for the calculation of reagent utilization. As with the heap leach module, prior work was utilized from SGS for the capital estimation of the precipitation module. A 1.036 factor to account for inflation and bring cost estimates to today's dollars was utilized. The various portions of their report were incorporated as shown in Figure 102. It is important to note that the process which was costed by SGS did not include oxalic acid, or sulfide roasting, as currently proposed, but rather had a rewash step and drying. Because of the nature of this concept study and degree of accuracy, it was felt that this swap was acceptable for conceptual evaluation purposes.

Operational costs from reagent utilization were calculated according to the model in Figure 101 (page 16), with the associated costs shown in Figure 102 (page 17) based on the reagent prices shown in Table 65 (page 17). Further, 72 process operators are assumed to operate this module comprising round the clock coverage. Note that the solvent extraction (SX) is not referenced in the flowsheet but appears in the mass balance as a placeholder for future work. From these calculations the estimated CapEx is $166,685,158 and OpEx is $100,979,051 $/yr.

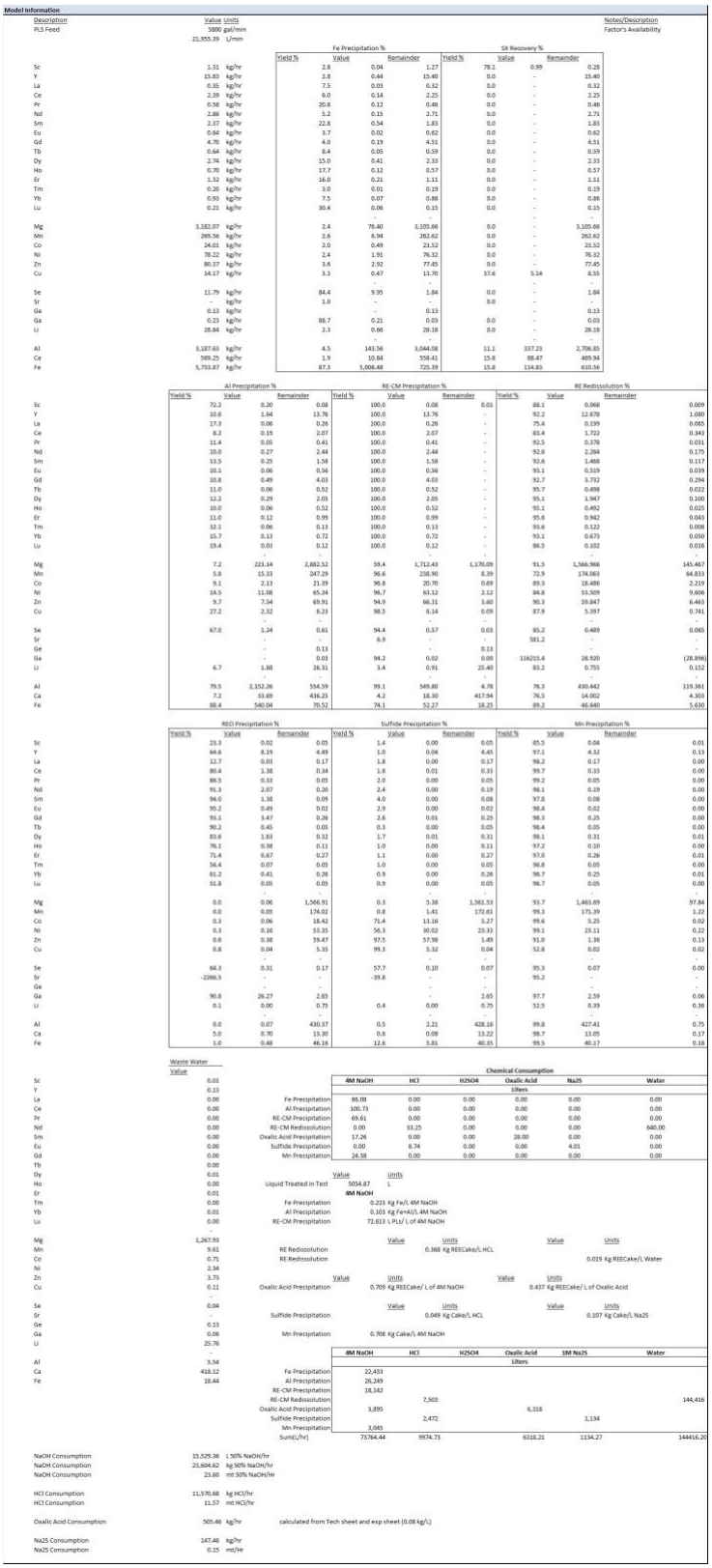

Model Information

| Description | Value | Units | Notes/Description |
|---|---|---|---|
| PLS Feed | 5800 | gal/min | Factor's Availability |
| | 21,955.39 | L/min | |

Fe Precipitation %

| | Yield % | Value | Remainder |
|---|---|---|---|
| Sc | | 2.8 | 0.04 |
| Y | | 15.83 | kg/hr | | 2.8 | 0.44 | 15.40 |
| La | | 0.35 | kg/hr | | 7.5 | 0.03 | 0.32 |
| Ce | | 2.39 | kg/hr | | 6.0 | 0.14 | 2.25 |
| Pr | | 0.58 | kg/hr | | 20.8 | 0.12 | 0.46 |
| Nd | | 2.86 | kg/hr | | 5.2 | 0.15 | 2.71 |
| Sm | | 2.37 | kg/hr | | 22.8 | 0.54 | 1.83 |
| Eu | | 0.64 | kg/hr | | 3.7 | 0.02 | 0.62 |
| Gd | | 4.70 | kg/hr | | 4.0 | 0.19 | 4.51 |
| Tb | | 0.64 | kg/hr | | 8.4 | 0.05 | 0.59 |
| Dy | | 2.74 | kg/hr | | 15.0 | 0.41 | 2.33 |
| Ho | | 0.70 | kg/hr | | 17.7 | 0.12 | 0.57 |
| Er | | 1.32 | kg/hr | | 16.0 | 0.21 | 1.11 |
| Tm | | 0.20 | kg/hr | | 3.0 | 0.01 | 0.19 |
| Yb | | 0.93 | kg/hr | | 7.5 | 0.07 | 0.86 |
| Lu | | 0.21 | kg/hr | | 30.4 | 0.06 | 0.15 |
| | | - | | | - | - | - |
| Mg | | 3,182.07 | kg/hr | | 2.4 | 76.40 | 3,105.66 |
| Mn | | 269.56 | kg/hr | | 2.6 | 6.94 | 262.62 |
| Co | | 24.01 | kg/hr | | 2.0 | 0.49 | 23.52 |
| Ni | | 78.22 | kg/hr | | 2.4 | 1.91 | 76.32 |
| Zn | | 80.37 | kg/hr | | 3.6 | 2.92 | 77.45 |
| Cu | | 14.17 | kg/hr | | 3.3 | 0.47 | 13.70 |
| | | - | | | - | - | - |
| Se | | 11.79 | kg/hr | | 84.4 | 9.95 | 1.84 |
| Sr | | - | kg/hr | | 1.0 | - | - |
| Ge | | 0.13 | kg/hr | | - | - | 0.13 |
| Ga | | 0.23 | kg/hr | | 88.7 | 0.21 | 0.03 |
| Li | | 28.84 | kg/hr | | 2.3 | 0.66 | 28.18 |
| | | - | | | - | - | - |
| Al | | 3,187.63 | kg/hr | | 4.5 | 143.56 | 3,044.08 |
| Ca | | 569.25 | kg/hr | | 1.9 | 10.84 | 558.41 |
| Fe | | 5,733.87 | kg/hr | | 87.3 | 5,008.48 | 725.39 |

SX Recovery %

| | Yield % | Value | Remainder |
|---|---|---|---|
| Sc | 78.1 | 0.99 | 0.28 |
| Y | 0.0 | - | 15.40 |
| La | 0.0 | - | 0.32 |
| Ce | 0.0 | - | 2.25 |
| Pr | 0.0 | - | 0.46 |
| Nd | 0.0 | - | 2.71 |
| Sm | 0.0 | - | 1.83 |
| Eu | 0.0 | - | 0.62 |
| Gd | 0.0 | - | 4.51 |
| Tb | 0.0 | - | 0.59 |
| Dy | 0.0 | - | 2.33 |
| Ho | 0.0 | - | 0.57 |
| Er | 0.0 | - | 1.11 |
| Tm | 0.0 | - | 0.19 |
| Yb | 0.0 | - | 0.86 |
| Lu | 0.0 | - | 0.15 |
| | - | - | - |
| Mg | 0.0 | - | 3,105.66 |
| Mn | 0.0 | - | 262.62 |
| Co | 0.0 | - | 23.52 |
| Ni | 0.0 | - | 76.32 |
| Zn | 0.0 | - | 77.45 |
| Cu | 37.6 | 5.14 | 8.55 |
| | - | - | - |
| Se | 0.0 | - | 1.84 |
| Sr | 0.0 | - | - |
| Ge | 0.0 | - | 0.13 |
| Ga | 0.0 | - | 0.03 |
| Li | 0.0 | - | 28.18 |
| | - | - | - |
| Al | 11.1 | 337.23 | 2,706.85 |
| Ca | 15.8 | 88.47 | 469.94 |
| Fe | 15.8 | 114.83 | 610.56 |

Al Precipitation %

| | Yield % | Value | Remainder |
|---|---|---|---|
| Sc | 72.2 | 0.20 | 0.08 |
| Y | 10.6 | 1.64 | 13.76 |
| La | 17.3 | 0.06 | 0.28 |
| Ce | 8.2 | 0.19 | 2.07 |
| Pr | 11.4 | 0.05 | 0.41 |
| Nd | 10.0 | 0.27 | 2.44 |
| Sm | 13.5 | 0.25 | 1.58 |
| Eu | 10.1 | 0.06 | 0.56 |
| Gd | 10.8 | 0.49 | 4.03 |
| Tb | 11.0 | 0.06 | 0.52 |
| Dy | 12.2 | 0.29 | 2.05 |
| Ho | 10.0 | 0.06 | 0.52 |
| Er | 11.0 | 0.12 | 0.99 |
| Tm | 32.1 | 0.06 | 0.13 |
| Yb | 15.7 | 0.13 | 0.72 |
| Lu | 19.4 | 0.03 | 0.12 |
| | - | - | - |
| Mg | 7.2 | 223.14 | 2,882.52 |
| Mn | 5.8 | 15.33 | 247.29 |
| Co | 9.1 | 2.13 | 21.39 |
| Ni | 14.5 | 11.08 | 65.24 |
| Zn | 9.7 | 7.54 | 69.91 |
| Cu | 27.2 | 2.32 | 6.23 |
| | - | - | - |
| Se | 67.0 | 1.24 | 0.61 |
| Sr | | - | - |
| Ge | | - | 0.13 |
| Ga | | - | 0.03 |
| Li | 6.7 | 1.88 | 26.31 |
| | | - | - |
| Al | 79.5 | 2,152.26 | 554.59 |
| Ca | 7.2 | 33.69 | 436.25 |
| Fe | 88.4 | 540.04 | 70.52 |

RE-CM Precipitation %

| | Yield % | Value | Remainder |
|---|---|---|---|
| Sc | 100.0 | 0.08 | 0.01 |
| Y | 100.0 | 13.76 | - |
| La | 100.0 | 0.26 | - |
| Ce | 100.0 | 2.07 | - |
| Pr | 100.0 | 0.41 | - |
| Nd | 100.0 | 2.44 | - |
| Sm | 100.0 | 1.58 | - |
| Eu | 100.0 | 0.56 | - |
| Gd | 100.0 | 4.03 | - |
| Tb | 100.0 | 0.52 | - |
| Dy | 100.0 | 2.05 | - |
| Ho | 100.0 | 0.52 | - |
| Er | 100.0 | 0.99 | - |
| Tm | 100.0 | 0.13 | - |
| Yb | 100.0 | 0.72 | - |
| Lu | 100.0 | 0.12 | - |
| | - | - | - |
| Mg | 59.4 | 1,712.43 | 1,170.09 |
| Mn | 96.6 | 238.90 | 8.39 |
| Co | 96.8 | 20.70 | 0.69 |
| Ni | 96.7 | 63.12 | 2.12 |
| Zn | 94.9 | 66.31 | 3.60 |
| Cu | 98.5 | 6.14 | 0.09 |
| | - | - | - |
| Se | 94.4 | 0.57 | 0.03 |
| Sr | 6.9 | - | - |
| Ge | - | - | 0.13 |
| Ga | 94.2 | 0.02 | 0.00 |
| Li | 3.4 | 0.91 | 25.40 |
| | - | - | - |
| Al | 99.1 | 549.80 | 4.78 |
| Ca | 4.2 | 18.30 | 417.94 |
| Fe | 74.1 | 52.27 | 18.25 |

RE Redissolution %

| | Yield % | Value | Remainder |
|---|---|---|---|
| Sc | 88.1 | 0.068 | 0.009 |
| Y | 92.2 | 12.678 | 1.080 |
| La | 75.4 | 0.199 | 0.065 |
| Ce | 83.4 | 1.722 | 0.343 |
| Pr | 92.5 | 0.378 | 0.031 |
| Nd | 92.8 | 2.264 | 0.175 |
| Sm | 92.6 | 1.468 | 0.117 |
| Eu | 93.1 | 0.519 | 0.039 |
| Gd | 92.7 | 3.732 | 0.294 |
| Tb | 95.7 | 0.498 | 0.022 |
| Dy | 95.1 | 1.947 | 0.100 |
| Ho | 95.1 | 0.492 | 0.025 |
| Er | 95.6 | 0.942 | 0.043 |
| Tm | 93.6 | 0.122 | 0.008 |
| Yb | 93.1 | 0.673 | 0.050 |
| Lu | 86.5 | 0.102 | 0.016 |
| | - | - | - |
| Mg | 91.5 | 1,566.966 | 145.467 |
| Mn | 72.9 | 174.063 | 64.833 |
| Co | 89.3 | 18.486 | 2.219 |
| Ni | 84.8 | 53.509 | 9.606 |
| Zn | 90.3 | 59.847 | 6.463 |
| Cu | 87.9 | 5.397 | 0.741 |
| | - | - | - |
| Se | 85.2 | 0.489 | 0.085 |
| Sr | 581.2 | - | - |
| Ge | - | - | - |
| Ga | 116215.4 | 28.920 | (28.896) |
| Li | 83.2 | 0.755 | 0.152 |
| | - | - | - |
| Al | 78.3 | 430.442 | 119.361 |
| Ca | 76.5 | 14.002 | 4.303 |
| Fe | 89.2 | 46.640 | 5.630 |

REO Precipitation %

| | Yield % | Value | Remainder |
|---|---|---|---|
| Sc | 23.3 | 0.02 | 0.05 |
| Y | 64.6 | 8.19 | 4.49 |
| La | 12.7 | 0.03 | 0.17 |
| Ce | 80.4 | 1.38 | 0.34 |
| Pr | 86.5 | 0.33 | 0.05 |
| Nd | 91.3 | 2.07 | 0.20 |
| Sm | 94.0 | 1.38 | 0.09 |
| Eu | 95.2 | 0.49 | 0.02 |
| Gd | 93.1 | 3.47 | 0.26 |
| Tb | 90.2 | 0.45 | 0.05 |
| Dy | 83.6 | 1.63 | 0.32 |
| Ho | 78.1 | 0.38 | 0.11 |
| Er | 71.4 | 0.67 | 0.27 |
| Tm | 56.4 | 0.07 | 0.05 |
| Yb | 61.2 | 0.41 | 0.26 |
| Lu | 51.8 | 0.05 | 0.03 |
| | - | - | - |
| Mg | 0.0 | 0.00 | 1,566.91 |
| Mn | 0.0 | 0.05 | 174.02 |
| Co | 0.3 | 0.06 | 18.42 |
| Ni | 0.3 | 0.16 | 53.35 |
| Zn | 0.6 | 0.38 | 59.47 |
| Cu | 0.8 | 0.04 | 5.35 |
| | - | - | - |
| Se | 66.3 | 0.31 | 0.17 |
| Sr | -2266.5 | - | - |
| Ge | | - | - |
| Ga | 90.8 | 26.27 | 2.65 |
| Li | 0.1 | 0.00 | 0.75 |
| | - | - | - |
| Al | 0.0 | 0.07 | 430.37 |
| Ca | 5.0 | 0.70 | 13.30 |
| Fe | 1.0 | 0.48 | 46.16 |

Sulfide Precipitation %

| | Yield % | Value | Remainder |
|---|---|---|---|
| Sc | 1.4 | 0.00 | 0.05 |
| Y | 1.0 | 0.04 | 4.45 |
| La | 1.8 | 0.00 | 0.17 |
| Ce | 1.6 | 0.01 | 0.33 |
| Pr | 2.0 | 0.00 | 0.05 |
| Nd | 2.4 | 0.00 | 0.19 |
| Sm | 4.0 | 0.00 | 0.08 |
| Eu | 2.9 | 0.00 | 0.02 |
| Gd | 2.6 | 0.01 | 0.25 |
| Tb | 0.3 | 0.00 | 0.05 |
| Dy | 1.7 | 0.01 | 0.31 |
| Ho | 1.0 | 0.00 | 0.11 |
| Er | 1.1 | 0.00 | 0.27 |
| Tm | 1.0 | 0.00 | 0.05 |
| Yb | 0.9 | 0.00 | 0.26 |
| Lu | 0.9 | 0.00 | 0.05 |
| | - | - | - |
| Mg | 0.3 | 5.38 | 1,561.53 |
| Mn | 0.8 | 1.41 | 172.61 |
| Co | 71.4 | 13.16 | 5.27 |
| Ni | 56.3 | 30.02 | 23.33 |
| Zn | 97.5 | 57.98 | 1.49 |
| Cu | 99.3 | 5.32 | 0.04 |
| | - | - | - |
| Se | 57.7 | 0.10 | 0.07 |
| Sr | -39.8 | - | - |
| Ge | | - | - |
| Ga | | - | 2.65 |
| Li | 0.4 | 0.00 | 0.75 |
| | - | - | - |
| Al | 0.5 | 2.21 | 428.16 |
| Ca | 0.6 | 0.08 | 13.22 |
| Fe | 12.6 | 5.81 | 40.35 |

Mn Precipitation %

| | Yield % | Value | Remainder |
|---|---|---|---|
| Sc | 85.5 | 0.04 | 0.01 |
| Y | 97.1 | 4.32 | 0.13 |
| La | 98.2 | 0.17 | 0.00 |
| Ce | 99.7 | 0.33 | 0.00 |
| Pr | 99.2 | 0.05 | 0.00 |
| Nd | 98.1 | 0.19 | 0.00 |
| Sm | 97.8 | 0.08 | 0.00 |
| Eu | 98.4 | 0.02 | 0.00 |
| Gd | 98.3 | 0.25 | 0.00 |
| Tb | 98.4 | 0.05 | 0.00 |
| Dy | 98.1 | 0.31 | 0.01 |
| Ho | 97.2 | 0.10 | 0.00 |
| Er | 97.0 | 0.26 | 0.01 |
| Tm | 96.8 | 0.05 | 0.00 |
| Yb | 96.7 | 0.25 | 0.01 |
| Lu | 96.7 | 0.05 | 0.00 |
| | - | - | - |
| Mg | 93.7 | 1,463.69 | 97.84 |
| Mn | 99.3 | 171.39 | 1.22 |
| Co | 99.6 | 5.25 | 0.02 |
| Ni | 99.1 | 23.11 | 0.22 |
| Zn | 91.0 | 1.36 | 0.13 |
| Cu | 52.8 | 0.02 | 0.02 |
| | - | - | - |
| Se | 95.3 | 0.07 | 0.00 |
| Sr | 95.2 | - | - |
| Ge | | - | - |
| Ga | 97.7 | 2.59 | 0.06 |
| Li | 52.5 | 0.39 | 0.36 |
| | - | - | - |
| Al | 99.8 | 427.41 | 0.75 |
| Ca | 98.7 | 13.05 | 0.17 |
| Fe | 99.5 | 40.17 | 0.18 |

Waste Water

| | Value |
|---|---|
| Sc | 0.01 |
| Y | 0.13 |
| La | 0.00 |
| Ce | 0.00 |
| Pr | 0.00 |
| Nd | 0.00 |
| Sm | 0.00 |
| Eu | 0.00 |
| Gd | 0.00 |
| Tb | 0.00 |
| Dy | 0.01 |
| Ho | 0.00 |
| Er | 0.01 |
| Tm | 0.00 |
| Yb | 0.01 |
| Lu | 0.00 |
| | - |
| Mg | 1,267.93 |
| Mn | 9.61 |
| Co | 0.71 |
| Ni | 2.34 |
| Zn | 1.73 |
| Cu | 0.11 |
| | - |
| Se | 0.04 |
| Sr | - |
| Ge | 0.13 |
| Ga | 0.06 |
| Li | 25.76 |
| | - |
| Al | 3.54 |
| Ca | 418.12 |
| Fe | 18.44 |

Chemical Consumption

| | 4M NaOH | HCl | H2SO4 | Oxalic Acid | Na2S | Water |
|---|---|---|---|---|---|---|
| | Liters | | | | | |
| Fe Precipitation | 86.08 | 0.00 | 0.00 | 0.00 | 0.00 | 0.00 |
| Al Precipitation | 100.73 | 0.00 | 0.00 | 0.00 | 0.00 | 0.00 |
| RE-CM Precipitation | 69.61 | 0.00 | 0.00 | 0.00 | 0.00 | 0.00 |
| RE-CM Redissolution | 0.00 | 33.25 | 0.00 | 0.00 | 0.00 | 640.00 |
| Oxalic Acid Precipitation | 17.26 | 0.00 | 0.00 | 28.00 | 0.00 | 0.00 |
| Sulfide Precipitation | 0.00 | 8.74 | 0.00 | 0.00 | 4.01 | 0.00 |
| Mn Precipitation | 24.38 | 0.00 | 0.00 | 0.00 | 0.00 | 0.00 |

| | Value | Units |
|---|---|---|
| Liquid Treated in Test | 5054.87 | L |

4M NaOH

| | |
|---|---|
| Fe Precipitation | 0.223 Kg Fe/L 4M NaOH |
| Al Precipitation | 0.103 Kg Fe+Al/L 4M NaOH |
| RE-CM Precipitation | 72.613 L PLs/ L of 4M NaOH |

| | Value | Units | Value | Units |
|---|---|---|---|---|
| RE Redissolution | | 0.368 Kg REECake/L HCL | | |
| RE Redissolution | | | | 0.019 Kg REECake/L Water |

| | Value | Units | Value | Units |
|---|---|---|---|---|
| Oxalic Acid Precipitation | 0.709 Kg REECake/ L of 4M NaOH | | 0.437 Kg REECake/ L of Oxalic Acid | |

| | Value | Units | Value | Units |
|---|---|---|---|---|
| Sulfide Precipitation | 0.049 Kg Cake/L HCL | | 0.107 Kg Cake/L Na2S | |

Mn Precipitation 0.708 Kg Cake/L 4M NaOH

| | 4M NaOH | HCl | H2SO4 | Oxalic Acid | 1M Na2S | Water |
|---|---|---|---|---|---|---|
| | Liters | | | | | |
| Fe Precipitation | 22,433 | | | | | |
| Al Precipitation | 26,249 | | | | | |
| RE-CM Precipitation | 18,142 | | | | | |
| RE-CM Redissolution | - | 7,503 | | | | 144,416 |
| Oxalic Acid Precipitation | 3,895 | | | 6,318 | | |
| Sulfide Precipitation | - | 2,472 | | | 1,134 | |
| Mn Precipitation | 3,045 | | | | | |
| Sum(L/hr) | 73764.44 | 9974.73 | | 6318.21 | 1134.27 | 144416.20 |

| | | | |
|---|---|---|---|
| NaOH Consumption | 15,529.26 | L 50% NaOH/hr | |
| NaOH Consumption | 23,604.62 | kg 50% NaOH/hr | |
| NaOH Consumption | 23.60 | mt 50% NaOH/Hr | |
| | | | |
| HCl Consumption | 11,570.68 | kg HCl/hr | |
| HCl Consumption | 11.57 | mt HCl/hr | |
| | | | |
| Oxalic Acid Consumption | 505.46 | kg/hr | calculated from Tech sheet and exp sheet (0.08 kg/L) |
| | | | |
| Na2S Consumption | 147.46 | kg/hr | |
| Na2S Consumption | 0.15 | mt/Hr | |

Figure 101. Precipitation yield model for the calculation of reagent consumption. Note: Please see accompanying Microsoft Excel TEA model for a more expansive reference.

**Equipment Cost (CapEX)**

| ID | Unit Equipment | No. of Units | Capacity of Unit | Units | Installed Capacity | Utilization | Utilized Capacity | Unit Cost | Total | Notes/Description |
|---|---|---|---|---|---|---|---|---|---|---|
| 1 | PC: Heap Pumping System | 1 | 1 | each | 1 | 100% | 1 | $ 19,081,825 | $ 19,081,825 | |
| 2 | PC:Civil Works (In-Plant) | 1 | 1 | each | 1 | 100% | 1 | $ 10,324,002 | $ 10,324,002 | |
| 3 | PC:Non-Process Buildings - Allowance - 1200m2 Bui | 1 | 1 | each | 1 | 100% | 1 | $ 1,243,200 | $ 1,243,200 | |
| 4 | PC:Structural Steelwork | 1 | 1 | each | 1 | 100% | 1 | $ 6,770,513 | $ 6,770,513 | |
| 5 | PC:Mechanical Equipment (Excl Tanks + Plateworks | 1 | 1 | each | 1 | 100% | 1 | $ 28,802,301 | $ 28,802,301 | |
| 6 | PC:Tanks + Plateworks | 1 | 1 | each | 1 | 100% | 1 | $ 17,260,109 | $ 17,260,109 | |
| 7 | PC:In-Plant Piping & Valves | 1 | 1 | each | 1 | 100% | 1 | $ 7,826,002 | $ 7,826,002 | |
| 8 | PC:Electrical | 1 | 1 | each | 1 | 100% | 1 | $ 5,755,898 | $ 5,755,898 | |
| 9 | PC:Sub-Station Allowance | 1 | 1 | each | 1 | 100% | 1 | $ 1,554,000 | $ 1,554,000 | |
| 10 | PC:Instrumentation | 1 | 1 | each | 1 | 100% | 1 | $ 4,796,582 | $ 4,796,582 | |
| 11 | PC:Civils P&G's | 1 | 1 | each | 1 | 100% | 1 | $ 4,645,801 | $ 4,645,801 | |
| 12 | PC:SMPP P&G's | 1 | 1 | each | 1 | 100% | 1 | $ 22,093,583 | $ 22,093,583 | |
| 13 | PC:E&I P&G's | 1 | 1 | each | 1 | 100% | 1 | $ 4,842,592 | $ 4,842,592 | |
| 14 | PC:Transportation of Equipment to site | 1 | 1 | each | 1 | 100% | 1 | $ 1,461,815 | $ 1,461,815 | |
| 15 | PC:Commissioning Spares | 1 | 1 | each | 1 | 100% | 1 | $ 1,066,752 | $ 1,066,752 | |
| 16 | PC:Critical Spares | 1 | 1 | each | 1 | 100% | 1 | $ 2,133,504 | $ 2,133,504 | |
| 17 | PC:First fill of lubricants and oil | 1 | 1 | each | 1 | 100% | 1 | $ 133,344 | $ 133,344 | |
| 18 | PC:Vendor assist during Constr & Comm | 1 | 1 | each | 1 | 100% | 1 | $ 1,466,784 | $ 1,466,784 | |
| 19 | PC:EPCM Excl Heap Pumping System | 1 | 1 | each | 1 | 100% | 1 | $ 21,991,821 | $ 21,991,821 | |
| 20 | PC:Engineering Interface - Heap Pumping System | 1 | 1 | each | 1 | 100% | 1 | $ 3,434,729 | $ 3,434,729 | |
| 21 | PC:Bonds Guarantees etc @ 055% of TNC | 1 | 1 | each | 1 | 100% | 1 | $ 916,768 | $ 916,768 | |
| 22 | NaOH | | | $/mt | 0 | 0% | 0 | | | |
| 23 | HCl | | | $/mt | 0 | 0% | 0 | | | |
| 24 | H2SO4 | | | $/mt | 0 | 0% | 0 | | | |
| 25 | Oxalic Acid | | | $/kg | 0 | 0% | 0 | | | |
| 26 | Na2S | | | $/mt | 0 | 0% | 0 | | | |
| 27 | | | | | | | | | | |
| 28 | | | | | | | | | | |
| 29 | | | | | | | | | $ - | |
| 30 | | | | | | | | | $ - | |
| | | | | | | | | | $ 167,601,926 | |

Figure 102. Assumed capital costs adapted from prior work of SGS.

**Consumables & Reagents (OpEX)**

| ID | Unit Equipment | Type/Value | | Cost | Total Cost | |
|---|---|---|---|---|---|---|
| 1 | PC: Heap Pumping System | 0.0% | $ | - | $ - | |
| 2 | PC:Civil Works (In-Plant) | 0.0% | $ | - | $ - | |
| 3 | PC:Non-Process Buildings - Allowance - 1200m2 Buildings | 0.0% | $ | - | $ - | |
| 4 | PC:Structural Steelwork | 0.0% | $ | - | $ - | |
| 5 | PC:Mechanical Equipment (Excl Tanks + Plateworks) | 0.0% | $ | - | $ - | |
| 6 | PC:Tanks + Plateworks | 0.0% | $ | - | $ - | |
| 7 | PC:In-Plant Piping & Valves | 0.0% | $ | - | $ - | |
| 8 | PC:Electrical | 0.0% | $ | - | $ - | |
| 9 | PC:Sub-Station Allowance | 0.0% | $ | - | $ - | Anticipated Consumption Per Year |
| 10 | PC:Instrumentation | 0.0% | $ | - | $ - | Anticipated Consumption Per Year |
| 11 | PC:Civils P&G's | 0.0% | $ | - | $ - | |
| 12 | PC:SMPP P&G's | 0.0% | $ | - | $ - | |
| 13 | PC:E&I P&G's | 0.0% | $ | - | $ - | |
| 14 | PC:Transportation of Equipment to site | 0.0% | $ | - | $ - | |
| 15 | PC:Commissioning Spares | 0.0% | $ | - | $ - | |
| 16 | PC:Critical Spares | 0.0% | $ | - | $ - | |
| 17 | PC:First fill of lubricants and oil | 0.0% | $ | - | $ - | |
| 18 | PC:Vendor assist during Constr & Comm | 0.0% | $ | - | $ - | |
| 19 | PC:EPCM Excl Heap Pumping System | 0.0% | $ | - | $ - | |
| 20 | PC:Engineering Interface - Heap Pumping System | 0.0% | $ | - | $ - | |
| 21 | PC:Bonds Guarantees etc @ 055% of TNC | 0.0% | $ | - | $ - | |
| 22 | NaOH | 100.0% | $ | 3,057 | $ 26,777,555 | |
| 23 | HCl | 100.0% | $ | 3,237 | $ 28,352,193 | |
| 24 | H2SO4 | 100.0% | | | $ - | |
| 25 | Oxalic Acid | 100.0% | $ | 314 | $ 2,752,321 | |
| 26 | Na2S | 100.0% | $ | 55 | $ 481,755 | |
| 27 | Laboratory | | | | $ 174,671 | |
| 28 | Mobile Equipment | | | | $ 202,752 | |
| 29 | Tailings | | | | $ 2,563,811 | |
| 30 | | | | | | |
| | | | | | $ 61,305,059 | |

Figure 103. Assumed operational costs for the precipitation module.

Table 65. Reagent costs for precipitation step (Cost basis from DE-FE0031827 for continuity).

| Consumable | Unit | $/Unit |
|---|---|---|
| Sodium Hydroxide (NaOH) 50% Solution | 125.00 | $/mt |
| Hydrochloric Acid (HCl) 31-38% | 270.00 | $/mt |
| Sulfuric Acid ($H_2SO_4$) 98% | 220.00 | $/mt |

| | | |
|---|---|---|
| Oxalic Acid 99.6% pure | 0.60 | $/kg |
| Sodium Sulfide ($Na_2S$) 60% | 360.00 | $/mt |

*RE Metal Making (3RE)* – The REM Making tab considers a plasma furnace comprised of a radio frequency (RF) argon lance to generate the plasma and a graphite crucible as shown in

Figure 104. The University of Alabama has indicated that the condensed metallic phase in the quench chamber is a fine and easy to remove powder which lends itself well to removal. It is important to note that it is recommend that this process be run batch wise, as continuous operation would lead to higher concentrations in the slag phase of vapor phase elements, leading to greater loss of those materials. In a batch operation the concentration of the vapor phase elements is expected to approach zero in the slag phase, thereby improving recoveries.

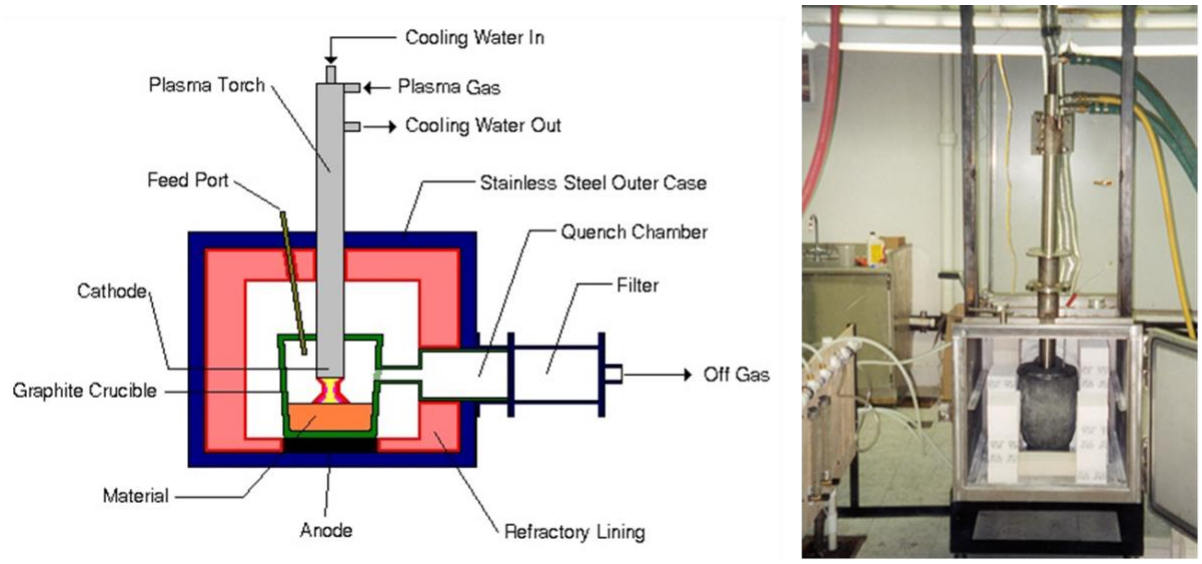


Figure 104. Schematic (left) and picture of plasma reactor (right).

The yields of each stage of the process are defined in the Microsoft Excel model with 99% mass yield being assumed for accounting purposes. The estimated graphite crucible costs over operational life were included in the operational costs. With regard to the ionic liquid cost estimations, the voltages and specific production capacity was estimated with the current density to determine the number of electrodes, size of the cell, and volume of electrolyte needed. See Figure 105 for documentation of that model.

To estimate the capital expense of the module, information and estimates were provided by the University of Alabama (UA) on the equipment which was constructed in their lab. As the plasma reactor is based on the surface area of the slag and vapor phase it was assumed that the reactors could not scale beyond the largest demonstrated size. Thus, a key attribute of the TEA model was determining the number of plasma reactors. The electrolytic cells were sized based on 1 m X 1m

electrodes and estimated expenses. The costs provided by UA were adjusted for inflation to current dollars. A summary of the capital expenses is show in Figure 106 indicating the type, number, and description of needed capital elements.

For operational costs, power consumption factors predominantly, although the specific consumption of argon gas, methane, graphite crucibles, and an assumption of electrolyte replacement three times per year are included. Also, it is assumed that 24 people will be needed to operate the plant.

The total CapEx costs are estimated at $5,433,694 with the OpEx at $5,361,167.

| | | | |
|---|---|---|---|
| Plasma Furnace Charge Size | 10.00 | kg/each | |
| Plasma Furnace cycle time | 1.50 | hr/each | |
| Curcible life time | 150.00 | hr/each | |
| Power | 35.00 | Kw | |
| Argon Flow Rate | 4.00 | L/min/Unit | |
| Natural Gas Flow Rate | 1.75 | L/min/Unit | |
| | | | |
| Electrode | 1.00 | m^2 | |
| Electrode Spacing | 0.03 | m | |
| Electrode Edge spacing | 0.05 | m | |
| Interior Tank Edge Bottom | 1.10 | m | |
| Interior Tank Height | 1.10 | m | |
| Volume for one Anode/Cathode | 0.04 | m^3 | |
| | | | |
| Metal Production Rate | 132.93 | g/(h*m^2) | |
| | 0.13 | kg/(h*m^2) | |
| Current Density | 410.00 | A/m^2 | |
| Rate Per Current | 0.32 | g/(A*h) | |
| | | | |
| **EW Sm** | 1.35 | kg/hr | |
| Area Needed | 10.17 | m^2 | |
| Electrodes needed | 11.00 | Electrode pairs (Cathode/Anode) | |
| Electrolyte Volume | 0.40 | m^3 | |
| Current | 4,510.00 | A | |
| Volts | 1.90 | V | |
| Power | 8.57 | Kw | |
| Electrode Material | W | | |
| | | | |
| **EW Dy** | 1.60 | kg/hr | |
| Area Needed | 12.00 | m^2 | |
| Electrodes needed | 13.00 | Electrode pairs (Cathode/Anode) | |
| Electrolyte Volume | 0.47 | m^3 | |
| Current | 5,330.00 | A | |
| Volts | 3.20 | V | |
| Power | 17.06 | Kw | |
| Electrode Material | W | | |
| | | | |
| **EW Al** | 0.07 | kg/hr | |
| Area Needed | 0.51 | m^2 | |
| Electrodes needed | 1.00 | Electrode pairs (Cathode/Anode) | |
| Electrolyte Volume | 0.04 | m^3 | |
| Current | 410.00 | A | |
| Volts | 1.50 | V | |
| Power | 0.62 | Kw | |
| Electrode Material | Cu | | |
| | | | |
| **EW Gd** | 3.44 | kg/hr | |
| Area Needed | 25.88 | m^2 | |
| Electrodes needed | 26.00 | Electrode pairs (Cathode/Anode) | |
| Electrolyte Volume | 0.94 | m^3 | |
| Current | 10,660.00 | A | |
| Volts | 1.75 | V | |
| Power | 18.66 | Kw | |
| Electrode Material | W | | |
| | | | |
| **EW Nd/Pr** | 2.37 | kg/hr | |
| Area Needed | 17.84 | m^2 | |
| Electrodes needed | 18.00 | Electrode pairs (Cathode/Anode) | |
| Electrolyte Volume | 0.65 | m^3 | |
| Current | 7,380.00 | A | |
| Volts | 2.50 | V | |
| Power | 18.45 | Kw | |
| Electrode Material | W | | |
| | | | |
| **EW Y** | 8.10 | kg/hr | |
| Area Needed | 60.97 | m^2 | |
| Electrodes needed | 61.00 | Electrode pairs (Cathode/Anode) | |
| Electrolyte Volume | 2.21 | m^3 | |
| Current | 25,010.00 | A | |
| Volts | 2.60 | V | |
| Power | 65.03 | Kw | |
| Electrode Material | W | | |

| | | |
|---|---|---|
| Total EW Ampeage | 53,300.00 | A |
| Total EW Power | 128.37 | Kw |
| Total Electrolyte | 5.19 | m^3 |
| Total Electrolyte | 1,370.49 | gal |
| W Electrodes | 65.00 | |
| Cu Electrodes | 1.00 | |
| | | |
| Total Rectifier units | 71.07 | Units |
| | | |
| Cruibles needed | 175.20 | |
| EW Argon | 5 | L/(min*m^3) |
| | 25.94 | L/min |
| | | |
| | | |
| Total Argon | 37.94 | L/min |
| Total Methane | 5.25 | L/min |

Figure 105. Capacity model for plasma and ionic liquid capital and operational cost calculations.

| Equipment Cost (CapEX) | | | | | | | | | | | | |
|---|---|---|---|---|---|---|---|---|---|---|---|---|
| ID | Unit Equipment | No. of Units | Capacity of Unit | Units | Installed Capacity | Utilization | Utilized Capacity | Unit Cost | | Total | | Notes/Description |
| 1 | RF Power Supply | 5 | 1 | 10 kg/each | 5 | 100% | 5 | $ | 672,302 | $ | 3,361,511 | |
| 2 | Plasma Gun | 5 | 1 | 10 kg/each | 5 | 100% | 5 | $ | 92,201 | $ | 461,007 | |
| 3 | Furnace Assembly | 5 | 1 | 10 kg/each | 5 | 100% | 5 | $ | 172,878 | $ | 864,389 | |
| 4 | Furnace Ancillaries | 5 | 1 | 10 kg/each | 5 | 100% | 5 | $ | 187,476 | $ | 937,381 | |
| 5 | Glass Lined EW Cell (REE) | 1 | 1 | 5 m^2/each | 1 | 100% | 1 | $ | 111,722 | $ | 111,722 | |
| 6 | Power Supply | 71.07 | 1 | 750 A/each | 71.06666667 | 100% | 71.06666667 | $ | 2,585 | $ | 183,695 | |
| 7 | Cathode | 65.00 | 1 | each | 65 | 100% | 65 | $ | 5,180 | $ | 336,700 | |
| 8 | Anode | 65.00 | 1 | each | 65 | 100% | 65 | $ | 2,072 | $ | 134,680 | |
| 9 | Electrode Press (1000 Ton) | 1 | 1 | each | 1 | 100% | 1 | $ | 139,860 | $ | 139,860 | |
| 10 | Electrolyte | 5,187.85 | 1 | $/L | 5187.851056 | 100% | 5187.851056 | $ | 52 | $ | 268,731 | |
| 11 | Argon | | | $/L | 0 | | 0 | | | | | |
| 12 | Methane | | | $/L | 0 | | 0 | | | | | |
| 13 | Graphite Crucibles | | | $/each | 0 | | 0 | | | | | |
| 14 | | | | | 0 | | 0 | | | | | |
| 15 | | | | | 0 | | 0 | | | | | |
| 16 | | | | | 0 | | 0 | | | | | |
| 17 | | | | | 0 | | 0 | | | | | |
| 18 | | | | | 0 | | 0 | | | | | |
| 19 | | | | | 0 | | 0 | | | | | |
| 20 | | | | | 0 | | 0 | | | | | |
| 21 | | | | | 0 | | 0 | | | | | |
| | | | | | | | | | | $ | 6,799,675 | |

Figure 106. Capital cost estimation of the REM making process.

*Sulfide Metal Making (4SU)* – The process of metal making from metal sulfides follows the REM production process generally, but per the flowsheet, does not require a plasma reactor and requires the conversion to an oxide first. Instead, a chlorination reactor is added in its place for the conversion of metals. As the model is in the same general form as the REM making step, the reader is encouraged to consult the TEA model for specifics. It is anticipated that a staff of 36 members will be required to operate this facility.

The total CapEx costs are estimated at $12,038,146 with the OpEx at $16,585,277 per year.

*MgMn Metal Making (5MM)* – The magnesium and manganese subcircuit being part of circuit 4, is nearly identical to the REM stage for costing purposes except in the scale. It is assumed that 162 plasma reactors are required due to the increased metal throughput in this step. The reader is encouraged to consult the TEA model for specifics. It is anticipated that a staff of 90 members will be required to operate this facility.

The total CapEx costs are estimated at $232,707,293 with the OpEx at $67,332,813 per year.

*LiSr Recovery (6Li)* – At the time of this writing insufficient data exists for the estimation of costs for the Li/Sr recovery circuit. See next section for a further discussion.

*Tax & Insurance (7TI)* – This is included as a model placeholder for a future date where a specific location is known and tax and insurance implications are better known.

*Site Services (8SS)* – Site services are included to provide estimation of power and water hookups which don't include the heap and precipitation plant. Items such as transformers, transmission lines, and water and sewer hookup are included (See Figure 107). The CapEx comes to $3,466,599 for this module.

Equipment Cost (CapEX)

| ID | Unit Equipment | No. of Units | Capacity of Unit | Units | Installed Capacity | Utilization | Utilized Capacity | Unit Cost | Total | Notes/Description |
|---|---|---|---|---|---|---|---|---|---|---|
| 1 | 13200V to 4160V Transformer | 4 | 1 | each | 4.0 | 100% | 4.0 | $ 305,000 | $ 1,220,000 | |
| 2 | 4160V to 480V Transformer | 4 | 1 | each | 4.0 | 100% | 4.0 | $ 30,000 | $ 120,000 | |
| 3 | Transmission Line | 4 | 1 | km | 4.0 | 100% | 4.0 | $ 439,520 | $ 1,758,080 | |
| 4 | Water and Sewer Hook Up | 3 | 1 | km | 3.0 | 100% | 3.0 | $ 84,400 | $ 253,199 | |
| 5 | | | | | 0 | | 0 | | | |
| 6 | | | | | 0 | | 0 | | | |
| 7 | | | | | 0 | | 0 | | | |
| 8 | | | | | 0 | | 0 | | | |
| 9 | | | | | 0 | | 0 | | | |
| 10 | | | | | 0 | | 0 | | | |
| 11 | | | | | 0 | | 0 | | | |
| 12 | | | | | 0 | | 0 | | | |
| 13 | | | | | 0 | | 0 | | | |
| 14 | | | | | 0 | | 0 | | | |
| 15 | | | | | 0 | | 0 | | | |
| 16 | | | | | 0 | | 0 | | | |
| 17 | | | | | 0 | | 0 | | | |
| 18 | | | | | 0 | | 0 | | | |
| 19 | | | | | 0 | | 0 | | | |
| 20 | | | | | 0 | | 0 | | | |
| 21 | | | | | 0 | | 0 | | | |
| | | | | | | | | | $ 3,351,279 | |

Figure 107. Capital equipment estimation for metal recovery and administrative needs.

*Facilities and buildings (9FB)* – The scope of the facilities and buildings assumes requirements for refining and metal making but does not include the heap or precipitation plant. The assumed buildings are: a change room with dimensions of 60'x60'x14' H and 3" of concrete; a warehouse with dimensions of 80'x100'x14' H and 6" of concrete; a shop with dimensions of 50'x50'x14' H and 6" of concrete; a process house with dimensions of 360'x100'x20' H and 6" of concrete; an office with dimensions of 30'x40'x10' H and 3" of concrete; a guard shack with dimensions of 15'x15'x10' H and 3" of concrete; a storage pad with dimensions of 50'x50' and 6" of concrete; a scale with dimensions of 50'x50' and 6" of concrete; and a waste storage pad with dimensions of 50'x50' and 6" of concrete. The materials requirements for these buildings were calculated and aggregated to determine the capital requirements as shown in Figure 108. The OpEx for this module was calculated based on the lighting and HVAC power requirements by area. 3 staff for janitorial services are assumed.

The total CapEx costs are estimated at $5,503,237 with the OpEx at $267,182 per year.

Equipment Cost (CapEX)

| ID | Unit Equipment | No. of Units | Capacity of Unit | Units | Installed Capacity | Utilization | Utilized Capacity | Unit Cost | Total | Notes/Description |
|---|---|---|---|---|---|---|---|---|---|---|
| 1 | Concrete | 700.31 | 1 | m^3 | 700.3 | 100% | 700.3 | $ 295 | $ 206,652 | |
| 2 | Rebar | 4,828.63 | 1 | m^2 | 4828.6 | 100% | 4828.6 | $ 25 | $ 119,543 | |
| 3 | Concrete Pumping | 700.31 | 1 | m^3 | 700.3 | 100% | 700.3 | $ 36 | $ 25,006 | |
| 4 | Form Rental | 4,828.63 | 1 | m^2 | 4828.6 | 100% | 4828.6 | $ 64 | $ 306,653 | |
| 5 | Concrete Forming | 4,828.63 | 1 | m^2 | 4828.6 | 100% | 4828.63 | $ 148 | $ 714,137 | |
| 6 | Concrete Finishing | 4,828.63 | 1 | m^2 | 4828.6 | 100% | 4828.63 | $ 2 | $ 10,135 | |
| 7 | Subgrade 6" Base | 4,828.63 | 1 | m^2 | 4828.6 | 100% | 4828.63 | $ 39 | $ 187,110 | |
| 8 | Building 14' Basic | 1,442.32 | 1 | m^2 | 1442.3 | 100% | 1442.32 | $ 307 | $ 442,307 | |
| 9 | Building Finish Cost | 699.10 | 1 | m^2 | 699.1 | 100% | 699.10 | $ 484 | $ 338,625 | |
| 10 | Building 23' | 3,344.51 | 1 | m^2 | 3344.5 | 100% | 3344.51 | $ 775 | $ 2,592,000 | |
| 11 | Building Interior Lights | 4,786.83 | 1 | m^2 | 4786.8 | 100% | 4786.83 | $ 73 | $ 350,370 | |
| 12 | Office Building HVAC | 699.10 | 1 | m^2 | 699.1 | 100% | 699.10 | $ 301 | $ 210,700 | |
| 13 | | | | | 0 | | 0 | | | |
| 14 | | | | | 0 | | 0 | | | |
| 15 | | | | | 0 | | 0 | | | |
| 16 | | | | | 0 | | 0 | | | |
| 17 | | | | | 0 | | 0 | | | |
| 18 | | | | | 0 | | 0 | | | |
| 19 | | | | | 0 | | 0 | | | |
| 20 | | | | | 0 | | 0 | | | |
| 21 | | | | | 0 | | 0 | | | |
| | | | | | | | | | $ 5,503,237 | |

Figure 108. CapEx estimations for Facilities and Buildings.

*General & Administrative (10GA)* – The general and administrative (G&A) costs include office, and staff for the administration of the project as shown in Figure 109 and

Figure 110. The success of any industrial project largely depends on the efficient management and operation of the plant. The management and administration of a plant involve a diverse range of responsibilities and duties and are summarized as follows. The plant manager is responsible for

overseeing all plant operations and ensuring that they are carried out efficiently and safely. The plant superintendent is responsible for the day-to-day operation of the plant, including maintenance, production, and safety. The plant safety and environmental personnel ensure that the plant meets all safety and environmental regulations. The foremen oversee and coordinate the work of the production and maintenance personnel. The administrative staff, including accounting and payroll personnel, manage the financial and administrative aspects of the plant. The processing metallurgist is responsible for overseeing the extraction operations and processing of metals. The lab techs carry out the necessary tests and analyses to ensure that the materials meet the required standards. The purchasing department is responsible for procuring the necessary equipment, materials, and supplies. The electricians and maintenance personnel ensure that the plant's equipment is functioning properly and that any maintenance or repairs are carried out promptly. Finally, the security personnel ensure that the plant is secure and protected from any potential threats. G&A assumes a total of 44 staff.

The total CapEx costs are estimated at $51,360 with the OpEx at $5,410,582 per year.

**Consumables & Reagents (OpEX)**

| ID | Unit Equipment | No. of Units | Capacity of Unit | Units | Installed Capacity | Utilization | Utilized Capacity | Unit Cost | Total | Notes/Description |
|---|---|---|---|---|---|---|---|---|---|---|
| 1 | Telephone - 3 lines | 120 | 1 | $/Month | 120.0 | 100% | 120.0 | $ 175 | $ 21,000 | |
| 2 | Cell phones | 100 | 1 | $/Month | 100.0 | 100% | 100.0 | $ 100 | $ 10,000 | |
| 3 | Hi-speed internet connection | 120 | 1 | $/Month | 120.0 | 100% | 120.0 | $ 200 | $ 24,000 | |
| 4 | Plotter (Lease purchase) | - | 1 | $/Month | 0.0 | 100% | 0.0 | $ 200 | $ - | |
| 5 | Copy Machine (Lease purchase) | 36 | 1 | $/Month | 36 | 100% | 36 | $ 150 | $ 5,400 | |
| 6 | Office supplies & expenses | 120 | 1 | $/Month | 120 | 100% | 120 | $ 1,500 | $ 180,000 | |
| 7 | Rescue Training | 24 | 1 | $/Month | 24 | 100% | 24 | $ 200 | $ 4,800 | |
| 8 | Phone system | - | 1 | $ | 0 | 100% | 0 | $ 1,500 | $ - | |
| 9 | Computers, Printers, Software | 4 | 1 | $/4 years | 3.75 | 100% | 3.75 | $ 20,000 | $ 75,000 | |
| 10 | Software | 1 | 1 | $/Year | 1 | 100% | 1 | $ 15,000 | $ 15,000 | |
| 11 | Relocation | 1 | 1 | $ | 1 | 100% | 1 | $ 20,000 | $ 20,000 | |
| 12 | Washer/Dryer replacement | 1 | 1 | $/Year | 1 | 100% | 1 | $ 4,335 | $ 4,335 | |
| 13 | Air Fare | - | 1 | $/Month | 0 | 100% | 0 | $ 600 | $ - | |
| 14 | Lodging | - | 1 | $/Night | 0 | 100% | 0 | $ 200 | $ - | |
| 15 | Vehicle | - | 1 | $/Month | 0 | 100% | 0 | $ 0.57 | $ - | Note this is milage |
| 16 | Meals | - | 1 | $/Meal | 0 | 100% | 0 | $ 30 | $ - | |
| 17 | Internal Audit | - | 1 | $/Year | 0 | 100% | 0 | $ 20,000 | $ - | |
| 18 | Tax Preparation | - | 1 | $/Year | 0 | 100% | 0 | $ 5,000 | $ - | |
| 19 | Travel/From/to/US | - | 1 | $/Year | 0 | 100% | 0 | $ 12,000 | $ - | |
| 20 | Crew Van | - | 1 | each | 0 | 100% | 0 | $ 23,184 | $ - | |
| 21 | Pickup | 1 | 1 | each | 1 | 100% | 1 | $ 4,788 | $ 4,788 | |
| 22 | GM Vehicle | - | 1 | each | 0 | 100% | 0 | $ 11,300 | $ - | |
| 23 | Country Office | - | 1 | $/Year | 0 | 100% | 0 | $ 52,630 | $ - | |
| | | | | | | | | | $ 364,323 | |

Figure 109. Supplies and consumables for G&A costs.

**Labor (OpEX)**

| ID | Position Description | Labor Type | Shift | Shifts | People Per Shift | People | Cost Per Day | Total Cost |
|---|---|---|---|---|---|---|---|---|
| 1 | | Plant Manager | 5/2 | 2 | 1 | 2 | $ 948.10 | $ 346,056 |
| 2 | | Plant Superintend | 5/2 | 2 | 1 | 2 | $ 758.48 | $ 276,845 |
| 3 | | Plant Safety and E | 5/2 | 1 | 1 | 1 | $ 284.43 | $ 103,817 |
| 4 | | Foremen | 5/2 | 3 | 1 | 3 | $ 829.59 | $ 302,799 |
| 5 | | Admin | 5/2 | 1 | 1 | 1 | $ 189.62 | $ 69,211 |
| 6 | | Accounting and Pa | 5/2 | 1 | 2 | 2 | $ 474.05 | $ 173,028 |
| 7 | | Processing Metalli | 5/2 | 1 | 4 | 4 | $ 1,516.96 | $ 553,690 |
| 8 | | Lab Tech | 5/2 | 1 | 4 | 4 | $ 948.10 | $ 346,056 |
| 9 | | Purchasing | 5/2 | 2 | 2 | 4 | $ 1,185.12 | $ 432,570 |
| 10 | | Electricians/Maint | 5/2 | 3 | 2 | 6 | $ 1,991.01 | $ 726,718 |
| 11 | | Maintenance | 5/2 | 3 | 4 | 12 | $ 3,982.01 | $ 1,453,435 |
| 12 | | Security | 4/3 | 3 | 1 | 3 | $ 711.07 | $ 259,542 |
| 13 | | | | | | 0 | | |
| 14 | | | | | | | | |
| 15 | | | | | | | | |
| 16 | | | | | | | | |
| 17 | | | | | | | | |
| 18 | | | | | | | | |
| 19 | | | | | | | | |
| 20 | | | | | | | | |
| 21 | | | | | | | $ - | $ - |
| 22 | | | | | | | $ - | $ - |
| 23 | | | | | | | | |
| | | | | | | 44 | | $ 5,043,766 |

Figure 110. Position and labor requirements

*Mobile Equipment (11MA)* – The mobile equipment needs of the project require a range of vehicles, including a dump truck for general use and road maintenance, skid steers for maneuvering and transporting smaller loads, a flatbed truck for larger equipment and materials, a crew van for transporting personnel to and from job sites, a pickup truck for general use and smaller loads, and a GM (general manager) vehicle for management and administrative purposes. Each vehicle has a specific purpose and is essential for the efficient functioning of the project and ensures that equipment and personnel are in the right place at the right time. Proper maintenance and operation of these vehicles is crucial for the safety and success of the project. Please consult the TEA model for specifics.

The total CapEx costs are estimated at $959,600 with the OpEx at $88,724 per year.

#### *2.11.1.1 Section References:*


[1] Rosenthal, M., 2022. "A Unique Collaboration of Coal-based REEs and the U.S.'s Largest Rare Earth Producer" Final Technical Report, MP Materials/DOE, Project Number: 89243320CFE000053-0001; 221 pages.

[2] Honaker, R.Q., Werner, J., Nawab, A., Zhang, W., Noble, A., Yang, X. and Free, M., 2023. "Demonstration of Scaled-Production of Rare Earth Oxides and Critical Materials from Coal-Based Sources," DOE Contract No. DE-FE0031827, Final Technical Report, 1080 pages.


### *2.11.2 Li-Sr Addendum*

The technical literature described previously provides suitable fundamental and empirical evidence for the technical viability of the proposed REE and CM recovery flowsheets. In particular, the Li/Sr technologies (e.g. adsorption, nanofiltration) have been proven to be effective in similar dilute, highly contaminated aqueous solutions, such as geothermal brines (see [2]), while producing high purity lithium carbonate and lithium hydroxide products. While process validation and verification testing will be needed to prove the technologies in the proposed coal-based leachate application, the degree of technical risk is relatively low.

Given the high likelihood of technical viability, preliminary cost models were developed to assess the economic comparative merits of Li/Sr flowsheets shown in Figure 74 and Figure 75. Due to the preliminary nature of these process flowsheets, the cost models were largely based on literature data and assumed parameters, rather than bottom-up estimates based on heat and material balances. While the accuracy of these models for the proposed application is quite limited, they do provide the opportunity to evaluate sensitivities and derive benchmarks for future process development efforts. For the purposes of this study, only the lithium production route was assessed. The technical literature for lithium production has detailed information on processing costs, and as stated above the technologies described in this project have been evaluated in similarly complex systems. Alternatively, indicative costs strontium processing route were not available in the technical literature, thus suggesting that a bottom-up estimate from a detailed heat and material balance is needed.

*Selective Adsorption* - Flowsheet I (Figure 74), which primarily uses selective adsorption as the method of lithium recovery was modeled using data provided by Warren (2021). In this study, the

author provides a detailed technical and economic analysis of seven direct lithium extraction (DLE) technologies applied to geothermal, evaporite, and oilfield brines. Technologies evaluated the study primarily included ion exchange/adsorption with a single study (#6) evaluating solvent extraction. As such, these processes can be considered suitable analogues for the proposed flowsheet technology. Moreover, Lithium concentrations in the various brines ranged from 65 to 500 ppm, similar in magnitude to the expected feed solution to the lithium recovery circuit. Products from the DLE processes included both lithium carbonate and lithium hydroxide depending on the process under evaluation. Salient data from the Warren (2021) study is shown in Table 66.

Table 66. Lithium Production and Cost Data [4].

| Ref ID | Brien Type/Technology | Brine Conc. (mg/L) | Recovery (%) | Production (t/y) | CAPEX ($1,000) | OPEX ($1,000/yr) |
|---|---|---|---|---|---|---|
| 1 | Geothermal, Ion Exchange | 400 | 90% | 20,000 | $52,300 | $76,900 |
| 2 | Geothermal, Adsorption | 181 | 90% | 40,000 | $1,287,600 | $128,688 |
| 3 | Evaporite, Ion Exchange | 168 | 90% | 20,900 | $437,162 | $90,259 |
| 4 | Oilfield, Ion Exchange | 75 | 90% | 20,000 | $602,000 | $73,200 |
| 5 | Evaporite, Ion Exchange | 300 | 75% | 15,000 | $120,000 | $68,180 |
| 6 | Evaporite, Solvent Extraction | 221 | 90% | 11,500 | $358,601 | $36,516 |
| 7 | Salar, Ion Exchange | 289 | 83% | 25,500 | $544,000 | $106,539 |

To develop the cost model, the Warren [4] data was first pre-processed to determine processing capital and operating costs on a volumetric feed basis ($/lpm of feed solution). Volumetric feed data for the seven processes ranged from 21,000 to over 100,000 lpm, while CAEX varied from $52 million to $1.3 billion. Operating costs ranged from $0.0015 / L to $0.0074 /L. These costs were then adjusted to reflect the coal-based system under consideration. Fixed parameters used in the cost model are shown in

Table 67. Note that the feed flowrate (32,000 lpm) corresponds to a REE/CM processing plant treating approximately 500 tph of coal refuse. This value has been used as standard for various techno-economic analyses conducted by the project team (see reports for (DE-FE0027035 and DE-FE0031827). From these parameters, the total lithium carbonate production was calculated by multiplying the flow rate, lithium concentration, process recovery and the lithium carbonate to lithium ratio.

Table 67. Fixed Economic Parameters used in the Cost Models.

| Parameter | Unit | Value |
|---|---|---|
| Feed Flow Rate | lpm | 32,000 |
| Feed Lithium Concentration | mg/L Li | 100 |
| Process Recovery | % | 90% |
| Operating Hours per Year | Hr/yr | 8064 |
| Discount Rate | % | 10% |
| Operating Period | Year | 20 |
| $Li_2CO_3$ / Li | m/m | 5.32 |

The capital costs for the modeled circuit was determined according to a power scaling law:

$$CAPEX_{New} = CAPEX_{Ref}\left(\frac{Q_{New}}{Q_{Ref}}\right)^{Exp}$$

where $CAPEX_{New}$ is the capital cost of the modeled system, $CAPEX_{Ref}$ is the capital cost for one of the reference systems given in Warren [4], $Q_{New}$ is the volumetric flow rate in the modeled system, $Q_{Ref}$ is the volumetric flowrate for the reference system, and *Exp* is the scaling exponent, which was fixed at 0.6 for this study.

Likewise, operating costs were determined using a simple linear trend based on a constant unit cost per volume of solution processed.

Using the approach described above, the total capital cost, annual operating cost, and annual production were determined for the modeled system. Capital costs were then annualized over a 20-year operating period with a 10% discount rate. These results were then combined to determine the breakeven lithium carbonate price (pre-tax), which was the primary output response evaluated in the study.

Since the economic model is primarily driven by the input assumptions, the selection of an appropriate reference system will have significant impacts on the results. Figure 111, for example, shows the calculated breakeven lithium carbonate price for the modeled system (32,000 lpm, 100 mg/L Li) as a function of the reference system selected for the model parameters. As shown, the data typically varies from $12,000 to $18,000 / t lithium carbonate with an anomalous low for ID4, which is $8,000. By comparison, the 2022 average-nominal spot price for battery-grade lithium carbonate was $37,000 /t, which was significantly higher than the prior trailing average of approximately $12,200 for years 2018 to 2021 [3].

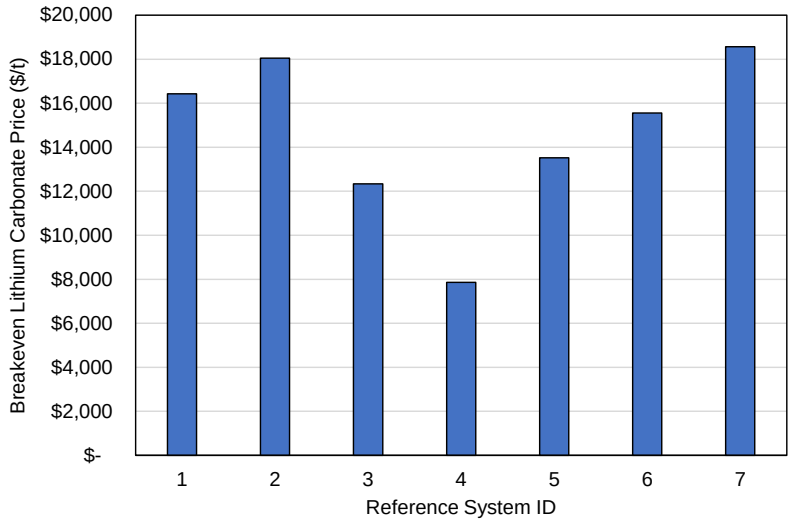


Figure 111. Breakeven lithium carbonate price for modeled system (adsorption/solvent extraction-based recovery) as a function of reference system used in the model parameter. Model parameters given in

Table 67, Reference system data given in Table 66 after [4].

To assess the model sensitivity to grade and recovery, a two-factor sensitivity analysis was conducted using reference system 5 as the model inputs. System ID 5 was selective given the similar technology employed and since it represents the approximate median of the datasets shown in Figure 111. The cost model was reevaluated with lithium solution concentrations ranging from 50 to 400 mg/L, while recovery was varied to levels of 50%, 75%, and 90%. Results from this analysis are shown in Figure 112. As indicated, breakeven price follows an exponential trend with respect to solution concentration. The greatest increases are shown for concentrations <150 ppm, which are likely to be present in most coal-based solutions. This result shows the critical need to preconcentrate lithium prior to and adsorption-based recovery system. In addition, this data suggests that incremental gains associated with high recoveries may not be necessary, as the difference between 75% recovery and 90% recovery is not as significant as that of 50% and 75%.

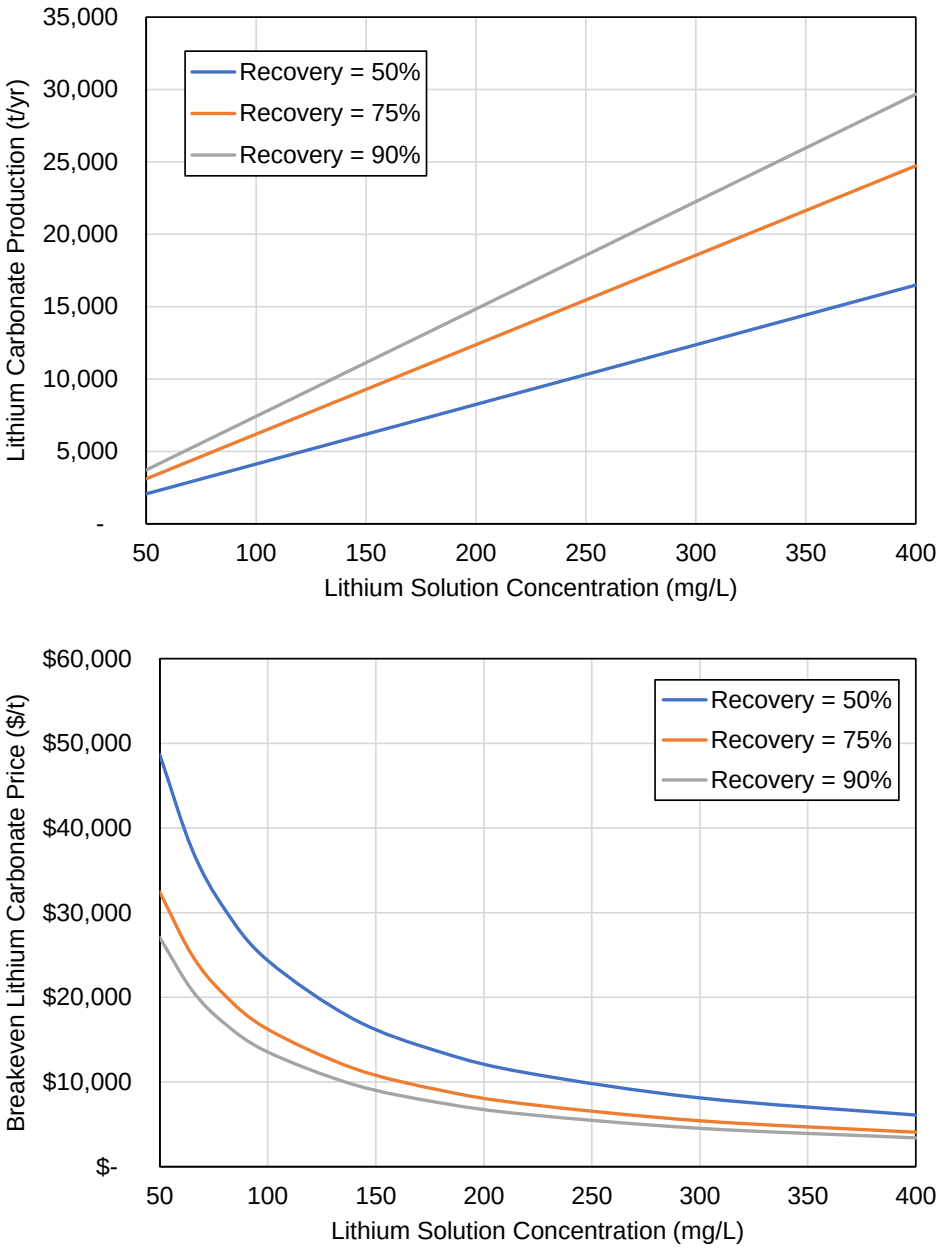


Figure 112. Two factor sensitivity analysis showing the impact of solution concentration and recovery on lithium production (top) and breakeven lithium carbonate price for adsorption/solvent extraction-based solvent extraction system.

*Reverse Osmosis/Nanofiltration*- Flowsheet II (Figure 75) was also modeled using a similar methodology. The fixed model parameters shown in

Table 67 were retained; however, the input cost model was adapted to account for the membrane-based separations. Processing costs for the membrane-based systems were derived from Xu et al. [5] and included $1.02 / 1,000 gallon for reverse osmosis and $0.89 / 1,000 gallon for nanofiltration. The energy and materials for carbonate precipitation were determined using material and energy data from Huang et al., 2021, including a sodium carbonate consumption of 2.049 tonnes per tonne of lithium carbonate produced and an energy use of 349 kW-hr/tonne of production. A fixed sodium carbonate price of $380 / tonne was assumed, and annualized capital costs were assumed to be 54% of the total annual cost using the worst-case scenario included in [4]. Between each stage of reverse osmosis and filtration, a conservative volume reduction of 50% was assumed to account for the solution enrichment occurring throughout the process. As was the case for Flowsheet I, the final result was determined as the breakeven lithium carbonate price assuming a 10% discount rate and 20-year operational period.

Results from a two-factor sensitivity analysis (grade and recovery) are shown in Figure 113. As was the case for Flowsheet I (Figure 74), the breakeven lithium carbonate price follows an exponential trend with respect to lithium solution concentration, reaching an asymptote at approximately $2,000 / t. This value is approximately the base thermodynamic cost associated with the minimum sodium carbonate and energy needed to precipitate the lithium carbonate. Overall, this analysis shows that the reverse osmosis/nanofiltration route may be economically superior to the selective adsorption route, provided that the various processing assumptions and performance parameters are validated.

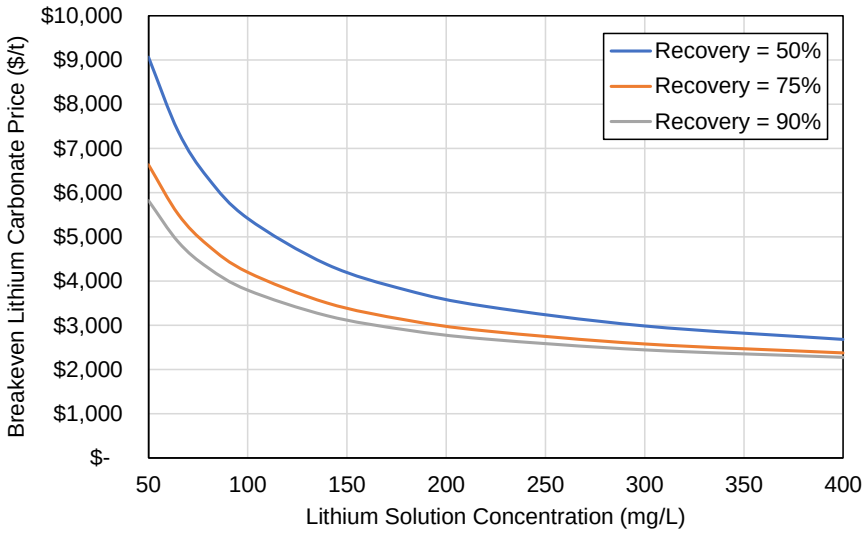


Figure 113. Two factor sensitivity analysis showing the impact of solution concentration and recovery) on breakeven lithium carbonate price for reverse osmosis/nano filtration-based solvent extraction system.

### *2.11.2.1 Section References:*


[1] Huang, T. Y., Perez-Cardona, J. R., Zhao, F., Sutherland, J. W., & Paranthaman, M. P. (2021). Life cycle assessment and techno-economic assessment of lithium recovery from geothermal brine. ACS Sustainable Chemistry & Engineering, 9(19), 6551-6560.

[2] Stringfellow, W. T., & Dobson, P. F. (2021). Technology for the recovery of lithium from geothermal brines. Energies, 14(20), 6805.

[3] United States Geological Survey (2023). Lithium. Mineral Commodity Summaries. Available: https://pubs.usgs.gov/periodicals/mcs2023/mcs2023-lithium.pdf

[4] Warren, Ian. Techno-Economic Analysis of Lithium Extraction from Geothermal Brines. United States: N. p., 2021. Web. doi:10.2172/1782801.

[5] Xu, P., Drewes, J. E., & Heil, D. (2008). Beneficial use of co-produced water through membrane treatment: technical-economic assessment. Desalination, 225(1-3), 139-155.


### *2.11.3 Purity Estimation*

Based on the information presented in the technical economic analysis and somewhat in the technical research plan the following estimates for the process are proposed. For additional information please see referenced documentation.

Table 68. Anticipated Purities

| **Element** | **Method** | **Estimated Purity** | **Final Form Factor** |
|---|---|---|---|
| REEs | | | |
| Y | Thermal Distillation>IL EW | 98%±2% | Y Metal |
| Nd/Pr | Thermal Distillation>IL EW | 98%±2% | Nd/Pr Metal |
| Gd | Thermal Distillation>IL EW | 98%±2% | Gd Metal |
| Dy | Thermal Distillation>IL EW | 98%±2% | Dy Metal |
| Sm | Thermal Distillation>IL EW | 98%±2% | Sm Metal |
| CMs | | | |
| Ga | Thermal Distillation>IL EW | TBD (95%+) | Ga Metal |
| Sr | Precipitate | TBD (95%+) | Sr Carbonate |
| Li | SAM or Precipitate | TBD (95%+) | Li Carbonate or Li Metal |
| Ni | Thermal Distillation>IL EW | 98%±2% | Electrowon Plate |

| | | | |
|---|---|---|---|
| Zn | Thermal Distillation>Water Leach | 95%+ | Metal Sponge |
| Ge | Thermal Distillation>IL EW | TBD (95%+) | Ga Metal |
| Co | Thermal Distillation>Ni>IL EW | 98%±2% | Electrowon Plate |
| Mn | Thermal Distillation>Thermal | 98%±2% | Metal Powder |

*2.11.4 Resource Quantity Estimation*

*Introduction* - Funding Opportunity Announcement (FOA) DE-FOA-0002404 included a future phase involving circuits for (1) possible application in the U.S. Department of Energy's 1 – 3 tonnes mixed rare earth oxide/mixed rare earth salt (MREO/MRES) engineering prototype facility, as well as (2) integration with downstream supply chain processing of these materials for manufacturing and production of end use consumer products, or critical clean energy and/or defense products. This document defines the amount of feed needed to produce the 1 – 3 tonnes of MREO for the two feedstocks studied in this project.

To assess the amount of MREO produced from a given amount of the resource, data collected from previous laboratory and pilot plant studies from projects funded by the U.S Department of Energy (DOE)/National Energy Technology Laboratory (NETL), i.e., [1] and [4]). Recovery values for the downstream purification and metal making processes are estimated from fundamental studies and previously performed experiments.

*West Kentucky No. 13 Coarse Refuse*

*Resource Requirement* - Heap leaching is a commonly used process for the recovery of copper from low grade ores dues to lower capital costs relative to a concentration plant [2] . Due to the low concentrations of rare earth elements and other critical minerals as well as the inability to achieve sufficient pre-concentration prior to hydrometallurgical processing, heap leaching is likely be the most economically viable approach for coarse coal refuse generated from the cleaning of bituminous coals [1], [3],[5]. A previous study tested a 65' x 65' heap leach pad for rare earth element (REE) recovery for the production of a high purity mixed rare earth oxide from West Kentucky No. 13 coarse refuse [4] Approximately 2000 short tons of West Kentucky No. 13 coarse refuse was placed on the pad and leached using an irrigation rate of 0.005 gpm/ft$^2$ of pad area. It can be assumed that the production of REE containing pregnant leach solution (PLS) is approximately equal to the irrigation rate. As such, PLS production was determined to be around 21 gpm (gallons per minute):

$$65 \text{ ft} * 65 \text{ ft} * 0.005 \frac{\text{gpm}}{\text{ft}^2} = 21.125 \text{ gpm}$$

The average total REE concentration of the PLS generated from the heap was determined to be around 28.7 ppm and with an element distribution according to

Table 69.

Table 69. Rare earth element and oxide concentrations of the heap leach pregnant leach solution.

| Rare Earth Element | REE Concentration (mg/L) | Rare Earth Oxide | Oxide Conversion Factor | REO Concentration (mg/L) |
|---|---|---|---|---|
| Sc | 0.99 | $Sc_2O_3$ | 1.5185 | 1.52 |
| Y | 12.02 | $Y_2O_3$ | 1.2699 | 15.26 |
| La | 0.26 | $La_2O_3$ | 1.1728 | 0.30 |
| Ce | 1.82 | $CeO_2$ | 1.2287 | 2.24 |
| Pr | 0.44 | $Pr_6O_{11}$ | 1.2082 | 0.53 |
| Nd | 2.17 | $Nd_2O_3$ | 1.1664 | 2.53 |
| Sm | 1.80 | $Sm_2O_3$ | 1.1596 | 2.09 |
| Eu | 0.49 | $Eu_2O_3$ | 1.1579 | 0.57 |
| Gd | 3.57 | $Gd_2O_3$ | 1.1526 | 4.11 |
| Tb | 0.49 | $Tb_4O_7$ | 1.1762 | 0.58 |
| Dy | 2.08 | $Dy_2O_3$ | 1.1477 | 2.39 |
| Ho | 0.53 | $Ho_2O_3$ | 1.1455 | 0.61 |
| Er | 1.00 | $Er_2O_3$ | 1.1435 | 1.14 |
| Tm | 0.15 | $Tm_2O_3$ | 1.1421 | 0.17 |
| Yb | 0.70 | $Yb_2O_3$ | 1.1387 | 0.80 |
| Lu | 0.16 | $Lu_2O_3$ | 1.1372 | 0.18 |
| **Total** | 28.67 | | 1.2215 | 35.02 |

A conversion factor of 4 can be used for water to convert gpm to tons per hour (tph):

$$M_W = \frac{\left(Q_W \frac{gal}{min}\right)\left(0.133681 \frac{ft^3}{gal}\right)\left(62.4 \frac{lbs}{ft^3}\right)\left(60 \frac{min}{hr}\right)}{\left(2000 \frac{lbs}{short\ ton}\right)} = \frac{Q_W}{4} ;$$

where $M_W$ is the mass flow rate of water in short tons/hour and $Q_W$ the volume flow rate of water in gallons/min. As such, the 21 gpm of PLS production has an equivalent weight of 5.25 tph:

$$21 \text{ gpm} \div 4 \frac{\text{tph}}{\text{gpm}} = 5.25 \text{ tph}$$

Therefore, using $35.02/10^6$ (35.02 mg/L or ppm) as the concentration of the PLS, the total equivalent rare earth oxide (REO) production from the heap pad is determined to be 0.00419 tons/day (tpd):

$$5.25 \text{ tph} \times 24 \frac{\text{hours}}{\text{day}} \times \left(\frac{35.02}{10^6}\right) = 0.0044 \text{ tpd}$$

Therefore, the minimum number of 65 x 65 $ft^2$ heap leach pads needed to meet the daily REO production of target of 1 tonne per day of REO is approximately 250, which would require 500,000 tons of coarse refuse:

$$\left(1 \frac{tonne}{day} \times \frac{2.2 \; tons}{2.0 \; tonnes}\right) \div 0.0044 \frac{tons/day}{heap \; leach \; pad} = 250 \text{ heap leach pads}$$

$$2000 \frac{\text{tons course refuse}}{\text{heap leach pad}} \times 250 \text{ heap leach pads} = 500{,}000 \text{ tons course refuse}$$

This value can be assumed to represent the annual resource feed requirement, since the heap was found to be productive over a one-year period.

However, rare earth element (REE) recovery from the downstream processes used to produce a high grade MREO product is significantly less than 100%. The techno-economic analysis (TEA) in this study was performed assuming a PLS volume flow rate of 5800 gpm, which is higher than the PLS solution from all 250 heap leach pads, which equals 5280 gpm. The rare earth element production for the 5800 gpm operation considering the process recovery values is summarized in Table 70. This scenario produces 25.35 kg/hr. of high purity mixed rare earth oxide (MREO). If operated 24 hours daily, the production is 608 kg/day, which is approximately 60% of the desired 1 tonne per day production of MREO:

$$25.35 \frac{kg}{hr} \times 24 \frac{hrs}{day} = 608 \text{ kg MREO} 608 \; kg \times \left(\frac{1 \; tonne}{1000 \; kg}\right) = 0.608 \text{ tonnes MREO}$$

The total amount of PLS needed to achieve the desired REO production can be estimated by:

$$5{,}800 \text{ gpm} \times \left(\frac{1 \frac{tonne \; MREO}{day} \text{ @ new flow rate}}{0.608 \frac{tonne \; MREO}{day} \text{ @ } 5800 \text{ gpm}}\right) = 9{,}540 \text{ gpm}$$

Therefore, the required resource is 2000 tons per heap leach pad, 454 heap leach pads providing 21 gpm of PLS each, and approximately 908,000 tons of coarse refuse annually:

$$\frac{9{,}540 \text{ gpm}}{21 \frac{\text{gpm}}{\text{heap leach pad}}} = 454 \text{ heap leach pads}$$

$$2000 \frac{\text{tons}}{\text{heap leach pad}} \times 454 \text{ heap leach pads} = 908{,}000 \text{ tons coarse refuse}$$

Table 70. Mass flow of REE in PLS feed and final mixed products.

| REE | REE Mass Flow (kg/hr.) | | REO Product (kg/hr.) |
|---|---|---|---|
| | Feed | Product | |
| Sc | 1.305 | 0.02 | 0.03 |
| Y | 15.83 | 8.19 | 10.40 |
| La | 0.35 | 0.03 | 0.04 |
| Ce | 2.39 | 1.38 | 1.70 |
| Pr | 0.58 | 0.33 | 0.40 |
| Nd | 2.86 | 2.07 | 2.41 |
| Sm | 2.37 | 1.38 | 1.60 |
| Eu | 0.64 | 0.49 | 0.57 |
| Gd | 4.70 | 3.47 | 4.00 |
| Tb | 0.64 | 0.45 | 0.53 |
| Dy | 2.74 | 1.63 | 1.87 |
| Ho | 0.70 | 0.38 | 0.44 |
| Er | 1.32 | 0.67 | 0.77 |
| Tm | 0.20 | 0.07 | 0.07 |
| Yb | 0.93 | 0.41 | 0.47 |
| Lu | 0.21 | 0.05 | 0.05 |
| **Total** | **37.77** | **21.02** | **25.35** |

Given that the total amount of West Kentucky No. 13 coarse refuse available is approximately18,800,000 tons, the heap leach pilot facility could operate approximately for 21 4 years:

$$18{,}800{,}000 \text{ tons } \div 908{,}000 \, \frac{\text{tons}}{\text{yr}} = 21 \text{ years}$$

*Refined Product Quantities*

The techno-economic analysis (TEA) for this project (DE-FE0032119) utilized preliminary data for the purification and metal making processing to estimate product purities and quantities. The production rates of the refined individual rare earth metals (REMs) are provided in Table 3 and the other metal products are provided in Table 4. The production values were based on 24 hours per day of operation and 365 days per year.

**Table 3.** Rare earth metal production from the treatment of West Kentucky No. 13 coarse refuse.

| Rare Earth Metal | Elemental Process Feed Rate (kg/hr.) | Product Production Rate (kg/day) | Product Production Rate (mt/yr.) | Annual Revenue Value ($/yr.) |
|---|---|---|---|---|
| Yttrium | 31.6 | 390 | 142 | $1,128,854 |
| Praseodymium | 1.2 | 16 | 6 | $586,340 |
| Neodymium | 4.4 | 98 | 36 | $4,062,450 |
| Samarium | 4.8 | 64 | 24 | $53,310 |
| Gadolinium | 9.4 | 166 | 60 | $3,413,052 |
| Dysprosium | 5.4 | 76 | 28 | $9,264,906 |
| **Total** | **56.8** | **810** | **296** | **$18,508,912** |

**Table 4.** Critical metal production from the treatment of West Kentucky No. 13 coarse refuse.

| Rare Earth Metal | Elemental Process Feed Rate (kg/hr.) | Product Production Rate (kg/day) | Product Production Rate (mt/yr.) | Annual Revenue Value ($/yr.) |
|---|---|---|---|---|
| Germanium | 0.26 | *ND | - | - |
| Gallium | 0.02 | 0.53 | 0.19 | $59,545 |
| Manganese | 539.12 | 66 | 24 | $118,032 |
| Cobalt | 48.02 | 600 | 220 | $7,611,696 |
| Nickel | 156.44 | 1426 | 520 | $13,823,856 |

| | | | | |
|---|---|---|---|---|
| Zinc | 160.74 | 2756 | 1006 | $3,177,676 |
| Strontium | *ND | - | - | - |
| Lithium | 57.68 | 1174 | 428 | $26,363,942 |
| **Total** | **962.28** | **7270** | **2654** | **$189,497,392** |

*ND = Not determined

*Lignite Resource*

*Resource Requirement* - The lignite resource is a higher-grade material containing around 2000 ppm of total rare earth elements (TREE), 300 ppm cobalt, 700 ppm nickel, and 1000 ppm zinc. Leaching studies revealed that over 95% of most metals can be recovered from the lignite by leaching with a 0.5 M sulfuric acid ($H_2SO_4$) solution (Honaker et al., 2023). As a result, tank leaching is the preferred processing approach, following grinding of the material to an 80% passing size of around 150 microns.

An algorithm was developed to assess the amount of the resource needed to achieve the targeted high-purity mixed rare earth oxide (MREO) production of one metric ton per day. The total resource requirement to meet the production goal was determined to be 60 mt/h. This value was calculated using the elemental concentrations in the feed and the downstream elemental recovery values obtained from the treatment of the heap leach West Kentucky No. 13 PLS as determined by the ratio of the product and feed flow rates in Table 70. Table 71 and Table 72 shows the estimated daily production of high purity MREE and MREO, respectively. The feed REE mass flow rate ($M_{F_i}$) was calculated using the 60 mt/h and the elemental concentration in the feed stream ( $C_{F_i}$ ) for the *i*th rare earth element: $M_{F_i}\frac{kg}{hr} = \left(60\,\frac{mt}{hr}\right) \times \left(1000\,\frac{kg}{mt}\right) \times \left(C_{F_i}\,\frac{mg\,REE_i}{kg\,solids}\right) \div \left(10^6\,\frac{mg\,REE_i}{kg\,REE_i}\right)$.

The calculation for yttrium is provided as an example:

$$M_{F_Y}\,\frac{kg}{hr} = \left(60\,\frac{mt}{hr}\right) \times \left(1000\,\frac{kg}{mt}\right) \times \left(390\,\frac{mg\,REE_i}{kg\,solids}\right) \div \left(10^6\,\frac{mg\,REE_i}{kg\,REE_i}\right) = 23.40\,\frac{kg}{hr}.$$

The estimation of the mass flow rate of a given rare earth to the product stream ($M_{P_i}$) was obtained by considering the elemental recovery values during leaching ( $R_{L_i}\%$ ) and downstream concentration and purification processes ($R_{D_i}\%$):

$$M_{P_i} = M_{F_i} \times \left(\frac{R_{L_i}\,\%}{100}\right) \times \left(\frac{R_{D_i}\,\%}{100}\right).$$

For yttrium, the product mass flow rate was calculated by:

$$M_{P_Y} = \left(23.40\,\frac{kg}{hr}\right) \times \left(\frac{95}{100}\right) x \left(\frac{51.2}{100}\right) = 11.38\,\frac{kg}{hr}.$$

Table 71. Estimated high purity rare earth element production from a waste lignite source using tank leaching and downstream concentration and purification processes.

| Rare Earth Element | Feed REE Concentration (mg/kg) | Feed REE Mass Flow (kg/hr) | REE Leach Recovery (%) | Downstream REE Recovery (%) | Product REE Mass Flow (kg/hr) |
|---|---|---|---|---|---|
| Yttrium | 390 | 23.40 | 95.0 | 51.2 | 11.38 |
| Praseodymium | 109 | 6.54 | 95.0 | 55.2 | 3.43 |
| Neodymium | 320 | 19.20 | 95.0 | 71.7 | 13.08 |
| Samarium | 75 | 4.50 | 95.0 | 57.0 | 2.44 |
| Gadolinium | 61 | 3.66 | 95.0 | 73.2 | 2.55 |
| Dysprosium | 62 | 3.72 | 95.0 | 58.4 | 2.06 |
| **Total** | **1017** | **61.02** | | | **34.94** |

The daily mass production of MREO was determined by multiplying the individual product mass flow rates for each REE by a corresponding conversion factor that was determined by a molecular weight ratio of its oxide form and the element and summing the individual REO daily production rates. The daily operating hours used in the calculation was 24. As shown in Table 6, 60 mt/hr provides a daily production of high purity MREO equal to 1008 kg or 1 metric tonne.

Table 72. Estimated high purity rare earth oxide production from a waste lignite source.

| Rare Earth Element | Product REE Mass Flow (kg/hr) | Oxide Conversion Factor | Product REO Mass Flow (kg/hr) | Product REO Mass Flow (kg/day) |
|---|---|---|---|---|
| Yttrium | 11.38 | 1.2699 | 14.45 | 347 |
| Praseodymium | 3.43 | 1.2082 | 4.14 | 99 |
| Neodymium | 13.08 | 1.1664 | 15.25 | 366 |
| Samarium | 2.44 | 1.1596 | 2.83 | 68 |
| Gadolinium | 2.55 | 1.1526 | 2.93 | 70 |
| Dysprosium | 2.06 | 1.1477 | 2.37 | 57 |
| **Total** | **34.94** | | **41.98** | **1,008** |

The daily production of the other critical elements were performed in the same manner. However, the end product was left in its elemental form as opposed to a presumed end product. The product rate for each critical element is provided in Table 73. Three of the elements were not detected in the resource, which explains the empty cells in Table 73 corresponding to these elements.

Table 73. Estimated critical element production from a waste lignite source using tank leaching and downstream concentration and purification processes.

| Critical Element | Feed REE Concentration (mg/kg) | Feed REE Mass Flow (kg/hr) | REE Leach Recovery (%) | Downstream REE Recovery (%) | Product REE Mass Flow (kg/hr) |
|---|---|---|---|---|---|
| Germanium | *ND | | | | |
| Gallium | *ND | | | | |
| Manganese | 2,836 | 161.7 | 95.0 | 62.9 | 101.7 |
| Cobalt | 179 | 10.2 | 95.0 | 52.1 | 5.3 |
| Nickel | 649 | 37.0 | 95.0 | 38.0 | 14.1 |
| Zinc | 146 | 8.3 | 95.0 | 71.4 | 5.94 |
| Strontium | *ND | | | | |
| Lithium | 514 | 29.3 | 95.0 | 84.8 | 24.8 |
| **Total** | | **246.5** | | | **151.8** |

*ND = not detected in the feed

*Refined Product Quantities* - Based on the 60 mt/h feed rate and the associated process efficiencies, the production rate of refined, high purity, metal products is provided in

*Table 74 and 2.11.4.1 Section References:*


[1] Honaker, R.Q., Werner, J., Nawab, A., Zhang, W., Noble, A., Yang, X. and Free, M., 2023. "Demonstration of Scaled-Production of Rare Earth Oxides and Critical Materials from Coal-Based Sources," DOE Contract No. DE-FE0031827, Final Technical Report, 1080 pages.

[2] Scheffel, R.E., 2002. "Copper Heap Leach Design and Practice," Mineral Processing Plant Design, Practice, and Control (editors: A.L. Mular, D.N. Halbe, and D.J. Baratt), Society for Mining, Metallurgy and Exploration, Littleton, Colorado, Volume 2, Chapter 12. pp. 1571-1605.

[3] Ji, B., Li, Q. and Zhang, W., 2022. "Rare earth elements (REEs) recovery from coal waste of the Western Kentucky No. 13 and Fire Clay Seams. Part I: Mineralogical characterization using SEM-EDS and TEM-EDS," *Fuel*, 307, 121854.

[4] Rosenthal, M., 2022. "A Unique Collaboration of Coal-based REEs and the U.S.'s Largest Rare Earth Producer" Final Technical Report, MP Materials/DOE, Project Number: 89243320CFE000053-0001; 221 pages.

| | |
|---|---|
| [5] | Zhang, W. and Honaker, R.Q., 2020, "Process Development for the Recovery of Rare Earth Elements and Critical Metals from an Acidic Mine Leachate," *Minerals Engineering*, 153, https://doi.org/10.1016/j.mineng.2020.106382. |


Table 75.

Table 74. Rare earth element production and value estimates from the treatment of the lignite material produced as a waste product from construction sand.

| Rare Earth Oxide | Product REO Mass Flow Rate (kg/day) | Product REO Annual Production (mt/yr) | REO Market Value ($/mt) | Annual Revenue Value ($/yr.) |
|---|---|---|---|---|
| $Y_2O_3$ | 347 | 127 | $7,950 | $1,006,584 |
| $Pr_6O_{11}$ | 99 | 36 | $103,500 | $3,756,849 |
| $Nd_2O_3$ | 366 | 134 | $113,250 | $15,133,306 |
| $Sm_2O_3$ | 68 | 25 | $2,250 | $55,694 |
| $Gd_2O_3$ | 70 | 26 | $56,630 | $1,455,275 |
| $Dy_2O_3$ | 57 | 21 | $331,500 | $6,878,526 |
| **Total** | **1008** | **368** | | **$28,286,234** |

*2.11.4.1 Section References:*


[1] Honaker, R.Q., Werner, J., Nawab, A., Zhang, W., Noble, A., Yang, X. and Free, M., 2023. "Demonstration of Scaled-Production of Rare Earth Oxides and Critical Materials from Coal-Based Sources," DOE Contract No. DE-FE0031827, Final Technical Report, 1080 pages.

[2] Scheffel, R.E., 2002. "Copper Heap Leach Design and Practice," Mineral Processing Plant Design, Practice, and Control (editors: A.L. Mular, D.N. Halbe, and D.J. Baratt), Society for Mining, Metallurgy and Exploration, Littleton, Colorado, Volume 2, Chapter 12. pp. 1571-1605.

[3] Ji, B., Li, Q. and Zhang, W., 2022. "Rare earth elements (REEs) recovery from coal waste of the Western Kentucky No. 13 and Fire Clay Seams. Part I: Mineralogical characterization using SEM-EDS and TEM-EDS," *Fuel*, 307, 121854.

[4] Rosenthal, M., 2022. "A Unique Collaboration of Coal-based REEs and the U.S.'s Largest Rare Earth Producer" Final Technical Report, MP Materials/DOE, Project Number: 89243320CFE000053-0001; 221 pages.

[5] Zhang, W. and Honaker, R.Q., 2020, "Process Development for the Recovery of Rare Earth Elements and Critical Metals from an Acidic Mine Leachate," *Minerals Engineering*, 153, https://doi.org/10.1016/j.mineng.2020.106382.

Table 75. Critical mineral production and value estimates from the treatment of the lignite material produced as a waste product from construction sand.

| Rare Earth Metal | Product Mass Flow Rate (kg/day) | Product Annual Production(mt/yr) | Elemental Market Value($/mt) | Annual Revenue Value ($/yr.) |
|---|---|---|---|---|
| Germanium | *ND | | - | - |
| Gallium | *ND | | - | - |
| Manganese | 2,440 | 891 | $4,840 | $4,311,031 |
| Cobalt | 128 | 47 | $34,755 | $1,618,404 |
| Nickel | 337 | 123 | $26,550 | $3,269,428 |
| Zinc | 143 | 52 | $3,160 | $164,482 |
| Strontium | *ND | | - | - |
| Lithium | 596 | 218 | $61,500 | $13,384,836 |
| **Total** | 3,644 | 1,330 | - | $22,748,181- |

## 3.0 PRODUCTS

### I. Journal Articles

None.

### II. Peer-Reviewed Conference Articles

None.

### III. Non-Reviewed Conference Articles

None.

### IV. Abstract & Conference Presentation

None.

### V. Other Publication Products

None.

### VI. Patents & Patent Applications

None.

## 4.0 PARTICIPANTS & COLLABORATING ORGANIZATIONS

The work outlined in this report has been performed as a collaboration among university researchers and industrial professionals. The team includes three academic institutions, i.e., University of Kentucky, Virginia Tech and the University of Alabama. Industrial participants include Alliance Coal and MP Materials. Alliance Coal is providing support by assisting with resource assessment and the techno-economic analysis. MP Materials is providing manpower and experience in rare earth markets, rare earth refining and metal production. Table 76 provides a list of key researchers involved in the project along with their affiliation and email address.

Table 76. Listing of key project personnel.

| Personnel | Business Association | Primary Contact E-Mail |
|---|---|---|
| Rick Honaker | University of Kentucky | honaker@uky.edu |
| Josh Werner | University of Kentucky | jmwe256@uky.edu |
| Xinbo Yang | University of Kentucky | xinbo.yang@uky.edu |
| Aaron Noble | Virginia Tech | noble54@vt.edu |
| Wencai Zhang | Virginia Tech | wencaizhang@vt.edu |
| Ramana Reddy | University of Alabama | rreddy@eng.ua.edu |
| Ernie Thacker | Alliance Coal | Ernie.Thacker@arlp.com |
| Michael Rosenthal | MP Materials | mrosenthal@mpmaterials.com |
| Joe Pascoe | MP Materials | chuck@krpky.com |
| Alan Lund | MP Materials | ALund@mpmaterials.com |
| Judson Marte | MP Materials | JMarte@mpmaterials.com |
| John Hryn | Argonne National Laboratory | jhryn@anl.gov |
| Matthew Earlam | Argonne National Laboratory | mearlam@anl.gov |

## 5.0 PROJECT IMPACT

There are no major project impacts to highlight for this quarter. However, the work to be performed under this project is expected to have a variety of important impacts in terms of (i) providing new scientific understanding, (ii) developing highly trained human resources, and (iii) contributing to process development and technology transfer.

## 6.0 CHANGES/PROBLEMS

None.

## 7.0 SPECIAL REPORTING REQUIREMENTS

There were no developments, events or actions that required special reporting during this progress reporting period.

# 8.0 BUDGETARY INFORMATION

The total budget for the project was $261,398 of which the federal share was $199,989. Cost share was being provided by MP Materials, Alliance Coal and the University of Kentucky in the form of manpower contributions plus associated F&A costs. A breakdown of the budget and expenditures by quarter is provided in Table 77.

As of the completion of the project on February 28, 2023, the total federal expenditures was $195,039. The University of Alabama failed to report expenditures from the last quarter of the report in time for the final invoice submission. As such, a total of $4,950 was expended but not billed to the project and shows as a remaining (positive) value in the federal share line of Table 9. Expenditures that occurred as cost-share provided by MP Materials, Alliance Coal and the University of Kentucky was slightly higher than the original budget as a result of extra funds provided by Alliance Coal to support the analysis of the heap leach data for the report. Cost-share expenditures were $4,777 higher than the original budget. As such, total expenditure were $173 lower that the original budget.

Table 77. Quarter-by-quarter planned and actual federal, non-federal and total expenditures.

| Budget Reporting Quarter | FY22 Q01 | | FY22 Q02 | | FY22 Q03 | | FY22 Q04 | | FY23 Q01 | | FY22 Q04 | |
|---|---|---|---|---|---|---|---|---|---|---|---|---|
| | 10/01/21 - 12/31/21 | | 01/01/22 - 03/31/22 | | 04/01/22 - 06/30/22 | | 07/01/22 - 09/30/22 | | 10/01/22 - 12/31/22 | | 01/01/23 - 03/31/23 | |
| | Q1 | Cumulative Total | Q2 | Cumulative Total | Q3 | Cumulative Total | Q4 | Cumulative Total | Q5 | Cumulative Total | Q6 | Cumulative Total |
| **Baseline Cost Plan** | | | | | | | | | | | | |
| Federal Share | $16,667 | $16,667 | $50,000 | $66,667 | $45,000 | $111,667 | $45,000 | $156,667 | $25,000 | $181,667 | $18,322 | $199,989 |
| Non-Federal Share | $6,823 | $6,823 | $20,470 | $27,293 | $6,000 | $33,293 | $6,000 | $39,293 | $20,116 | $59,409 | $2,000 | $61,409 |
| Total Planned | $23,490 | $23,490 | $70,470 | $93,960 | $51,000 | $144,960 | $51,000 | $195,960 | $45,116 | $241,076 | $20,322 | $261,398 |
| **Actual Incurred Cost** | | | | | | | | | | | | |
| Federal Share | $0 | $0 | $53,818 | $53,818 | $36,119 | $89,937 | $25,656 | $115,593 | $37,586 | $153,179 | $41,860 | $195,039 |
| Non-Federal Share* | $0 | $0 | $4,667 | $4,667 | $3,246 | $7,913 | $2,125 | $10,038 | $18,832 | $28,870 | $37,316 | $66,186 |
| Total Incurred Cost | $0 | $0 | $58,485 | $58,485 | $39,365 | $97,850 | $27,781 | $125,631 | $56,418 | $182,049 | $79,176 | $261,225 |
| **Variance** | | | | | | | | | | | | |
| Federal Share | $16,667 | $16,667 | ($3,818) | $12,849 | $8,881 | $21,730 | $19,344 | $41,074 | ($12,586) | $28,488 | ($23,538) | $4,950 |
| Non-Federal Share* | $6,823 | $6,823 | $15,803 | $22,626 | $2,754 | $25,380 | $3,875 | $29,255 | $1,284 | $30,539 | ($35,316) | ($4,777) |
| Total Variance | $23,490 | $23,490 | $11,985 | $35,475 | $11,635 | $47,110 | $23,219 | $70,329 | ($11,302) | $59,027 | ($58,854) | $173 |